Department of Aeronautics and Astronautics
Stanford University
Stanford, California

THE CONTROL AND USE OF DRAG-FREE SATELLITES

by

B. Lange

SUDAER No. 194

June 1964

ACKNOWLEDGMENTS

ABSTRACT

A scientific earth satellite which is guided in a drag-free orbit by a shielded, free-falling proof-mass has been proposed by a number of investigators. The outer satellite, which completely encloses the proof-mass, has a jet-activated translation-control system that causes it to pursue the proof-mass such that the two never touch. This thesis examines the feasibility and some of the applications of this scheme.

The complete system equations of motion are derived, and the various special cases which apply for different missions and types of attitude control are delineated. In addition, a set of linear equations for both translation and libration of a satellite in orbit are derived. These represent a combined version of the linear form of Hill's Lunar Equations and Lagrange's Libration Equations.

The control and guidance system is analyzed with respect to system performance and gas usage requirements, and an exact solution of the fuel consumption integrals is presented in closed form for a linear pressure-scale-height model of the atmosphere.

A linear-feedback control-synthesis method is developed for a class of even-ordered dynamical plants which possess a property that is defined as "frequency symmetry." This method allows a simple linear-feedback law to be computed which is stable for all positive values of the control gain so that it is useful for the synthesis of contactor control systems.

The principal trajectory errors which are due to vehicle gravity, stray electric and magnetic fields, and sensor forces are investigated. It is found that drag and solar radiation pressure forces may be effectively reduced by three to five orders of magnitude for 100 to 500 statute mile orbits, and that the deviation from a purely-gravitational orbit may be made as small as one meter per year. Such a satellite may be used to make precise measurements in geodesy and aeronomy.

Finally, if a spherical proof-mass is spun as a gyroscope, its random drift rate would be very small because all the drift-producing torques which are associated with the support forces are eliminated. The sources of gyroscope drift which are not associated with support forces are analyzed, and it is found that the random drift would probably be less than 0.1 second of arc per year. Such a gyroscope could be used to measure the effects which would ultimately limit the performance of the best terrestrial or satellite-borne gyroscopes, and it might also be good enough to perform the experiment proposed by G. E. Pugh and L. I. Schiff to test general relativity.

TABLE OF CONTENTS

LIST OF TABLES

LIST OF ILLUSTRATIONS

LIST OF ILLUSTRATIONS (CONT)

TABLE OF CONTENTS (CONT)

LIST OF SYMBOLS

Symbol	Definition
A	area
$\underline{A}$	direction cosine matrix
A,B,C	principal moments of inertia of gyro rotor
A_B	ball projected area (πR_B^2)
A_C	area of capacitive plates
A_S	satellite reference area
A_1, A_2, A_3	ellipsoidal magnetization integrals
a	satellite orbit semi-major axis or real part of the complex roots of Eq. (3-64)
a,b	poles of the integrand of I_n, j_n
a,b,c	principal axis distances of ellipsoidal gyro rotor
$\vec{B}$	magnetic induction vector
$\vec{B}_e$	earth's magnetic induction vector
$\vec{B}_o$	constant external-applied magnetic-induction field
B'_o	that component of $\vec{B}_o$ which gives the largest component of torque in Eq. (5-62)
B_{ox}, B_{oy}, B_{oz}	gyro body-axis components of a constant external magnetic field
$\vec{B}_\perp$	the part of $\vec{B}$ perpendicular to $\vec{\omega}_B$
$\vec{B}_\parallel$	the part of $\vec{B}$ parallel to $\vec{\omega}_B$
b	a constant defined by Eq. (1-44), the imaginary part of the complex roots of Eq. (3-64), or atmospheric rotation resistance defined by Eq. (5-85)
C_D	drag coefficient
C_k^n	binomial coefficient
c	cosine or speed of light in vacuum

Symbol	Definition
D	a function defined by Eq. (5-21)
$\underline{D}$	distribution matrix
$\underline{D}^D$	normal coordinate distribution matrix
D_n	normalized drag force
d, d_2	a distance characteristic of the satellite size
d_b	width of light beam
d_g	capacitive pick-up gap width
Δd_g	departure of proof-mass from the point where the electric forces from a capacitive pick-up are zero
d_1	radius or characteristic size of the cavity
E	eccentric anomaly, electric field, or Young's modulus
E_{av}	average value of the electric field over the surface of the proof-mass
E_{max}	maximum value of the electric field over the surface of the proof-mass
E_n	normal component of the electric field
e	eccentricity of the satellite orbit, electronic charge, or the largest eccentricity of the gyro rotor considered as an oblate spheroid
e/m	charge to mass ratio of the electron
e_P	gyro rotor eccentricity due to a permanent or built-in bulge
e_R	gyro rotor eccentricity due to a bulge caused by rotation
$\vec{e}_\omega$	unit vector parallel to $\vec{\omega}_B$
e_1, e_2	gyro rotor eccentricities
$\vec{F}$	force

Symbol	Definition
$\underline{F}$	matrix defined by Eqs. (4-5) and (4-6)
$\underline{F}^D$	matrix defined by Eqs. (4-7) and (4-8)
F_C	control force
$\vec{F}_{CS}$	control force on the satellite
$\vec{F}_D$	all terms on the right side of Eq. (1-6) except $- m_B/m_S \ \vec{F}_{CS}$
$\vec{F}_{DRAG}$	aerodynamic drag force plus solar radiation force
$\Delta\vec{F}_G$	$\vec{F}_{GB} - \dfrac{m_B}{m_S} \vec{F}_{GS}$
ΔF_{Gx}	the x component of $\Delta\vec{F}_G$
$\vec{F}_{GB}$	force of gravity on the ball
$\vec{F}_{GK} = \vec{F}_{GS}$	force of gravity on the satellite
$\vec{F}_{GSi}$	gravitational force on the ith mass element of the satellite
$\vec{F}_P$	perturbing force from all sources except gravity, drag, and control
$\vec{F}_{PB}$	any nongravitational force on the ball except those due to the satellite
$\vec{F}_{PBx}$	the x component of $\vec{F}_{PB}$
$\vec{F}_{PS}$	the sum of all forces on the satellite except those due to gravity, drag, and control
$\vec{F}_S$	any force acting on the satellite
$\vec{F}_{SB}$	force which the satellite exerts on the ball
F_{SBx}	the x component of $\vec{F}_{SB}$
$\vec{f}$	a specific force or acceleration, $\vec{F}/m$

Symbol	Definition
f	the magnitude of $\vec{f}$ except in Chapter III where $f = f_x + jf_y$ is a complex specific force
f_{BVG}	specific force on the ball due to gravitational attraction of the satellite
$\vec{f}_C$	control acceleration, $-\vec{F}_C/m_S$
f_C	magnitude of $\vec{f}_C$ except in Chapter III where $f_C = f_{Cx} + j\, f_{Cy}$ is a complex specific control force
$\underline{f}_C$	3×1 column matrix with components of $\vec{f}_C$ resolved in x_C, y_C, z_C reference frame
$\underline{f}'_C$	3×1 column matrix with components of $\vec{f}_C$ resolved in x'_C, y'_C, z'_C reference frame
f_{Cx}, f_{Cy}, f_{Cz}	components of $\vec{f}_C$ resolved in the x_C, y_C, z_C reference frame
$\vec{f}_D$	disturbing acceleration, $\vec{F}_D/m_B$
f_D	magnitude of $\vec{f}_D$ except in Chapter III where $f_D = f_{Dx} + j\, f_{Dy}$ is a complex specific disturbing force
$\underline{f}_D$	3×1 column matrix with components of $\vec{f}_D$ resolved in x_C, y_C, z_C reference frame
$\underline{f}'_D$	3×1 column matrix with components of $\vec{f}_D$ resolved in x'_C, y'_C, z'_C reference frame
$\vec{f}_{DB}$	$\vec{f}_{PB} + \vec{f}_{SB}$
$f_{DB\xi}, f_{DB\eta}, f_{DB\zeta}$	components of $\vec{f}_{DB}$ along with ξ, η, ζ axes
$f_{DB\xi I}, f_{DB\eta I}, f_{DB\zeta I}$	assumed constant components of $\vec{f}_{DB}$ resolved in a nonrotating reference frame which was coincident with the ξ, η, ζ reference frame at time $t = 0$
$f_{DB\xi o}, f_{DB\eta o}, f_{DB\zeta o}$	assumed constant components of $\vec{f}_{DB}$ in the ξ, η, ζ reference frame

LIST OF SYMBOLS (CONT)

Symbol	Definition
f_{Dgas}	specific force on the ball due to random molecular collisions from gas in the cavity
f_{DRAG}	F_{DRAG}/m_S
$f_{DRAG,R}$	f_{DRAG} at the reference altitude
f_{Dx}, f_{Dy}, f_{Dz}	components of $\vec{f}_D$ resolved in the x_C, y_C, z_C reference frame
Δf_G	$\Delta F_G/m_B$
$\vec{f}_{GB}$	gravitational acceleration on the ball, $\vec{F}_{GB}/m_B$
$\vec{f}_{PB}$	$\vec{F}_{PB}/m_B$
$f_{\lambda}, f_{\phi}, f_z$	cylindrical components of $\vec{f}$
$\vec{f}_{SB}$	$\vec{F}_{SB}/m_B$
f_ξ, f_η, f_ζ	components of $\vec{f}$ in ξ, η, ζ reference frame
$f_{\xi I}, f_{\eta I}, f_{\zeta I}$	$f_{DB\xi I}, f_{DB\eta I}, f_{DB\zeta I}$
$f_{\xi o}, f_{\eta o}, f_{\zeta o}$	$f_{DB\xi o}, f_{DB\eta o}, f_{DB\zeta o}$
f_1, f_2	contactor control switching functions
G	universal gravitational constant
G_1, G_2, G_3	satellite radii of gyration, $(I_1/m_S)^{\frac{1}{2}}, (I_2/m_S)^{\frac{1}{2}}, (I_3/m_S)^{\frac{1}{2}}$
g	acceleration of gravity
g_e	acceleration of gravity at the earth's surface
g_H	gyromagnetic ratio of a material
$\vec{H}$	magnetic field vector

Symbol	Definition
H	pressure-scale-height $= kT/gm_{av}$ filter transfer function, or magnetic field magnitude
$\underline{\tilde{H}}$	3 × 1 column matrix with components of the magnetic field inside the gyro rotor resolved in the gyro rotor principal axes
H_e	earth's magnetic field
$\vec{H}_o$	$\vec{B}_o/\mu_o$, constant external applied magnetic field
$\underline{H}_o$	3 × 1 column matrix with components of $\vec{H}_o$ resolved in the gyro rotor principal axes
H_o''	that component of $\vec{H}_o$ which gives the largest component of torque in Eq. (5-62)
H_{ox}, H_{oy}, H_{oz}	components of $\vec{H}_o$ in the gyro rotor principal axes
H_R	pressure-scale-height at reference altitude, h_R
$\vec{h}$	angular momentum
h	altitude or effective length of cold gas valve in jet damping calculations
$\vec{h}_B$	angular momentum of the ball
h_P	perigee altitude
h_R	reference altitude at which the atmospheric pressure-scale-height is linearized
h_S	length of cylindrically shaped satellite
$\vec{I}$	vector component of $\vec{m}_H/2\pi B_{\perp} R_3^3$ with direction shown in Fig. 5-3 and magnitude given by Eq. (5-34)
$\underline{I}$	matrix of components of satellite moment of inertia tensor resolved in the principal axis reference frame
$\underline{\underline{I}}$	satellite moment of inertia dyadic
I_o, I_1, I_2, I_3, I_n	integrals defined by Eqs. (2-26) through (2-29)

Symbol	Definition
I_{SP}	control gas specific impulse
I_1, I_2, I_3	satellite principal moments of inertia
$I_{\frac{1}{2}}(v)$, $I_{-\frac{1}{2}}(v)$	spherical Bessel's functions with imaginary argument
i	orbit inclination angle
J_o, J_1, J_2, J_3, J_n	integrals defined by Eq. (2-30)
j	$\sqrt{-1}$
K_a	feed-back gain for adaptive limit cycle size control
$(K_a)_{i+1}$	value of K_a at the $i + 1$th sample instant
K_C	defined by Eq. (4-57)
K_G	numerical factor which depends on vehicle geometry defined by Eq. (4-39)
K_{G2}	defined by Eqs. (4-41) and (4-42)
K_P	constant position feed-back gain
K_T	defined by Eq. (2-50)
K_V	constant velocity feed-back gain
k	gravitational constant of the earth, Gm_E; reciprocal slope of contactor switching line; or Boltzmann constant
k_P, k_V	parameters of Eq. (3-72)
L	Lagrangian
ℓ	radius of a spherical satellite
$\vec{M}$	moment or torque vector
$\underline{M}$	3×1 column matrix with components of $\vec{M}$ resolved in the gyro rotor principal axes

LIST OF SYMBOLS (CONT)

Symbol	Definition
M_{Bx}, M_{By}, M_{Bz}	principal axis components of torque acting on the gyro rotor
$\vec{M}_{CS}$	satellite control-moment vector
$\underline{M}_{CS}$	3×1 column matrix with components of $\vec{M}_{CS}$ resolved in the satellite principal axes
$M_{CSx}, M_{CSy}, M_{CSz}$	principal-axis components of $\vec{M}_{CS}$ resolved in the satellite
$\vec{M}_{DS}$	satellite disturbing-moment vector
$M_{DSx}, M_{DSy}, M_{DSz}$	principal-axis components of $\vec{M}_{DS}$
$\vec{M}_{GS}$	satellite gravity-gradient torque
$\underline{M}_{GS}$	3×1 column matrix with components of $\vec{M}_{GS}$ resolved in the satellite principal axes
$\vec{M}_{GSi}$	satellite gravity-gradient moment on the ith mass element
$\vec{M}_{PS}$	the sum of all moments acting on the satellite except those due to gravity-gradient and control torques
$\underline{M}_{PS}$	3×1 column matrix with components of $\vec{M}_{PS}$ resolved in the satellite principal axes
M_1, M_2, M_3	components of $\vec{M}$ in the ξ, η, ζ reference frame
$M_\perp$	component of $\vec{M}$ perpendicular to $\vec{\omega}_B$
$M_\parallel$	component of $\vec{M}$ parallel to $\vec{\omega}_B$
m	mass or moment of inertia ratio $(I_1 - I_3)/I_1$
m_{av}	average molecular mass of the atmosphere in the satellite
m_B	mass of the ball, proof-mass, or gyro rotor
m_E	mass of the earth

Symbol	Definition
m_g	mass of the control gas
$\vec{m}_H$	magnetic moment vector
$\vec{m}_{HB}$	magnetic moment of the ball
$\vec{m}_{HS}$	magnetic moment of the satellite
m_i	ith mass element
m_S	mass of the satellite and control gas
m_{So}	initial mass of the satellite and control gas
m_{SS}	mass of spherical satellite shell structure
N	photomultiplier tube noise equivalent power
n	moment of inertia ratio, I_3/I_1; or index of integrals defined by Eqs. (2-26) to (2-30)
P_2	second Legendre polynomial
p	atmospheric velocity-resistance coefficient
Q	complex torque ratio, $M_x/I_1 + jM_y/I_1 = Q_x + jQ_y$ or $Q_1 + jQ_2$
Q_C	complex control torque ratio, $Q_{Cx} + jQ_{Cy}$
Q_D	complex dusturbing torque ratio, $Q_{Dx} + jQ_{Dy}$
q	electric charge or complex angular velocity, $\omega_x + j\omega_y$
q_B	electric charge on the ball
$\vec{R}$	vector component of $\vec{m}_H/2\pi B_\perp R_B^3$ with direction shown in Fig. 5-3 and magnitude given by Eq. (5-33)
$\underline{R}$	Euler rate matrix defined by Eqs. (1-28) and (1-30)
R_B	radius of the ball or gyro rotor

Symbol	Definition
R_e	radius of the earth
$\vec{r}$	radius vector
$\underline{r}$	3×1 column matrix with components of $\vec{r}$ resolved in a rotating reference frame
$\underline{r}'$	3×1 column matrix with components of $\vec{r}$ resolved in a nonrotating reference frame
$\delta\vec{r}$	small variation in $\vec{r}_{ES}$ given by $\vec{r}_{ES} - \vec{r}_N$
$\delta\vec{r}_i'$	radius vector from satellite center of mass to ith mass particle
$\vec{r}_B, \vec{r}_{BK}$ $\vec{r}_C, \vec{r}_{CB}, \vec{r}_{CZ}$ $\vec{r}_{EB}, \vec{r}_{EK}, \vec{r}_{IB}, \vec{r}_{IS}$ $\vec{r}_S, \vec{r}_{SB}, \vec{r}_{SC}, \vec{r}_{ZB}$	all defined by Fig. 1-1, vector begins at first subscript point and terminates at the second (for single-letter subscripts see footnote on page 10)
$\underline{r}_C$	3×1 column matrix with components of $\vec{r}_C$ resolved in the x_C, y_C, z_C reference frame
$\underline{r}_C'$	3×1 column matrix with components of $\vec{r}_C$ resolved in the x_C', y_C', z_C' reference frame
$\vec{r}_{ES}$	radius vector from the center of the earth to the satellite center of mass
$\vec{r}_i$	radius vector from the center of mass of the earth to the ith mass particle
$\vec{r}_N$	radius vector from the center of the earth to nominal circular orbit
r_P	perigee radius
r_Q	distance to a point charge from the center of a spherical cavity

Symbol	Definition
r_R	radius from earth's center to the reference altitude, $r_R = R_e + h_R$
λ, ϕ, z	cylindrical coordinates
$\underline{S}$	3×3 square matrix defined by Eq. (5-75)
S_B	surface area of the ball
$d\vec{S}_B$	vector surface area element of the ball
S_d	desired value of S_i
S_i	limit-cycle-size at the ith sample instant
s, s'	Laplace transform variables
$\sim$	sine
T	kinetic energy, period of one control limit cycle, or absolute temperature
$\underline{T}$	matrix transformation to normal coordinates defined by Eqs. (4-3) and (4-4)
T_C	length of time when control is on
T_{CW}	total time control is on during T_W, i.e., while gas is being wasted
T_D	length of time control is off
T_i	length of time control is off during ith limit cycle, approximately equal to the period of the ith limit cycle
T_L	fuel lifetime or control time delay
T_{LC}	fuel lifetime in a circular orbit
T_O	orbit period
T_r	translation-control time constant

Symbol	Definition
T_W	period of one saturated limit cycle (when $f_D = 0$)
T_ω	attitude or rotation-control time constant
t	time
t_{DB}	the time after perigee passage when the control limit cycle first begins to saturate
t_i	assumed thickness or depth of penetration of surface eddy currents
U	energy of an ellipsoid in a constant external magnetic field
$\underline{\underline{U}}$	unit dyadic
u	control variable
$\underline{u}$	2×1 column matrix of control variables
V	potential energy, voltage, or volume
V'	the part of the satellite potential energy containing the coupling terms between the center-of-mass and attitude motions
V_B	potential between the ball and the cavity
V_C	capacitive pick-up input voltage
v	complex dimensionless parameter given by $(j\mu_o \sigma\omega_B)^{\frac{1}{2}} R_B$
v_e	effective exhaust velocity of control gas
$\vec{v}_O$	satellite orbital velocity
W	light power incident on the ball
W_g	weight of the control gas
W_{gw}	weight of the wasted control gas
x	dimensionless parameter given by $(2\mu_o \sigma\omega_B)^{\frac{1}{2}} R_B$

Symbol	Definition
x,y,z	components of $\vec{r}$ in a rotating reference frame
x',y',z'	components of $\vec{r}$ in a nonrotating reference frame
x_B, y_B, z_B	gyro rotor principal-axis components
x_C, y_C, z_C	components of $\vec{r}_C$ (reference frame fixed in the satellite) (These are the basic quantities indicated by the ball position sensor.
x_I, y_I, z_I	inertial reference frame components (see Fig. 1-1)
x_L, x_R, x_S $\dot{x}_B, \dot{x}_T$	defined by Fig. 2-2
x_S, y_S, z_S	satellite principal-axis reference frame components
y	dimensionless parameter defined by Eqs. (2-18) through (2-20)
z	complex variable $= e^{jE}$ or z-transform variable
α, β, γ	angles between $\vec{\omega}_B$ and x_B, y_B, z_B
α	slope of the pressure-scale-height line versus altitude or complex attitude angle, $\emptyset + j\theta$ or $\emptyset_1 + j\emptyset_2$ (see Fig. 1-3 and Eq. (3-70))
$\underline{\alpha}$	4 × 1 column matrix of normal coordinates defined by Eqs. (4-3) and (4-4)
β	constant value of ω_z or $(1 + \alpha)/\alpha$
γ	complex "star-tracker" or "sun-seeker" variable given by $\gamma_x + j\gamma_y + \alpha e^{-j\beta t}$
γ_x, γ_y	real and imaginary parts of γ

Symbol	Definition

<u>Symbol</u>   <u>Definition</u>

$\Delta d_g, \Delta \vec{F}_G, \Delta F_{Gx}$

$\Delta f_G, \delta \vec{r},$ see English alphabetical listing

$\delta \vec{r}_i'$

δ contactor threshold level

δ_i δ at the ith sample instant

ϵ_o permitivity of free space

ϵ_P ellipticity due to a built-in or permanent bulge

ϵ_R ellipticity due to a bulge caused by rotation

$\epsilon_1, \epsilon_2, \epsilon_3$ gyro rotor ellipticities

η complex coordinate given by $x_C' + j\, y_C'$ or see also (ξ, η, ζ)

θ Euler angle defined by Fig. 1-2

$\dot{\vec{\theta}}$ $\dot{\theta}$ written as a vector angular velocity with a direction parallel to the instantaneous direction of rotation of θ

$\dot{\theta}_{max}$ equivalent initial attitude rate caused by an impulsive disturbance

$\dot{\theta}_{ML}$ translation jet misalignment angle

$\theta_1, \theta_2, \theta_3$ small-amplitude vehicle-attitude angles with respect to the ξ, η, ζ reference frame (defined by Fig. 1-6)

μ complex attitude angle given by $\mu_R + j\, \mu_I = \alpha e^{-j \frac{n\beta}{2} t}$

μ_o permeability of free space

Symbol	Definition
μ_1, μ_2	permeability matrices defined by Eqs. (5-71) and (5-72)
ν	arbitrary frequency variable (see Eqs. (3-65) and (3-71))
ξ	complex coordinate given by $x_c + jy_c$
$\underline{\xi}$	4 × 1 column matrix of state variables defined by Eqs. (4-3) and (4-4)
ξ, η, ζ	local tangent reference frame defined by Fig. 1-6 or an intermediate reference frame in the Euler angle transformation
ξ', η', ζ'	intermediate reference frame in the Euler angle transformation defined by Fig. 1-2
ρ	atmospheric mass density
ρ_m	mass density of the proof-mass or gyro rotor
ρ_R	atmospheric mass density at the reference altitude
σ	gyro rotor electrical conductivity or real part of s
σ_A	conductivity per unit area of the satellite skin
σ_x	RMS position error
$\sigma_{\dot{x}}$	RMS velocity error
τ	dummy integration variable
$\underline{\Phi}$	3 × 1 column matrix with components ϕ, θ, ψ
$\delta\underline{\Phi}$	3 × 1 column matrix of infinitesimal rotations
ϕ	Euler angle defined by Fig. 1-2, angle of the gyro spin axis with respect to some initial reference, or gravitational potential function
$\vec{\dot{\phi}}$	$\dot{\phi}$ written as a vector angular velocity with a direction parallel to the instantaneous direction of rotation of ϕ

Symbol	Definition
$\left\langle \phi^2 \right\rangle_{av}$	mean square value of ϕ when the gyro is disturbed by random atmospheric torques
ϕ_1, ϕ_2	small amplitude yaw, roll angles for a vehicle in orbit acted on by gravity-gradient torques
ϕ_2	second term in the series expansion of the gravitational potential of the satellite
χ_m	magnetic susceptability of isotropic material
$\underline{\chi}_m$	3 × 3 square matrix with components of the magnetic susceptability tensor resolved in the principal axis set
$\chi_{mx}, \chi_{my}, \chi_{mz}$	Eigenvalues of $\underline{\chi}_m$
χ_m', χ_m''	Eigenvalues of $\underline{\chi}_m$ for the primed and double-primed axes respectively where the primes are associated with whatever axes give the largest component of torque in Eq. (5-81)
ψ	Euler angle defined by Fig. 1-2 or angle between $\vec{\omega}_B$ and $\vec{h}_B$
$\vec{\psi}$	$\dot{\psi}$ written as a vector angular velocity with a direction parallel to the instantaneous direction of rotation of ψ
$\underline{\Omega}$	3 × 1 antisymmetric matrix of angular velocities defined by Eq. (1-27)
ω	imaginary part of s
ω_B	angular velocity of the gyro rotor
$\omega_{Bx}, \omega_{By}, \omega_{Bz}$	components of $\vec{\omega}_B$ in the gyro rotor principal axes
$\vec{\omega}_e$	earth's angular velocity vector
$\vec{\omega}_{field}$	apparent angular velocity of a constant external magnetic field which would be seen by an observer riding on the gyro rotor

LIST OF SYMBOLS (CONT)

Symbol	Definition
ω_ℓ	Larmour precession frequency
$\vec{\omega}_O$	orbit angular velocity vector
$\vec{\omega}_S$	satellite angular velocity vector
$\underline{\omega}_S$	3×1 column matrix with components of $\vec{\omega}_S$ resolved in the satellite principal axes
$\omega_x, \omega_y, \omega_z$	components of $\vec{\omega}_S$ in the satellite principal axes
ω_1, ω_2	natural frequencies of the dynamical system defined by Eq. (3-69) or cutoff frequencies of the filter defined by Eq. (4-52)

LIST OF SUBSCRIPTS

Subscript	Definition
a	adaptive
av	average
B	ball (proof-mass or gyro rotor) or bottom
BVG	vehicle gravity acting on the ball
b	beam
C	control center, control, or capacitive
D	disturbing
d	desired
DB	dead band
DRAG	atmospheric drag plus solar radiation force
E or e	earth
FL	fuel lifetime
G	gravitational
g	gas or gap
H	magnetic
I	inertial
i	dummy index or thickness
K	center of gravity
L	left or lag
ML	misalignment
m	mass or magnetic
max	maximum
min	minimum
N	nominal

LIST OF SUBSCRIPTS (CONT)

Subscript	Definition
n	normal
O	orbit
o	initial or constant value
P	perturbing, permanent, position, or perigee
Q	charge
R	right, reference, or rotation
r	translation
S	satellite or switch
Sp	specific
T	top or total
V or $\dot{x}$	vehicle or velocity
W	wasted
x	position
Z	zero self-gravity
ω	rotation
$\parallel$	parallel
$\perp$	perpendicular
$\underline{\quad}$	matrix

LIST OF SUPERSCRIPTS

Superscript	Definition
$(\vec{})$	Gibb's vector
$(\ )^{*}$	complex conjugate
$(\ )^{D}$	diagonalized or normal coordinate form
$(\cdot) = \dfrac{d'(\ )}{dt}$	time rate of change seen by an observer in a nonrotating reference frame
$(^{o}) = \dfrac{d(\ )}{dt}$	time rate of change seen by an observer in a rotating reference frame
$(\ )^{-}$	internal
$(\ )^{-1}$	matrix inverse
$(\ )'$	nonrotating with respect to an inertial reference or component associated with maximum value of some quantity
$(\ )^{T}$	transpose of a matrix

A. STATEMENT OF THE PROBLEM

The term "drag-free satellite" as used in this thesis will refer to a system consisting of a small, spherical proof-mass or ball inside of a completely enclosed cavity in a larger satellite. The outer satellite has a jet-activated translation-control system that causes it to pursue the proof-mass such that the two never touch. Since the cavity is closed, the ball is shielded from gas drag and solar-radiation pressure; and, in the ideal case when the effects of other disturbing forces are negligible, the orbit of the proof-mass will be determined only by the forces of gravity. The only disturbing forces which can act on the proof-mass will arise from the satellite itself or from any interactions which can penetrate the shield. Forces due to the satellite can arise from vehicle gravity, stray electric and magnetic fields, gas in the satellite cavity, and the interaction of the position sensor.

Several possible uses or missions for such a satellite have been proposed.

1. GEODESY

The departure of the figure of the earth from a perfect sphere introduces higher harmonics in the earth's gravitational potential. These harmonics perturb the orbit of an earth satellite, and it is possible to measure the harmonics of the earth's gravitational field by observing the changes in a satellite's orbit elements. However, the atmosphere also perturbs the satellite orbit, and this effect must be corrected for in accurate geodetic calculations based on measurements of satellite orbits. The rather elaborate techniques for making these corrections are explained in detail by Kaula (1). A drag-free satellite would remove the necessity of correcting for the uncertainties of atmospheric drag and solar-radiation pressure in satellite observations of the higher harmonics of the earth's gravitational field. In addition, sustained operation would be possible at lower altitudes where the effects of higher harmonics are stronger and where the orbits of conventional satellites are quickly dissipated.

2. AERONOMY

Conventionally, upper-atmosphere density determinations (2) are made by observing the change in the satellite period over several orbits and essentially determining the average density over the entire time and altitude range. This type of data is not as useful in studies of the upper atmosphere as instantaneous density measurements. By contrast, the proof-mass in the zero-g satellite essentially constitutes a very sensitive accelerometer which could be used to measure the instantaneous atmospheric drag (plus radiation pressure) at any altitude.

For a spherically-shaped satellite, the drag coefficient, C_D, is 2 in free molecular flow at high Mach numbers, regardless of the accommodation coefficient; and the calibration of the instrument would not depend on knowing the accommodation coefficient as does, for example, Sharp's density gauge (3). The actual drag forces may be inferred from the jet-plenum-chamber temperatures and pressures, or even more precisely from the relative motion between the proof-mass and the satellite, or from strain-gage measurement of the forces between the jets and the satellite. The latter technique is feasible because the jet forces are typically one to three orders-of-magnitude larger than the drag force, due to the fact that the jets are on for only a small fraction of the total time.

3. PRECISION GYROSCOPES

If the spherical proof-mass is spun at a very rapid rate, it becomes a gyroscope. Since there are no support forces, only extremely small disturbing torques are present. These will arise from gravity-gradient effects, electromagnetic interactions, relativity effects, and read-out torques. It appears possible to construct in this way a gyroscope whose random drift rates would be as low as 0.1 second of arc per year. Such an instrument would be very useful to study all the effects, not connected with the support forces, which would ultimately become important in the construction of extremely low-drift gyroscopes, and it would be possible to do this many years in advance of the time when it might be possible to construct such instruments on earth.

SEL-64-067

4. THE PUGH-SCHIFF GYROSCOPE EXPERIMENT

L. I. Schiff (4) has shown that, while Newtonian theory predicts no precession of the spin axis of a spherically-symmetric gyroscope in free-fall about the earth, General Relativity predicts a geodetic precession arising from motion through the earth's gravitational field, and a Lense-Thirring precession due to the difference between the gravitational field of a rotating and nonrotating earth. The geodetic precession of a gyro in a satellite is about 7 seconds of arc/year and the Lense-Thirring precession is about 0.1 second of arc/year. The design and preliminary development of this experiment in a satellite has been under way at Stanford University for about two years, and is described by Cannon in (5).

5. TIME DEPENDENCE OF GRAVITY

R. H. Dicke (6) has suggested that such a satellite could be used as a clock whose rate would depend on the universal constant of gravity, G. Such a clock could be compared to precision atomic clocks on earth. Any change in the rate of the gravitational clock could be interpreted as a change in the "constant" G. The value of G as a function of time has important consequences in the theories of relativity. The tracking accuracies necessary for this experiment are dictated by the very small size of the effect (about one part in 10^{10} per year), which yields an accumulated lag in the satellite's position of about 0.2 second of arc/year. This is discussed in (7) in detail.

6. ORBIT SUSTAINING

For certain missions, it is desirable to operate a satellite at very low altitudes. Such a satellite would quickly re-enter if its drag were not counteracted in some manner. Rider (8), Bruce (9), and Roberson (10) have discussed various ways of doing this. The free-falling ball could be used to control thrust such that the satellite would remain in a purely-gravitational orbit until the gas supply

is exhausted. This technique would also be especially useful to control precisely the entry points of satellites and of large, potentially-dangerous, spent booster stages. It could also be used to establish a true equiperiod orbit (where the orbit dips very low into the atmosphere) for rendezvous practice.

7. ZERO-G LABORATORIES

It has been proposed that the central parts of manned space stations be used as zero-g laboratories. For experiments of long duration, such a drag cancellation scheme would be necessary to prevent the apparatus from contacting the laboratory walls.

The problem which this thesis will consider is the analysis and design of suitable control systems for the various drag-free satellite missions, and the analysis of the performance of the drag-free satellite in its various applications.

B. PREVIOUS RESULTS

A system similar to the drag-free satellite was first used by researchers who investigated the state of weightlessness (11). Airplanes were flown in weightless trajectories by keeping a small object centered in free space in the cabin. The same system has also been suggested as a guidance scheme to cause ballistic missiles to re-enter along a path which is undisturbed by aerodynamic forces. Ericke (12) also has suggested launching a half-airplane half-satellite which would fly at altitudes between 90 km and 180 km and use some thrust to cancel drag. He calls such a vehicle a "satelloid" and points out that it may also fly at sub-circular velocities using aerodynamic lift to sustain it.

The first suggestions of this scheme, purely in connection with a satellite, apparently were made independently from 1959 to 1961 by a number of investigators. Martin Schwarzschild (6) at Princeton, R.A. Ferrell (in an unpublished report), G. E. Pugh (13), and Gordon J. F. MacDonald (14) at U.C.L.A. have proposed various forms of the drag-free

satellite. It was also suggested independently by C. W. Sherwin of Aerospace and by the author at the Stanford Conference on Experimental Tests of Theories of Relativity in July 1961 (15).

There has been no previous attempt to write the equations of motion of the drag-free satellite system, but the analysis of these equations rests in part on the recent efforts to apply the linearized version of Hill's lunar equations to orbit mechanics and on the use of a complex variable formalism in the theory of symmetric rigid bodies.

In 1878, G. W. Hill wrote the equations of motion of the moon in a rectangular coordinate system centered at the earth and rotating at the sun's mean orbital rate. Hill's equations included the nonlinear gravitational attraction between the earth and the moon, and it was not until 1957 that Wheelon (16) (and independently Geyling (17) in 1959) realized that the linear version without the gravitational terms was a very useful way to calculate orbit partials and perturbations. This approach has also been applied by Eggleston (18) and Tempelman (19) to the problems of rendezvous and guidance. These linearized equations are used to analyze the effect of acceleration errors in Chapter IV.

One of the most important modes of operation of the drag-free satellite is as a symmetric spin-stabilized vehicle. It has been known for a long time that Euler's equations and the small-angle attitude equations for a symmetric body were most conveniently represented in complex form. This method has been applied to spinning missiles in the atmosphere by Nelson (20) and Kanno(21) and to space vehicles by Leon (22) and Freed (23). Freed has worked out the basic attitude-control equations for strapped-down inertial guidance of a spinning space vehicle including the basic requirement of filters tuned to the spin speed, and this work has been extended by Reeves[*] to a space station whose equations of motion include cross product of inertia terms and which uses a control-moment gyro to apply control torques.

---

[*]Reeves, E. I., Space Technology Laboratories, Inc., Redondo Beach, Calif. Stanford University Flight Control Seminar, 1963.

MacDonald (14) has made a few numerical calculations of the fuel lifetime of a drag-free satellite. These results are tied to specific booster and launch configurations. Bruce (9) has computed the fuel lifetime for a circular orbit, and Roberson (10) has presented a technique for computing the jet firing or equivalently, the control switching times for a different kind of orbit-sustaining technique.

Since the drag-free satellite translation-control system operates in a limit cycle at the origin most of the time, it is important to analyze this mode of behavior. Gaylord (24) and Dahl (25) have published calculations of limit-cycle behavior for $1/s^2$ type plants. Gaylord presents a control synthesis based on the use of minimum impulse-bit, logically-controlled pulses, and Dahl considers the effects of very specially-shaped switching surfaces at the origin on fuel consumption in the presence of external torques.

Precision spherical-rotor gyroscopes have been under development for several years in a number of university and industrial laboratories, most notably Minneapolis-Honeywell, Autonetics, University of Illinois, Jet Propulsion Laboratories, General Electric, and General Motors. These researchers were interested in gyroscopes with random drift rates of the order of 10^{-2} to 10^{-4} degrees per hour; and consequently, they were concerned primarily with torques caused by rotor imbalance, magnetic eddy-currents, electric or magnetic support fields acting on a nonspherical rotor, and poor vacuum. The unsupported mode of operation of a spherical free-rotor gyroscope in the vacuum of outer space leaps over the above difficulties and brings into importance a host of much smaller torque-producing effects. Of these only the effects of gravity-gradient and magnetic eddy-current torques on spherical rotors have been previously discussed in the literature. Cannon (5) derives the magnitude of the drift rate caused by gravity-gradient torque on an almost-spherical-rotor gyroscope. Smythe (26) has given the basic equations for magnetic eddy-currents in spherical shells and solid spheres, and Houston (27) and Alers (28) have computed this torque in detail for a solid spherical rotor. However, they did not include the term which is the dominant cause of eddy-current drift for a silicon free-rotor gyroscope.

SEL-64-067

C. OUTLINE OF NEW RESULTS

In Chapter I the author derives the basic 9-degree-of-freedom dynamical equations of the drag-free satellite system and delineates the various special cases of these equations which apply to different kinds of satellite mission and attitude control. The equations of motion take into account the important fact that the center of mass, the center of gravity, the point where the proof-mass position sensor reads zero, and the point where the gravitational attraction of the vehicle is zero are not coincident. In addition, the linearized orbit-perturbation equations of Hill (29) and Wheelon (16) and the small-amplitude attitude equations of Lagrange (30) Roberson (31), and DeBra(32) are combined and extended to include the complete 6-degree-of-freedom, small-amplitude linearized equations of motion of a librating rigid body in orbit. These equations exhibit the coupling between orbit and attitude motions in an explicit manner and allow a quantitative evaluation of the effect of the attitude motions on the orbit. It is necessary to analyze the effects of the attitude motions on the orbit because the close proximity of the satellite and proof-mass might make even small motions important. It turns out, however, that these effects are negligible even for this application except for certain very special resonance conditions.

In Chapter II the author analyzes the basic problems associated with contactor control of a drag-free satellite with perfect attitude control to an inertial reference. The drag force on the satellite is computed from the linear-scale-height model proposed by Groves (33), Jacchia (34), and Smelt (35). An analytic technique is presented which makes it possible to solve the fuel-lifetime integrals in closed form, and the fuel lifetime is calculated for a typical drag-free satellite. It is shown that the dynamics of the plant do not affect the minimum fix fuel consumption as long as the control force always opposes the drag force. Typical limit cycles are presented for various orbits, and a rather interesting control is discussed which employs adaptive limit-cycle-size.

In Chapter III the author attacks the problem of the translation control of a drag-free satellite in the complete absence of attitude control. The intuitive concept of considering the plant in an inertially-nonrotating reference frame leads to a simple synthesis of a linear, time-varying control law. This concept can be generalized to arbitrary 2nth-order plants which are derived from nth-order plants by a transformation which is analogous to the transformation into an inertial reference frame. In the special case that the new 2nth-order plant has constant coefficients, it is possible to plot the locus of the roots of its characteristic equation by shifting the root locus of the corresponding nth-order plant along the plus and minus j axis in the s plane. This technique is then applied to the attitude control of a symmetric, spinning, rigid body as an example. The symmetric rigid body is described by a fourth-order plant and the corresponding second-order plant is the harmonic oscillator. There appears to be no intuitive interpretation of the transformation between these two plants as was possible with the drag-free satellite translation control.

In Chapter IV are analyzed the effects on the trajectory of the drag-free satellite of the perturbations which act on the proof-mass. The basic technique is to extend the results of Wheelon (16) and Tempelman (19) to include two interesting types of forced motion. The advantage of this approach is that it presents the results of linear perturbation analysis in a very simple and intuitive manner. Every force which could perturb the motion of the proof-mass is listed, and an expression for its magnitude is derived. The numerical values of these perturbations are presented for a typical drag-free satellite.

In Chapter V the author considers the sources of random drift for an unsupported gyroscope and concludes that drift rates less than 0.1 second of arc/year are possible. An exhaustive list of torques is computed based on the approximation that the rotor is not a perfect sphere, but rather is slightly ellipsoidal in shape. In addition, all of the torques which depend on atomic or crystalline anisotropy are computed.

CHAPTER I

DERIVATION OF THE DYNAMICAL EQUATIONS

The object of this chapter is to derive the relevant equations
of motion which will be used

1) In the analysis and synthesis of the control system,
   and

2) In the computation of the magnitude and effects of
   the system errors.

A particle moving in empty space under the influence of gravity
alone is dynamically in balance between gravitational and inertial
forces. Thus a reference frame whose origin is at the particle is
"locally inertial" at its origin in the sense that an accelerometer
located exactly at the origin would read zero. If, in addition, the
reference frame is nonrotating with respect to inertial space, it is
reasonable to expect that in this frame the equations of motion of a
particle which is "close" to the origin would be very close to the
form that Newton's laws assume when they are written in an inertial
reference.

The above concept provides the intuitive framework into which the
exact equations of motion of the drag-free satellite will be cast.
Conceptually, the center of the spherical proof-mass or "ball" would
correspond to the origin of the "locally inertial" frame if there
were no nongravitational forces acting on the ball. Since, however,
there are important nongravitational forces which act on the ball,
the approach of this chapter will be to derive the _relative_ equations
of motion between the ball and the satellite. The attitude motions
of a perfect spherical proof-mass are completely ignorable (except in
the case of the unsupported gyroscope, which is treated in Chapter V).
Thus, the complete drag-free satellite dynamical system has six trans-
lational and three rotational degrees-of-freedom. By deriving the
difference or relative equations of motion, it is possible to reduce
the entire system to that of a point mass in either a rotating or

nonratoting reference frame with unaccelerated origin. In keeping with this viewpoint, certain small terms are included on the right-hand side of the equations as perturbing forces, even though they are not independent terms.

A. GENERAL EQUATIONS OF MOTION

Figure 1-1 shows the geometry for a drag-free satellite with a proof-mass in free-fall and with three-axis position control. The center of mass and the center of gravity of the satellite do not coincide in general; and, in addition, the center of gravity is not even fixed in the body but is a function of body orientation. Furthermore, although the design objective would be to obtain coincidence of the control center (the point at which the position indicator reads zero or, equivalently, the point to which the control system tries to drive the ball), the center of mass, and the point of zero self-gravity,[*] due to various uncertainties in manufacture these points will not be the same and the variations cannot be neglected.

The equation of motion of the proof mass is[**]

$$ m_B \, \ddot{\vec{r}}_B = \vec{F}_{GB} + \vec{F}_{SB} + \vec{F}_{PB} \qquad (1-1) $$

---

[*]A point of zero self-gravity or Z.S.G. point is a point where all of the gravitational forces due to the satellite alone sum to zero. See Chapter IV.

[**]Notation:

1) Position Vectors: Fig. 1-1 shows the position vectors used in this analysis. The first subscript indicates where the vector begins, and the second subscript shows where the vector terminates. The various points are labeled in Fig. 1-1 and are defined in the list of subscripts. The vectors $\vec{r}_{IB}$, $\vec{r}_{IS}$, and $\vec{r}_{CB}$ will be abbreviated to $\vec{r}_B$, $\vec{r}_S$, and $\vec{r}_C$ respectively because they occur so often.

2) Forces: The definition of each force is given in the list of symbols. The first subscript indicates the source or cause of the force, and the second indicates the object the force acts upon or the position where it acts. For example, $\vec{F}_{GB}$ is the force of gravity acting on the ball, and $\vec{F}_{CS}$ is the control force applied to the satellite. The first subscript is omitted if the source of the force is unspecified.

3) Differentiation: The symbol $\cdot\cdot = d'/dt$ and $^o = d/dt$ will denote the time derivatives of a vector as seen by an observer in the primed (i.e., inertially fixed or nonrotating) coordinate system and the time derivative of a vector as seen by an observer in the rotating (i.e., body fixed) coordinate system.
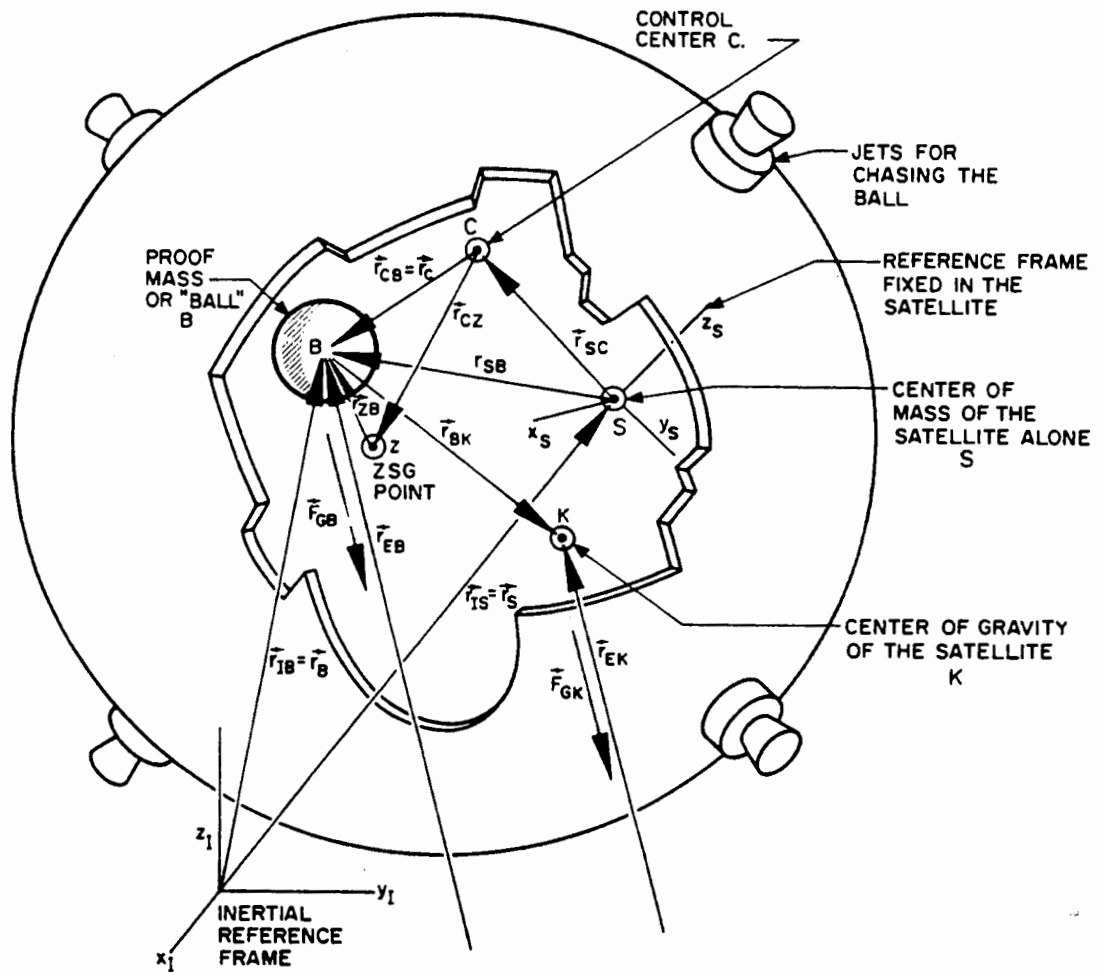
FIG. 1-1.   DRAG-FREE SATELLITE GEOMETRY

where the subscripts $B, G, S, P,$ and C stand for ball, gravity, satellite, perturbation, and control respectively; and the equation of motion of the center of mass of the satellite is

$$m_S \ddot{\vec{r}}_S = \vec{F}_{GS} + \vec{F}_{PS} + \vec{F}_{CS} - \vec{F}_{SB} . \tag{1-2}$$

Since $\vec{r}_B = \vec{r}_S + \vec{r}_{SB}$, Eqs. (1-1) and (1-2) may be combined to yield the equation of motion of the ball with respect to a reference frame fixed in the vehicle:

$$m_B \ddot{\vec{r}}_{SB} = \left(\vec{F}_{GB} - \frac{m_B}{m_S} \vec{F}_{GS} \right) + \left(1 + \frac{m_B}{m_S} \right) \vec{F}_{SB}$$

$$\tag{1-3}$$

$$+ \left(\vec{F}_{PB} - \frac{m_B}{m_S} \vec{F}_{PS} \right) - \frac{m_B}{m_S} \vec{F}_{CS} .$$

Notice that when the equation is written in this form any forces applied to the satellite appear to be applied to the proof-mass through the scale factor $(-m_B/m_S)$. It will often be convenient to speak of "applying a force to the proof-mass," and this terminology will mean $-(m_B/m_S)\vec{F}_S$ whenever the force is actually applied to the satellite.

While the vector $\vec{r}_{SB}$ describes the position of the ball with respect to the satellite mass center, the position-sensing apparatus in the satellite actually measures the vector $\vec{r}_C$ where $\vec{r}_{SB} = \vec{r}_{SC} + \vec{r}_C$, i.e., it measures the position of the ball with respect to the control center. The vector $\vec{r}_{SC}$ will be assumed to be fixed in the satellite; or, equivalently, it will be assumed that the relative motion between the center of mass, S, and the control center, C, during the expulsion of gas, will be so slow and so small that it may be neglected in the present study of dynamic behavior.

With this assumption, the equations of motion now become

$$m_B (\ddot{\vec{r}}_{SC} + \ddot{\vec{r}}_C) = \Delta\vec{F}_G + \left(1 + \frac{m_B}{m_S} \right) \vec{F}_{SB} + \left(\vec{F}_{PB} - \frac{m_B}{m_S} \vec{F}_{PS} \right) - \frac{m_B}{m_S} \vec{F}_{CS} \tag{1-4}$$

where

$$\Delta \vec{F}_G \triangleq \left(\vec{F}_{GB} - \frac{m_B}{m_S} \vec{F}_{GS} \right).$$

Due to the rotation, $\vec{\omega}_S$, of the satellite,[*]

$$\ddot{\vec{r}}_{SC} + \ddot{\vec{r}}_C = \overset{\circ\circ}{\vec{r}}_C + 2\vec{\omega}_S \times \overset{\circ}{\vec{r}}_C + \dot{\vec{\omega}}_S \times (\vec{r}_C + \vec{r}_{SC}) + \vec{\omega}_S \times [\vec{\omega}_S \times (\vec{r}_C + \vec{r}_{SC})]; \quad (1\text{-}5)$$

and the relative translation equations written in terms of the vector, $\vec{r}_C$, measured by the position sensor are

$$m_B[\overset{\circ\circ}{\vec{r}}_C + 2\vec{\omega}_S \times \overset{\circ}{\vec{r}}_C + \dot{\vec{\omega}}_S \times \vec{r}_C + \vec{\omega}_S \times (\vec{\omega}_S \times \vec{r}_C)] = \left\{ m_B[-\dot{\vec{\omega}}_S \times \vec{r}_{SC} - \vec{\omega}_S \times (\vec{\omega}_S \times \vec{r}_{SC})] \right.$$

$$\left. + \Delta \vec{F}_G + \left(1 + \frac{m_B}{m_S} \right) \vec{F}_{SB} + \left(\vec{F}_{PB} - \frac{m_B}{m_S} \vec{F}_{PS} \right) \right\} - \frac{m_B}{m_S} \vec{F}_{CS} . \quad (1\text{-}6)$$

For convenience a single symbol, $\vec{F}_D$, defined to be equal to the sum of the terms in the braces will be used when this equation is used later.

Equations (1-1) and (1-6) are the basic equations of motion of the drag-free satellite. Equation (1-1) is the only one that is needed to compute the satellite trajectory since it will be assumed that the translation-control system constrains the satellite to follow the ball. It will be discussed in Chapter IV. Equation (1-6) is the dynamical plant which the translation-control system must control. It determines the control-system requirements and will be discussed in Chapters II and III.

---

[*] See footnote on page 10. Note also that $\cdot = \circ + \vec{\omega}_S \times$.

B. THE FORCING TERMS AND THEIR RELATIVE MAGNITUDES

Since the satellite is constrained by the translation control system to follow the proof-mass, the orbit of the satellite will be determined solely by Eq. (1-1). The proof-mass will be disturbed from a purely-gravitational orbit only by the forces $\vec{F}_{SB}$ and $\vec{F}_{PB}$. These are shown in Table 4-1, page 130, to correspond to accelerations which are less than $10^{-11} g_e$.*

The terms on the right-hand side of Eq. (1-6) determine the relative motion between the satellite and the ball, and their magnitudes are important only in determining the requirements on the translation-control system.

If one considers only the gravitational attraction of a spherical earth

$$\Delta\vec{F}_G \stackrel{\triangle}{=} \vec{F}_{GB} - \frac{m_B}{m_S}\vec{F}_{GS} \approx Gm_E m_B \left[\frac{\vec{r}_{BK}}{r_{EB}^3} - 3\frac{\vec{r}_{EB}(\vec{r}_{EB} \cdot \vec{r}_{BK})}{r_{EB}^5} \right] \quad (1\text{-}7)$$

$$\Delta F_G \approx \frac{Gm_E m_B r_{BK}}{r_{EB}^3} \quad (1\text{-}8)$$

---

*It is not correct to conclude immediately from these numbers that the drag is only cancelled to $10^{-11} g_e$ since the effect of $\vec{F}_{SB}$ and $\vec{F}_{PB}$ on the ball's orbit are not the same as the drag. This is true because the drag always acts along the velocity vector. See the section on System Errors (pp. 126 to 128).

$$\frac{\Delta f_G}{g_e} \triangleq \frac{\Delta F_G}{m_B g_e} \approx \frac{r_{BK}}{r_{EB}} \approx 10^{-10} \text{ to } 10^{-11} . \tag{1-9}$$

Likewise, from Table 4-1,[*] page 13Q, since $m_B/m_S \ll 1$ and since it is assumed that the control system can maintain $r_Z < 0.1 \, d_1$,

$$\frac{1}{m_B} \left(1 + \frac{m_B}{m_S}\right) F_{SB} \approx 10^{-11} g_e . \tag{1-10}$$

Finally,

$$\frac{1}{m_B} \left| \vec{F}_{PB} - \frac{m_B}{m_S} \vec{F}_{PS} \right| \approx \frac{-F_{DRAG}}{m_S} \approx 10^{-4} \text{ to } 10^{-8} g_e. \tag{1-11}$$

Thus, for low orbits the aerodynamic drag force, $\vec{F}_{DRAG}$, is the dominant translation disturbance; and in order that the control keep the ball centered, the average control force must equal the average drag force,

$$\left\langle \vec{F}_{CS} \right\rangle_{av} \approx - \left\langle \vec{F}_{DRAG} \right\rangle_{av} , \tag{1-12}$$

so that $\vec{F}_{DRAG}$ may be measured by observing $\vec{F}_{CS}$.

C. TRANSLATION CONTROL EQUATIONS FOR VARIOUS TYPES OF ATTITUDE CONTROL

1. THREE-AXIS ATTITUDE CONTROL TO AN INERTIAL REFERENCE

If the drag-free satellite possessed perfect attitude control to an inertial reference, $\vec{\omega}_S$ and $\dot{\vec{\omega}}_S$ would be identically zero; and Eq. (1-6) would become

---

[*]The expressions in Table 4-1 are derived in Chapter IV.

$$m_B \ddot{\vec{r}}_C = \Delta\vec{F}_G + \left(1 + \frac{m_B}{m_S}\right)\vec{F}_{SB} + \left(\vec{F}_{PB} - \frac{m_B}{m_S}\vec{F}_{PS}\right) - \frac{m_B}{m_S}\vec{F}_{CS}. \quad (1\text{-}13)$$

Equation (1-13) is equivalent to three scalar equations of the form

$$\ddot{x}_C = \frac{1}{m_B}\left[\Delta F_{Gx} + \left(1 + \frac{m_B}{m_S}\right)F_{SBx} + \left(F_{PBx} - \frac{m_B}{m_S}F_{PSx}\right)\right] - \frac{F_{CSx}}{m_S} = f_{Dx} + f_{Cx}. \quad (1\text{-}14)$$

In order for these equations to be valid, the attitude control must act such that the neglected terms in $\vec{\omega}_S$ and $\dot{\vec{\omega}}_S$ are much smaller than $\ddot{\vec{r}}_C$. To investigate the conditions under which this is true, assume, for simplicity, that the control acts such that the position and attitude responses are second-order critically damped, with time constants T_r and T_ω respectively. Then it turns out that the above assumptions will be satisfied if $T_\omega \geq T_r$ and if an equivalent impulsive disturbance in attitude, $\dot{\theta}_{max}$ satisfies

$$\dot{\theta}_{max} \ll \frac{1}{T_r} . \qquad (1\text{-}15)$$

The control associated with the plant represented by Eq. (1-13) will be discussed in order to illustrate the basic problems; but, in general, it is more convenient (and for geodetic missions more desirable) not to control attitude at all.

2. CONSTANT SPIN ABOUT A PREFERRED AXIS

If the satellite is symmetric such that $I_1 = I_2 \neq I_3$, and if the satellite is stably oriented with respect to the orbit plane (36), and if the other disturbing torques are negligible, then $\vec{\omega}_S = \vec{\omega}_z$ is constant and Eq. (1-6) is

$$\ddot{\vec{r}}_C + 2\vec{\omega}_S \times \dot{\vec{r}}_C + \vec{\omega}_S \times (\vec{\omega}_S \times \vec{r}_C) = \vec{f}_D + \vec{f}_C . \qquad (1\text{-}16)$$

In a reference frame with the z axis parallel to the spin axis, this becomes

$$\ddot{x}_C - \omega_S^2 x_C - 2\omega_S \dot{y}_C = f_{Dx} + f_{Cx}$$

$$+ 2\omega_S \dot{x}_C + \ddot{y}_C - \omega_S^2 y_C = f_{Dy} + f_{Cy} \tag{1-17}$$

$$\ddot{z}_C = f_{Dz} + f_{Cz} \; .$$

3. ATTITUDE UNCONTROLLED, ARBITRARY SPIN

For

$$\vec{\omega}_S = \begin{pmatrix} \omega_x \\ \omega_y \\ \omega_z \end{pmatrix} , \tag{1-18}$$

equation (1-6) becomes

$$\ddot{x}_C - (\omega_y^2 + \omega_z^2)x_C - 2\omega_z\dot{y}_C + (\omega_x\omega_y - \dot{\omega}_z)y_C + 2\omega_y\dot{z}_C + (\omega_x\omega_z + \dot{\omega}_y)z_C = f_{Dx} + f_{Cx}$$

$$2\omega_z\dot{x}_C + (\omega_x\omega_y + \dot{\omega}_z)x_C + \ddot{y}_C - (\omega_z^2 + \omega_x^2)y_C - 2\omega_x\dot{z}_C + (\omega_y\omega_z - \dot{\omega}_x)z_C = f_{Dy} + f_{Cy} \tag{1-19}$$

$$-2\omega_y\dot{x}_C + (\omega_z\omega_x - \dot{\omega}_y)x_C + 2\omega_x\dot{y}_C + (\omega_z\omega_y + \dot{\omega}_x)y_C + \ddot{z}_C - (\omega_x^2 + \omega_y^2)z_C = f_{Dz} + f_{Cz} \; .$$

It will be shown in Chapter III that it is possible to build a translation-control system in which the satellite attitude is uncontrolled and is allowed to "run free." However, not all drag-free satellites will be flown with no attitude control. For the geodesy and aeronomy vehicles and for the satellites which carry low-precision unsupported gyroscopes, it is desirable to use a spin-stabilized attitude-control system; and for existing vehicles which already have an attitude control system or for carriers of high-precision unsupported

gyroscopes, a three-axis attitude-control system is desirable. There-fore, a brief discussion of the satellite attitude equations will be included in this chapter.

D. GENERAL ATTITUDE EQUATIONS (A SHORT REVIEW OF CLASSICAL RIGID-BODY DYNAMICS)

The orientation of a set of arbitrarily rotated axes (x,y,z) with respect to a reference frame (x',y',z') in terms of the non-classical Euler angles, ϕ, θ, and ψ is depicted in Fig. 1-2.[*] The components of the vector $\vec{r}$ will be denoted by the 3×1 column matrix

$$\underline{r} \triangleq \begin{pmatrix} x \\ y \\ z \end{pmatrix} \tag{1-20}$$

with a similar notation for $\underline{r}'$. The components of $\underline{r}$ and $\underline{r}'$ are related by the 3×3 direction cosine matrix

$$\underline{r} = \underline{A}\,\underline{r}' \,. \tag{1-21}$$

The components of $\underline{A}$ may be written in terms of ϕ, θ, and ψ by multiplying together the matrices which correspond to the three ordered rotations about x', η', and ζ.

$$\underline{A} = \begin{bmatrix} c\psi c\theta & s\psi c\phi + c\psi s\theta s\phi & s\psi s\phi - c\psi s\theta c\phi \\ -s\psi c\theta & c\psi c\phi - s\psi s\theta s\phi & c\psi s\phi + s\psi s\theta c\phi \\ s\theta & -c\theta s\phi & c\theta c\phi \end{bmatrix} \tag{1-22}$$

_____

[*] Reference frames (x',y',z'), (x,y,z) and a general vector $\vec{r}$ will be used in this section to maintain generality. (x',y',z') corresponds to a nonrotating reference frame at the satellite center of mass and (x,y,z) corresponds to (x_S, y_S, z_S).

ROTATE φ ABOUT x'   ROTATE θ ABOUT η'   ROTATE ψ ABOUT ζ
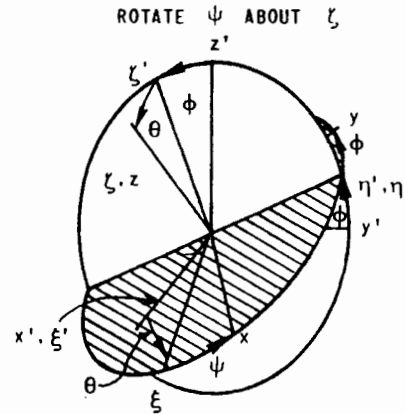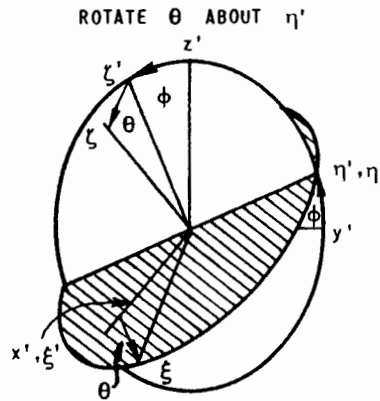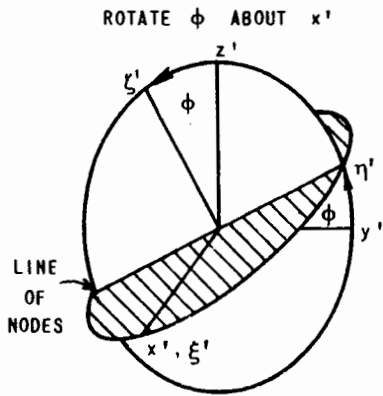
PRINCIPAL PLANE REPRESENTATION (PRINCIPAL PLANES BEGIN PERPENDICULAR)
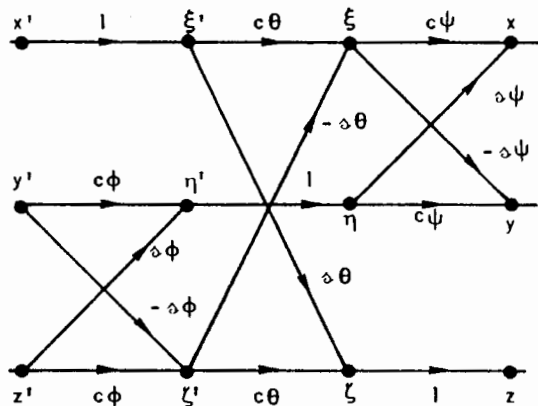
SIGNAL-FLOW-GRAPH REPRESENTATION
Due to Emory Curtis (37)
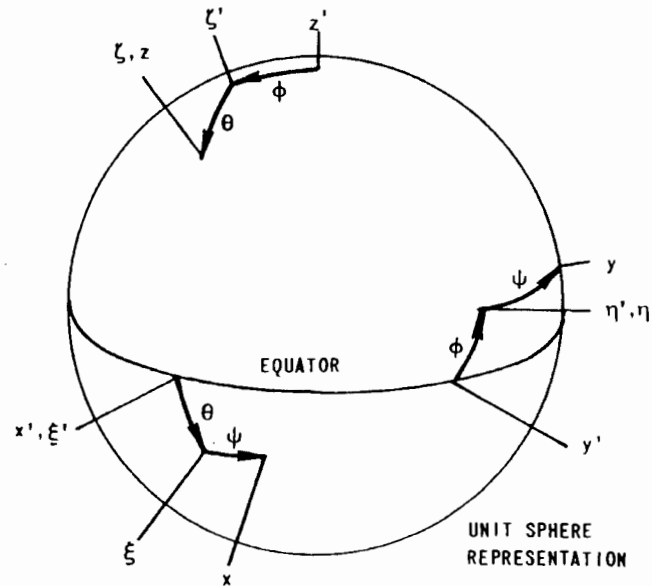
UNIT SPHERE
REPRESENTATION

FIG. 1-2.   AIRCRAFT OR NONCLASSICAL EULER SET

By differentiating the inverse of Eq. (1-21),

$$\underline{r}' = \underline{A}^T \underline{r} \, , \qquad (1\text{-}23)$$

and premultiplying by $\underline{A}$, one obtains

$$\underline{A} \, \underline{\dot{r}}' = \underline{A} \, \frac{d}{dt} \, (A^T)\underline{r} + \underline{\dot{r}} \, . \qquad (1\text{-}24)$$

Direct comparison of Eq. (1-24) with the Coriolis law

$$\vec{\dot{r}} = \vec{\overset{\circ}{r}} + \vec{\omega}_S \times \vec{r} \qquad (1\text{-}25)$$

shows that

$$\underline{\dot{A}} = - \, \underline{\Omega} \, \underline{A} \qquad (1\text{-}26)$$

in which

$$\underline{\Omega} \triangleq \begin{bmatrix} 0 & -\omega_z & \omega_y \\ \omega_z & 0 & -\omega_x \\ -\omega_y & \omega_x & 0 \end{bmatrix} \qquad (1\text{-}27)$$

is an antisymmetric matrix of body angular rates which yields the components of $\vec{\omega}_S \times \vec{r}$ resolved in the (x,y,z) reference frame when postmultiplied by $\underline{r}$. Equation (1-26) is one form of the differential equations of the satellite orientation.

By resolving the 3 vectors $\vec{\phi}$, $\vec{\theta}$, and $\vec{\psi}$ in the (x,y,z) frame, it may be shown that

$$\underline{\omega}_S = \underline{R} \, \underline{\dot{\phi}} \qquad (1\text{-}28)$$

where

$$\underline{\Phi} \triangleq \begin{pmatrix} \phi \\ \theta \\ \psi \end{pmatrix} \qquad\qquad (1\text{-}29)$$

and

$$\underline{R} \triangleq \begin{bmatrix} c\psi c\theta & \varDelta\psi & 0 \\ -\varDelta\psi c\theta & c\psi & 0 \\ \varDelta\theta & 0 & 1 \end{bmatrix} . \qquad\qquad (1\text{-}30)$$

Thus, another form of the orientation differential equation is

$$\underline{\dot{\Phi}} = \underline{R}^{-1} \underline{\omega}_S = \frac{1}{c\theta} \begin{bmatrix} c\psi & -\varDelta\psi & 0 \\ \varDelta\psi c\theta & c\psi c\theta & 0 \\ -c\psi\varDelta\theta & \varDelta\psi\varDelta\theta & c\theta \end{bmatrix} \underline{\omega}_S . \qquad (1\text{-}31)$$

In this same notation Euler's equations become

$$\underline{\dot{\omega}}_S = \underline{I}^{-1} \underline{\Omega} \underline{I} \underline{\omega}_S + \underline{I}^{-1}(\underline{M}_{PS} + \underline{M}_{GS} + \underline{M}_{CS}) \qquad (1\text{-}32)$$

where $\underline{I}$ is a matrix of the body components of the moment of inertia tensor. Equation (1-32) combined with Eq. (1-31) or (1-26) are the general satellite-attitude equations of motion. The attitude equations are coupled to the trajectory equations through the terms $\Delta\vec{F}_G$, $\vec{F}_{PS}$, $\vec{F}_{CS}$, $\vec{M}_{PS}$, $\vec{M}_{GS}$, and $\vec{M}_{CS}$; but with the exception of the control jets, this coupling is rather weak.

It is not necessary to consider the most general form of the attitude equations for most vehicles, since the equations may be written in simpler form for various satellite types.

E. ATTITUDE CONTROL EQUATIONS

1. THREE-AXIS ATTITUDE CONTROL TO AN INERTIAL REFERENCE

In this case, the well known small-amplitude linear form of Eqs. (1-31) and (1-32) is adequate

$$\underline{I} \, \vec{\ddot{\phi}} = \vec{M}_{PS} + \vec{M}_{GS} + \vec{M}_{CS} \; . \tag{1-33}$$

Equation (1-33) has been extensively studied in the controls literature (38) and will not be considered in this thesis except in Chapter II where the translation control equations for the case of no rotation have the same form.

2. SYMMETRIC RIGID BODY SPINNING ABOUT ITS SYMMETRY AXIS

Leon (22) and Freed (23) show how to reduce the equations of motion of a spinning, symmetric rigid body to a more convenient complex form. This procedure is briefly reviewed here.

If $I_1 = I_2 \neq I_3$, Euler's equations become

$$\dot{\omega}_x - \frac{I_1 - I_3}{I_1} \, \omega_z \omega_y = \frac{M_x}{I_1} \tag{1-34}$$

$$\dot{\omega}_y + \frac{I_1 - I_3}{I_1} \, \omega_z \omega_x = \frac{M_y}{I_1} \tag{1-35}$$

$$\dot{\omega}_z = \frac{M_z}{I_3}$$

If $q \triangleq \omega_x + j\omega_y$, $m \triangleq (I_1 - I_3)/I_1$, $n \triangleq I_3/I_1$, $\omega_z \triangleq \beta$, and $Q \triangleq M_x/I_1 + j \, M_y/I_1$, Eqs. (1-34) and (1-35) reduce to

$$\dot{q} + j \, m \, \beta \, q = Q. \tag{1-36}$$

Since $e^{j\psi} = c\psi + j \not{\!\!\!\;} \psi$, the first two lines of Eq. (1-28) may also be written in the complex form

$$q = (\dot{\phi}\, c\theta + j\dot{\theta})e^{-j\psi} \ . \tag{1-37}$$

When $\theta \ll 1$, Eq. (1-37) becomes

$$\dot{\phi} + j\dot{\theta} = q\, e^{j\psi} = q\, e^{j\beta t} \tag{1-38}$$

if ψ is chosen to be zero when $t = 0$.

Now define the complex attitude angle, α,

$$\alpha \triangleq \phi + j\theta \ . \tag{1-39}$$

Figure 1-3 shows the interpretation of α. The angles ϕ and θ give the orientation of the symmetry axis in the inertial reference frame (x',y',z'). By differentiating Eq. (1-39) and substituting in Eq. (1-38),

$$\dot{\alpha} = q\, e^{j\beta t} \ . \tag{1-40}$$

Equations (1-36) and (1-40) are one form of the attitude equations of a symmetric rigid body. They may be combined to form a single equation in α.

$$\ddot{\alpha} - j\, n\, \beta\, \dot{\alpha} = Q\, e^{j\beta t} \ . \tag{1-41}$$

Figures 1-4 and 1-5 show block diagrams of these equations in both real and complex form. The control of these equations is discussed in Chapter III.

WHEN θ AND ϕ ARE SMALL,
α MAY BE INTERPRETED AS THE
PROJECTION OF THE TIP OF THE
z AXIS IN THE x,y PLANE.
THE EQUATIONS OF MOTION, HOWEVER,
ARE VALID FOR ARBITRARILY LARGE ϕ.
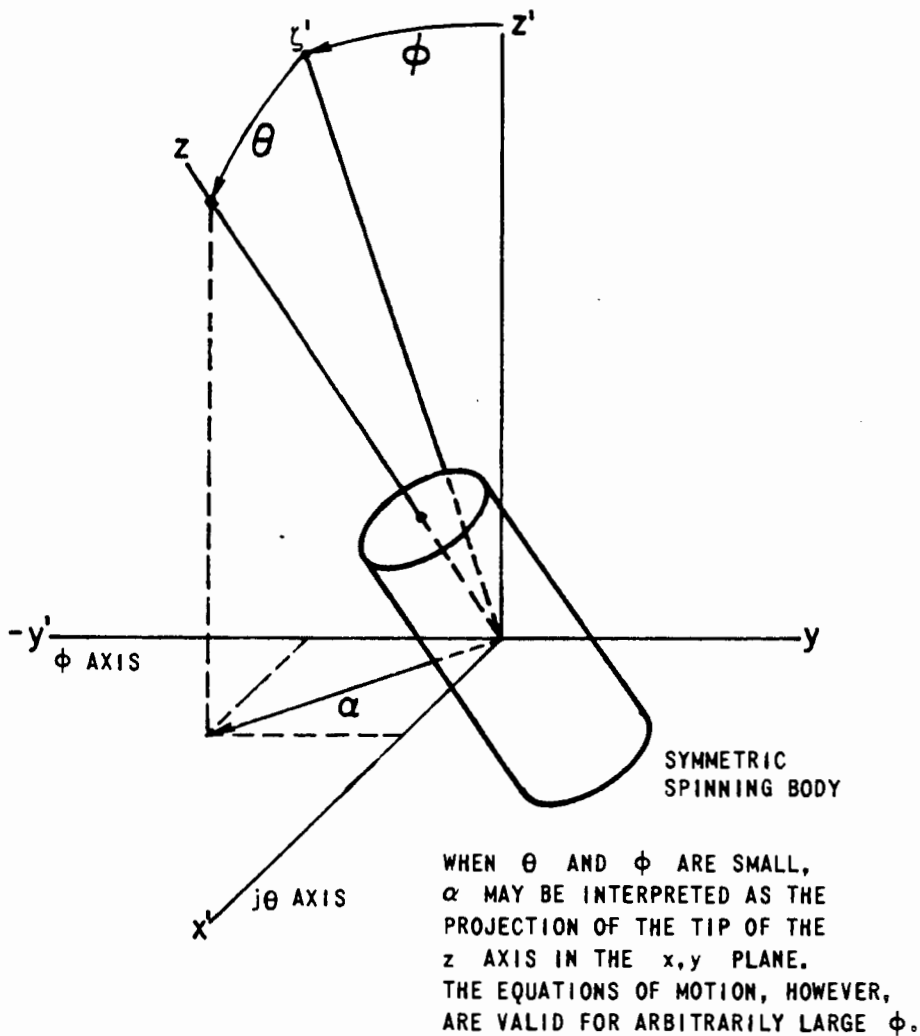
FIG. 1-3.   INTERPRETATION OF THE COMPLEX ATTITUDE ANGLE, $\alpha \triangleq \phi + j\theta$

3.   ISOINERTIAL SATELLITE WITH SPIN DIRECTION CONTROL

It is desirable to point the spin vector normal to the orbit
plane to minimize various trajectory disturbances (cf. Chapter IV), and
the satellite with the least amount of internal vehicle gravity will also
be isoinertial. If $I_1 = I_2 = I_3$, the attitude-control equations are simply

$$\underline{I}\ \underline{\dot{\omega}}_S = \underline{M}_{PS} + \underline{M}_{GS} + \underline{M}_{CS} \tag{1-42}$$

and will not be discussed.

COMPLEX FORM
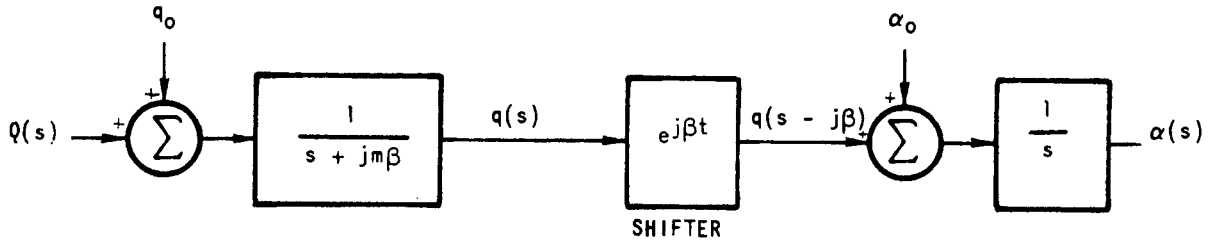
REAL FORM
$$\alpha = \phi + j\theta$$
$$q = \omega_x + j\omega_y$$
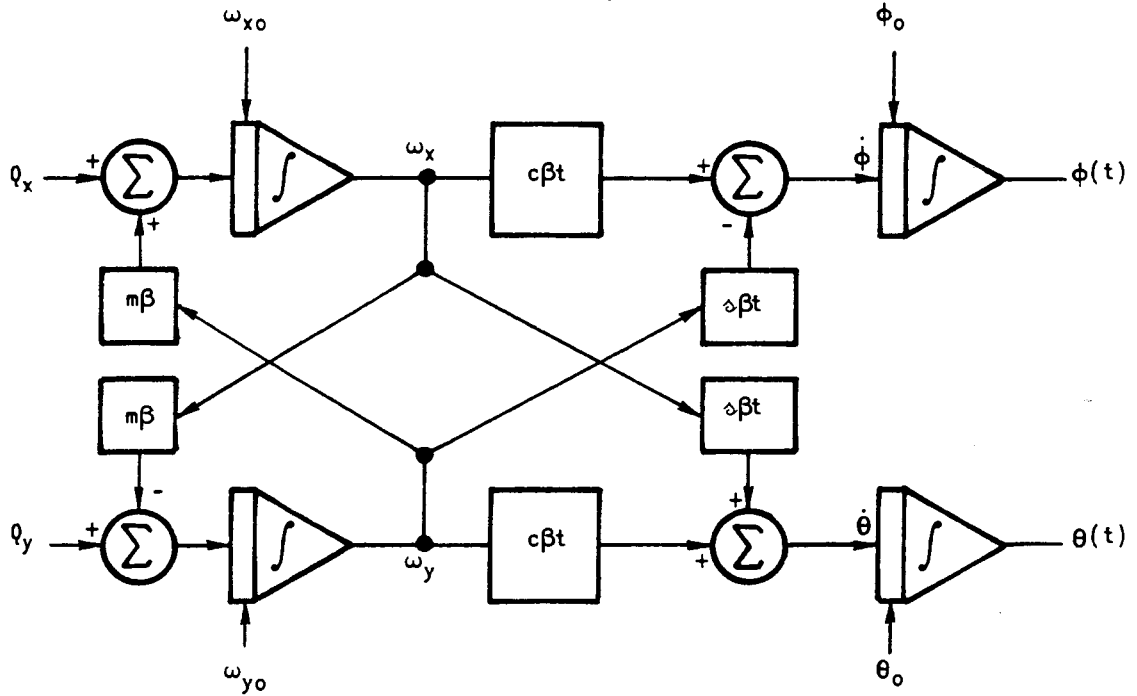
FIG. 1-4. BLOCK DIAGRAM OF THE SYMMETRIC SPINNING RIGID-BODY DYNAMICAL
EQUATIONS $\dot{q} + jm\beta q = Q$ and $\dot{\alpha} = q\, e^{j\beta t}$

SEL-64-067

COMPLEX FORM
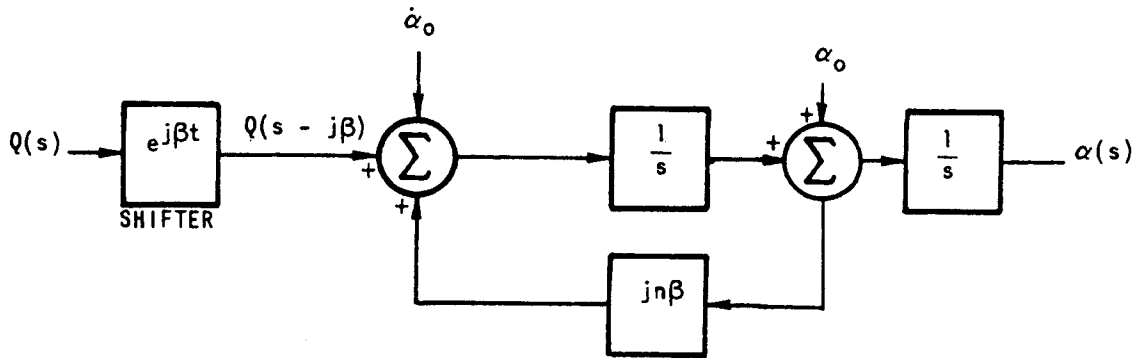
REAL FORM
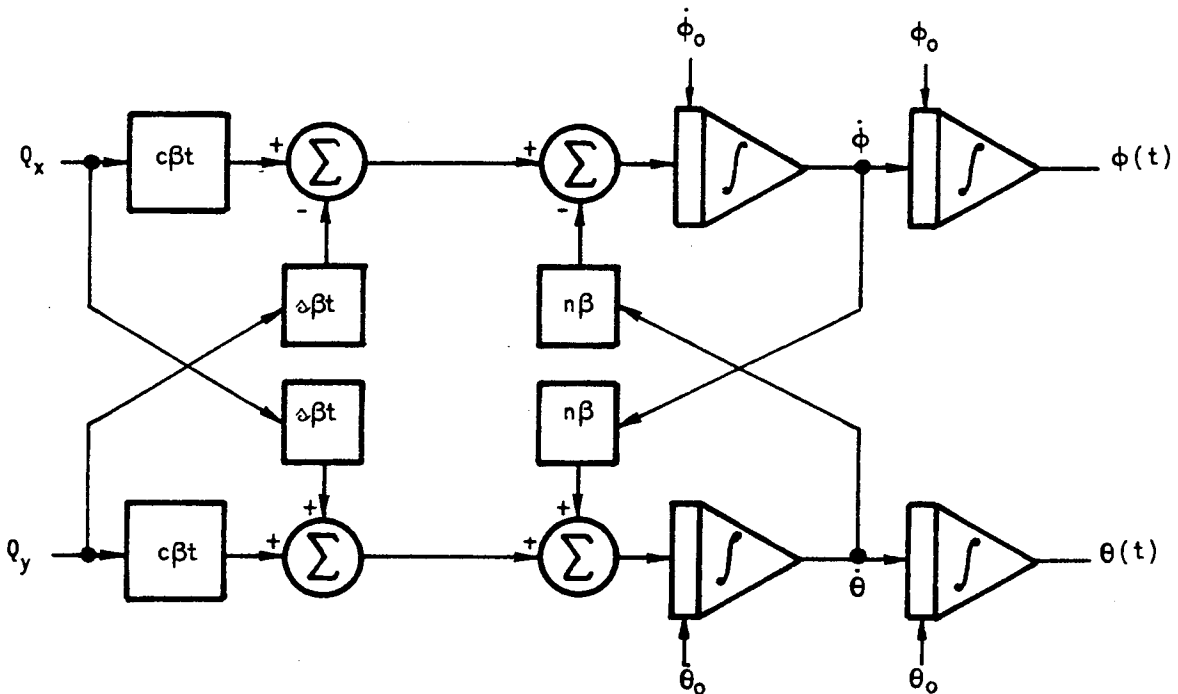
FIG. 1-5. BLOCK DIAGRAM OF THE SYMMETRIC SPINNING RIGID-BODY DYNAMICAL EQUATIONS $\ddot{\alpha} - jn\beta\dot{\alpha} = Q\, e^{j\beta t}$

4. ATTITUDE UNCONTROLLED, EXPECTED SPIN RATE FROM TRANSLATION JET MISALIGNMENT

For the purpose of an order of magnitude estimate assume that:

1) the drag-free satellite consists of a hollow spherical shell of radius, ℓ, and mass, m_{SS}, with a single gas jet of "effective" length, h, and assume that the center of mass of the satellite does not shift as gas is expelled,

2) the thrust line of this jet makes an angle, θ_{ML}, with a line drawn from the jet to the center of mass of the satellite,

3) the jet runs continuously at a thrust level equal to the average drag force acting on the satellite so that
$$m_S = m_{SS} + m_{go} + \dot{m}_g t,$$

4) the velocity field of the control gas is zero with respect to the satellite everywhere except where it passes through the jet and that it is parallel to the jet axis of symmetry and equal to v_e everywhere inside the jet,

5) effects due to centrifugal acceleration and $\dot{\omega}_S$ may be neglected in comparison with the Coriolis acceleration,

6) the only external moment acting on the satellite arises from eddy-current damping in the earth's magnetic field (26) given by $- [2/3 \; B_e^2 \; \ell^4 \sigma_A \cos (\vec{\omega}_S, \vec{B}_e)] \; \omega_S$.

Under these conditions, the gas stream exerts a lateral force, $2\omega_S \dot{m}_S h$, on the jet wall due to the Coriolis acceleration of the moving fluid in the rotating satellite.

Under these conditions, the attitude equation of the satellite may be approximated by

$$\frac{d}{dt}(I\omega) = -b\,\omega_S + 2\,\dot{m}_g\,\ell\,h\,\omega_S + \dot{m}_g\,v_e\,\ell\,\theta_{ML} \qquad (1\text{-}43)$$

where

$$b = \frac{2}{3}B_e^2\,\ell^4\,\sigma_A\,\cos(\vec{\omega}_S,\,\vec{B}_e)\ . \qquad (1\text{-}44)$$

$$\left(m_{SS} + \frac{2}{5}m_{go} + \frac{2}{5}\dot{m}_g t\right)\dot{\omega}_S + \left[-\frac{2}{5}\dot{m}_g\left(\frac{5h}{\ell} - 1\right) + \frac{b}{\ell^2}\right]\omega_S = \frac{\dot{m}_g v_e \theta_{ML}}{\ell}\ . \qquad (1\text{-}45)$$

The solution of Eq. (1-45) is

$$\omega_S = \frac{5v_e\theta_{ML}/2\ell}{\dfrac{5h}{\ell} - 1 - \dfrac{5b}{2\dot{m}_g\ell^2}}\left[\left(1 + \frac{\dfrac{2}{5}\dot{m}_g t}{m_{SS} + \dfrac{2}{5}m_{go}}\right)^{\left(\frac{5h}{\ell} - 1 - \frac{5b}{2\dot{m}_g\ell^2}\right)} - 1\right]\ . \qquad (1\text{-}46)$$

Since the total mass of control gas would be typically only about one tenth of the total vehicle mass, $\left|\dot{m}_g t\right| \ll \left|m_{SS} + \dfrac{2}{5}m_{go}\right|$ and

$$\omega_S \approx \frac{v_e\theta_{ML}\,\dot{m}_g t}{\ell(m_{SS} + 2m_{go}/5)} = \frac{F_{DRAG}\,\theta_{ML}\,\ell\,t}{m_{SS}\ell^2 + 2m_{go}\ell^2/5} = 6.6 \times 10^{-7}\,t/\text{sec}^2 \qquad (1\text{-}47)$$

for a drag-free satellite in a 400 km circular orbit (cf. pages 43 and 44) with a misalignment angle of one degree. In one year, ω_S can typically build up to about 20 rad/sec $\approx$ 200 RPM. Thus, for some

missions, the uncontrolled rates will not be excessive; but for long lifetimes or low altitudes, a rate-limiting control system may be necessary even in those cases where attitude control is unnecessary or where spin is desirable.

F. SMALL-AMPLITUDE LINEAR MOTION OF A SATELLITE INCLUDING GRAVITY-GRADIENT EFFECTS

The librations of a satellite will in general couple into the center-of-mass motion, and the center-of-mass motions will couple into the attitude motions. The latter effect is well known and has been studied extensively (32), and the former is, in general, quite small. For the drag-free satellite, however, any motions of the center of mass in which the proof-mass does not share are important. In order to determine their exact size, these motions will be investigated by analyzing the six coupled center-of-mass and attitude equations after they have been linearized about a nominal circular orbit. These equations may be derived in two ways: 1) from Lagrange's equations, or 2) directly from Newton's Laws. Furthermore, the resulting equations must reduce to the linearized form of Hill's equations for a point mass (29) and to Lagrange's attitude equations (30) for a circular orbit. (See page 36 and see the discussion beginning on page 110.)

1. DERIVATION OF THE COMBINED SIX-DEGREE-OF-FREEDOM TRANSLATION AND ATTITUDE EQUATIONS

For the coordinates as shown in Fig. 1-6, the Lagrangian of the satellite is given by

$$L = T - V = \frac{1}{2} m_S \dot{\vec{r}}_{ES}^2 + \frac{1}{2} \vec{\omega}_S \cdot \underline{\underline{I}} \cdot \vec{\omega}_S + \frac{km_S}{r_{ES}} - \frac{3}{2} \frac{k}{r_{ES}^5} \vec{r}_{ES} \cdot \underline{\underline{I}} \cdot \vec{r}_{ES}$$

$$\tag{1-48}$$

$$+ \frac{1}{2} \frac{k \text{ Trace } \underline{\underline{I}}}{r_{ES}^3} .$$

x_S

BODY FIXED
REFERENCE FRAME

y_S

m_i

ARBITRARY
RIGID BODY

ith MASS
ELEMENT, m_i

$\delta \overline{r_i'}$

CM

z_S

ξ

θ_1

$\delta \overline{r}$

LOCAL TANGENT
REFERENCE FRAME

η

θ_2

γ

NOMINAL
CIRCULAR
ORBIT

θ_3

$\overline{r}_{ES} = \overline{r}_N + \delta\overline{r}$

$\overline{r}_i = \overline{r}_N + \delta\overline{r} + \delta\overline{r_i'}$

ζ

$\overline{r}_i$

$\overline{r}_{ES}$

$\overline{r}_N$

ANGULAR VELOCITY OF
NOMINAL CIRCULAR
ORBIT $= \overline{\omega_0}$

FIXED ATTRACTING CENTER
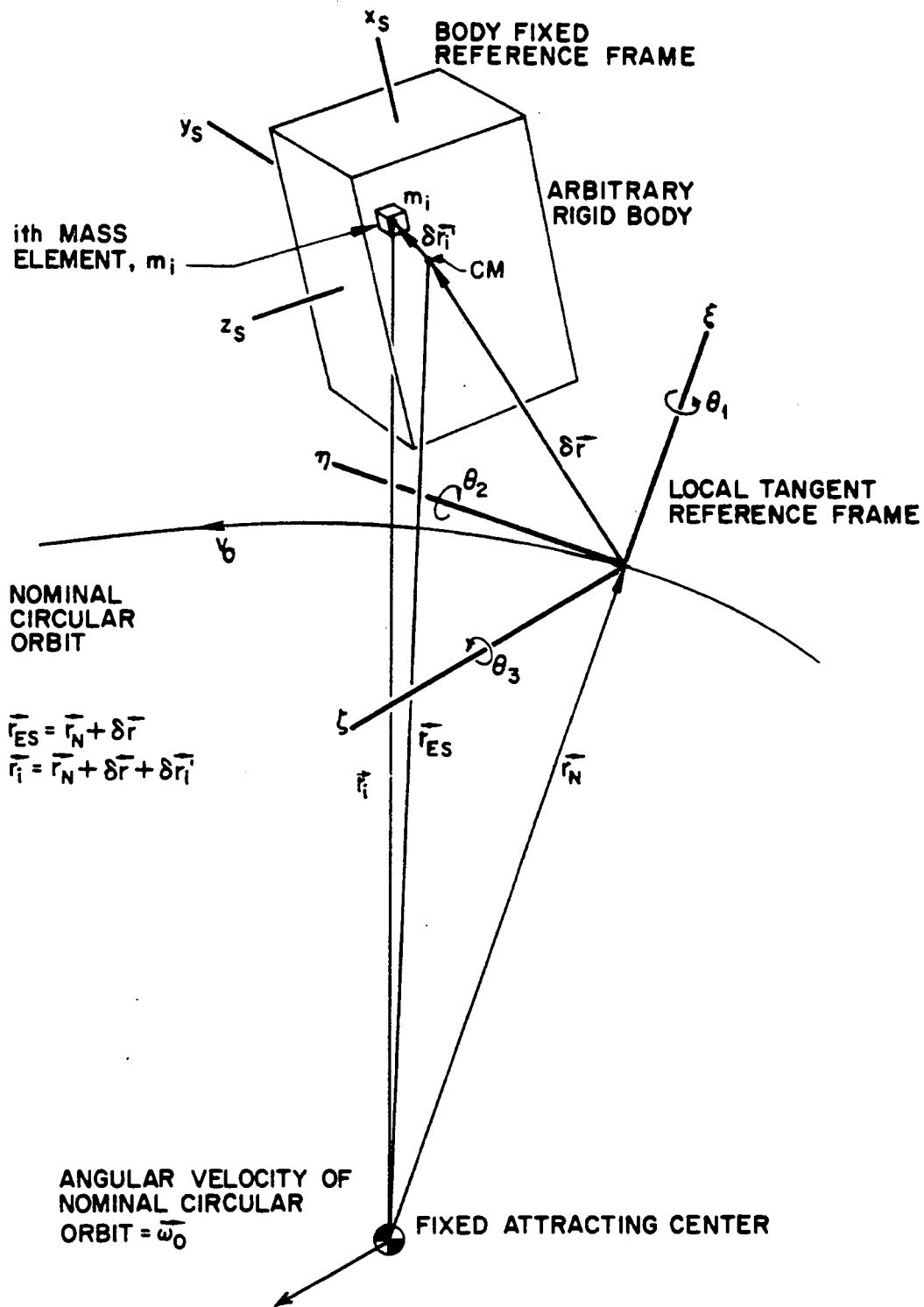
FIG. 1-6. SATELLITE COORDINATES

where $k \triangleq Gm_E$ is the earth's gravitational constant and $\underline{\underline{I}}$ is the satellite moment-of-inertia dyadic. (Dyadics will be denoted by a double underscore.) Clearly, when the linearization is about a nominal circular orbit, $1/2\ m_S\ \dot{\vec{r}}_{ES}^2 + km_S/r_{ES}$ must yield the linearized form of Hill's equations (since these terms deal only with the center-of-mass motions as do Hill's equations); and $1/2\ \vec{\omega}_S \cdot \underline{\underline{I}} \cdot \vec{\omega}_S$ must yield the inertial terms in the Lagrange attitude equations (since they deal only with the attitude motions). Hence, the terms of interaction in the equations of motion may be obtained by differentiating only

$$V' = \frac{3}{2}\ \frac{k}{r_{ES}^5}\ \vec{r}_{ES} \cdot \underline{\underline{I}} \cdot \vec{r}_{ES} - \frac{1}{2}\ \frac{k\ \text{Trace}\ \underline{\underline{I}}}{r_{ES}^3}\ . \quad (1\text{-}49)$$

If the vehicle attitude angles $\phi, \theta,$ and ψ are called θ_1, θ_2 and θ_3 , then (when they are small enough that their products may be neglected) the direction cosine matrix (Eq. (1-22)) becomes

$$\underline{A} = \begin{pmatrix} 1 & \theta_3 & -\theta_2 \\ -\theta_3 & 1 & \theta_1 \\ \theta_2 & -\theta_1 & 1 \end{pmatrix} . \quad (1\text{-}50)$$

In addition, if

$$\vec{r}_{ES} \triangleq \vec{r}_N + \delta\vec{r} \quad (1\text{-}51)$$

where

$$\delta\underline{r} \triangleq \begin{pmatrix} \xi \\ \eta \\ \zeta \end{pmatrix} \quad (1\text{-}52)$$

then Eq. (1-49) may be expanded to second order in the independent variables $\xi, \eta, \zeta, \theta_1, \theta_2,$ and θ_3 .

$$V' = \frac{3}{2}\ \frac{\omega_0^2}{r_N^2}\left\{I_1\left[r_N+\ \xi\ -\ \frac{r_N}{2}\,(\theta_2^2\ +\ \theta_3^2)+\ \theta_3\eta-\ \theta_2\zeta\right]\left[r_N-\ 4\xi+\ \frac{5}{2}\left(\frac{4\xi^2-\eta^2-\zeta^2}{r_N}\right)\right.\right.$$

$$-\ \frac{r_N}{2}(\theta_2^2\ +\ \theta_3^2)+\ \theta_3\eta\ -\ \theta_2\zeta\right]+\ I_2\left[\eta\ -\ r_N\theta_3\right]^2+\ I_3\left[\zeta\ +\ r_N\theta_2\right]^2\right\}\qquad(1\text{-}53)$$

$$-\ \frac{\omega_0^2(I_1\ +\ I_2\ +\ I_3)}{2}\ \left[1\ -\ \frac{3\xi}{r_N}\ -\ \frac{3}{2}\left(\frac{-4\xi^2\ +\ \eta^2\ +\ \zeta^2}{r_N^2}\right)\right].$$

The interaction terms are then given by:

$$\frac{1}{m_S}\ \frac{\partial V'}{\partial\xi} = 6\ \omega_0^2\ \left(\frac{2G_1^2\ -\ G_2^2\ -\ G_3^2}{r_N^2}\right)\ \xi\ -\ \frac{3\omega_0^2}{2}\left(\frac{2G_1^2-\ G_2^2-\ G_3^2}{r_N}\right)\qquad(1\text{-}54)$$

$$\frac{1}{m_S}\ \frac{\partial V'}{\partial\eta} = -\ \frac{3\omega_0^2}{2}\ \left(\frac{4G_1^2-\ 3G_2^2\ -\ G_3^2}{r_N^2}\right)\eta\ +\ 3\omega_0^2\ \left(\frac{G_1^2\ -\ G_2^2}{r_N}\right)\theta_3\qquad(1\text{-}55)$$

$$\frac{1}{m_S}\ \frac{\partial V'}{\partial\zeta} = -\ \frac{3\omega_0^2}{2}\ \left(\frac{4G_1^2-\ G_2^2\ -3G_3^2}{r_N^2}\right)\ \zeta\ +\ 3\omega_0^2\ \left(\frac{G_3^2\ -\ G_1^2}{r_N}\right)\theta_2\qquad(1\text{-}56)$$

$$\frac{\partial V'}{\partial\theta_1} = 0\qquad(1\text{-}57)$$

$$\frac{\partial V'}{\partial\theta_2} = 3\omega_0^2\ (I_3\ -\ I_1)\theta_2\ +\ 3\omega_0^2\ (I_3\ -\ I_1)\ \frac{\zeta}{r_N}\qquad(1\text{-}58)$$

$$\frac{\partial V'}{\partial\theta_3} = 3\omega_0^2\ (I_2\ -\ I_1)\theta_3\ +\ 3\omega_0^2\ (I_1\ -\ I_2)\ \frac{\eta}{r_N}\ .\qquad(1\text{-}59)$$

To obtain these results directly from Newton's Laws, it is necessary to sum all the forces and torques acting on the ith mass element and then to integrate these over the entire body.

$$\vec{F}_{GSi} = \frac{-k\ m_i\ \vec{r}_i}{r_i^3} \quad \text{where} \quad \vec{r}_i = \vec{r}_N + \delta\vec{r} + \delta\vec{r}_i' \qquad (1\text{-}60)$$

and

$$\vec{M}_{GSi} = \delta\vec{r}_i' \times \vec{F}_{GSi} \ . \qquad (1\text{-}61)$$

Expanding $1/r_i^3$ to the third order, and neglecting terms in $(\delta r)^2$ and $(\delta r_i')^3$ and higher, and noting that

$$\underset{i}{S}\ m_i(\delta\vec{r}_i')^2 = \frac{1}{2}\ \text{Trace}\ \underline{\underline{I}}\ , \qquad (1\text{-}62)$$

and

$$\underset{i}{S}\ m_i\ \delta\vec{r}_i'\ \delta\vec{r}_i' = -\underline{\underline{I}} + \underline{\underline{U}}\ \frac{\text{Trace}\ \underline{\underline{I}}}{2}\ , \qquad (1\text{-}63)$$

(where the symbol $\underset{i}{S}$ has the meaning of sum or integral as the case may require and $\underline{\underline{U}}$ is the unit dyadic), the following expression, for the force and torque terms are obtained by integrating $\vec{F}_{GSi}$ and $\vec{M}_{GSi}$ over the body.

SEL-64-067

$$- \frac{\vec{F}_{GS}}{\omega_0^2} = \left[m_S - 3m_S \left(\frac{\delta\vec{r} \cdot \vec{r}_N}{r_N^2} \right) + \frac{3}{2} \frac{\text{Trace } \underline{\underline{I}}}{r_N^2} \left(1 - 5 \frac{\delta\vec{r} \cdot \vec{r}_N}{r_N^2} \right) \right.$$

$$\left. - \frac{15}{2} \frac{(\delta\vec{r}+\vec{r}_N) \cdot \underline{\underline{I}} \cdot (\delta\vec{r}+\vec{r}_N)}{r_N^4} + \frac{105}{2} \frac{(\delta\vec{r}\cdot\vec{r}_N)(\vec{r}_N\cdot\underline{\underline{I}}\cdot\vec{r}_N)}{r_N^6} \right] \vec{r}_N$$

$$+ \left[m_S + \frac{3}{2} \frac{\text{Trace } \underline{\underline{I}}}{r_N^2} - \frac{15}{2} \frac{\vec{r}_N \cdot \underline{\underline{I}} \cdot \vec{r}_N}{r_N^4} \right] \delta\vec{r}$$

$$+ \frac{3\underline{\underline{I}} \cdot (\delta\vec{r} + \vec{r}_N)}{r_N^2} \left[1 - 5 \frac{\delta\vec{r} \cdot \vec{r}_N}{r_N^2} \right] \tag{1-64}$$

and

$$\vec{M}_{GS} = \frac{3\omega_0^2}{r_N^2} (\vec{r}_N \times \underline{\underline{I}} \cdot \vec{r}_N)\left(1 - 5 \frac{\delta\vec{r}\cdot\vec{r}_N}{r_N^2} \right) + \frac{3\omega_0^2}{r_N^2}(\delta\vec{r} \times \underline{\underline{I}}\cdot\vec{r}_N + \vec{r}_N \times \underline{\underline{I}}\cdot\delta\vec{r}).$$

$$\tag{1-65}$$

When coordinatized as in Fig. 1-6, the interaction terms in Eqs. (1-64) and (1-65) reduce to Eqs. (1-54) through (1-59). The complete coupled set is shown below.

$$\ddot{\xi} - 3\omega_0^2\left[1 - \frac{4G_1^2 - 2G_2^2 - 2G_3^2}{r_N^2}\right]\xi - 2\omega_0\dot{\eta} + 0 + 0 + 0 + 0 = \frac{3}{2}\omega_0^2\left[\frac{2G_1^2 - G_2^2 - G_3^2}{r_N}\right] \qquad (1\text{-}66)$$

$$2\omega_0\dot{\xi} + \ddot{\eta} - \frac{3\omega_0^2}{2}\left[\frac{4G_1^2 - 3G_2^2 - G_3^2}{r_N^2}\right]\eta + 0 + 0 + 0 + 3\omega_0^2\left[\frac{G_1^2 - G_2^2}{r_N}\right]\theta_3 = 0 \qquad (1\text{-}67)$$

$$0 + 0 + \ddot{\zeta} + \omega_0^2\left[1 - \frac{3}{2}\frac{4G_1^2 - G_2^2 - 3G_3^2}{r_N^2}\right]\zeta + 0 + 3\omega_0^2\left[\frac{G_3^2 - G_1^2}{r_N}\right]\theta_2 + 0 = 0 \qquad (1\text{-}68)$$

$$0 + 0 + 0 + I_1\ddot{\theta}_1 + (I_3 - I_2)\omega_0^2\theta_1 - \omega_0\dot{\theta}_2(I_1 + I_2 - I_3) + 0 = 0 \qquad (1\text{-}69)$$

$$0 + 0 + 3\omega_0^2(I_3 - I_1)\frac{\zeta}{r_N} + \omega_0\dot{\theta}_1(I_1 + I_2 - I_3) + I_2\ddot{\theta}_2 + 4(I_3 - I_1)\omega_0^2\theta_2 + 0 = 0 \qquad (1\text{-}70)$$

$$0 + 3\omega_0^2(I_1 - I_2)\frac{\eta}{r_N} + 0 + 0 + 0 + I_3\ddot{\theta}_3 + 3\omega_0^2(I_2 - I_1)\theta_3 = 0 \qquad (1\text{-}71)$$

Equations (1-66), (1-67), and (1-68) reduce to Hill's equations (without the nonlinear gravitational terms) when the satellite becomes a point mass; and Eqs. (1-69), (1-70), and (1-71) become the Lagrange attitude equations when ξ, η and ζ are zero.

Hill's equations describing the linearized motions of a point mass with respect to a nominal circular orbit

$$\ddot{\xi} - 3\omega_0^2\xi - 2\omega_0\dot{\eta} = f_\xi \qquad (1\text{-}72)*$$

$$2\omega_0\dot{\xi} + \ddot{\eta} = f_\eta \qquad (1\text{-}73)*$$

$$\ddot{\zeta} + \omega_0^2 \zeta = f_\zeta \qquad (1\text{-}74)*$$

Lagrange's attitude equations describing the linearized libratory motions of a satellite in a circular orbit

$$I_1\ddot{\theta}_1 + (I_3-I_2)\omega_0^2\theta_1 - \omega_0\dot{\theta}_2(I_1+I_2-I_3) = M_1 \qquad (1\text{-}78)$$

$$\omega_0\dot{\theta}_1(I_1+I_2-I_3) + I_2\ddot{\theta}_2 + 4(I_3-I_1)\omega_0^2\theta_2 = M_2 \qquad (1\text{-}79)$$

$$I_3\ddot{\theta}_3 + 3\omega_0^2(I_2-I_1)\theta_3 = M_3 \qquad (1\text{-}80)$$

---

*It is important to note that the correspondence

$$\xi \longleftrightarrow \mathcal{R}$$

$$\eta \longleftrightarrow r_N\phi$$

leads to a set of equations like (1-72), (1-73), and (1-74) in cylindrical coordinates

$$\ddot{\mathcal{R}} - 3\omega_0^2 \mathcal{R} - 2\omega_0 r_N\dot{\phi} = f_{\mathcal{R}} \qquad (1\text{-}75)$$

$$2\omega_0 \dot{\mathcal{R}} + r_N\ddot{\phi} = f_\phi \qquad (1\text{-}76)$$

$$\ddot{\zeta} + \omega_0^2 \zeta = f_\zeta \qquad (1\text{-}77)$$

Equations (1-75), (1-76), and (1-77) may be derived directly from the orbit equations written in cylindrical form. When this is done ϕ may be arbitrarily large (in Eq. (1-72) and (1-73), ξ and η must be small), but $\dot{\phi}$ and $\ddot{\phi}$ must be small (in Eq. (1-72) and (1-73), ξ and $\dot{\eta}$ may be arbitrarily large). The cylindrical coordinate (or with planar motion, the polar coordinate) interpretation is much more accurate when the solution of Hill's equations contain large terms in η. See Ref. (19).

In order to analyze completely the effects of the disturbing forces on the ball, the form of Eqs. (1-72), (1-73), and (1-74) with the second-order nonlinearities included will be needed in Chapter IV. These will be derived next.

2. DERIVATION OF THE HIGHER-ORDER NONLINEARITIES IN HILL'S ORBIT EQUATIONS

Hill's equations may also be derived by substituting

$$\dot{\vec{r}}_{ES} = \delta\vec{r} + \vec{r}_N \tag{1-81}$$

directly into the orbit equation

$$\ddot{\vec{r}}_{ES} + \frac{k \vec{r}_{ES}}{r_{ES}^3} = \vec{f}. \tag{1-82}$$

The equation in $\vec{r}_N$ is assumed to satisfy

$$\ddot{\vec{r}}_N + \frac{k \vec{r}_N}{r_N^3} = 0 \, , \tag{1-83}$$

and

$$r_{ES}^{-3} = r_N^{-3} \left(1 + \frac{(\delta r)^2}{r_N^2} + \frac{2\delta\vec{r} \cdot \vec{r}_N}{r_N^2} \right)^{-\frac{3}{2}} \tag{1-84}$$

is expanded as a power series in $\delta r/r_N$. If Eq. (1-84) is carried to third order, Hill's orbit equations become

$$\ddot{\delta\vec{r}} + \frac{k\delta\vec{r}}{r_N^3} - 3\omega_0^2 \frac{\delta\vec{r} \cdot \vec{r}_N}{r_N^2} \vec{r}_N = \vec{f} + \omega_0^2 \left\{ 3 \frac{\delta\vec{r} \cdot \vec{r}_N}{r_N^2} \delta\vec{r} - \frac{3}{2} \left[5 \frac{(\delta\vec{r} \cdot \vec{r}_N)^2}{r_N^4} - \frac{(\delta r)^2}{r_N^2} \right]\vec{r}_N \right\}$$

$$- \omega_0^2 \left\{ \frac{3}{2} \left[5 \frac{(\delta\vec{r} \cdot \vec{r}_N)^2}{r_N^4} - \frac{(\delta r)^2}{r_N^2} \right] \delta\vec{r} + \frac{5}{2} \left[3 \frac{\delta\vec{r} \cdot \vec{r}_N(\delta\vec{r})^2}{r_N^4} - 7 \frac{(\delta\vec{r} \cdot \vec{r}_N)^3}{r_N^6} \right] \vec{r}_N \right\}. $$

$$- 37 - \tag{1-85}$$

Equation (1-85) may be written in scalar form

$$\ddot{\xi} - 3\omega_0^2 \xi - 2\omega_0 \dot{\eta} = f_\xi - \frac{3}{2} \omega_0^2 \frac{2\xi^2 - \eta^2 - \zeta^2}{r_N} + \omega_0^2 \frac{4\xi^3 - \xi\eta^2 - \xi\zeta^2}{r_N^2} \quad (1-86)$$

$$2\omega_0 \dot{\xi} + \ddot{\eta} = f_\eta + 3\omega_0^2 \frac{\xi\eta}{r_N} - \frac{3}{2} \omega_0^2 \frac{4\xi^2\eta - \eta^3 - \eta\zeta^2}{r_N^2} \quad (1-87)$$

$$\ddot{\xi} + \omega_0^2 \zeta = f_\zeta + 3\omega_0^2 \frac{\xi\zeta}{r_N} - \frac{3}{2} \omega_0^2 \frac{4\xi^2\zeta - \eta^2\zeta - \zeta^3}{r_N^2}. \quad (1-88)$$

Equation (1-88) will be needed to compute the effect of the disturbing forces when the satellite spin vector is normal to the orbit plane.

CHAPTER II

TRANSLATION CONTROL WITH PERFECT THREE-AXIS ATTITUDE CONTROL

The object of this chapter is to discuss the basic translation-control problem (including fuel consumption) associated with the operation of a nonrotating drag-free satellite. The case where the satellite does not rotate with respect to an inertial reference is of interest for precision-gyroscope experiments where the gyroscope spin axis must be compared with a fixed direction in inertial space. In addition, omitting the satellite rotation makes it easier to present the basic properties of the translation control without the added complexity due to the rotation.

The control must accomplish two things:

1) keep the vector $\vec{r}_C$ within some specified bound in the presence of the disturbing forces, and

2) do this with a minimum expenditure of fuel.

The bound on $\vec{r}_C$ will be dictated by the type of mission. For example, in the case of an aeronomy mission, it is merely necessary that the proof-mass not contact the cavity walls very much; and for geodesy experiments, it is desirable that the proof-mass be controlled in such a manner that the force interactions between it and the satellite are as small as possible. For precision-gyroscope experiments, however, it is necessary that the rotor <u>never</u> contact the cavity walls; and for some readout schemes, it is necessary that the rotor be very stationary with respect to the satellite during the readout period.

A. TRANSLATION-CONTROL SYSTEM DESIGN FOR MINIMUM-FUEL CONSUMPTION

In order to consider the fuel consumption, it is necessary to examine the nature of the control system disturbances given in Eq. (1-6) and also on page 15. They are

1) $\Delta\vec{F}_G/m_B$ (the difference between the acceleration of gravity acting on the ball and that acting on the satellite) $\approx 10^{-10}$ to $10^{-11} g_e$.

2) $(1 + m_B/m_S)\vec{F}_{SB}/m_B$ (the acceleration due to the force interactions between the ball and the satellite) $\approx 10^{-11} g_e$. (See Table 4-1, page 130.)

3) $(\vec{F}_{PB} - m_B/m_S \; \vec{F}_{PS})/m_B$ (the acceleration due to outside perturbations).

$(\vec{F}_{PB} - m_B/m_S \; \vec{F}_{PS})/m_B$ arises from

a) Meteorite collisions with the satellite,

b) Motion of a charged satellite through the earth's magnetic field,

c) Undesired expulsion of matter due to outgassing or control gas leaks,

d) Solar radiation pressure, and

e) Atmospheric drag.

(1) and (2) are negligibly small but (3) must be considered in detail. Each of these disturbances will be discussed below.

1. EXTERNAL PERTURBING ACCELERATIONS

a. Meteorite Collisions with the Satellite

From elementary momentum considerations, it can be shown that a meteorite collision with a typical relative velocity of 40,000 ft/sec between a 45 kilogram satellite and a 0.2 milligram meteorite[*] would impart a velocity change of 10^{-2} cm/sec to the satellite. (This velocity change is typical of the limit-cycle-size for the control system. See Fig. 2-7, page 62 .) Data on the frequency of meteorite collisions is still rather poor; but the indications are that collisions with meteorites of this mass or larger are extremely rare, occurring approximately every one to 1000 years (40).

---

[*] This mass was chosen as a worst-case example. A collision with a much larger meteorite would probably do serious damage to the satellite.

b. Motion of a Charged Satellite Through the Earth's Magnetic Field

A charge will accumulate on a satellite moving through the ionized upper atmosphere because of the different mobilities of the electrons and ions, and it can be shown theoretically that the potential of this charge will not exceed a few volts (41). (However, there is at least one instance of a potential of several hundred volts being measured on a satellite.) If one takes 100 volts as a reasonable upper bound, the disturbing acceleration caused by moving this charge through the earth's magnetic field will be of the order of $4 \times 10^{-12} g_e$.

c. Undesired Expulsion of Matter Due to Outgassing or Control Gas Leaks

Cold gas control valves have typical leakage rates which vary between 10^{-3} and 10^{-5} standard cc/sec. By careful design and quality control, it is reasonable to expect total gas leakages of the order of about 10 standard liters per year. Such leakage values correspond to flow rates which would cause negligible control-system disturbance.

Gas leaks which result from system malfunctions or outgassing could result in sizable disturbing forces. There is no way to analyze these in advance, but the disturbances will be relatively constant. They will make the drag-free satellite uncontrollable if their magnitudes exceed the control force, or they will only waste gas while still allowing the control system to function if their magnitudes are less than the control force.

d. Solar-Radiation Pressure

Solar-radiation pressure is about 1 dyne/meter^2. This causes a disturbing acceleration of about $10^{-8} g_e$ on a 45 kilogram satellite with an area of 0.5 meters^2. This disturbance is constant except for two times during the orbit when the satellite enters or leaves the earth's shadow.

e. Atmospheric Drag

Consider again Eq. (1-14) (with some of the subscripts dropped)

$$\ddot{x}_C = f_D + f_C.\qquad (2\text{-}1)$$

For most orbits the dominant contribution to f_D is the atmospheric drag, and it is instructive to compute the drag as a function of time and orbit. The linear-scale-height model of the atmosphere, as proposed by Groves (33), Jacchia (34), and Smelt (35), provides a more accurate representation than the conventional constant-scale-height exponential model, and will be the one which is used in this calculation.

The drag force on a body moving at orbit speed v_0, through a rarified atmosphere of density, ρ, is given by

$$F_{DRAG} = 1/2 \, \rho \, v_0^2 \, C_D \, A_S \qquad (2\text{-}2)$$

where A_S = satellite reference area, and

                         C_D = drag coefficient.

The atmospheric density, ρ, used in these calculations will be obtained by integrating the equation of hydrostatic equilibrium using a pressure-scale-height, H, which varies linearly with altitude.

$$H = H_R + \alpha(h - h_R) \qquad (2\text{-}3)$$

where R stands for "reference" and α is the slope of the scale height line versus h. The result is

$$\rho = \rho_R \left(\frac{H_R}{H}\right)^{\beta} \left(\frac{r_{ES}}{r_R}\right)^2 \qquad (2\text{-}4)$$

where

$$\beta \overset{\triangle}{=} \frac{1 + \alpha}{\alpha} \ .$$

h_R is the reference altitude about which the scale height is linearized, and r_{ES} and r_R are the radii from the center of mass of the earth to the satellite and to the reference altitude respectively. Equation (2-4) is derived by Smelt (35).

Later in this chapter in the evaluation of the fuel-lifetime integrals, it will be most convenient to have r_{ES} and v_O^2 expressed in terms of the eccentric anomaly, E.*

$$r_{ES} = a(1 - e \ c \ E) \tag{2-5}$$

$$v_O^2 = (\omega_O^2 a^2) \frac{1 + e \ c \ E}{1 - e \ c \ E} = \left(\frac{g_e \ R_e^2}{a} \right) \frac{1 + e \ c \ E}{1 - e \ c \ E} \ . \tag{2-6}$$

If we define the normalized drag force, D_n, as the drag divided by the drag at the reference altitude (except for the factor $R_e^2 a / r_R^3$), then substituting Eqs. (2-3) through (2-6) into Eq. (2-2) yields

$$D_n = \frac{F_{DRAG}}{r_R A_S \rho_R g_e \left(\dfrac{C_D}{2} \right)} = \left(\frac{R_e^2 a}{r_R^3} \right) \frac{1 - e^2 \ c^2 \ E}{\left[1 + \dfrac{\alpha(a - r_R - ae \ c \ E)}{H_R} \right]^{\beta}} \ . \tag{2-7}$$

Equation (2-7) is plotted in Fig. 2-1 using constants interpolated from the 1962 ARDC Model Atmosphere (42). The following values for the constants were assumed:

$$h_R = 400 \text{ km} = 250 \text{ sm}$$

$$H_R = 72 \text{ km} = 45 \text{ sm}$$

---

*See Ref. (29) for a definition and discussion of eccentric anomaly.

$$R_e = 6380 \text{ km} = 3960 \text{ sm} \qquad (2\text{-}8)$$

$$\alpha = 1/7$$

$$\rho_R = 6.5 \times 10^{-15} \text{gm/cm}^3 \; .$$

As an example, consider a satellite with $C_D = 2$ and $A_S = 0.5 \text{ m}^2 = 5.38 \text{ ft}^2$, then

$$r_R A_S \rho_R g_e \left(\frac{R_e}{r_R} \right)^2 = 2.08 \times 10^{-4} \text{ntns} = 4.68 \times 10^{-5} \text{ lbs}; \quad (2\text{-}9)$$

and if $m_S g_e = 445 \text{ ntns} = 100 \text{ lbs}$, then the nominal drag, $r_R A_S \rho_R g_e (R_e/r_R)^2$, expressed in g_e's is

$$\frac{f_{DRAG,R}}{g_e} = \frac{r_R A_S \rho_R \dfrac{R_e^2}{r_R}}{m_S} = 4.68 \times 10^{-7} \; . \qquad (2\text{-}10)$$

Thus $(R_e/r_R)^2$ times Eq. (2-10) gives the drag acceleration, f_{DRAG}/g_e, in a nominal circular orbit at the reference altitude of 400 km, and Eq. (2-9) or (2-10) may be used in conjunction with Fig. 2-1 to determine the drag forces for other orbits.

From the preceding discussion, it can be seen that the disturbing accelerations fall into five general classes:

1) Negligibly small,

2) Causing small step changes in velocity about once per year (meteorite collisions),

3) Causing small step changes in a constant disturbing acceleration about twice per orbit (solar-radiation pressure),

4) Relatively constant, but possibly not negligible (leaks or outgassing), and

5) Periodic with period $2\pi/\omega_0$ (atmospheric drag).
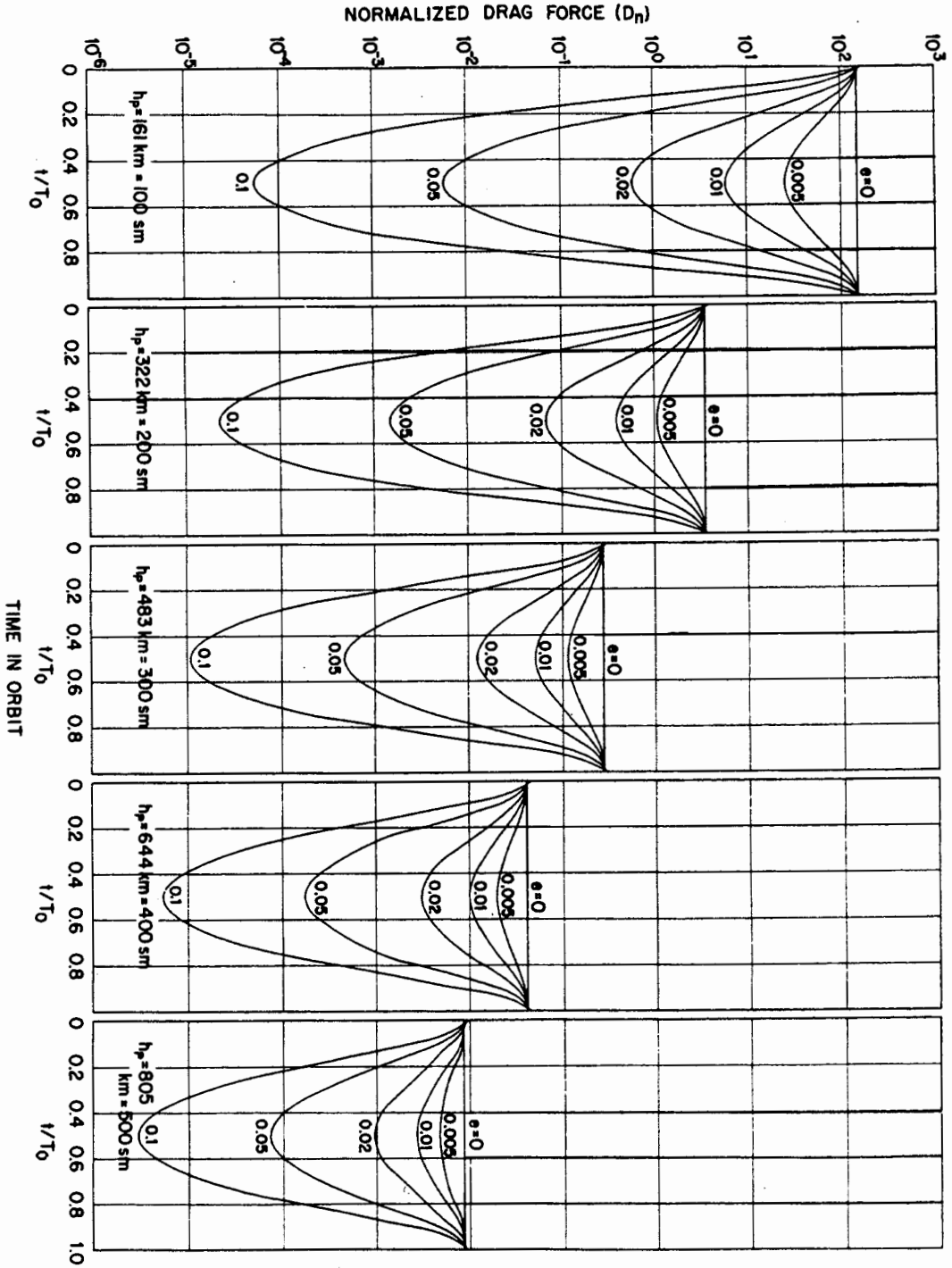
FIG. 2-1.   NORMALIZED DRAG FORCE

Except for orbits with very large eccentricities, all of these disturbances are relatively constant during the period of one control-limit-cycle (cf. Fig. 2-7) and thus the control system will spend most of its life in limit cycles at the origin. The problem of minimum-fuel consumption will be discussed next based on this assumption.

2. CONTACTOR TRANSLATION CONTROL

Since leak-free valves for the control jets are most easily built when they are the full-on or full-off type, it is convenient to use on-off, or contactor, translation control in the satellite. The general problem of using contactor control with linear switching is discussed in a number of basic control-theory texts (see for example Flügge-Lotz (43)) and the $1/s^2$ plant is covered in detail by Graham and McRuer (38). The general state of the art of contactor control is reviewed by Flügge-Lotz in Ref. (44).

a. Justification of the Assumption of Constant Disturbances

The control of the nonrotating drag-free satellite is the same as the classical control problem discussed in the references above if the drag force is considered as a constant over one control-limit-cycle. For most orbits this is a reasonable assumption. If $|f_C + f_D| \gg |f_D|$, then the period of one limit cycle is approximately

$$\left[\frac{8(x_S - x_L)}{f_D}\right]^{\frac{1}{2}} = 40 \text{ seconds for } x_S - x_L = 0.1 \text{ cm and } f_D = 5 \times 10^{-4} \text{cm/sec}^2,$$

where x_S and x_L are defined by Fig. 2-2.[*]

---

[*]See page 64 for the reasons underlying the choice of the typical numbers used in control examples in this chapter.

$$\dot{x}_C$$

$$t = T_C + T_D$$

$$t = 0$$

$$\dot{x}_T$$

$$\frac{1}{2} \dot{x}_C^2 = + (f_C + f_D)(x_C - x_R)$$

$$f_C < -|f_D|$$

$$x_L \qquad x_S \qquad x_R \qquad x_C$$

$$\frac{1}{2} \dot{x}_C^2 = f_D(x_C - x_L)$$

$$\dot{x}_B \qquad t = T_C$$

$$T_C = \frac{\dot{x}_T - \dot{x}_B}{-(f_C + f_D)} \quad \text{AND} \quad T_D = \frac{\dot{x}_T - \dot{x}_B}{f_D}$$
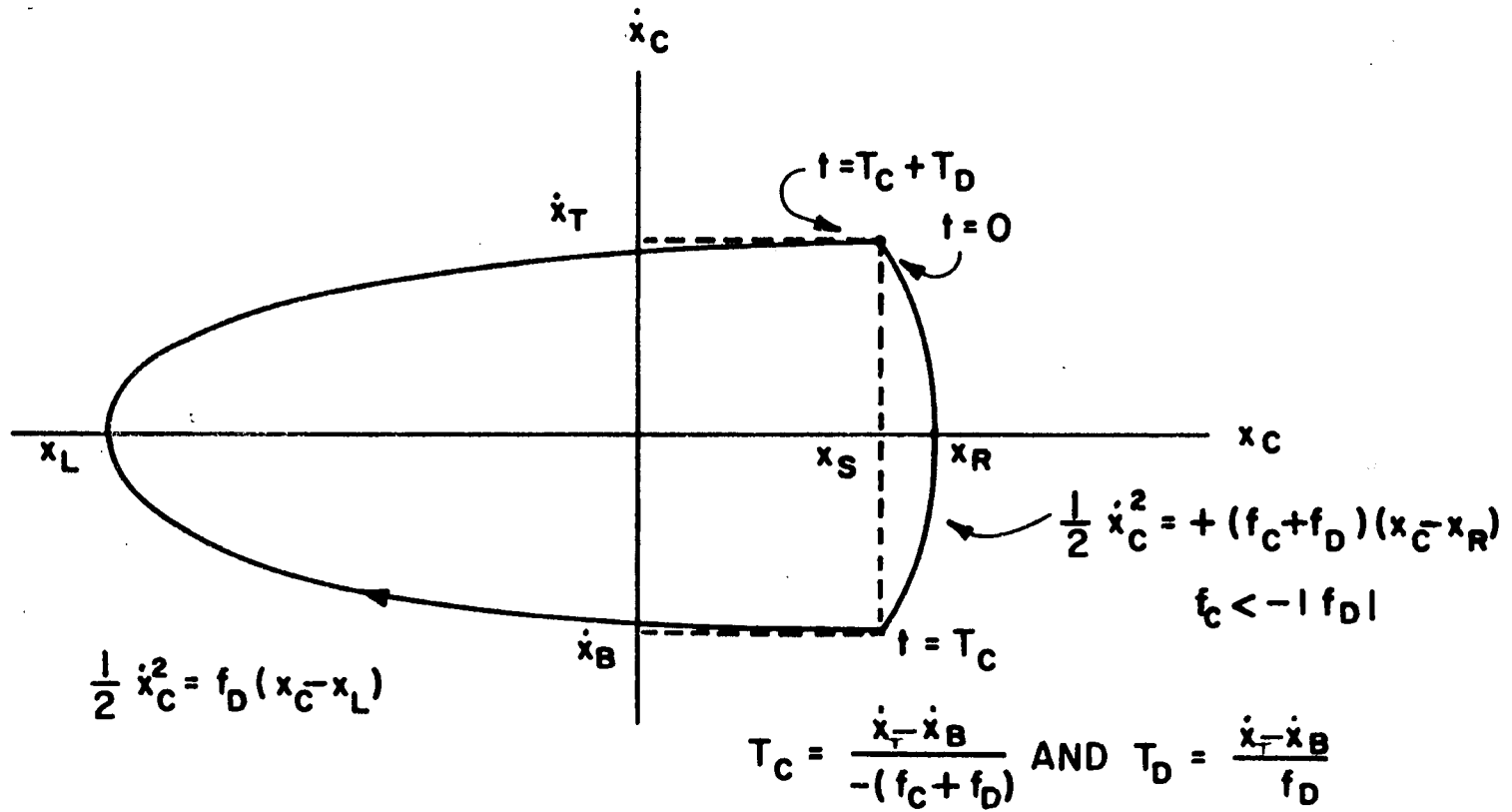
FIG. 2-2. MINIMUM-FUEL CONTROL LIMIT CYCLE

As can be seen from Fig. 2-1, the number can vary from one to several thousand seconds. For simplicity, it will be assumed in the following sections that f_D is approximately constant during this time interval, although this is not true when

$$\left[\frac{8(x_S - x_L)}{f_D} \right]^{\frac{1}{2}} \quad \text{is of the same order as one orbit period.}$$

b. <u>Minimum-Fuel-Consumption Limit Cycles</u>

When "on-off" or contactor control is used there is nearly always the possibility of limit cycles near the origin due to threshold, dead-zone, and delay in the sensors and actuators. The effect of these limit cycles on gas consumption is an important question. Due to the presence of f_D it is possible to find limit cycles which consume no more fuel than that which is required to offset the effect of f_D. Indeed within certain limits the amount of gas consumed is independent of the functional form of f_D.

Since, for a gas jet, the control force, F_C, is given by

$$F_C = - g_e I_{SP} \dot{m}_g \tag{2-11}$$

where

$$I_{SP} = \text{control gas specific impulse, and}$$

$$m_g = \text{mass of control gas,}$$

Eq. (2-1) becomes

$$m_B \ddot{x}_C = - \frac{m_B}{m_S} F_D + \frac{m_B}{m_S} g_e I_{SP} \dot{m}_g$$

or

$$\dot{m}_g = \frac{1}{g_e I_{SP}} \left[F_D + m_S \ddot{x}_C \right] . \tag{2-12}$$

As long as the control always acts such that the sign of $\dot{m}_g$ is the same as the sign of F_D (i.e., if the control always opposes the drag force); then during any period of time when the sign of F_D does not change, $|\dot{m}_g|$ is either always $+\dot{m}_g$ or always $-\dot{m}_g$. For definiteness, assume that $F_D \geq 0$. Then $\dot{m}_g \geq 0$ and $|\dot{m}_g| = \dot{m}_g$, so that the total amount of fuel consumed in time t, $m_g(t)$, is given by

$$m_g(t) \overset{\Delta}{=} \int_0^t |\dot{m}_g|\,d\tau = \int_0^t \dot{m}_g\,d\tau = \frac{1}{g_e I_{SP}}\left\{\int_0^t F_D\,d\tau + m_S[\dot{x}_C(t) - \dot{x}_C(0)]\right\}. \quad (2\text{-}13)$$

Under these circumstances the value of $m_g(t)$ depends only on the right side of Eq. (2-13) and not on the functional form of $\dot{m}_g$. For the case of a limit cycle of period T, the gas consumed, $m_g(T)$, depends only on the integral $\int_0^T F_D\,dt$. Furthermore,

$$\frac{1}{g_e I_{SP}} \int_0^T F_D\,dt$$

is the minimum amount of fuel needed during one period to hold the system in a limit cycle near the origin, and the system must consume this much fuel to balance out the effect of the drag force.

As an example, it is instructive to examine this in detail for the case where F_D is a constant. Figure 2-2 shows the phase-plane plot of one possible limit cycle of period T bounded by a maximum excursion $(x_R - x_L)$. The control jet switches on when $x_C = x_S$ and $\dot{x}_C = \dot{x}_T$ and switches off at $x_C = x_S$ and $\dot{x}_C = \dot{x}_B$.

The gas used per cycle is

$$m_g(T) = \frac{-F_C T_C}{g_e I_{SP}} = \frac{-F_C T}{g_e I_{SP}} \cdot \frac{T_C}{T_C + T_D} = \frac{-F_C T}{g_e I_{SP}} \cdot \frac{1}{1 + \dfrac{T_D}{T_C}}. \quad (2\text{-}14)$$

However, since the time T_C or T_D is given by $(\dot{x}_T - \dot{x}_B)$ divided by the acceleration

$$-T_C(F_C + F_D) = T_D F_D \ ,$$

so that

$$\frac{T_D}{T_C} = - \ \frac{F_C + F_D}{F_D} \tag{2-15}$$

and by substituting Eq. (2-16) into Eq. (2-14), the gas consumed per limit cycle is

$$m_g(T) = \frac{F_D T}{g_e I_{SP}} \ . \tag{2-16}$$

To reiterate, as long as the control force always opposes F_D, the gas consumed does not depend on the shape of the control-force impulse but only on its area, which must be equal to $F_D T$. This very simple but important result makes it possible to compute the total fuel consumption by integrating the drag force over a complete orbit.

$$\frac{m_g}{ORBIT} = \frac{1}{g_e I_{SP}} \int_0^{T_O} F_{DRAG} dt = \frac{T_O}{2\pi g_e I_{SP}} \int_0^{2\pi} F_{DRAG}(1 - e \ c \ E)dE$$

$$\frac{m_g}{ORBIT} = r_R A_S \rho_R \left(\frac{T_O}{I_{SP}}\right)\left(\frac{C_D}{2}\right)\left(\frac{aR_e^2}{r_R^3}\right)\frac{1}{2\pi} \int_0^{2\pi} \frac{(1-ecE-e^2c^2E+e^3c^3E)dE}{\left[1 + \frac{\alpha(a-r_R-ae \ c \ E)}{H_R}\right]^\beta} \tag{2-17}$$

since from Kepler's equation $\dot{E} = 2\pi/[T_O(1 - e \ c \ E)]$.

Surprisingly, this integral is fairly easy to evaluate by contour integration. Figure 2-3 shows a series of fuel-lifetime plots obtained by evaluating this integral. The next section will show how to evaluate the integral in Eq. (2-17).

B. THE FUEL LIFETIME OF A DRAG-FREE SATELLITE

Bruce (9) has computed the fuel expenditure necessary to sustain a satellite in a drag-free circular orbit. He compares continuous correction with a series of discrete corrections in which the orbit is allowed to decay for a fixed period of time and then is restored with a Hohman transfer. He concludes that continuous correction requires less fuel than the series of discrete corrections. This result also follows from the conclusion of the previous section, since the control force acts in the same direction as the drag force during the second corrective impulse of a Hohman transfer, and since the discrete application allows the orbit to decay into the denser atmosphere.

In order to evaluate Eq. (2-17), which gives the fuel consumption for an arbitrary elliptic orbit using a linear pressure-scale-height model of the atmosphere, define

$$y \triangleq \frac{\alpha a e}{H_R + \alpha(a - r_R)} \qquad (2\text{-}18)$$

$$= \frac{\alpha\left(\dfrac{r_P}{1 - e}\right)e}{H_R + \alpha\left[\dfrac{r_P}{1-e} - r_R\right]} \qquad (2\text{-}19)$$

$$= \frac{e}{1 + (1 - e)\left[\dfrac{(\beta - 1)H_R - r_R}{r_P}\right]} \qquad (2\text{-}20)$$
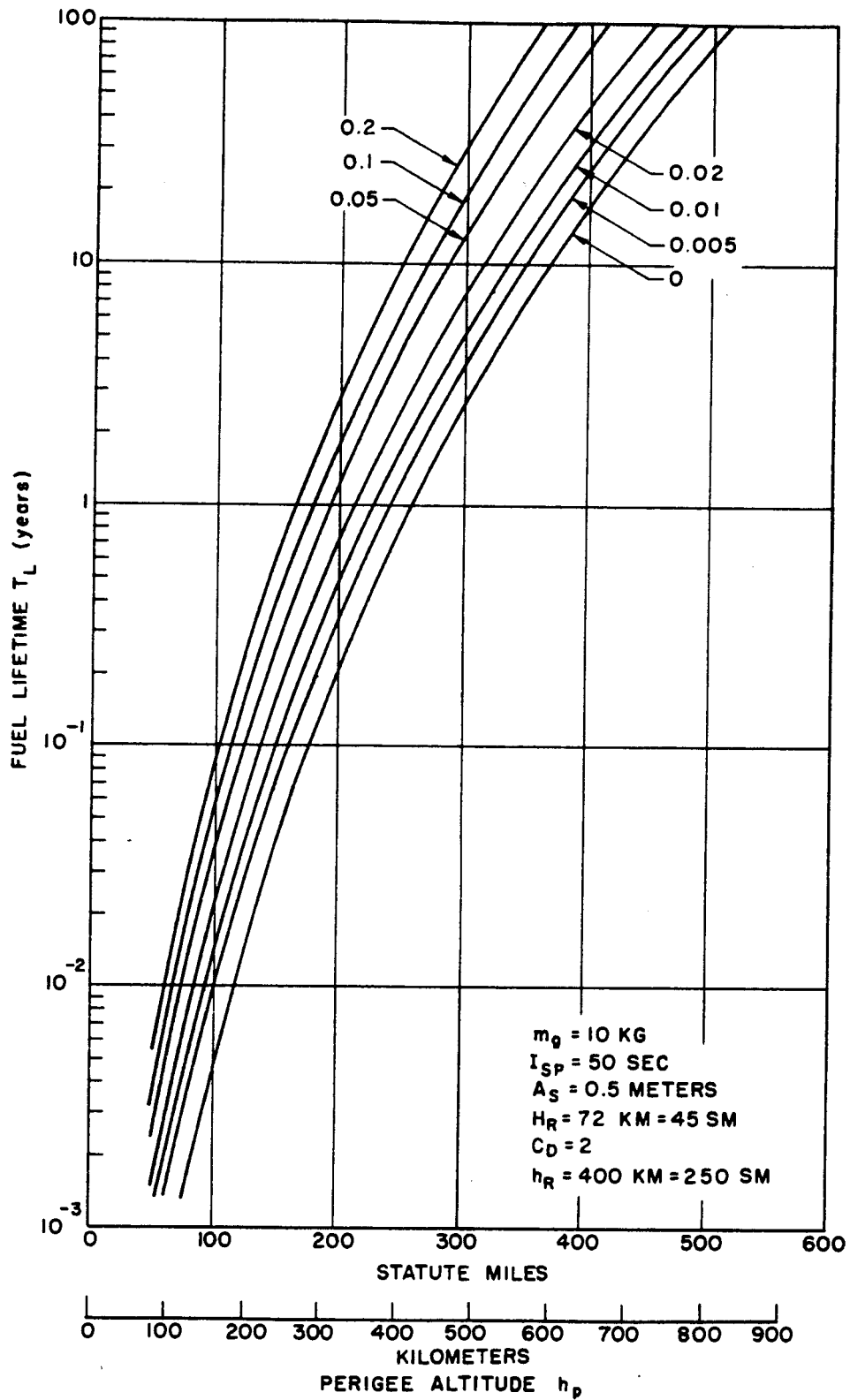
FIG. 2-3. FUEL LIFETIME OF A DRAG-FREE SATELLITE

A typical plot of y versus e is shown in Fig. 2-4.
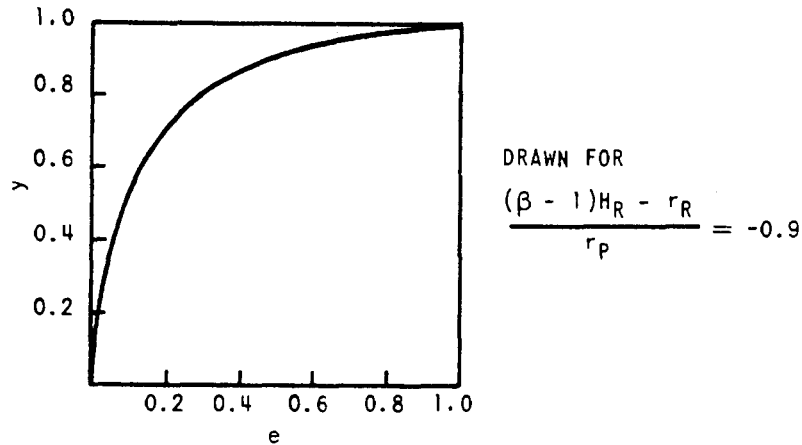
FIG. 2-4. TYPICAL PLOT OF y VERSUS e.

When Eq. (2-20) is substituted into Eq. (2-17), the fuel consumed per orbit becomes

$$\frac{m_g}{\text{ORBIT}} = r_R A_S \rho_R \left(\frac{T_O}{I_{SP}} \right) \left(\frac{C_D}{2} \right) \left(\frac{r_P R_e^2}{r_R^3} \right) \frac{\frac{1}{2\pi} \int_0^{2\pi} \frac{(1-ecE-e^2c^2E+e^3c^3E)dE}{(1-ycE)^\beta}}{\left[1 + \alpha \frac{r_P - r_R + er_R}{H_R(1-e)} \right]^\beta (1-e)}$$

(2-21)

Since the average rate of fuel consumption is given by

$$\left\langle \dot{m}_g \right\rangle_{av} \triangleq \frac{m_g/\text{ORBIT}}{T_O} ,$$

(2-22)

the fuel lifetime can be readily evaluated since

$$T_L = \frac{m_g}{\left\langle \dot{m}_g \right\rangle_{av}} \, . \qquad (2\text{-}23)$$

Now let

$$I(y,e) \triangleq \frac{1}{2\pi} \int_0^{2\pi} \frac{(1 - ecE - e^2 c^2 E + e^3 c^3 E)}{(1 - ycE)^\beta} \, dE \qquad (2\text{-}24)$$

$$\triangleq I_o(y) - eI_1(y) - e^2 I_2(y) + e^3 I_3(y) \qquad (2\text{-}25)$$

where

$$I_o(y) \triangleq \frac{1}{2\pi} \int_0^{2\pi} \frac{dE}{(1 - ycE)^\beta} \qquad (2\text{-}26)$$

$$I_1(y) \triangleq \frac{1}{2\pi} \int_0^{2\pi} \frac{cEdE}{(1 - ycE)^\beta} \qquad (2\text{-}27)$$

$$I_2(y) \triangleq \frac{1}{2\pi} \int_0^{2\pi} \frac{c^2 E \, dE}{(1 - ycE)^\beta} \qquad (2\text{-}28)$$

$$I_3(y) \triangleq \frac{1}{2\pi} \int_0^{2\pi} \frac{c^3 EdE}{(1 - ycE)^\beta} \qquad (2\text{-}29)$$

The integrals, I_n, may be evaluated numerically; however, if β is an integer, it is not difficult to compute them by contour integration. The restriction of β to integer values is not of serious consequence, since the value of α varies with the choice of h_R due to the fact that H_R is not constant versus altitude.

Thus, restricting β to integer values merely restricts the nominal point about which the density model is linearized to a series of discrete altitudes.

It is mathematically more convenient to evaluate the integral

$$J_n \triangleq \frac{1}{2\pi} \int_0^{2\pi} \frac{cnE\ dE}{(1 - ycE)^\beta} \tag{2-30}$$

and then to compute I_n in terms of J_n from the trigonometric multiple angle identities for the cosine function.

Let $z \triangleq e^{jE}$ so that $cE = \frac{z^2 + 1}{2z}$; \hfill (2-31)

then (since the integrals containing the sine terms in the numerator are zero)

$$J_n = \frac{(-2/y)^\beta}{2\pi j} \oint_{|z|=1} \frac{z^{n+\beta-1}dz}{(z-a)^\beta (z-b)^\beta} \tag{2-32}$$

where

$$b = \frac{1}{y} + \sqrt{\frac{1}{y^2} - 1} \tag{2-33}$$

$$a = \frac{1}{y} - \sqrt{\frac{1}{y^2} - 1}\ . \tag{2-34}$$

For $0 \leq y < 1$ Eqs. (2-33) and (2-34) yield $0 \leq a < 1$ and $b > 1$ so that

$$J_n = (-2/y)^\beta \ \text{Residue} \ \left. \frac{z^{n+\beta-1}}{(z-a)^\beta (z-b)^\beta} \right|_{z=a} \tag{2-35}$$

$$J_n = (-2/y)^\beta \ \underset{z \to a}{\text{Lim}} \ \frac{1}{(\beta-1)!} \ \frac{d^{\beta-1}}{dz^{\beta-1}} \left[\frac{z^{n+\beta-1}}{(z-b)^\beta} \right] \tag{2-36}$$

$$J_n = (-2/y)^\beta \lim_{z \to a} \frac{z^n}{(z-b)^\beta (\beta-1)!} \sum_{i=0}^{\beta-1} C_{n+i}^{n+\beta-1} C_i^{\beta-1+i} \left(\frac{z}{b-z}\right)^i \qquad (2\text{-}37)$$

$$= \frac{\left(1 - \sqrt{1-y^2}\right)^n}{y^n \left(\sqrt{1-y^2}\right)^\beta} \sum_{i=0}^{\beta-1} C_{n+i}^{n+\beta-1} C_i^{\beta-1+i} \left(\frac{\frac{1}{\sqrt{1-y^2}} - 1}{2}\right)^i \qquad (2\text{-}38)$$

where

$$C_k^n \triangleq \frac{n!}{k!(n-k)!} \quad . \qquad (2\text{-}39)$$

The values of the integrals $I_n(y,\beta)$ are tabulated in Table 2-1 and a plot of $I_o(y,\beta)$ is shown in Fig. 2-5.

From Eqs. (2-21), (2-22), and (2-23),

$$T_L = I_{SP} \left(\frac{m_g}{r_R A_S \rho_R}\right) \left(\frac{2}{C_D}\right) \left(\frac{r_R^3}{r_P R_e^2}\right) \frac{(1-e)\left[1 + \alpha \dfrac{r_P - r_R + er_R}{H_R(1-e)}\right]^\beta}{I(y,e)} \quad . \qquad (2\text{-}40)$$

It is convenient to express T_L in terms of the lifetime of a circular orbit of radius r_P. For a circular orbit

$$T_{LC} = I_{SP} \left(\frac{m_g}{r_R A_S \rho_R}\right) \left(\frac{2}{C_D}\right) \left(\frac{r_R^3}{r_P R_e^2}\right) \left[1 + \alpha \frac{r_P - r_R}{H_R}\right]^\beta \quad , \qquad (2\text{-}41)$$

so that

$$\frac{T_L}{T_{LC}} = \frac{(1-e)\left[1 + \alpha \dfrac{r_P - r_R + er_R}{H_R(1-e)}\right]^\beta}{\left[1 + \dfrac{\alpha(r_P - r_R)}{H_R}\right]^\beta I(y,e)} \quad . \qquad (2\text{-}42)$$

TABLE 2-1

TABULATED VALUES OF THE FUEL-CONSUMPTION INTEGRALS (EQS. (2-26) TO (2-29)

I0(Y,BETA)

Y BETA=	4	5	6	7	8	9	10
0.0000000E+00	1.000000E+00	1.000000E+00	1.000000E+00	1.000000E+00	1.000000E+00	1.000000E+00	1.000000E+00
5.0000000E-02	1.012582E+00	1.018915E+00	1.026548E+00	1.035497E+00	1.045782E+00	1.057425E+00	1.070450E+00
1.0000000E-01	1.051335E+00	1.077692E+00	1.109873E+00	1.148172E+00	1.192929E+00	1.244537E+00	1.303445E+00
1.5000000E-01	1.119456E+00	1.182823E+00	1.261909E+00	1.358379E+00	1.474237E+00	1.611880E+00	1.774148E+00
2.0000000E-01	1.222003E+00	1.346574E+00	1.505823E+00	1.704802E+00	1.957365E+00	2.267300E+00	2.648747E+00
2.5000000E-01	1.370940E+00	1.589638E+00	1.882230E+00	2.267805E+00	2.771513E+00	3.428408E+00	4.275772E+00
3.0000000E-01	1.576087E+00	1.946054E+00	2.461306E+00	3.176573E+00	4.164462E+00	5.526224E+00	7.402945E+00
3.5000000E-01	1.870230E+00	2.472286E+00	3.366303E+00	4.685262E+00	6.627690E+00	9.489817E+00	1.371388E+01
4.0000000E-01	2.282676E+00	3.264471E+00	4.821319E+00	7.288158E+00	1.118472E+01	1.737822E+01	2.724233E+01
4.5000000E-01	2.876306E+00	4.492598E+00	7.252705E+00	1.197843E+01	2.009911E+01	3.411250E+01	5.839352E+01
5.0000000E-01	3.763468E+00	6.472025E+00	1.151849E+01	2.096518E+01	3.874979E+01	7.241509E+01	1.364531E+02
5.5000000E-01	5.129618E+00	9.823333E+00	1.946710E+01	3.943166E+01	8.106685E+01	1.684554E+02	3.528805E+02
6.0000000E-01	7.343292E+00	1.585931E+01	3.542516E+01	8.082825E+01	1.871018E+02	4.376425E+02	1.031790E+03
6.5000000E-01	1.116230E+01	2.761081E+01	7.062044E+01	1.843305E+02	4.879845E+02	1.305065E+03	3.517503E+03
7.0000000E-01	1.831467E+01	5.298037E+01	1.582880E+02	4.824269E+02	1.490713E+03	4.652864E+03	1.463464E+04
7.5000000E-01	3.326732E+01	1.158004E+02	4.155676E+02	1.520854E+03	5.641697E+03	2.113699E+04	7.979563E+04
8.0000000E-01	7.001600E+01	3.049903E+02	1.369361E+03	6.267600E+03	2.907247E+04	1.361854E+05	6.427690E+05
8.5000000E-01	1.651080E+02	1.076654E+03	6.450055E+03	3.937976E+04	2.436225E+05	1.521928E+06	9.579096E+06
9.0000000E-01	7.408600E+02	6.471258E+03	5.818725E+04	5.330732E+05	4.947991E+06	4.637391E+07	4.378787E+08
9.5000000E-01	8.132677E+03	1.422138E+05	2.558755E+06	4.689784E+07	8.707976E+08	1.632523E+10	3.083334E+11

I1(Y,BETA)

Y BETA=	4	5	6	7	8	9	10
0.0000000E+00	0.000000E+00	0.000000E+00	0.000000E+00	0.000000E+00	0.000000E+00	0.000000E+00	0.000000E+00
5.0000000E-02	1.009430E-01	1.266530E-01	1.526490E-01	1.789830E-01	2.057031E-01	2.328014E-01	2.605105E-01
1.0000000E-01	2.076743E-01	2.635280E-01	3.218097E-01	3.829919E-01	4.475717E-01	5.160790E-01	5.898814E-01
1.5000000E-01	3.208996E-01	4.224481E-01	5.272449E-01	6.431276E-01	7.723877E-01	9.176212E-01	1.081785E+00
2.0000000E-01	4.600495E-01	6.188518E-01	7.962460E-01	1.004899E+00	1.252815E+00	1.549673E+00	1.907237E+00
2.5000000E-01	6.305081E-01	8.747906E-01	1.170391E+00	1.542278E+00	2.014830E+00	2.619579E+00	3.397457E+00
3.0000000E-01	8.534335E-01	1.273691E+00	1.717505E+00	2.364226E+00	3.292961E+00	4.539206E+00	6.255735E+00
3.5000000E-01	1.139613E+00	1.720160E+00	2.554334E+00	3.768454E+00	5.549795E+00	8.177507E+00	1.208875E+01
4.0000000E-01	1.531607E+00	2.454490E+00	3.892120E+00	6.157096E+00	9.751398E+00	1.548376E+01	2.466028E+01
4.5000000E-01	2.087530E+00	3.587317E+00	6.133571E+00	1.050160E+01	1.804597E+01	3.114065E+01	5.395784E+01
5.0000000E-01	2.906135E+00	5.417114E+00	1.009294E+01	1.869337E+01	3.556921E+01	6.733060E+01	1.280760E+02
5.5000000E-01	4.174926E+00	8.534028E+00	1.753413E+01	3.629919E+01	7.570036E+01	1.588863E+02	3.353183E+02
6.0000000E-01	6.237030E+00	1.419336E+01	3.260979E+01	7.567178E+01	1.771226E+02	4.175678E+02	9.902451E+02
6.5000000E-01	9.820175E+00	2.531710E+01	6.615097E+01	1.749508E+02	4.671478E+02	1.257046E+03	3.403752E+03
7.0000000E-01	1.656895E+01	4.953357E+01	1.504285E+02	4.830576E+02	1.440805E+03	4.517360E+03	1.425968E+04
7.5000000E-01	3.089950E+01	1.100174E+02	3.996890E+02	1.473715E+03	5.494457E+03	2.066039E+04	7.821152E+04
8.0000000E-01	6.630087E+01	2.937179E+02	1.330463E+03	6.122799E+03	2.850609E+04	1.338911E+05	6.332296E+05
8.5000000E-01	1.787955E+02	1.048677E+03	6.321640E+03	3.874085E+04	2.402856E+05	1.503889E+06	9.479022E+06
9.0000000E-01	7.239690E+02	6.367109E+03	5.746221E+04	5.276510E+05	4.905464E+06	4.602860E+07	4.350053E+08
9.5000000E-01	8.046278E+03	1.411379E+05	2.543720E+06	4.667272E+07	8.672630E+08	1.626782E+10	3.073770E+11

I2(Y,BETA)

Y BETA=	4	5	6	7	8	9	10
0.0000000E+00	5.000000E-01	5.000000E-01	5.000000E-01	5.000000E-01	5.000000E-01	5.000000E-01	5.000000E-01
5.0000000E-02	5.094437E-01	5.142001E-01	5.199350E-01	5.266441E-01	5.344019E-01	5.431673E-01	5.529806E-01
1.0000000E-01	5.386171E-01	5.584962E-01	5.828171E-01	6.118227E-01	6.457980E-01	6.850726E-01	7.300243E-01
1.5000000E-01	5.901845E-01	6.383234E-01	6.984453E-01	7.725509E-01	8.617343E-01	9.602235E-01	1.094428E+00
2.0000000E-01	6.690810E-01	7.640116E-01	8.869709E-01	1.043264E+00	1.239561E+00	1.484291E+00	1.787818E+00
2.5000000E-01	7.833946E-01	9.531300E-01	1.182404E+00	1.487544E+00	1.890212E+00	2.418992E+00	3.111515E+00
3.0000000E-01	9.459410E-01	1.234860E+00	1.645378E+00	2.222404E+00	3.029116E+00	4.154157E+00	5.721756E+00
3.5000000E-01	1.177040E+00	1.658134E+00	2.383355E+00	3.468912E+00	5.089546E+00	7.507748E+00	1.111785E+01
4.0000000E-01	1.509511E+00	2.307220E+00	3.590748E+00	5.662441E+00	8.985754E+00	1.433091E+01	2.294129E+01
4.5000000E-01	1.997960E+00	3.332859E+00	5.658342E+00	9.706733E+00	1.676527E+01	2.909973E+01	5.070843E+01
5.0000000E-01	2.737068E+00	5.017958E+00	9.351649E+00	1.760087E+01	3.335168E+01	6.352279E+01	1.214907E+02
5.5000000E-01	3.899039E+00	7.925639E+00	1.636382E+01	3.411828E+01	7.163849E+01	1.512508E+02	3.207818E+02
6.0000000E-01	5.817413E+00	1.326054E+01	3.069406E+01	7.176997E+01	1.690847E+02	4.007419E+02	9.544622E+02
6.5000000E-01	9.189467E+00	2.384142E+01	6.283057E+01	1.673751E+02	4.495338E+02	1.215229E+03	3.302624E+03
7.0000000E-01	1.562308E+01	4.706374E+01	1.441361E+02	4.466125E+02	1.396211E+03	4.395649E+03	1.391760E+04
7.5000000E-01	2.933796E+01	1.055039E+02	3.862290E+02	1.432034E+03	5.360989E+03	2.022125E+04	7.673463E+04
8.0000000E-01	6.356596E+01	2.842713E+02	1.295931E+03	5.990420E+03	2.797912E+04	1.317313E+05	6.241730E+05
8.5000000E-01	1.727023E+02	1.074214E+03	6.203260E+03	3.814024E+04	2.371115E+05	1.486592E+06	9.362509E+06
9.0000000E-01	7.090849E+02	6.770156E+03	5.677233E+04	5.224320E+05	4.864237E+06	4.569260E+07	4.321962E+08
9.5000000E-01	7.964431E+03	1.400964E+05	2.529042E+06	4.645157E+07	8.637792E+08	1.621112E+10	3.064307E+11

I3(Y,BETA)

Y BETA=	4	5	6	7	8	9	10
0.0000000E+00	0.000000E+00	0.000000E+00	0.000000E+00	0.000000E+00	0.000000E+00	0.000000E+00	0.000000E+00
5.0000000E-02	7.578606E-02	9.512802E-02	1.147092E-01	1.345711E-01	1.547558E-01	1.753065E-01	1.962670E-01
1.0000000E-01	1.564061E-01	1.987903E-01	2.432090E-01	2.900567E-01	3.397527E-01	3.927456E-01	4.495171E-01
1.5000000E-01	2.473090E-01	3.209256E-01	4.021463E-01	4.927041E-01	5.945561E-01	7.099280E-01	8.413654E-01
2.0000000E-01	3.553051E-01	4.746533E-01	6.147962E-01	7.814663E-01	9.815822E-01	1.223551E+00	1.517636E+00
2.5000000E-01	4.896216E-01	6.789419E-01	9.170939E-01	1.220564E+00	1.610668E+00	2.115124E+00	2.770090E+00
3.0000000E-01	6.635498E-01	9.630621E-01	1.368395E+00	1.928420E+00	2.689040E+00	3.750137E+00	5.225331E+00
3.5000000E-01	8.971970E-01	1.374553E+00	2.072059E+00	3.101594E+00	4.630361E+00	6.909149E+00	1.031457E+01
4.0000000E-01	1.222336E+00	1.994273E+00	3.217135E+00	5.170917E+00	8.308262E+00	1.336289E+01	2.152594E+01
4.5000000E-01	1.691384E+00	2.966398E+00	5.167740E+00	8.996423E+00	1.568564E+01	2.740990E+01	4.801044E+01
5.0000000E-01	2.394934E+00	4.561780E+00	8.667382E+00	1.649844E+01	3.150162E+01	6.034221E+01	1.159359E+02
5.5000000E-01	3.496108E+00	7.321092E+00	1.534215E+01	3.228084E+01	6.821856E+01	1.447496E+02	3.082383E+02
6.0000000E-01	5.321503E+00	1.240577E+01	2.905587E+01	6.845985E+01	1.621913E+02	3.860954E+02	9.228670E+02
6.5000000E-01	8.537035E+00	2.254147E+01	5.998330E+01	1.608378E+02	4.340903E+02	1.177992E+03	3.211377E+03
7.0000000E-01	1.470468E+01	4.491526E+01	1.386748E+02	4.321091E+02	1.356569E+03	4.284911E+03	1.360278E+04
7.5000000E-01	2.792750E+01	1.015545E+02	3.743010E+02	1.394406E+03	5.238607E+03	1.981368E+04	7.535144E+04
8.0000000E-01	6.115084E+01	2.758567E+02	1.264575E+03	5.868111E+03	2.748587E+04	1.296902E+05	6.155522E+05
8.5000000E-01	1.676187E+02	1.001684E+03	6.092995E+03	3.757292E+04	2.340838E+05	1.469977E+06	9.289315E+06
9.0000000E-01	6.953715E+02	6.178968E+03	5.611353E+04	5.173997E+05	4.824227E+06	4.536485E+07	4.294484E+08
9.5000000E-01	7.886256E+03	1.390863E+05	2.514479E+06	4.623424E+07	8.603449E+08	1.615509E+10	3.054943E+11

FIG. 2-5.   PLOT OF I_o (y,β) VERSUS y FOR FIXED β

Figure 2-3 is a plot of Eq. (2-42) for a typical satellite where I_{SP} = 50 sec and m_g = 10 kg.

C. <u>CONTROL SYSTEM MECHANIZATION</u>

1. CONTROL WITH LINEAR SWITCHING, THRESHOLD, AND DEADBAND

In the previous sections it was shown that any control, which does not allow the proof-mass to touch the cavity walls and which always acts such as to oppose the drag, will use the minimum amount of fuel; and this minimum was computed using a linear pressure-scale-height model of the atmosphere. The question arises how a control which has or approximates these properties might be mechanized. This section will consider one possible realization using linear switching, threshold, and deadband.*

Figure 2-6 shows typical switching surfaces in the phase plane with f_D always acting to the right. The finite width of the switching lines is due to contactor threshold which is built into the system as a design parameter, δ. The loop time delay, T_L, which is due primarily to the time required to operate the gas valves, is of the order of 5 to 25 milliseconds and is negligible for most limit cycles. When the time delay is not negligible, its effect is to alter the vertical width of the switching line an amount $f_C T_L$ and to alter its slope by T_L/k^2. Thus, time delay limits the system only in that it establishes a minimum width of the switching line.

---

*For other approaches see Gaylord and Keller (24) and Dahl, Aldrich, and Herman (25).
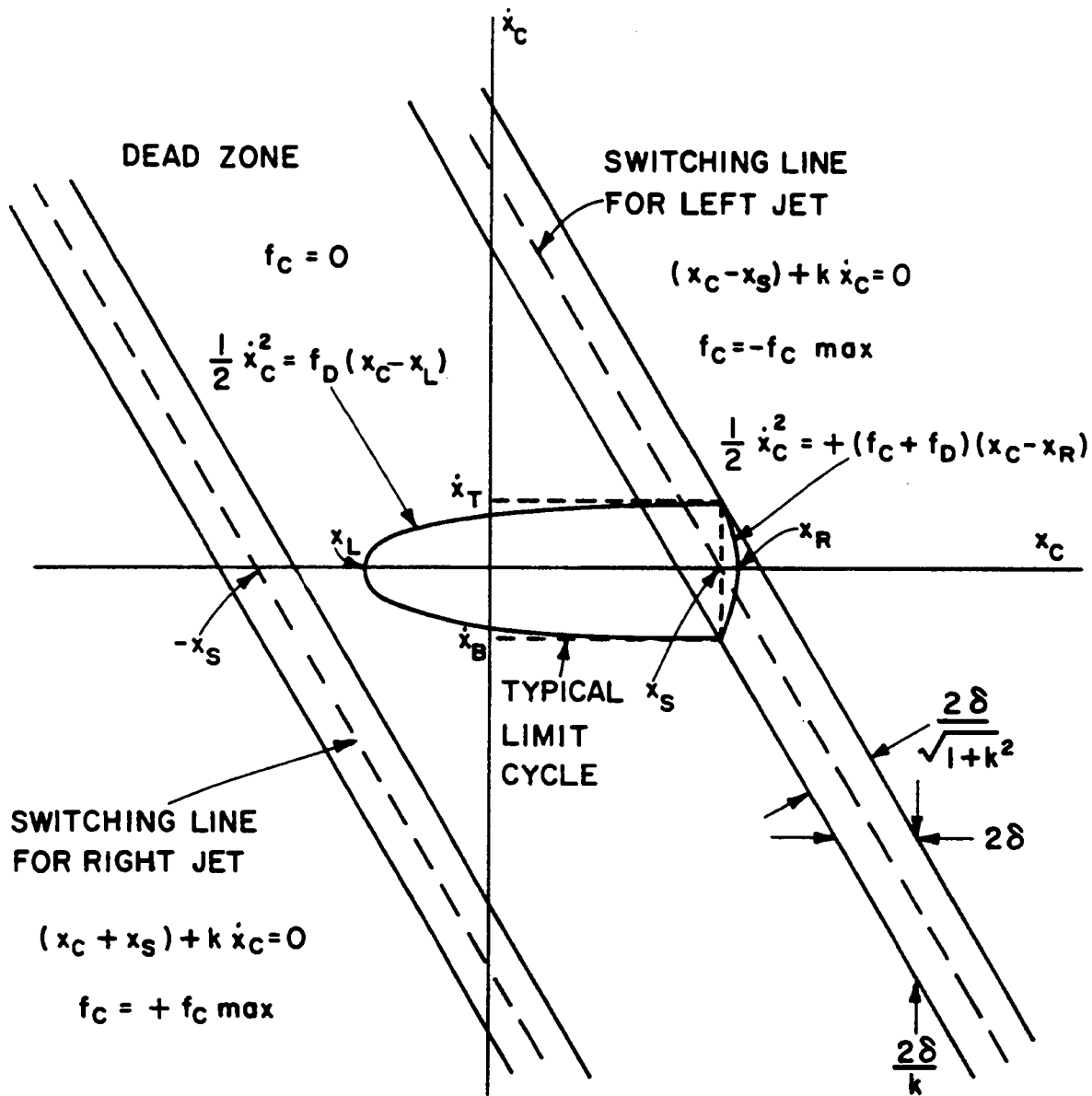
FIG. 2-6. ON-OFF CONTROL SWITCHING LINES

Within the figure:

DEAD ZONE

$f_C = 0$

$\frac{1}{2} \dot{x}_C^2 = f_D (x_C - x_L)$

SWITCHING LINE FOR LEFT JET

$(x_C - x_S) + k \dot{x}_C = 0$

$f_C = -f_C \text{ max}$

$\frac{1}{2} \dot{x}_C^2 = +(f_C + f_D)(x_C - x_R)$

$\dot{x}_C$

x_L

$\dot{x}_T$

x_R

x_C

$-x_S$

$\dot{x}_B$

TYPICAL LIMIT CYCLE

x_S

$\frac{2\delta}{\sqrt{1+k^2}}$

2δ

SWITCHING LINE FOR RIGHT JET

$(x_C + x_S) + k \dot{x}_C = 0$

$f_C = + f_C \text{ max}$

$\frac{2\delta}{k}$

Table 2-2 and Fig. 2-7 show the size and period for typical limit cycles versus f for three perigee altitudes. It is assumed in all calculations that f_D and $f_C + f_D$ are constant over one limit cycle. The minimum value of $x_S - x_L$ occurs at perigee and is chosen as 0.01 cm in this example.* The values for the drag acceleration at

---

*Subscripts of x and ẋ refer to quantities which are defined by labels in Fig. 2-6.

TABLE 2-2

TYPICAL LIMIT CYCLES FOR $1/s^2$ PLANT WITH DRAG

(Cf. Figs. 2-6, 2-7, and 2-8)

h_P	f_D** g_e's	$\dot{x}_S - \dot{x}_L$ cm	$\dot{x}_T - \dot{x}_B$* cm/sec	T_D sec	$\lvert f_C + f_D \rvert$** g_e's	$x_R - x_S$	T_C msec	T_C/T_D
161 km	0.73×10^{-4}	10^{-2}	0.76×10^{-1}	1.1	0.93×10^{-3}	0.78×10^{-3}	82	7.8×10^{-2}
or	0.73×10^{-5}	10^{-1}	0.76×10^{-1}	11	0.99×10^{-3}	0.74×10^{-3}	77	7.3×10^{-3}
100 sm	0.73×10^{-6}	1	0.76×10^{-1}	110	1.00×10^{-3}	0.73×10^{-3}	76	7.2×10^{-4}
	0	10^{-1}	0.76×10^{-1}	5.3	1.00×10^{-3}	0.73×10^{-3}	$150^{\dagger}$	2.8×10^{-3}
322 km	1.7×10^{-6}	10^{-2}	1.2×10^{-2}	7	0.83×10^{-5}	2.2×10^{-3}	1500	2.2×10^{-1}
or	1.7×10^{-7}	10^{-1}	1.2×10^{-2}	70	0.98×10^{-5}	1.9×10^{-3}	1200	1.7×10^{-2}
200 sm	1.7×10^{-8}	1	1.2×10^{-2}	700	1.00×10^{-5}	1.8×10^{-3}	1200	1.7×10^{-3}
	0	10^{-1}	1.2×10^{-2}	34	1.00×10^{-5}	1.8×10^{-3}	$2300^{\dagger}$	7.8×10^{-2}
483 km	1.4×10^{-7}	10^{-2}	3.3×10^{-3}	24	1.00×10^{-5}	1.3×10^{-4}	330	1.4×10^{-2}
or	1.4×10^{-8}	10^{-1}	3.3×10^{-3}	240	1.00×10^{-5}	1.3×10^{-4}	330	1.4×10^{-3}
300 sm	1.4×10^{-9}	1	3.3×10^{-3}	2400	1.00×10^{-5}	1.3×10^{-4}	330	1.4×10^{-4}
	0	10^{-1}	3.3×10^{-3}	120	1.00×10^{-5}	1.3×10^{-4}	$660^{\dagger}$	5.5×10^{-3}

* $\dot{x}_T - \dot{x}_B$ is chosen to make $x_S - x_L = 10^{-2}$ cm at perigee and is constant over any given orbit.

** For a given orbit the drag at perigee determines the maximum value of f_D and hence the required value of f_C. Limit cycles are also shown for smaller values of f_D which occur later in the orbit without giving the times or altitudes at which they occur.

†When f_D is zero, the control acts at both ends of the limit cycle and hence, T_C is longer.

perigee were obtained from Eq. (2-10) and Fig. 2-1, and they determine the required control acceleration and the size of $\dot{x}_T - \dot{x}_B$ and, hence, the value of δ since $\delta = (1/2)k(\dot{x}_T - \dot{x}_B)$. A value of f_D, which is 10^{-2} of that at perigee, would bang against the left switching line; but the values corresponding to the full unsaturated limit cycle are plotted for comparison.
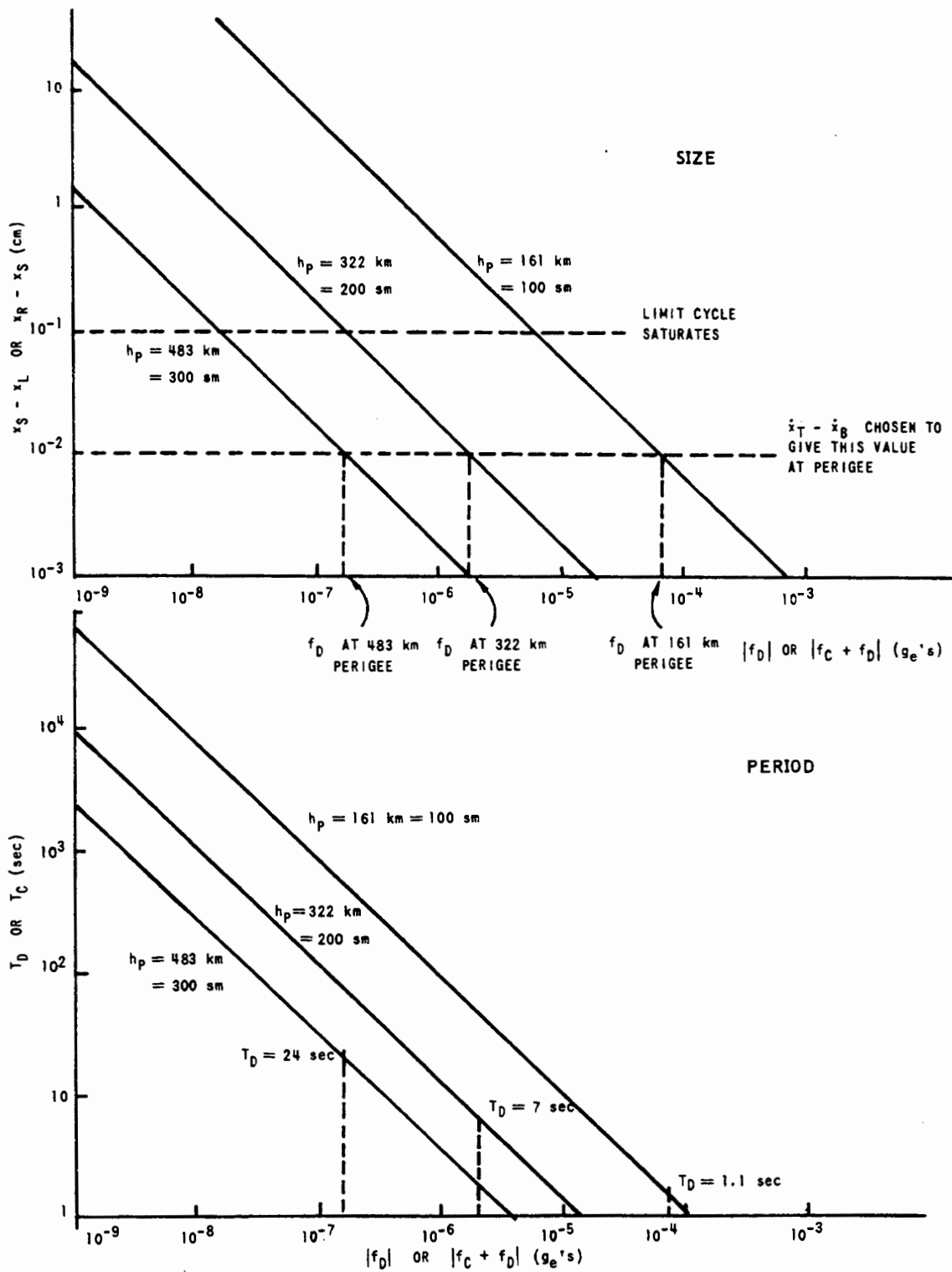
FIG. 2-7.   LIMIT CYCLE SIZE AND PERIOD VERSUS f
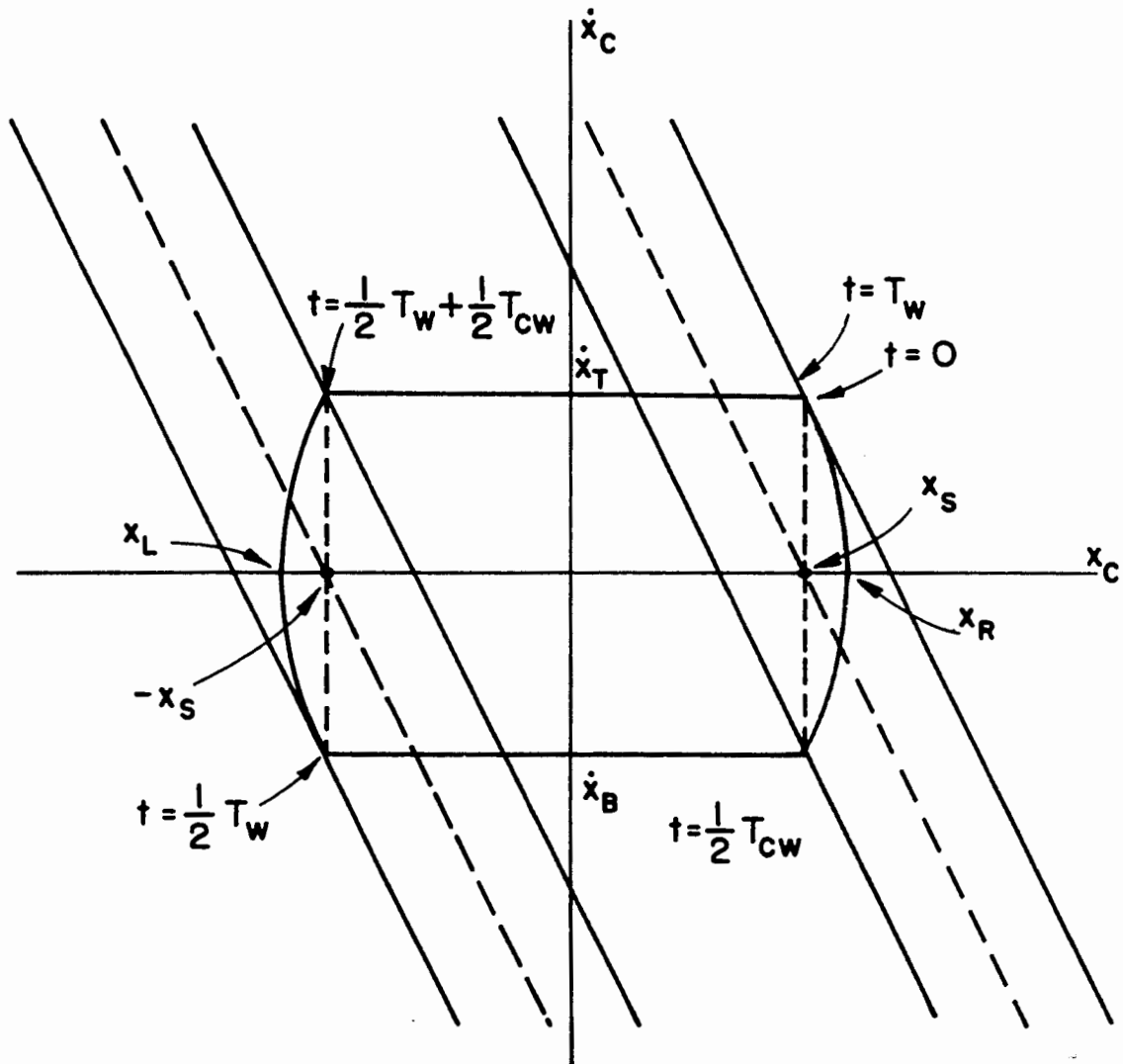
FIG. 2-8.   SATURATED LIMIT CYCLE (TYPICAL NUMERICAL VALUES ARE SHOWN IN
THE LAST LINE OF EACH BLOCK IN TABLE 2-2)

Table 2-2 also shows the values for saturated limit cycles
where f_D is taken as zero. This limit cycle has the form shown in
Fig. 2-8, and, of course, wastes gas. Here $2x_S$ is taken as 0.1 cm, and
T_C is the total time the control acts during the cycle. For the 300 mile
orbit, it is assumed that f_C can be no smaller than 10^{-2} cm/sec^2. This
corresponds to a typical lower limit of 10^{-3} lbs thrust on a 100 lb
vehicle.

It has been suggested to the author a number of times that the required thrusts would be much too small, or equivalently, the jet-nozzle areas or chamber pressures required would be much too small to make cold-gas-jet control of a drag-free satellite feasible. This is not so. Commercial cold-gas thrust systems are available "off-the-shelf" with thrusts in the 10^{-4} to 10^{-2} pound range, with rise and fall times on the order of a few milliseconds, and with leakage rates less than 10^{-4} standard cc/sec. The ratio T_C/T_D is equivalent to an effective thrust attenuation factor, and is the basic reason that very small jets are not required. Thus, it is seen from Fig. 2-7 and Table 2-2 that the control requirements are reasonable.

To summarize, the basic design procedure is to:

1) Choose the size of the deadband, $2x_S$, for mission reasons. This choice is dictated by:

   a) maintaining the nominal position of the ball to minimize the forces from the satellite which act on the ball (see Table 4-1 and the accompanying discussion),

   b) the fact that the position sensor errors may depend on the nominal gap between the ball and the cavity (see pages 138 to 141), and

   c) avoiding difficulties associated with the design of a special recovery system which would have to be employed for initial acquisition or in the event that the ball went outside the linear range of the sensor.

2) Choose the control acceleration, f_C. This should be as small as possible, but it should also be several times the drag acceleration at the nominal perigee altitude. The safety factor used in the numerical examples is to select f_C approximately 10 times f_{DRAG} at perigee. For orbits with high perigees, f_C cannot be chosen arbitrarily small, but it is limited by the fact that the thrust levels of the control jets cannot be set much smaller than 10^{-3} lbs.

3) Select $\dot{x}_T - \dot{x}_B = [8\, f_{DRAG}(x_S - x_L)]^{\frac{1}{2}}$ to avoid saturating at apogee. (This may not always be possible due to the amount of noise present in the $\dot{x}_C$ signal (see pages 138 to 142) and the time delay in the control loop.) For illustration, $x_S - x_L$ was set at 0.01 cm in the numerical examples, and $\dot{x}_T - \dot{x}_B$ calculated for this choice. (See Table 2-2.)

4) Select k based on the desired initial condition or "dead-beat" response to large initial conditions. See Ref.(38).

5) Select $\delta = \frac{1}{2}\, k(\dot{x}_T - \dot{x}_B)$.

2. GAS CONSUMED BY A NONIDEAL CONTROL SYSTEM

In the examples shown, when the drag acceleration falls below one tenth of its value at perigee, the jet for the left switching line begins to fire and gas is wasted. In general, it is impossible to avoid wasting some gas in high orbits; since as f_D approaches zero, the limit cycle becomes so long that $\dot{x}_T - \dot{x}_B$ cannot be made small enough, because of the noise in the $\dot{x}$ signal and time delay. It is instructive to compute an upper bound on this wasted gas.

Let t_{DB} be the time in orbit after passing perigee at which the limit cycle begins to touch the left line, and assume that from time t_{DB} to time $T_0 - t_{DB}$ that f_D is exactly zero. Then,

$$\frac{T_0 - 2t_{DB}}{T_W}\, T_{CW} = \begin{array}{l} \text{total time that thrust} \\ \text{is on during this period} \\ \text{of gas wasting} \end{array} \qquad (2\text{-}43)$$

where

T_0 = period of one orbit,

T_W = period of one limit cycle while $f_D = 0$, and

T_{CW} = total time control is on during T_W.

The weight of gas wasted per orbit is bounded by

$$\frac{W_{gw}}{ORBIT} \leqq \frac{(T_O - 2t_{DB})}{I_{SP}} \frac{T_{CW}}{T_W} F_C .$$ (2-44)

Equation (2-44) may be compared with the minimum possible gas used per orbit which is obtained from Fig. 2-3 using

$$\frac{W_{gmin}}{ORBIT} = W_{g \ total} \left(\frac{T_O}{T_L} \right) .$$ (2-45)

The ratio $\dfrac{W_{gw}/ORBIT}{W_{gmin}/ORBIT}$ is given in Table 2-3 for an eccentricity of $e = 0.02$. The amount of wasted gas decreases monotonically as $\dot{x}_T - \dot{x}_B$ decreases.

TABLE 2-3

TYPICAL UPPER BOUNDS ON WASTED GAS FOR $e = 0.02$

h_P (statute miles)	$W_{gw}/ORBIT$ (pounds)	$W_{gmin}/ORBIT$ (pounds)	W_{gw}/W_{gmin}
100	0.15	0.23	0.65
200	2.7×10^{-3}	8.2×10^{-3}	0.22
300	2.2×10^{-4}	7.6×10^{-4}	0.29

In a practical satellite, the gas consumption rate must be multiplied by an additional factor which is never larger than $\sqrt{3}$, due to the fact that the control force must be resolved along three mutually-perpendicular axes.

Finally, over the course of the lifetime of the satellite, some control gas will leak out and this must be considered in the final lifetime calculation. In conclusion, if h_P is greater than 100 sm, Fig. 2-3 is right, within a factor of two, for realistic vehicle design.

3. ADAPTIVE CONTROL — THRESHOLD FEEDBACK

The size of the limit cycle is given by

$$x_S - x_L = \frac{(\dot{x}_T - \dot{x}_B)^2}{8 \, f_D} = \frac{\delta^2}{2 \, f_D \, k^2} \; . \tag{2-46}$$

δ cannot be made arbitrarily small but is limited by the accuracy with which $\dot{x}$ can be measured and by the amount of time delay in the control loop. It may not be desirable, however, to make δ as small as possible even though such a choice would waste the least fuel (since the limit cycle would not saturate as soon). The reason for this is that it may be desirable to maintain the average value of x, the position of the proof-mass, fixed during the orbit in order to minimize the force interactions with the satellite, since these interactions generally depend on the position of the proof-mass. This may be accomplished by measuring $x_S - x_L$ during one limit cycle and adjusting δ^2 to achieve the desired value of $x_S - x_L$ during the following limit cycle. If $S_i \triangleq (x_S - x_L)_i$ and δ_i^2 are the values of S and δ^2 during the ith limit cycle, then one way to do this is to select δ_{i+1}^2 such that

$$\delta_{i+1}^2 = - K_a (\triangle S_i) + \delta_i^2 \tag{2-47}$$

where

$$\triangle S_i \triangleq S_i - S_d \tag{2-48}$$

and S_d is the desired value of $x_S - x_L$. A block diagram of this discrete process is shown in Fig. 2-9.

The transfer function is given, by z-transform analysis, as

$$S(z) = \frac{K_T \, z^{-1} \, S_d(z)}{1 + (K_T - 1)z^{-1}} \tag{2-49}$$

where

$$K_T \triangleq \frac{K_a}{2 \, f_D \, k^2} \; . \tag{2-50}$$

SEL-64-067

VARIABLE LIMIT CYCLE

$$x_S - x_L = \frac{\delta^2}{2f_D k^2}$$

$$T \approx \frac{2\delta}{f_D k}$$
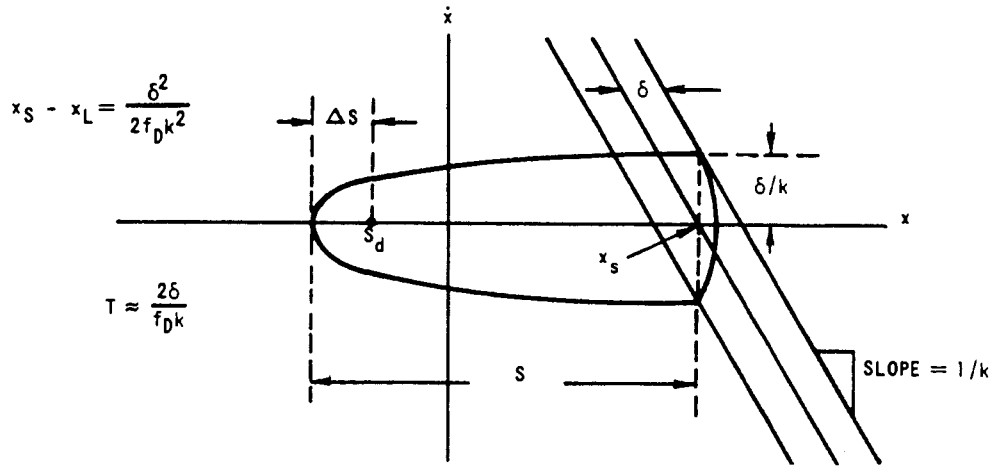
ADAPTIVE SYSTEM BLOCK DIAGRAM

$$\delta^2_{i+1} = -K_a(\Delta s_i) + \delta^2_i$$

$$(K_a)_{i+1} = 4\delta_i / T_i$$
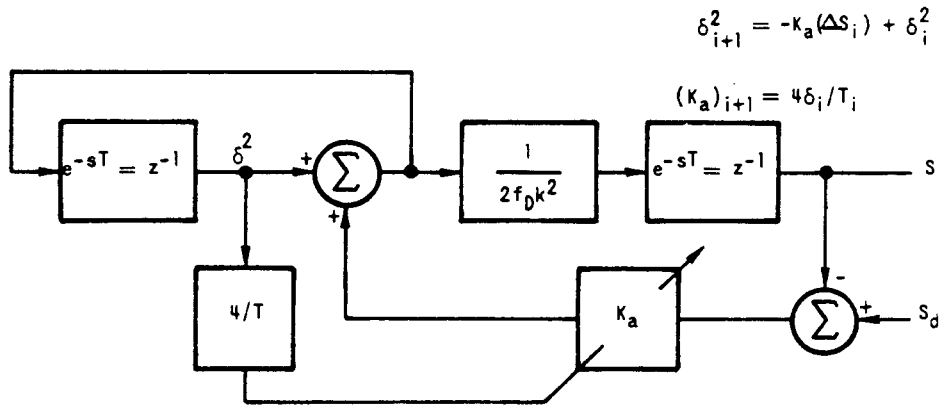
ADAPTIVE SYSTEM FLOW GRAPH

$$K_T = \frac{K_a}{2f_D k^2}$$

$$S(z^{-1}) = \frac{K_T z^{-1} S_d(z^{-1})}{1+(K_T-1)z^{-1}}$$
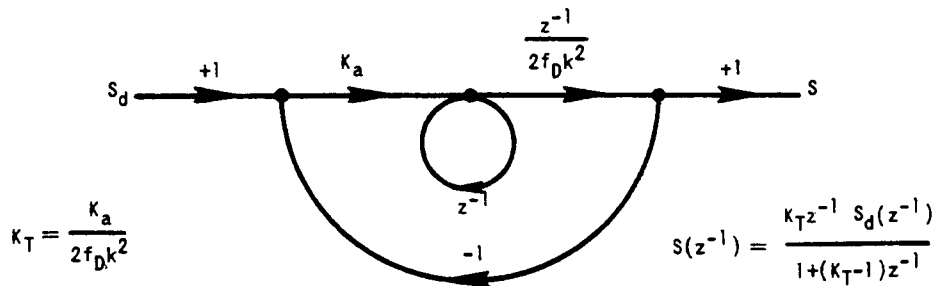
FIG. 2-9. LIMIT-CYCLE-SIZE CONTROL

This carries S_i into S_d in one cycle if $K_T = 1$ or, equivalently, if

$$K_a = 2 f_D k^2 . \qquad (2-51)$$

The solution of Eq. (2-49) for a step input in S_d such that

$$S_d(z) = \frac{S_{do}}{1 - z^{-1}} \qquad (2-52)$$

is

$$S_i = S_{do} [1 - (1 - K_T)^i] . \qquad (2-53)$$

If $0 < K_T < 2$, then $S_i \rightarrow S_{do}$ as $i \rightarrow \infty$; if $K_T = 2$, S_i alternates between 0 and $2S_{do}$; and if $K_T > 2$, the system is unstable.

Thus, it is necessary that $0 < K_T < 2$. Since f_D varies (although it was considered as constant in the above analysis), it is desirable in a practical system to make K_a time-varying so that K_T remains constant. This may be done approximately by measuring δ_i and T_i and setting

$$\left(K_a \right)_{i+1} = \frac{4 \delta_i}{T_i} , \qquad (2-54)$$

since the fractional variation of f_D will not be very great from one limit cycle to the next.

This system will saturate if f_D becomes too small and δ reaches δ_{min}, and will remain in saturation until f_D again falls within the linear range as the satellite approaches perigee.*

---

*Since the force interactions between the ball and satellite are not a serious problem (see Chapter IV), it is doubtful that it would ever be necessary to implement the above scheme in a practical drag-free satellite. The previous system was presented merely as an example of what might be done if the problem ever became important.

CHAPTER III

TRANSLATION CONTROL WITH PARTIAL OR NO ATTITUDE CONTROL WITH APPLICATIONS TO THE CONTROL OF SPINNING VEHICLES AND OTHER DYNAMICALLY SIMILAR PLANTS

In this chapter the author will discuss the modifications in the translation control of a drag-free satellite which are necessary if the satellite rotates or tumbles. The linear control-synthesis techniques developed here to handle this special case will be shown to have a much wider applicability than the translation control of the rotating drag-free satellite. Therefore in this chapter will also be discussed the applications of these methods to the synthesis of linear and contactor control for other dynamically-similar plants such as, for example, the attitude control of the symmetry axis of a symmetric, spinning space vehicle.

In Chapter I it was shown that the translation-control equations for the drag-free satellite reduce to Eq. (1-6) when the vehicle is tumbling with an arbitrary angular velocity $\vec{\omega}_S$. The simplest case of tumbling motion consists of a symmetric body with attitude control to keep it spinning at a constant rate about its symmetry axis. When the body z_C axis is chosen parallel to the spin axis, Eqs. (1-6) reduce to Eqs. (1-17)

$$\ddot{x}_C - \omega_S^2 x_C - 2\omega_S \dot{y}_C = f_{Dx} + f_{Cx}$$

$$+ 2\omega_S \dot{x}_C + \ddot{y}_C - \omega_S^2 y_C = f_{Dy} + f_{Cy} \qquad (1\text{-}17)$$

$$\ddot{z}_C = f_{Dz} + f_{Cz}$$

This special case will be discussed first because it provides a simple example of the basic method. Control for the general case of arbitrary $\vec{\omega}_S$ will be discussed at the end of the chapter (pages 102 to 107).

The equation in z_C is uncoupled from the x_C and y_C equations and is identical to the equation discussed in Chapter II. This leaves the fourth-order coupled set

$$\ddot{x}_C - \omega_S^2 \, x_C - 2\omega_S \, \dot{y}_C = f_{Dx} + f_{Cx}$$

$$2\omega_S \, \dot{x}_C + \ddot{y}_C - \omega_S^2 \, y_C = f_{Dy} + f_{Cy} \, , \qquad (3\text{-}1)$$

and the first problem of the present chapter will be to synthesize a linear control for this set.

Within the context of the drag-free satellite application, there are a number of practical constraints which apply to any control law for Eqs. (3-1). First, the most desirable control is still of the "on-off" or "bang-bang" type discussed in Chapter II because of the practical difficulties of constructing proportional gas jets. Second, it would be highly desirable if the limit cycles at the origin consumed, as nearly as possible, only the amount of fuel necessary to oppose the drag. (This minimum-fuel consumption cannot be completely realized unless very short pulses are used because the spinning jet will precisely oppose the drag force only at one instant during its entire time of firing.) Third, and possibly most important, the controller must be of the simplest possible form (consistent with the other requirements), since it must operate reliably on orbit, unattended for periods of the order of a year.

The synthesis approach, which will be employed in this chapter, will be first to find a linear, constant-coefficient, feed-back control law which makes the system stable for all positive values of the control gain, and then to replace the linear gain element with a relay control to operate the jet valves.[*] Synthesis methods, which optimize

_____

[*]This procedure was first suggested by Aizerman (45), who conjectured that if a linear system with a constant-gain element in its feed-back control loop were stable for all positive values of that gain, then it would also be stable if the gain element were replaced by a relay controller.

(An alternate approach is to employ the pulse-width, pulse-repetition rate-modulation system used on the Discoverer space-craft series as an approximation of the linear control.)

the initial condition or "dead-beat" response for some integral criterion, are not as useful here as in other applications; because (just as in Chapter II) the nature of the disturbances is such that the drag-free satellite translation-control system will spend almost all of its life in limit cycles at the origin.

The problem of finding a linear, constant-coefficient, feed-back control law for a dual-input, fourth-order dynamical plant which results in a stable system is not entirely straightforward (at least not when compared with the second- or third-order, single-input case); and once such a control law has been found, the analysis of the system perform-ance may involve tedious algebraic calculations. A synthesis method will be developed here which is straightforward and easy to apply, which guarantees stability for all positive values of the control gain, and which yields a system whose controlled performance is very easy to analyze. In addition, switching surfaces for the corresponding con-tactor control system constructed on the basis of Aizerman's conjecture will be shown to be two planes in three-dimensional sub-spaces of the states.

A. LINEAR CONSTANT-COEFFICIENT CONTROL OF THE $1/s^2$ PLANT IN A ROTATING REFERENCE FRAME

1. TRANSFORMATION TO COMPLEX COORDINATES

The substitution

$$\xi \triangleq x_c + j\, y_c \tag{3-2}$$

and

$$f \triangleq f_x + j\, f_y \tag{3-3}$$

transforms Eqs. (3-1) into the complex form

$$\ddot{\xi} + 2j\, \omega_s\, \dot{\xi} - \omega_s^2\, \xi = f \,. \tag{3-4}$$

This step is desirable because it greatly reduces the amount of algebra involved in the solutions of Eq. (3-4) and because these solutions are much easier to interpret in complex form. The coupling between the first and second of Eqs. (3-1), or the real and imaginary parts of Eq. (3-4), is due to the fact that the equations have been written down in a rotating reference frame. The equations were cast in this form because it is necessary to mechanize the final form of any control law in this reference frame. This is true because the control gas jets are fixed in the satellite body and because the ball-position sensor reads x_C and y_C. It is not necessary, however, to work in the x_C, y_C reference frame during the conceptual process of control synthesis. Thus, in the next section, Eq. (3-4) will be written in a nonrotating reference frame where the corresponding complex equation represents two uncoupled $1/s^2$ plants.

2. TRANSFORMATION TO A REFERENCE FRAME WHICH IS NONROTATING WITH RESPECT TO AN INERTIAL REFERENCE

The transformation

$$\eta = \xi e^{j\omega_S t} \tag{3-5}$$

with first and second derivatives

$$\dot{\eta} = (\dot{\xi} + j\,\omega_S\,\xi)e^{j\omega_S t} \tag{3-6}$$

$$\ddot{\eta} = (\ddot{\xi} + 2j\,\omega_S\,\dot{\xi} - \omega_S^2\,\xi)e^{j\omega_S t} \tag{3-7}$$

changes Eq. (3-4) into

$$\ddot{\eta} = f\,e^{j\omega_S t} \quad . \tag{3-8}$$

If x_C' and y_C' are defined to be the real and imaginary parts of η (which means that they are simply the in-plane components of $\vec{r}_C$ in a nonrotating reference frame), then Eq. (3-8) can be written as the equations of motion of two uncoupled $1/s^2$ plants in

the nonrotating reference frame x_C', y_C'.

$$\ddot{x}_C' = f_x \; c \; \omega_S t - f_y \; \diagup \omega_S t$$

$$(3-9)$$

$$\ddot{y}_C' = f_x \; \diagup \omega_S t + f_y \; c \; \omega_S t \; .$$

Equations (3-9), of course, are obvious physically and this discussion could have begun with them rather than with Eq. (3-1) or (3-4), but the method of presentation used here was chosen to illustrate the more general method which will be developed later in this chapter. A control law may be found for each of the uncoupled second-order equations represented by Eqs. (3-9), and that control law may then be transformed into the x_C, y_C reference frame which is fixed in the satellite.

3. THE CONTROL SYNTHESIS METHOD

A standard, constant-coefficient, linear feed-back control system using position feedback (with constant "position" gain, K_p) to return an initial disturbance to zero and rate feedback (with constant "velocity" gain, K_v) for damping may be synthesized for Eq. (3-8).

The input acceleration, f, can be divided into two parts, a control acceleration, f_C, and a disturbing acceleration, f_D.

$$f = f_C + f_D$$

or

$$f \; e^{j\omega_S t} = (f_C + f_D) \; e^{j\omega_S t} \; .$$

$$(3-10)$$

If this is done, the control acceleration in the nonrotating reference, $f_C \; e^{j\omega_S t}$, can then be chosen as

$$f_C \ e^{j\omega_s t} = - K_V \ \dot{\eta} - K_P \ \eta \ .$$

(3-11)

Then, Eq. (3-8) becomes

$$\ddot{\eta} + K_V \ \dot{\eta} + K_P \ \eta = f_D \ e^{j\omega_s t}.$$

(3-12)

K_V and K_P may be chosen in the usual manner to obtain any desired performance of Eq. (3-12). From the root locus of the characteristic equation of Eq. (3-12),

$$s'^2 + K_V s' + K_P = 0,$$

(3-13)

shown in Fig. 3-1, it may be seen that Eq. (3-12) is asymptotically stable for all positive K_V and K_P.
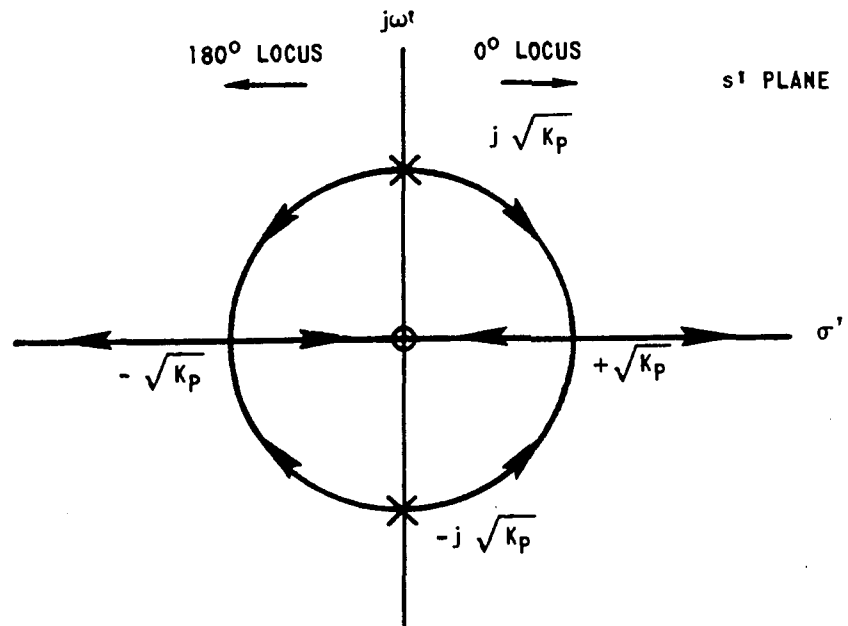
FIG. 3-1.   LOCUS OF THE ROOTS OF $s'^2 + K_V s' + K_P$ VS. K_V

When written in terms of ξ, the control law, Eq. (3-11),
becomes

$$f_C \, e^{j\omega_S t} = - K_V \, \dot{\eta} - K_P \, \eta \qquad\qquad (3\text{-}11)$$

$$f_C \, e^{j\omega_S t} = - K_V(\dot{\xi} + j\omega_S \, \xi)e^{j\omega_S t} - K_P \, \xi e^{j\omega_S t} \qquad\qquad (3\text{-}14)$$

so that

$$f_C = - K_V \, \dot{\xi} - (K_P + j\omega_S \, K_V)\xi \; . \qquad\qquad (3\text{-}15)$$

The complete controlled form of Eq. (3-4) is given by

$$\ddot{\xi} + (K_V + 2j\omega_S)\dot{\xi} + (-\omega_S^2 + K_P + j\omega_S \, K_V)\xi = f_D \; . \qquad\qquad (3\text{-}16)$$

Equation (3-15) corresponds to the pair of real control equations

$$f_{Cx} = - K_V \, (\dot{x}_C - \omega_S \, y_C) - K_P \, x_C$$

$$\qquad\qquad\qquad\qquad\qquad\qquad\qquad\qquad\qquad (3\text{-}17)^*$$

$$f_{Cy} = - K_V \, (\dot{y}_C + \omega_S \, x_C) - K_P \, y_C \; ,$$

---

*Notice that the signal multiplied by each of the rate gains, K_V, is obtained from the velocity of the plant as measured by an observer in the nonrotating reference by using the components of that velocity resolved in the rotating reference frame. That is, the form of the control in the rotating reference frame is identical to the form of the control in the nonrotating reference frame, but the damping is obtained from the rates in a nonrotating reference frame.

and Eq. (3-16) takes the real form,

$$\ddot{x}_C + K_V \dot{x}_C + (K_P - \omega_S^2)x_C - 2\omega_S \dot{y}_C - K_V \omega_S y_C = f_{Dx}$$

(3-18)

$$2\omega_S \dot{x}_C + K_V \omega_S x_C + \ddot{y}_C + K_V \dot{y}_C + (K_P - \omega_S^2)y_C = f_{Dy}.$$

4. TRANSFORMATION OF THE ROOT LOCUS

Since

$$\eta \overset{\Delta}{=} \xi \, e^{j\omega_S t} ,$$

(3-5)

the roots of the characteristic equation of Eq. (3-16)

$$s^2 + (K_V + 2j\omega_S)s + (K_P - \omega_S^2 + j\omega_S K_V) = 0$$

or

$$s^2 + K_V s + K_P - \omega_S^2 + 2j\omega_S (s + \frac{K_V}{2}) = 0 ,$$

(3-19)

are related to the roots of the characteristic Eq. (3-13) by the substitution

$$s = s' - j\omega_S .$$

(3-20)

This may also be seen by inserting Eq. (3-20) directly into Eq. (3-13) since this substitution yields Eq. (3-19). Thus, the root locus of Eq. (3-19) plotted versus K_V may be obtained by merely shifting the root locus of Eq. (3-13) down the $j\omega$ axis by an amount $-j\omega_S$. This is shown in Fig. 3-2.
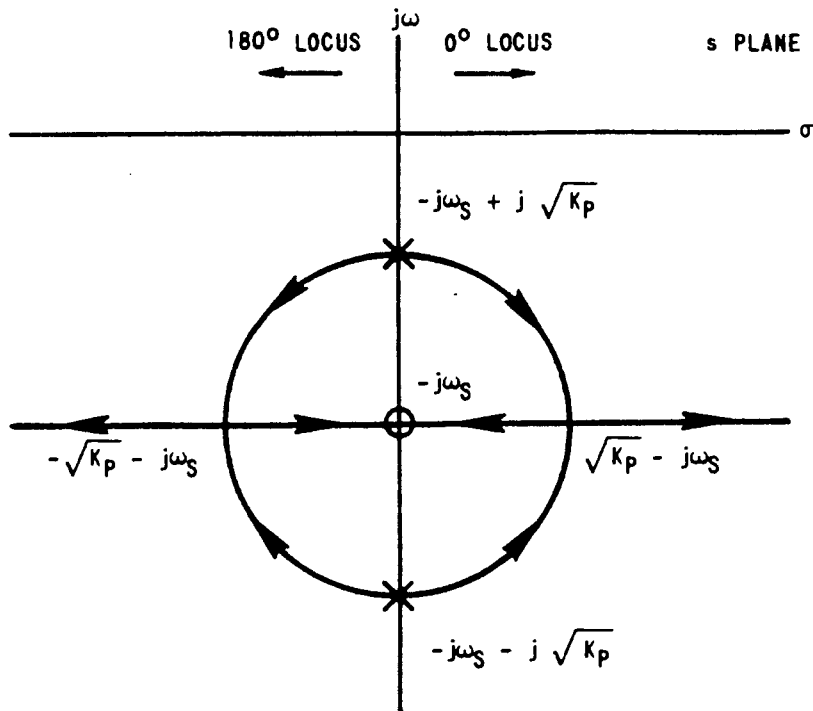
FIG. 3-2. LOCUS OF THE ROOTS OF $s^2+(K_V+2j\omega_S)s+(K_P-\omega_S^2+j\omega_S K_V)$
OR $(s^2+K_P s+K_P-\omega_S^2)+2j\omega_S(s+K_V/2) = 0$ VS K_V

It is clear, either from Eq. (3-5) or from Fig. 3-2, that Eq. (3-16) is asymptotically stable for all positive values of K_P and K_V.

5. ROOT LOCUS OF THE CORRESPONDING REAL SYSTEM (A SPECIAL CASE WHERE THE GAIN PARAMETERS ENTER BOTH AS LINEAR AND AS SQUARED TERMS)

Since

$$x_C = \frac{\xi + \xi^*}{2} \quad \text{and} \quad y_C = \frac{\xi - \xi^*}{2j} , \qquad (3-21)$$

where $\xi^* = x_C - j\,y_C$ and $\eta^* = x_C' - j\,y_C'$, the roots of the characteristic equation of the corresponding real system are given by

$$s = s' - j\,\omega_S$$

and $\hspace{8cm}$ (3-22)

$$s = s' + j\,\omega_S .$$
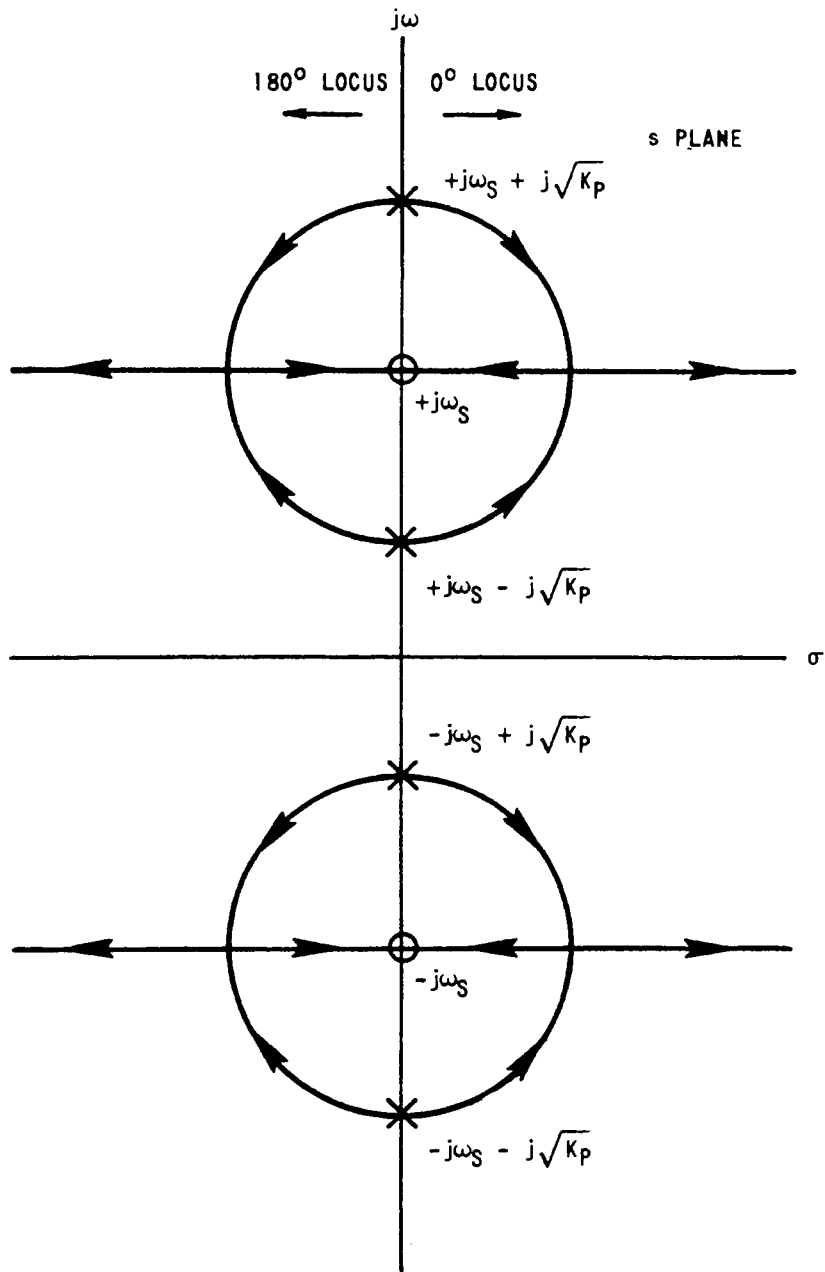
FIG. 3-3. LOCUS OF THE ROOTS OF $(s^2 + K_V s + K_P - \omega_S^2)^2 + 4\omega_S^2(s + K_V/2)^2 = 0$ VERSUS K_V
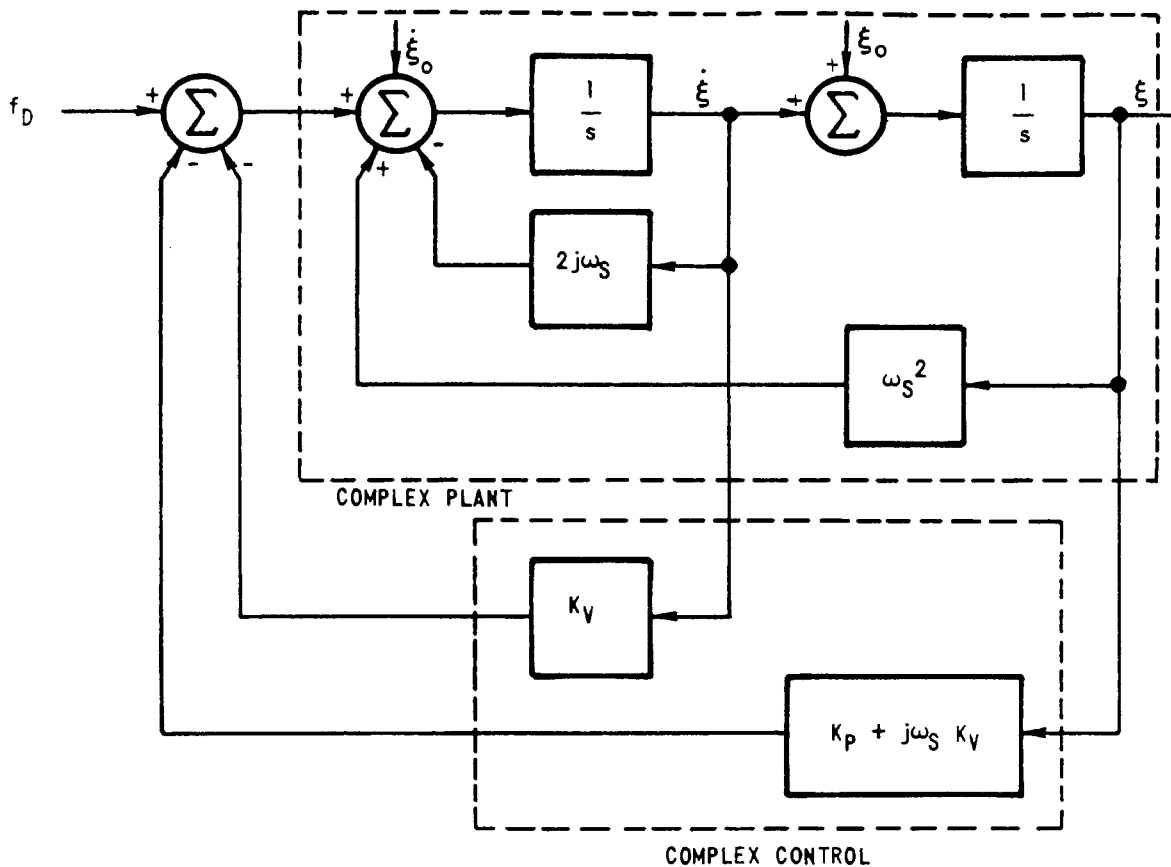
FIG. 3-4. BLOCK DIAGRAM OF COMPLEX CONTROL SYSTEM

This implies that the characteristic equation of Eqs. (3-18) is given by the magnitude squared of Eq. (3-19).

$$(s^2 + K_V s + K_P - \omega_S^2)^2 + 4\omega_S^2 \left(s + \frac{K_V}{2}\right)^2 = 0. \qquad (3\text{-}23)$$

The root locus of Eq. (3-23) versus K_V is shown in Fig. 2-3. Notice that K_V enters Eq. (3-23) both as K_V and as K_V^2, and notice that there is no locus on the real axis. The system represented by Eqs. (3-18) is also asymptotically stable for all positive values of K_P and K_V.

A block diagram of the feedback control for the complex system Eq. (3-16) is shown in Fig. 3-4 and of the real system Eq. (3-18) in Fig. 3-5.
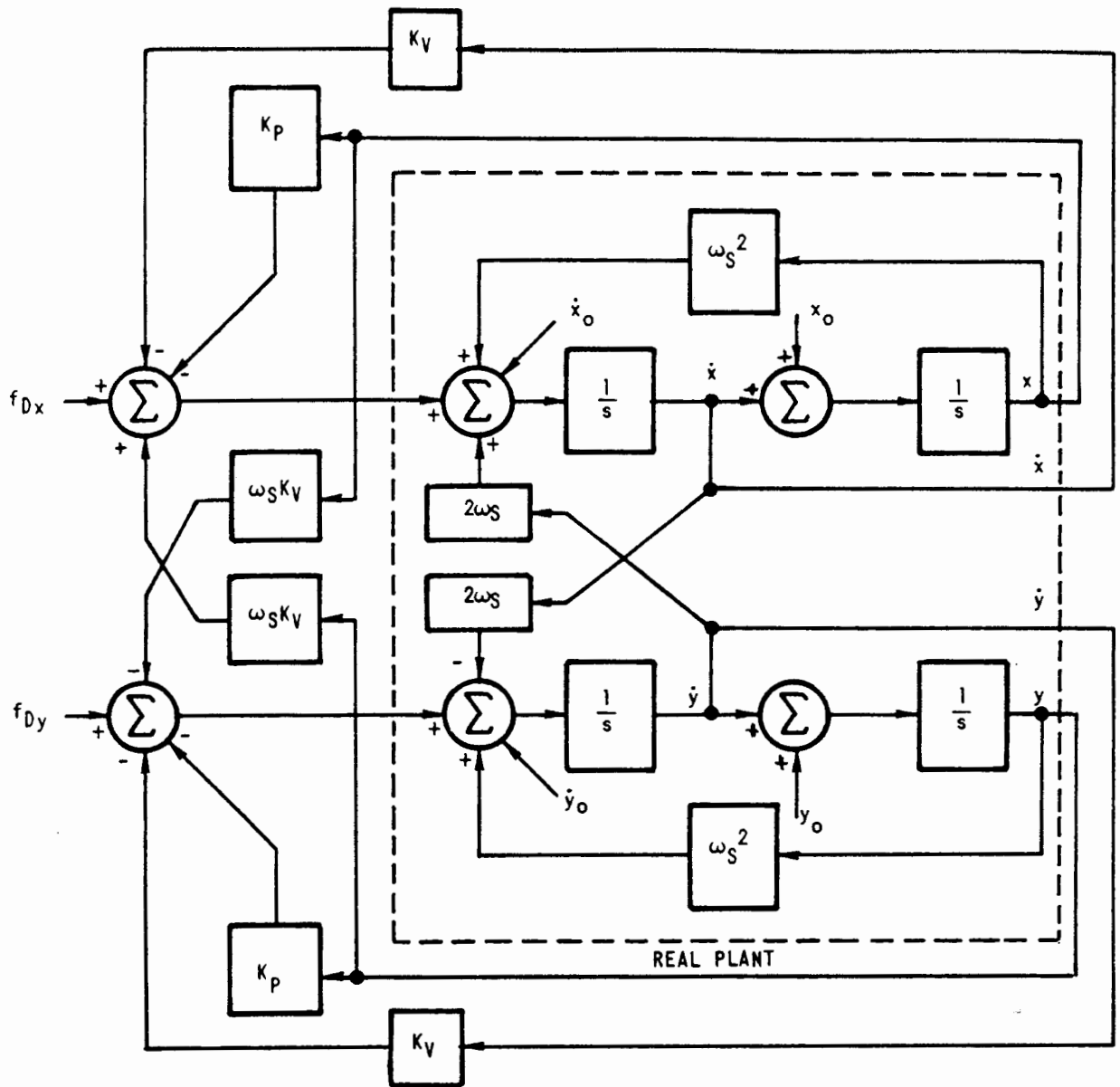
FIG. 3-5. BLOCK DIAGRAM OF REAL CONTROL SYSTEM

B. CONTACTOR CONTROL OF THE $1/s^2$ PLANT IN A ROTATING REFERENCE FRAME USING LINEAR SWITCHING

If Eqs. (3-17) are written with K_V as a multiplying factor and if $k \triangleq K_P/K_V$, then Eqs. (3-17) become

$$f_1 \triangleq - (f_{Cx}/K_V) = \dot{x}_C - \omega_S y_C + k x_C$$

$$f_2 \triangleq - (f_{Cy}/K_V) = \dot{y}_C + \omega_S x_C + k y_C \; . \tag{3-24}$$

Since the system Eq. (3-18) is asymptotically stable for all positive K_V, Aizerman's conjecture suggests that the linear constant gain K_V may be replaced with a relay controller. When this is done, f_1 and f_2 play the role of linear switching functions. The plane switching surfaces $f_1 = 0$ and $f_2 = 0$ are shown in Fig. 3-6.

SURFACE $f_1 = 0$

SURFACE $f_2 = 0$
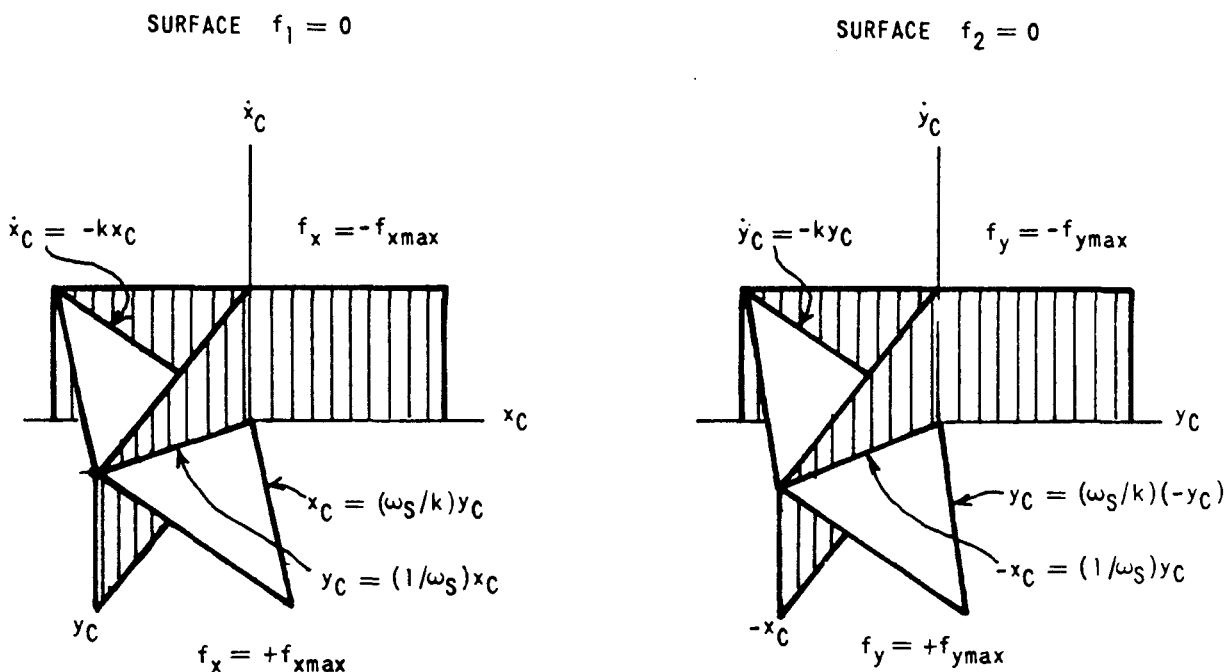
FIG. 3-6. LINEAR SWITCHING SURFACES SUGGESTED BY AIZERMAN'S CONJECTURE

A contactor control system using the switching surfaces given by Eqs. (3-24) for the dynamical plant represented by Eqs. (3-1) has been mechanized on a TR-48 Analog Computer, and the system is asymptotically stable for "reasonable" initial conditions.*

---

*An initial condition for the system Eqs. (3-1) which corresponds to a large velocity as seen from a nonrotating reference frame would carry the system outside the linear range of the computer, even though the controller could ultimately return the states to zero if saturation did not occur.

C. THE ATTITUDE CONTROL OF A SPINNING, SYMMETRIC RIGID BODY

The dynamical plant represented by Eqs. (3-1) is very special in the sense that there is coupling between the x_C and y_C equations only because of the rotation of the satellite. Within this context, it is of fourth order only because of the choice of coordinate system, and the method of the previous sections was based on writing the equations in a reference frame where they assumed their simplest form. It might be supposed these techniques represent an ad hoc approach which would be limited to the previous example. This is not the case. The methods of the previous section generalize to a wide class of dynamical plants, and included in these are a number of fourth-order, dual-input plants of interest in space-vehicle system design.

The attitude control of the symmetry axis of a spinning, symmetric space vehicle is an example of a control problem which may also be solved by the previous techniques. It is of interest in this thesis because it represents another example, and also because this is the attitude-control system currently planned for some of the early drag-free satellites.

1. EQUATIONS OF MOTION OF THE SYMMETRY AXIS OF A SPINNING VEHICLE

In Chapter I it was shown that the equation for the direction of the symmetry axis of a spinning rigid body could be written in the form

$$\ddot{\alpha} - j\,n\,\beta\,\dot{\alpha} = (Q_C + Q_D)\,e^{j\beta t} \tag{3-25}$$

where

$$n \triangleq I_3/I_1, \text{ the vehicle moment of inertia ratio,}$$

$$\beta \triangleq \omega_z, \text{ the constant z axis angular velocity,}$$

$$\alpha \triangleq \phi + j\theta, \text{ and} \tag{3-26}$$

$$Q \triangleq \frac{M_x}{I_1} + j\,\frac{M_y}{I_1}, \text{ the complex torque.}$$

α gives the Euler angles ϕ and θ as a single complex number, and Eq. (3-25) is the second-order complex form in α of the fourth-order coupled set in ϕ and θ,

$$\ddot{\phi} + n\beta\dot{\theta} = \frac{M_x}{I_1} c\beta t - \frac{M_y}{I_1} s\beta t$$

$$\tag{3-27}$$

$$-n\beta\dot{\phi} + \ddot{\theta} = \frac{M_x}{I_1} s\beta t + \frac{M_y}{I_1} c\beta t \ .$$

2. SYNTHESIS OF LINEAR FEED-BACK CONTROL

The approach of the previous sections essentially amounts to choosing a complex rotation transformation which eliminates the term with a j multiplier in Eq. (3-25). This is done because that term is the source of the coupling between the real and imaginary parts of Eq. (3-25).

The choice

$$\mu \overset{\triangle}{=} \alpha e^{-j \frac{n\beta}{2} t} \tag{3-28}$$

with derivatives

$$\dot{\mu} = (\dot{\alpha} - j \frac{n\beta}{2} \alpha) e^{-j \frac{n\beta}{2} t} \tag{3-29}$$

and

$$\ddot{\mu} = (\ddot{\alpha} - j n\beta\dot{\alpha} - \frac{n^2\beta^2}{4} \alpha) e^{-j \frac{n\beta}{2} t} \tag{3-30}$$

does just this. This result may be seen by writing Eq. (3-30) in the form

$$\ddot{\mu} e^{\frac{jn\beta}{2} t} + \frac{n^2\beta^2}{4} \alpha = \ddot{\alpha} - j n\beta\dot{\alpha} = Q e^{j\beta t} \tag{3-31}$$

or

$$\ddot{\mu} + \frac{n^2\beta^2}{4} \mu = Q \ e^{j(1-\frac{n}{2})\beta t} = (Q_C + Q_D)e^{j(1-\frac{n}{2})\beta t} \ . \tag{3-32}$$

If μ is separated into its real and imaginary parts

$$\mu \triangleq \mu_R + j \ \mu_I \ , \tag{3-33}$$

then Eq. (3-32) takes the form of two uncoupled harmonic oscillators of frequency $n\beta/2$.

$$\ddot{\mu}_R + \frac{n^2\beta^2}{4} \mu_R = Q_x \ c(1-\frac{n}{2})\beta t - Q_y \Delta (1-\frac{n}{2})\beta t$$

$$\tag{3-34}$$

$$\ddot{\mu}_I + \frac{n^2\beta^2}{4} \mu_I = Q_x \Delta (1-\frac{n}{2})\beta t + Q_y \ c(1-\frac{n}{2})\beta t.$$

If a control law of a form similar to that used in Eq. (3-11),

$$Q_C \ e^{j(1-\frac{n}{2})\beta t} = - K_V \ \dot{\mu} - K_P \ \mu \ , \tag{3-35}$$

is selected; then in terms of α and $\dot{\alpha}$

$$Q_C \ e^{j\beta t} = - K_V \ (\dot{\alpha} - j \ \frac{n\beta}{2} \ \alpha) - K_P \ \alpha \ . \tag{3-36}$$

The constants K_V and K_P are again "velocity" and "position" gains.

Equation (3-32) then becomes

$$\ddot{\mu} + K_V \ \dot{\mu} + (K_P + \frac{n^2\beta^2}{4})\mu = Q_D \ e^{j(1-\frac{n}{2})\beta t} \ , \tag{3-37}$$

and Eq. (3-25) becomes

$$\ddot{\alpha} + (K_V - jn\beta)\dot{\alpha} + (K_P - j\frac{n\beta}{2} K_V)\alpha = Q_D e^{j\beta t}. \qquad (3-38)$$

Equation (3-38) corresponds to the set of fourth-order real equations

$$\ddot{\phi} + K_V\dot{\phi} + K_P\phi + n\beta\dot{\theta} + \frac{n\beta}{2} K_V\theta = \frac{M_{DSx}}{I_1} c\beta t - \frac{M_{DSy}}{I_1} \beta t$$

$$(3-39)$$

$$- n\beta\dot{\phi} - \frac{n\beta}{2} K_V\phi + \ddot{\theta} + K_V\dot{\theta} + K_P\theta = \frac{M_{DSx}}{I_1} \beta t + \frac{M_{DSy}}{I_1} c\beta t.$$

The characteristic equations of Eqs. (3-37) and (3-38) are respectively

$$s'^2 + K_V s' + \frac{n^2\beta^2}{4} + K_P = 0 \qquad (3-40)$$

and

$$s^2 + (K_V - jn\beta)s + (K_P - j\frac{n\beta}{2} K_V) = 0$$

or

$$(3-41)$$

$$(s^2 + K_V s + K_P) - jn\beta(s + \frac{K_V}{2}) = 0 .$$

The root loci of Eqs. (3-40) and (3-41) versus K_V are shown in Figs. 3-7 and 3-8 respectively.
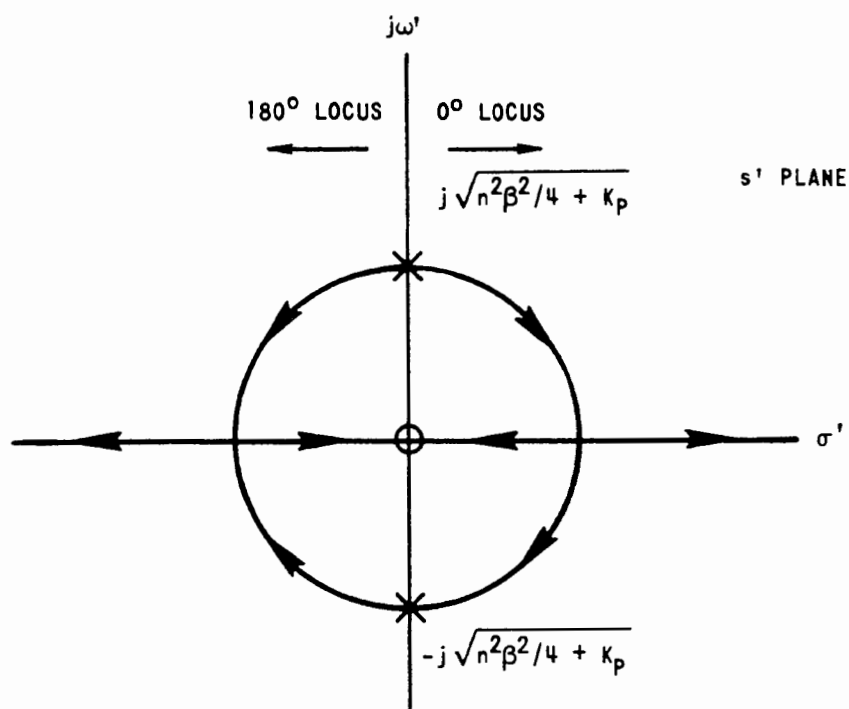
FIG. 3-7. LOCUS OF THE ROOTS OF $s'^2 + K_V s' + n^2\beta^2/4 + K_P = 0$ VS. K_V
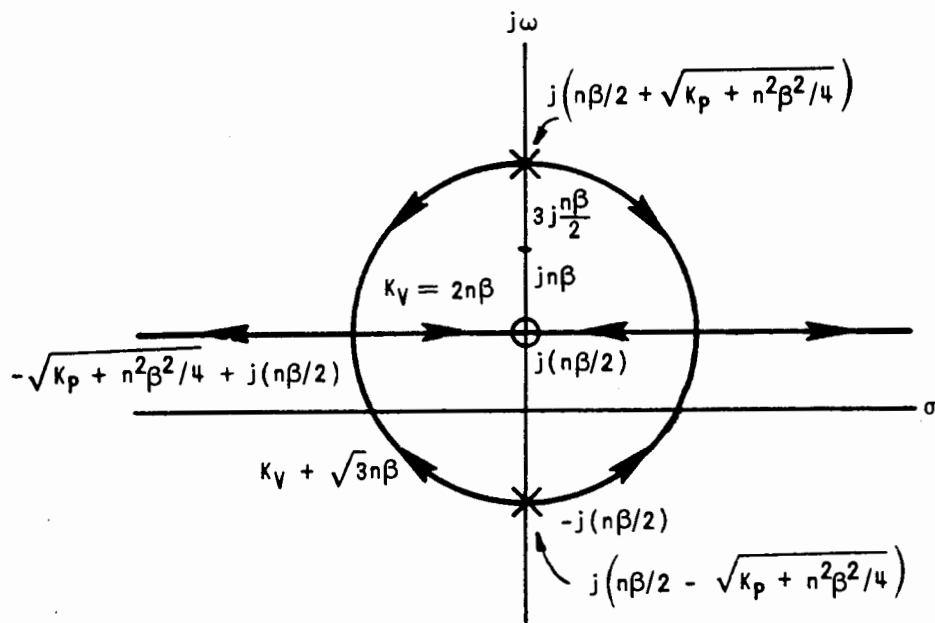
FIG. 3-8. LOCUS OF THE ROOTS OF $(s^2 + K_V s + K_P) - jn\beta(s + K_V/2) = 0$ VS. K_V. DRAWN FOR THE SPECIAL CASE $K_P = 3n^2\beta^2/4$

- 87 -

Again, since

$$\mu = \alpha e^{-j \frac{n\beta}{2} t} \, , \qquad\qquad (3\text{-}28)$$

$$s' = s - j \frac{n\beta}{2} \, ; \qquad\qquad (3\text{-}42)$$

and the locus in Fig. 3-8 is obtained by shifting the locus of Fig. 3-7 up a distance $jn\beta/2$ on the $j\omega$ axis.

Also, since

$$\phi = \frac{\alpha + \alpha^*}{2} \quad \text{and} \quad \theta = \frac{\alpha - \alpha^*}{2j} \, , \qquad (3\text{-}43) \text{ and } (3\text{-}44)$$

the characteristic equation of Eqs. (3-39) is the magnitude squared of the characteristic equation of Eq. (3-38).

$$(s^2 + K_V s + K_P)^2 + n^2 \beta^2 (s + \frac{K_V}{2})^2 = 0. \qquad\qquad (3\text{-}45)$$

The root locus of this equation is shown in Fig. 3-9. The case $K_P = 3 \, n^2 \beta^2 / 4$ was selected because it illustrates what happens with pole-zero cancellation. It is interesting to note that the choice $K_V = \sqrt{3} \, n\beta$ yields an example of a system which can slew the symmetry axis without exciting ω_x and ω_y, i.e., without wobbling.

Again, notice that K_P and K_V enter both as K_P, K_V and K_P^2, K_V^2 and that there is no locus on the real axis except at isolated points.
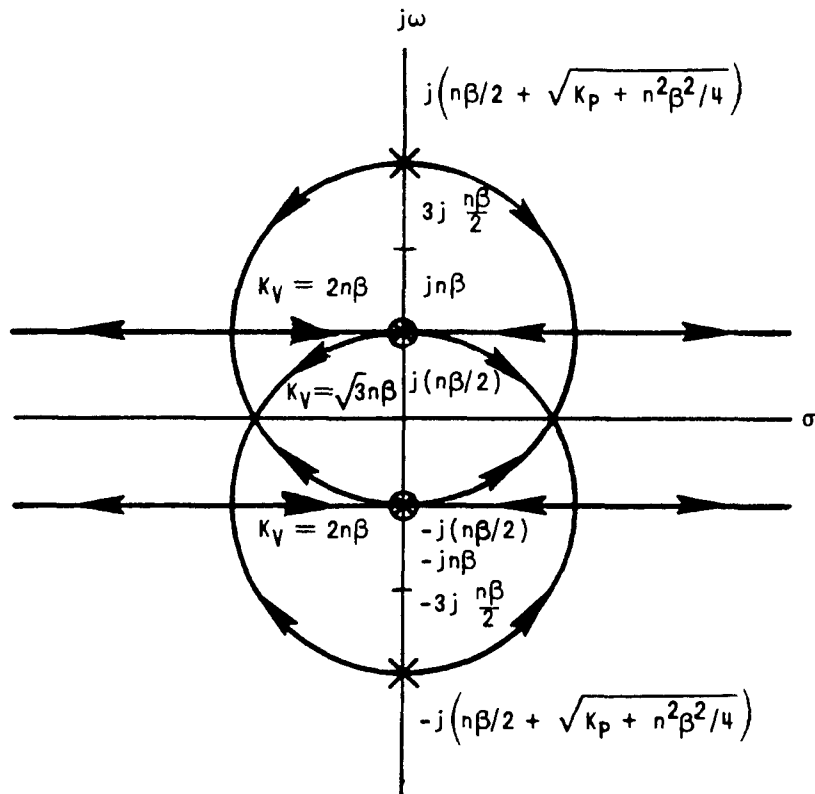
FIG. 3-9. LOCUS OF THE ROOTS OF $(s^2+K_V s+K_P)^2 + n^2\beta^2(s+K_V/2)^2 = 0$
VS. K_V. DRAWN FOR THE SPECIAL CASE $K_P = 3n^2\beta^2/4$

3. MECHANIZATION OF THE CONTROL LAW

The linear control law given by Eq. (3-36)

$$Q_C \, e^{j\beta t} = - K_V \dot{\alpha} - (K_P - j \, \frac{n\beta}{2} \, K_V)\alpha \qquad (3\text{-}36)$$

is not in a form which can be easily mechanized. However,

$$Q_C = - K_V \dot{\alpha} \, e^{-j\beta t} - (K_P - j \, \frac{n\beta}{2} \, K_V)\alpha \, e^{-j\beta t} , \qquad (3\text{-}46)$$

can be easily treated since

$$\dot{\alpha} = q \, e^{j\beta t} \, , \qquad\qquad (1-40)$$

where $q \overset{\Delta}{=} \omega_x + j\omega_y$. Equation (3-46) may then be written as

$$Q_C = - K_V \, q - (K_P - j \, \frac{n\beta}{2} \, K_V)\gamma \, . \qquad\qquad (3-47)$$

The new symbol, γ, which will be referred to as "the star-tracker" variable or complex angle, is defined as

$$\gamma \overset{\Delta}{=} \alpha \, e^{-j\beta t} \, . \qquad\qquad (3-48)$$

The additional quantity, γ, is introduced because it simplifies the form of Eq. (3-47) and (later) the presentation of the switching surfaces, and because it is very easy to obtain a signal proportional to γ from a star-tracker or sun sensor or from the gimbal angles of a three-axis stable platform.

The control law, Eq. (3-47), may be mechanized in either of two ways.

a. <u>Mechanization with an External Reference for α</u>

If it is desired to point the symmetry axis at the sun or at a bright star, then the quantity $\alpha e^{-j\beta t}$ may be read directly from an optical sensor if $|\alpha|$ is small. $q \overset{\Delta}{=} \omega_x + j\omega_y$ may be obtained from body mounted rate gyros, or $-K_V \, q$ may be obtained from a spin damper if $1 < n \leq 2$. The real form of Eq. (3-47) is

$$Q_{Cx} \overset{\Delta}{=} \frac{M_{CSx}}{I_1} = - K_V(\omega_x + \frac{n\beta}{2} \, \gamma_y) - K_P \, \gamma_x$$

$$\qquad\qquad (3-49)$$

$$Q_{Cy} = \frac{M_{CSy}}{I_1} = - K_V(\dot{\omega}_y - \frac{n\beta}{2} \, \gamma_x) - K_P \, \gamma_y$$

or, in terms of ϕ and θ,

$$\frac{M_{CSx}}{I_1} = - K_V \left[\omega_x + \frac{n\beta}{2} (-\phi \Delta \beta t + \theta c\beta t) \right] - K_P(\phi c\beta t + \theta \Delta \beta t)$$

$$\frac{M_{CSy}}{I_1} = - K_V \left[\omega_y - \frac{n\beta}{2} (\phi c\beta t + \theta \Delta \beta t) \right] - K_P(-\phi \Delta \beta t + \theta c\beta t).$$

(3-50)

The complete-system block diagram for the controlled complex plant is shown in Fig. 3-10, and the real plant is shown in Fig. 3-11. (See also page 22 and Fig. 1-4.)
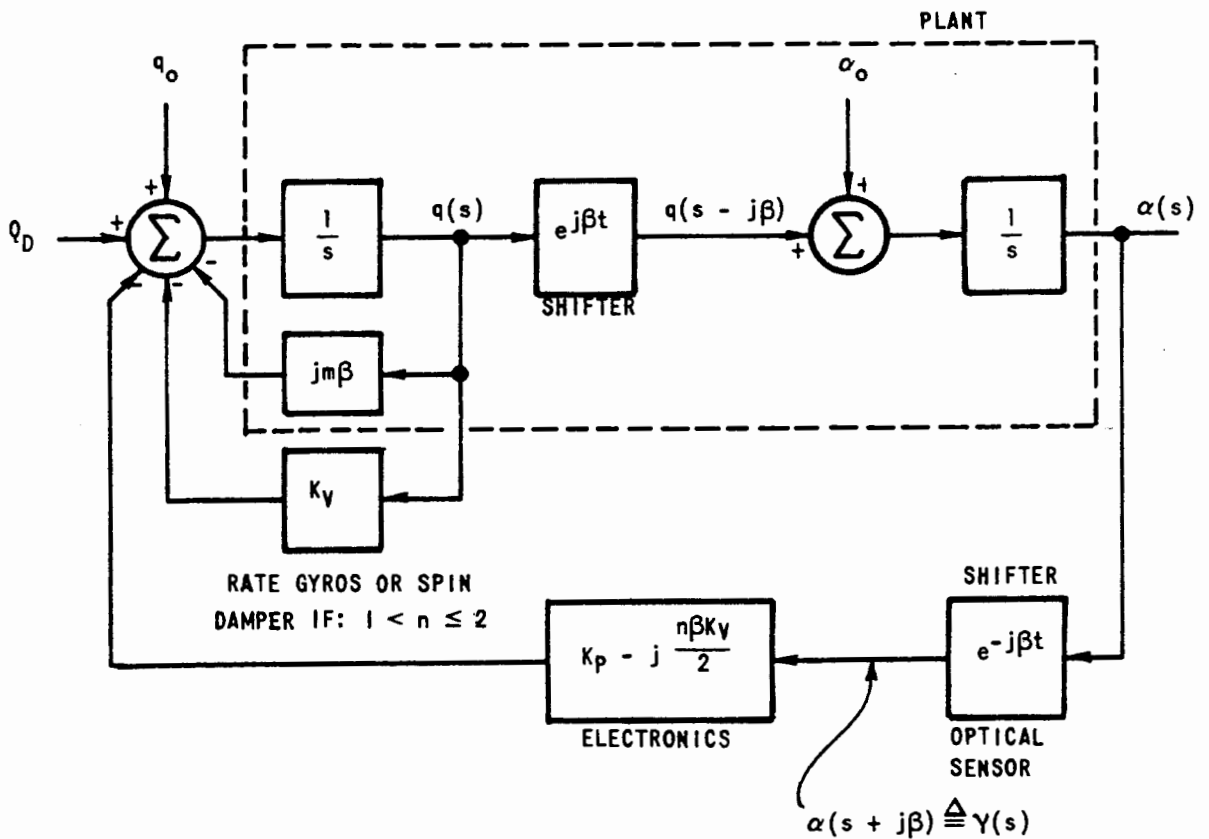
FIG. 3-10. SPINNING VEHICLE CONTROL WITH EXTERNAL REFERENCE – COMPLEX FORM

- 91 -
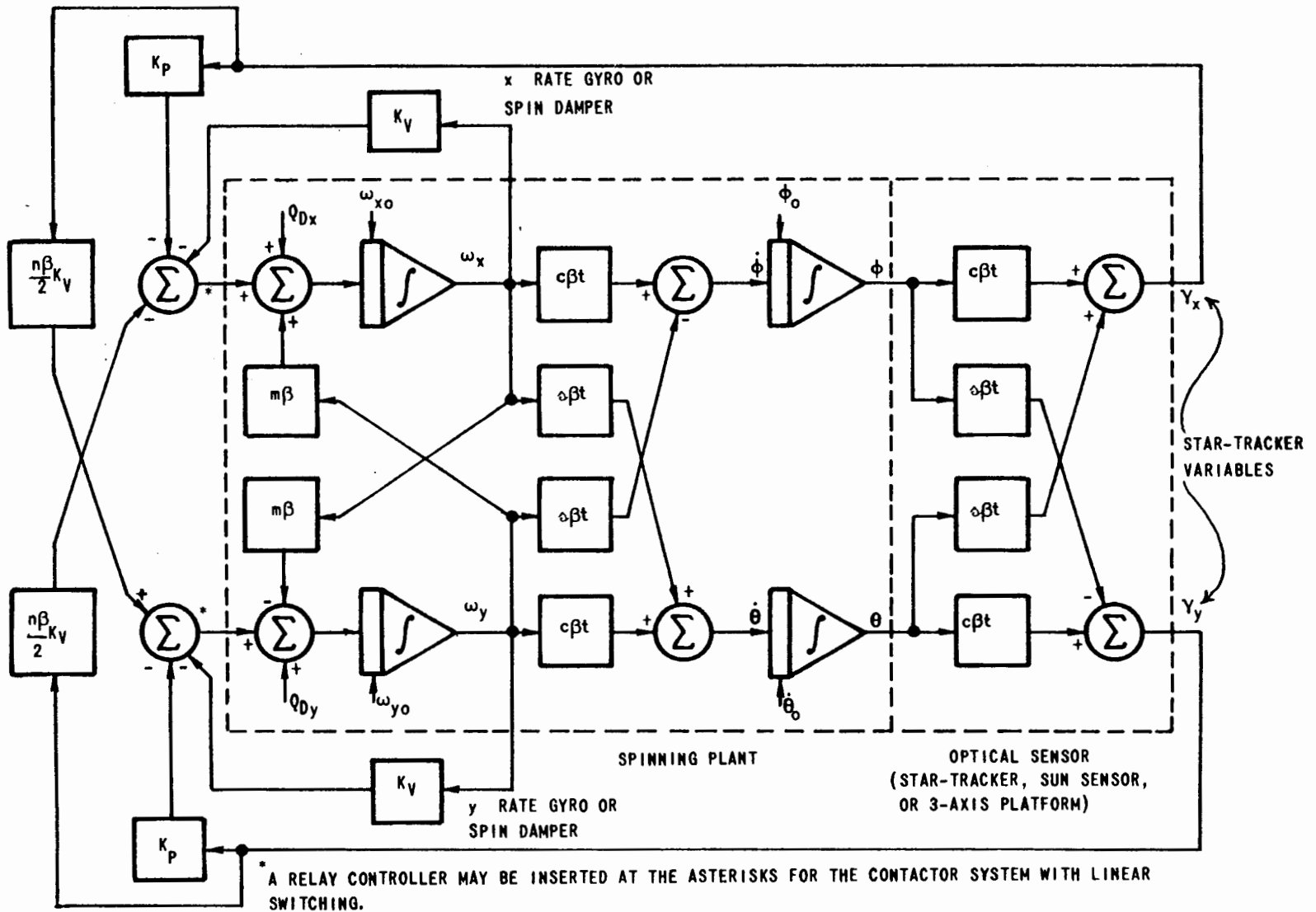
FIG. 3-11. SPINNING VEHICLE CONTROL WITH EXTERNAL REFERENCE — REAL FORM

b. Mechanization with a Strapped-Down Inertial Reference System

If no external reference for α is available, it is possible in principle to mechanize an all-inertial attitude-reference system. Such a system is difficult to realize in practice because it requires lossless filters accurately tuned to the spin frequency, $\dot{\beta}$.

Stable control may be accomplished if the quantity $\gamma \overset{\Delta}{=} \alpha e^{-j\beta t}$ can be computed from measurements of $q(t)$. Since

$$\dot{\alpha} = q(t)e^{j\beta t} \; , \tag{1-40}$$

$$\alpha(t)e^{-j\beta t} = \alpha_o e^{-j\beta t} + e^{-j\beta t} \int_0^t e^{j\beta \tau} q(\tau)d\tau. \tag{3-51}$$

Taking the Laplace transform of Eq. (3-51),

$$L\left[\alpha(t)e^{-j\beta t}\right] = L(s) = \frac{q(s) + \alpha_o}{s + j\beta} \; . \tag{3-52}$$

The control law then becomes

$$Q_C(s) = -K_v q(s) + \left[\frac{(K_p - j\frac{n\beta K_v}{2})}{s + j\beta}\right][q(s) + \alpha_o]. \tag{3-53}$$

The quantity

$$\frac{q(s)}{s + j\beta} = \frac{s\,q(s) - j\beta\,q(s)}{s^2 + \beta^2} \tag{3-54}$$

has the corresponding real form

$$\text{Real part} = \frac{s\,\omega_x(s) - \beta\,\omega_y(s)}{s^2 + \beta^2} \tag{3-55}$$

$$\text{Imag. part} = \frac{s\,\omega_y(s) - \beta\,\omega_x(s)}{s^2 + \beta^2} \; ; \tag{3-56}$$

and, hence, requires the synthesis of the filters

$$H(s) = \frac{1}{s^2 + \beta^2} \tag{3-57}$$

and

$$sH(s) = \frac{s}{s^2 + \beta^2} \tag{3-58}$$

to mechanize the control.

The synthesis of the filters represented by Eqs. (3-57) and (3-58) is best understood by considering the differential equation which γ obeys. If Eq. (3-51) is written in the form

$$\alpha(t)e^{-j\beta t} = \gamma(t) = \gamma_o e^{-j\beta t} + e^{-j\beta t} \int_0^t e^{j\beta \tau} q(\tau)d\tau; \tag{3-59}$$

since $\gamma_o = \alpha_o$, Eq. (3-59) is immediately recognizable as a solution of the differential equation

$$\dot{\gamma} + j\beta\gamma = q$$
$$\gamma_o = \alpha_o \tag{3-60}$$

or

$$\dot{\gamma}_x = \beta\gamma_y + \omega_x$$
$$\dot{\gamma}_y = -\beta\gamma_x + \omega_y. \tag{3-61}$$

Figure 3-12 shows the relatively simple form that the tuned filters assume when mechanized from Eq. (3-61) with operational amplifiers. In a practical system, the spin rate slowly decays; and the gains, β, must be maintained from some measurement of the spin speed such as a z-axis rate gyro, sun sensor, or platform gimbal rate sensor. In addition, some provision must be made to reset the integrators periodically to counteract the effects of drift and errors in the measurement of ω_x, ω_y, and the gain β.
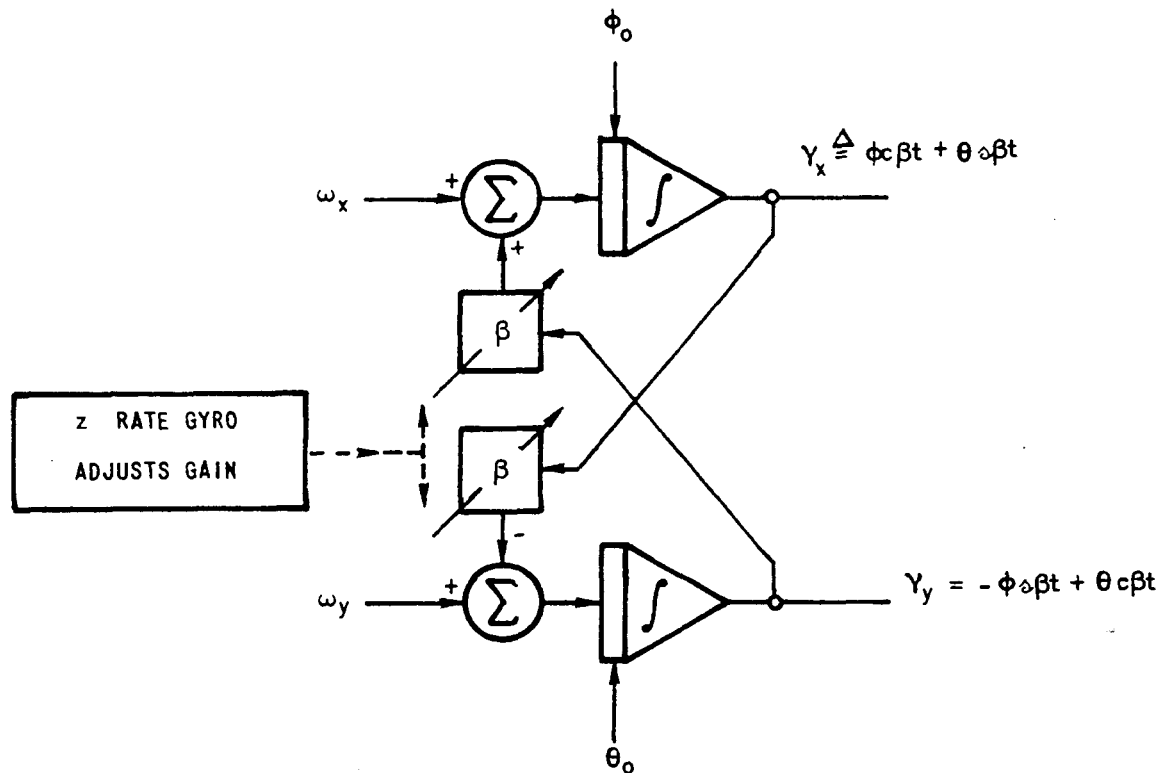
FIG. 3-12.   OPERATIONAL AMPLIFIER MECHANIZATION OF THE TUNED FILTERS TO COMPUTE γ

A block diagram of the complex form of the strapped-down inertial reference system is shown in Fig. 3-13.
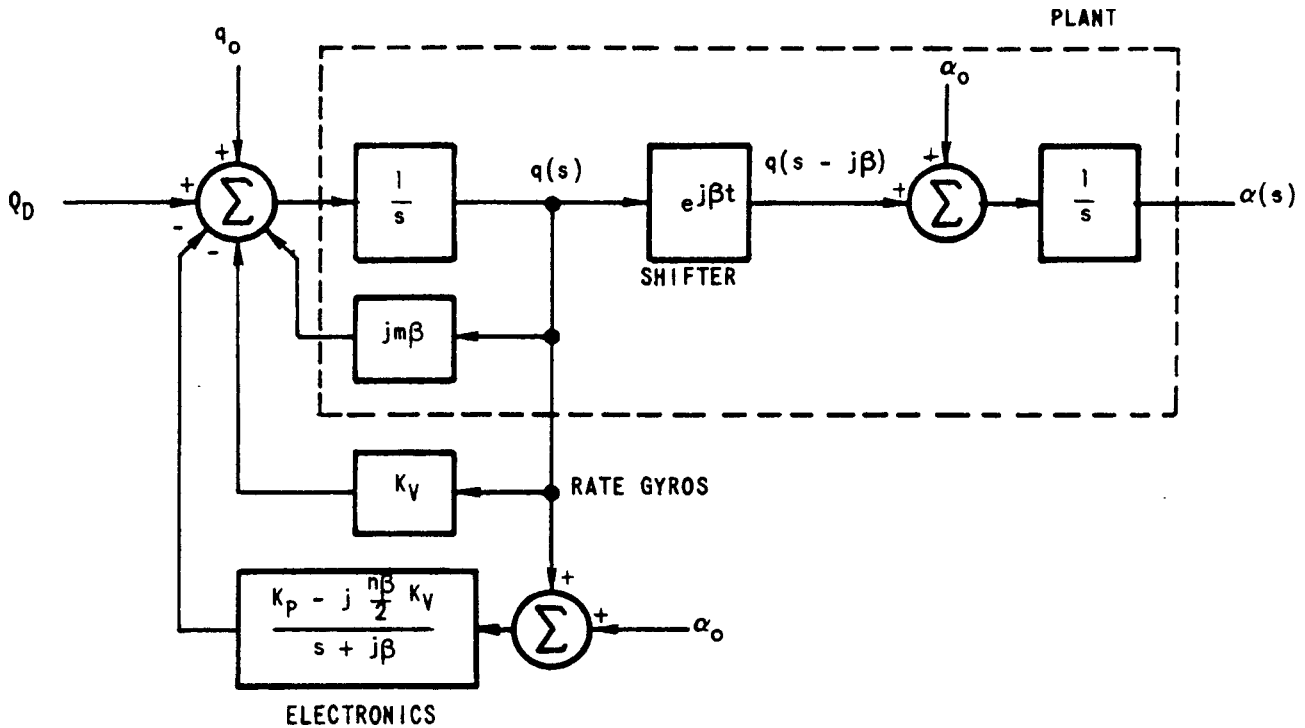
FIG. 3-13. SPINNING VEHICLE CONTROL WITH A STRAPPED-DOWN
INERTIAL REFERENCE - COMPLEX FORM

D. CONTACTOR CONTROL OF THE ATTITUDE OF THE SYMMETRY AXIS OF A SYMMETRIC, SPINNING SPACE VEHICLE USING LINEAR SWITCHING

Since the controlled form of Eq. (3-38) is stable for all positive values of K_V and for all values of $K_P > -n^2\beta^2/4$, stable switching surfaces may be constructed from Eqs. (3-49) if Aizerman's conjecture is true for this plant. Again, as was the case with Eqs. (3-24), define $k = K_P/K_V$ so that

$$ f_1 \overset{\triangle}{=} - \frac{Q_{Cx}}{K_V} = \omega_x + \frac{n\beta}{2}\gamma_y + k\gamma_x $$

$$ f_2 \overset{\triangle}{=} - \frac{Q_{Cy}}{K_V} = \omega_y - \frac{n\beta}{2}\gamma_x + k\gamma_y. $$

$$(3-62)$$

The switching surfaces described by Eqs. (3-62) are shown in Fig. 3-14.

SURFACE $f_1 = 0$ SURFACE $f_2 = 0$
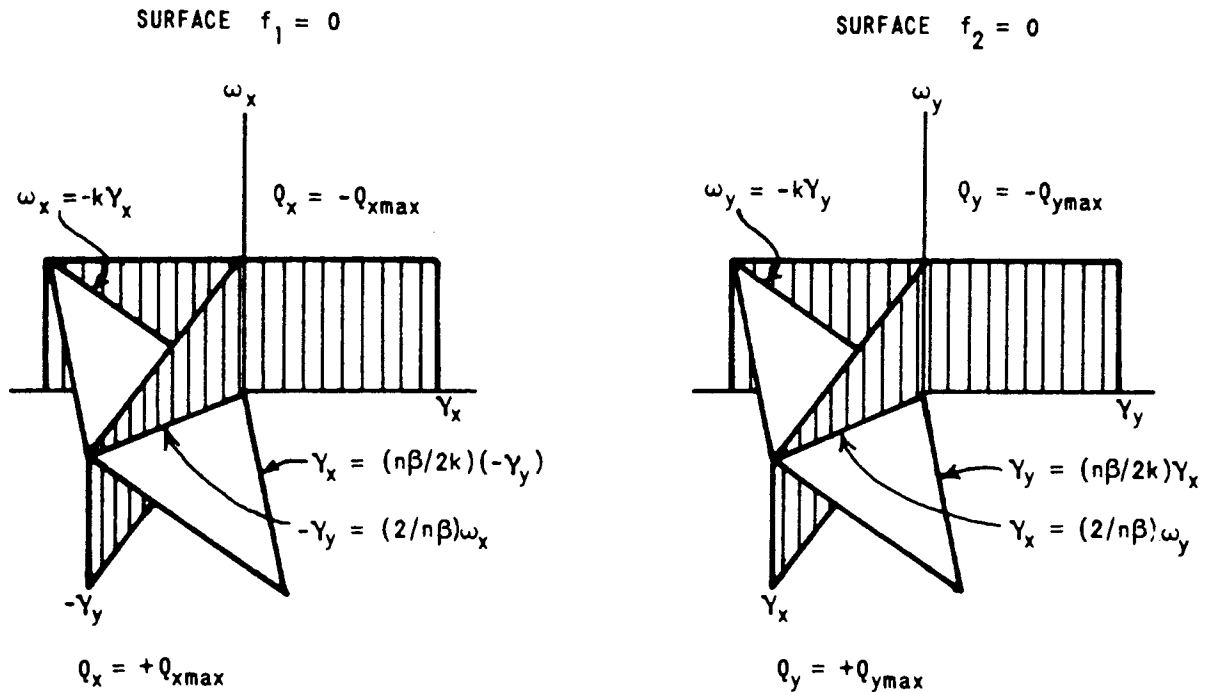
FIG. 3-14. LINEAR SWITCHING SURFACES FOR THE SPINNING VEHICLE
SUGGESTED BY AIZERMAN'S CONJECTURE

A contactor control system using the switching surfaces shown
in Fig. 3-14 has been mechanized on a TR-48 Analog Computer, and the
system was always observed to be asymptotically stable for the initial
conditions which were tested. In fact, the ϕ_0, θ_0, ω_{xo}, and ω_{yo}
space was continuously searched using the computer "Rep Op" mode,
and no points of instability were observed.

E. EXTENSION TO ARBITRARY, FREQUENCY-SYMMETRIC, LINEAR DYNAMICAL PLANTS

1. DEFINITION OF FREQUENCY SYMMETRY

Those even-ordered, linear, time-invariant dynamical systems whose pole-zero configurations may be generated by translations of the pole-zero configuration of some other linear-dynamical system (of one-half the order of the first) by equal distances up and down the $j\omega$ axis will be said to possess "frequency symmetry."

As an example consider the third-order plant

$$\dddot{\eta} + (2a + c)\ddot{\eta} + (a^2 + b^2 + 2ac)\dot{\eta} + (a^2 + b^2)c\eta = u\,e^{j\nu t} \tag{3-63}$$

with characteristic equation

$$(s' + c)[(s' + a)^2 + b^2] = 0. \tag{3-64}$$

Then the sixth-order dual-input plant, whose complex form may be generated by the substitution

$$\xi = \eta e^{-j\nu t}, \tag{3-65}$$

$$\dddot{\xi} + (3j\nu + 2a + c)\ddot{\xi} + [-3\nu^2 + 2j\nu(2a+c) + a^2 + b^2 + 2ac]\dot{\xi}$$

$$+[-j\nu^3 -(2a+c)\nu^2 + j\nu(a^2 + b^2 + 2ac) + (a^2 + b^2)c]\xi = u, \tag{3-66}$$

is frequency symmetric.

Equation (3-66) has characteristic equation given by the substitution in Eq. (3-64) of $s' = s + j\nu$

$$(s+c+j\nu)[(s+a+j\nu)^2+b^2] = \left\{(s+c)\,[(s+a)^2 + b^2 -\nu^2]-2\nu^2(s+a)\right\}$$

$$+ j\nu[(s+a)^2 + b^2 - \nu^2 + 2(s+a)(s+c)] = 0 . \tag{3-67}$$

The characteristic equation of the real sixth-order plant which cor-
responds to Eq. (3-66) is given by the magnitude squared of Eq. (3-67)

$$\left\{ (s+c)[(s+a)^2+b^2-v^2] -2v^2(s+a) \right\}^2 + v^2[(s+a)^2 +b^2-v^2+ 2(s+a)(s+c)]^2 = 0. \quad (3-68)$$

2. LINEAR CONTROL SYNTHESIS

Any constant-coefficient, linear control equation which
stabilizes Eq. (3-63) in terms of $\ddot{\eta}$, $\dot{\eta}$, and η will also stabilize
Eq. (3-66) with $(\ddot{\xi} + 2jv\dot{\xi} - v^2\xi)$, $(\dot{\xi} + jv\xi)$, and ξ substituted
in the control law for $\ddot{\eta}$, $\dot{\eta}$, and η respectively. If the control
law happens to be stable for all positive values of the control gain,
then the system will most likely be stable if the linear gain element
is replaced with a relay controller.

3. FREQUENCY-SYMMETRIC DYNAMICAL PLANTS WHOSE EQUATIONS OF MOTION CANNOT BE IMMEDIATELY WRITTEN IN COMPLEX FORM

The linearized form of Hill's Lunar equations (1-72) and (1-73)
with characteristic equation $s^2(s^2 + \omega_0^2) = 0$ and the Lagrange attitude
Eqs. (1-78) and (1-79) with characteristic equation $(s^2 + \omega_1^2)(s^2+ \omega_2^2) = 0$
(when stably oriented), provide examples of frequency-symmetric plants,
whose equations cannot be written as a single complex equation while
in their present form.

However, in the case of Eqs. (1-78) and (1-79), a linear
transformation can be found which changes them into a symmetric form
which can be written as the single complex equation

$$\ddot{\alpha} + j(\omega_1 + \omega_2)\dot{\alpha} - \omega_1\omega_2\alpha = Q, \quad (3-69)$$

which corresponds to the real fourth-order system

$$\ddot{\phi}_1 - \omega_1\omega_2\phi_1 - (\omega_1 + \omega_2)\dot{\phi}_2 = Q_1$$

$$(3-70)$$

$$(\omega_1 + \omega_2)\dot{\phi}_1 + \ddot{\phi}_2 - \omega_1\omega_2\phi_2 = Q_2$$

where $\alpha \overset{\Delta}{=} \phi_1 + j\phi_2$ and $Q \overset{\Delta}{=} Q_1 + jQ_2$.

Since Eqs. (3-70) and (1-78) and (1-79) have the same characteristic roots (none of which are repeated), there exists an invertible linear transformation from Eqs. (3-70) to Eqs. (1-78) and (1-79). In practice, this is found from the invertible linear transformations which change Eqs. (3-70) and Eqs. (1-78) and (1-79) into normal coordinates.

When this procedure is carried out for the general case, a rather strange complication arises. The control inputs to Eqs. (1-78) and (1-79) become distributed among all the states of Eqs. (3-70), rather than just among those states which correspond to the system velocities as in the case of Eqs. (1-78) and (1-79). When the control equations are modified to take care of this situation, it turns out that the control must be fed back through a linear filter instead of merely a constant-coefficient linear combination.

On the other hand, Hill's linear orbit Eqs. (1-72) and (1-73) are examples of a fourth-order, dual-input, frequency-symmetric, linear, time-invariant, dynamical plant which cannot be treated by the methods of this chapter. The characteristic equation $s^2(s^2 + \omega_0^2) = 0$ is frequency symmetric and can be shifted into an equation of the form $(s'^2 + \omega_0^2/4) = 0$, but the multiple root at zero causes a response in the original system which grows as t, and the roots at $\pm j\,\omega_0/2$ do not cause such a response in the shifted system.

In general, if the Jordan form of a frequency-symmetric plant has ones above its diagonal, the corresponding shifted, half-order plant cannot duplicate the character of its response unless it has a corresponding shifted, multiple root and also has corresponding ones above the diagonal in its Jordan form. (This is precisely the case for the $1/s^2$ plant in a rotating reference frame. It has a

characteristic equation $(s^2 + \omega_s^2)^2 = 0$, and the corresponding shifted $1/s^2$ plant has a characteristic equation $s'^2 = 0$.)

F. EXTENSION TO TIME-VARYING LINEAR DYNAMICAL SYSTEMS

As an example of this extension, the transformation

$$\eta = \xi\, e^{\displaystyle j\int_0^t \nu(\tau)d\tau} \qquad\qquad (3\text{-}71)$$

changes the general second-order, linear, time-invariant equation

$$\ddot{\eta} + k_V\dot{\eta} + k_P\eta = u\, e^{\displaystyle j\int_0^t \nu(\tau)d\tau} \qquad\qquad (3\text{-}72)$$

(where k_V and k_P are constants) into the time-varying, linear system

$$\ddot{\xi} + (k_V + 2j\nu)\dot{\xi} + (k_P - \nu^2 + j\dot{\nu} + jk_V)\xi = u_D + u_C . \qquad\qquad (3\text{-}73)$$

A control law of the form

$$u_C\, e^{\displaystyle j\int_0^t \nu d\tau} = -K_V\dot{\eta} - K_P\eta \qquad\qquad (3\text{-}74)$$

or

$$u_C = -K_V(\dot{\xi} + j\nu\xi) - K_P\, \xi , \qquad\qquad (3\text{-}75)$$

which stabilized Eq. (3-72), also stabilized Eq. (3-73). The concept of a characteristic equation of Eq. (3-73), of course, has no meaning; but the response of Eq. (3-73) may be easily computed from the response of Eq. (3-72).

The case where $k_V = k_P = 0$ is of interest here, because it represents the form of the drag-free satellite equations when the spin about the symmetry axis is not constant in time. The results of the previous analysis can be applied to this case in a straightforward way and will not be discussed here.

G. EXTENSION TO THE SYNTHESIS OF LINEAR CONTROL FOR THE GENERAL SIXTH-ORDER, THREE-DIMENSIONAL, TIME-VARYING EQUATIONS FOR SATELLITE TRANSLATION CONTROL

When a drag-free satellite with arbitrary moments of inertia has no attitude control but is allowed to tumble with arbitrary $\vec{\omega}_S$, Eq. (1-6) assumes the form

$$\ddot{x}_C - (\omega_y^2 + \omega_z^2)x_C - 2\omega_z\dot{y}_C + (\omega_x\omega_y - \dot{\omega}_z)y_C + 2\omega_y\dot{z}_C + (\omega_x\omega_z + \dot{\omega}_y)z_C = f_{Dx} + f_{Cx}$$

$$2\omega_z\dot{x}_C + (\omega_x\omega_y + \dot{\omega}_z)x_C + \ddot{y}_C - (\omega_z^2 + \omega_x^2)\,y_C - 2\omega_x\dot{z}_C + (\omega_y\omega_z - \dot{\omega}_x)z_C = f_{Dy} + f_{Cy} \quad (1\text{-}19)$$

$$-2\omega_y\dot{x}_C + (\omega_z\omega_x - \dot{\omega}_y)x_C + 2\omega_x\dot{y}_C + (\omega_z\omega_y + \dot{\omega}_x)\,y_C + \ddot{z}_C - (\omega_x^2 + \omega_y^2)\,z_C = f_{Dz} + f_{Cz}.$$

The formidable nature of Eq. (1-19) gives a first impression that to synthesize a linear control law, which would meet even the elementary requirement that it be stable, might be a very difficult task. It turns out, however, that this is not the case. It is possible to mechanize a very simple linear, time-varying, feed-back control law which is stable and is closely related to the linear, constant-coefficient feedback used in the previous sections of this chapter. This linear control also suggests a possible control scheme using contactor control.

1. THE EQUATIONS OF MOTION IN MATRIX FORM

It is convenient to distinguish between the measured position of the ball, $\vec{r}_C$, viewed as a physical vector and $\underline{r}_C$ viewed as a 3×1 column matrix. This is helpful because while $\vec{r}_C$, as a vector, is invariant under a rotation of coordinates, its components are not, but are variant scalars which transform according to the law

$$\underline{r}_C = \underline{A} \, \underline{r}_C'$$

(3-76)

where $\underline{A}$ is a 3×3 direction cosine matrix which represents a coordinate rotation. Let $\underline{r}_C'$ denote the components of the vector, $\vec{r}_C$, resolved in a reference frame which is nonrotating with respect to inertial space, and $\underline{r}_C$ denote the components of $\vec{r}_C$ resolved in a reference frame which is fixed in the satellite. Under these circumstances $\underline{\dot{r}}_C$ ($\underline{\dot{r}}_C'$) will simply mean the 3×1 column matrix whose elements are the time derivatives of $\underline{r}_C(\underline{r}_C')$, and this notation will not imply from what frame vector differentiation is performed as in the case of the dot and circle notation for vectors. It is clear that $\underline{\dot{r}}_C(\underline{\dot{r}}_C')$ consists of the components of $\overset{\circ}{\vec{r}}_C(\overset{\cdot}{\vec{r}}_C)$ resolved in a reference frame which is fixed in the satellite (which is nonrotating with respect to inertial space).

In this notation, Eq. (1-6), or equivalently Eq. (1-19), assumes the form

$$\underline{\ddot{r}}_C' = \underline{f}_D' + \underline{f}_C'$$

(3-77)

in the nonrotating frame and

$$\underline{\ddot{r}}_C + 2\underline{\Omega} \, \underline{\dot{r}}_C + \underline{\dot{\Omega}} \, \underline{r}_C + \underline{\Omega}^2 \, \underline{r}_C = \underline{f}_D + \underline{f}_C$$

(3-78)

in the rotating frame.

The symbol

$$\underline{\Omega} \stackrel{\Delta}{=} \begin{pmatrix} 0 & -\omega_z & \omega_y \\ \omega_z & 0 & -\omega_x \\ -\omega_y & \omega_x & 0 \end{pmatrix} \qquad (3\text{-}79)$$

represents an antisymmetric matrix of angular velocities, which yields the components of $\vec{\omega}_S \times \vec{r}_C$ in the satellite reference frame when post-multiplied by r_C. Equation (3-78) is the matrix form of Eq. (1-19).

By differentiating Eq. (3-76) and comparing it, term by term, with the Coriolis law, $\cdot = {}^\circ + \vec{\omega}_S \times$, it may be shown that

$$\underline{\dot{A}} = -\underline{\Omega}\,\underline{A} \qquad (3\text{-}80)$$

and that

$$\underline{A}\,\underline{\dot{r}}'_C = \underline{\dot{r}}_C + \underline{\Omega}\,\underline{A}\,\underline{r}'_C = \underline{\dot{r}}_C + \underline{\Omega}\,\underline{r}_C . \qquad (3\text{-}81)$$

Equations (3-80) and (3-81) will be needed in the next section in order to transform the control law.

2.   TRANSLATION CONTROL WITH ARBITRARY $\vec{\omega}_S$

Just as Eqs. (3-1) were complicated because of the reference frame in which they were expressed, so also Eq. (3-78) takes on the simple form of Eq. (3-77) when written in a nonrotating reference frame. Because Eq. (3-77) is so simple, a control law will be found which stabilizes it; and this control law will be transformed back into the rotating reference fixed in the satellite. This is identical to the procedure employed in the first part of this chapter, except that now the full three-dimensional equations will be used.

If, as in the previous cases, a control of the form

$$\underline{f}'_C = - K_V \dot{\underline{r}}'_C - K_P \underline{r}'_C \qquad (3\text{-}82)$$

is selected for the nonrotating reference frame, the resulting equation of motion obtained from Eq. (3-77) is

$$\ddot{\underline{r}}'_C + K_V \dot{\underline{r}}'_C + K_P \underline{r}'_C = \underline{f}'_D . \qquad (3\text{-}83)$$

This equation breaks into three independent, second-order, linear, constant-coefficient, scalar equations, and the constant-control gains, K_V and K_P, may be chosen to give any desired second-order performance.

Equation (3-83) is not very useful, however; since the jets which apply $\underline{f}_C$ are fixed in the satellite; and since the satellite relative-position sensor measures $\underline{r}_C$ and not $\underline{r}'_C$. That is, the sensor measures the components of the ball's position in a reference frame fixed in the satellite, not one which is nonrotating with respect to inertial space. If, however, Eq. (3-82) is transformed into the satellite reference frame, the expression for the jet forces may be written in terms of the variables actually measured by the position sensor. Since $\vec{f}_C$ is a space vector, its components transform in the same manner as the components of $\vec{r}_C$. So that from Eqs. (3-76) and (3-82),

$$\underline{f}_C = \underline{A}\,\underline{f}'_C = - K_V\,\underline{A}\,\dot{\underline{r}}'_C \; - K_P\,\underline{A}\,\underline{r}'_C$$

$$= - K_V(\dot{\underline{r}}_C + \underline{\Omega}\,\underline{r}_C) \; - K_P\,\underline{r}_C , \qquad (3\text{-}84)$$

or (in ordinary vector notation)

$$\vec{f}_C = - K_V\,(\overset{\circ}{\vec{r}}_C + \vec{\omega}_S \times \vec{r}_C) - K_P\,\vec{r}_C . \qquad (3\text{-}85)$$

SEL-64-067

Thus to mechanize a linear translation system for arbitrary $\vec{\omega}_S$, it is only necessary to measure $\vec{\omega}_S$ (for example with body-fixed rate gyros) and to feed back control commands as dictated by Eq. (3-84) or (3-85). For example, the x component of the control law would be

$$f_{Cx} = - K_V[\dot{x}_C + \omega_y(t)z_C - \omega_z(t)y_C] - K_P x_C , \qquad (3-86)$$

and the control is completely specified in terms of the state variables $\underline{r}_C$ and $\dot{\underline{r}}_C$.

The complete equations of motion with the above linear control law then are given by

$$\ddot{\underline{r}}_C + (K_V + 2\underline{\Omega})\dot{\underline{r}}_C + (\underline{\Omega}^2 + \dot{\underline{\Omega}} + K_P + K_V\underline{\Omega})\underline{r}_C = \underline{f}_D , \qquad (3-87)$$

or (in physical vector notation)

$$\overset{\circ\circ}{\vec{r}}_C + (K_V + 2\vec{\omega}_S\times)\overset{\circ}{\vec{r}}_C + [\vec{\omega}_S \times \vec{\omega}_S\times + \dot{\vec{\omega}}_S\times + K_P + K_V \vec{\omega}_S\times]\vec{r}_C = \vec{f}_D . \qquad (3-88)$$

Viewed in the light of the entire Eqs. (3-87) or (3-88) the previous results are obvious, since Eq. (3-88) results from the transformation of the vector form of Eq. (3-83) by the Coriolis law $\bullet = \circ + \vec{\omega}_S\times$. The control may be obtained then, by merely separating out the terms which are multiplied by K_V or K_P in Eq. (3-88).

Thus, it can be seen that the complete absence of attitude control does not unduly complicate the mechanization of the drag-free satellite translation-control system.

Equation (3-83) is asymptotically stable for all positive K_P and K_V and the choice $K_V = 2\sqrt{K_P}$ yields three second-order, critically-damped systems. Since

$$\underline{r}_C = \underline{A} \ \underline{r}'_C , \qquad (3-76)$$

the system of equations represented by Eqs. (3-87) or (3-88) is also asymptotically stable for all positive K_p and K_V. Furthermore, although, strictly speaking, the concept of critical damping has no meaning for the system (3-87) or (3-88), the choice $K_V = 2\sqrt{K_p}$ implies that an interval of time equal to several multiples of $1/\sqrt{K_p}$ after an initial disturbance will find $\underline{r}_C$ and $\underline{\dot{r}}_C$ smaller in some sense than any other choice of the value of K_V as a function of K_p.

H. CONCLUSION

It has been shown that for a certain class of plants there exists a rather simple time-varying transformation which reduces a 2nth-order system to two uncoupled nth-order systems. For the special case where the resulting nth-order plant is time invariant, the methods of classical control theory can synthesize an asymptotically stable control. Furthermore, if the original plant is also time invariant, then the roots of its characteristic equation are obtained from the roots of the nth-order system by translation along the j axis in the s plane. In the case of the translation control of the drag-free satellite, the time-varying transformation which was used made very good intuitive sense; since it corresponded simply to working in an inertial reference frame. For the symmetric, spinning space vehicle, however, the transformation appears to have no intuitive meaning; since the frequency $n\beta/2$ corresponds to none of the physical parameters of the system; and since the equation

$$\ddot{\mu} + \frac{n^2\beta^2}{4}\mu = Q\, e^{j(1-\frac{n}{2})\beta t} \qquad (3\text{-}32)$$

describes the behavior of no related system.

All control problems which involve plants which may be generated from a tractable one-half-order system by Eq. (3-65) are amenable to this technique, and they have the common property that their characteristic roots may be generated by the transformation

$$s = s' \pm j\,\omega_s \, . \qquad (3\text{-}22)$$

However, apparently not all plants whose roots have this property may be treated by this method, since a similarity transformation designed to reduce the differential equations to a symmetric form, where they can be written as a single complex equation, may not be possible. This is true because, while all similar matrices have the same characteristic equation, not all matrices with the same characteristic equation are similar.

CHAPTER IV

SYSTEM TRAJECTORY ERRORS

The effects of various types of drag-free satellite system errors fall into two general classes: those which cause the satellite orbit to deviate from a truly drag-free trajectory and those which affect the control-system requirements. In order to investigate those errors which affect the trajectory, it is only necessary to consider Eq. (1-1) which describes the motion of the proof-mass alone.

$$m_B \; \ddot{\vec{r}}_B = \vec{F}_{GB} + \vec{F}_{SB} + \vec{F}_{PB} \tag{1-1}$$

or

$$\ddot{\vec{r}}_B = \vec{f}_{GB} + \vec{f}_{SB} + \vec{f}_{PB} \overset{\Delta}{=} \vec{f}_{GB} + \vec{f}_{DB} \; . \tag{4-1}$$

It is not necessary to consider the equation of the satellite itself, since it is assumed that the control system constrains the satellite to follow the ball. If $\vec{f}_{GB} + \vec{f}_{PB} \overset{\Delta}{=} \vec{f}_{DB}$ were zero, the satellite motion would be that of a satellite acted on only by gravity so that the additional effect of $\vec{f}_{DB}$ may be found by a perturbation analysis. While it is not necessary to do so, the analysis is greatly simplified if the actual motion is compared with a nominal circular orbit about a spherically-symmetric earth. The results of this type of analysis will be valid for orbits with eccentricities up to about 0.1 to 0.3.

As was pointed out in Chapter I in the derivation of Eqs. (1-72), (1-73), and (1-74), ξ and η may be interpreted either in a rectangular or in a cylindrical coordinate system. The latter is chosen (although it will be convenient to represent the figures in rectangular plots). That is, to accommodate those results which contain large secular terms in η, ξ and η shall connote cylindrical coordinates, which can be visualized by thinking of the η axis as being "wrapped around" the nominal circular orbit (19).

A. FREE-RESPONSE OF HILL'S ORBIT EQUATIONS

The equations of motion of the satellite linearized about a nominal circular orbit are

$$\ddot{\xi} - 3 \omega_0^2 \xi - 2 \omega_0 \dot{\eta} = f_{DB\xi} \qquad (1\text{-}72)$$

$$2 \omega_0 \dot{\xi} + \ddot{\eta} = f_{DB\eta} \qquad (1\text{-}73)$$

$$\ddot{\zeta} + \omega_0^2 \zeta = f_{DB\zeta} \quad . \qquad (1\text{-}74)$$

Equations (1-72) and (1-73) have the fundamental matrix[*]

$$
\begin{bmatrix} \xi(t) \\ \dot{\xi}(t) \\ \eta(t) \\ \dot{\eta}(t) \end{bmatrix}
=
\begin{bmatrix}
4-3c\omega_0 t & \dfrac{s\omega_0 t}{\omega_0} & 0 & \dfrac{2}{\omega_0}(1-c\omega_0 t) \\
3\omega_0 s\omega_0 t & c\omega_0 t & 0 & 2s\omega_0 t \\
6(s\omega_0 t-\omega_0 t) & \dfrac{2}{\omega_0}(c\omega_0 t-1) & 1 & \dfrac{1}{\omega_0}(4s\omega_0 t-3\omega_0 t) \\
6\omega_0(c\omega_0 t-1) & -2s\omega_0 t & 0 & 4c\omega_0 t-3
\end{bmatrix}
\begin{bmatrix} \xi_0 \\ \dot{\xi}_0 \\ \eta_0 \\ \dot{\eta}_0 \end{bmatrix} \quad . \qquad (4\text{-}2)
$$

The responses of Eq. (4-2) are plotted in Fig. 4-1 for various initial conditions.

---

[*]Note that Eq. (1-74) which corresponds to orbit tilt is uncoupled from Eqs. (1-72) and (1-73) and that its form is that of the well-known simple harmonic oscillator.

- 111 -
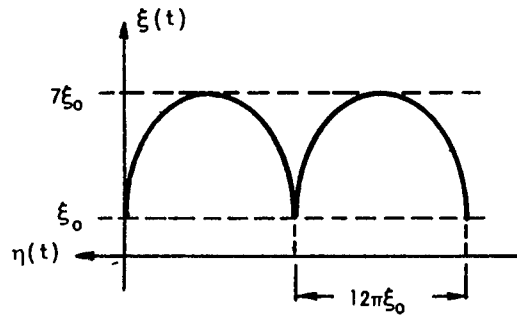
(η scale foreshortened) $\xi_0 \neq 0$, $\dot{\xi}_0 = \eta_0 = \dot{\eta}_0 = 0$

$$\Delta e = \frac{3\xi_0}{r_N} \ , \quad \Delta a = 4\xi_0, \quad \Delta T = \frac{12\pi\xi_0}{\omega_0 r_N} \ ,$$

to first order in e.
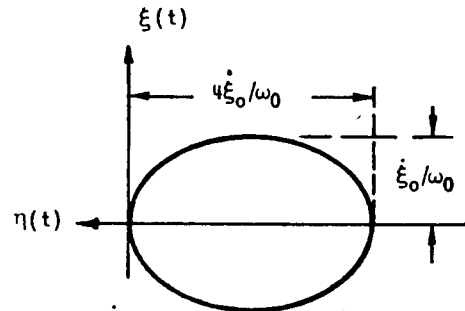
Change in perigee argument = $2\Delta e$

$\dot{\xi}_0 \neq 0$, $\xi_0 = \eta_0 = \dot{\eta}_0 = 0$

$$= \frac{2\dot{\xi}_0}{\omega_0 r_N} \ , \text{ to first order in e.}$$
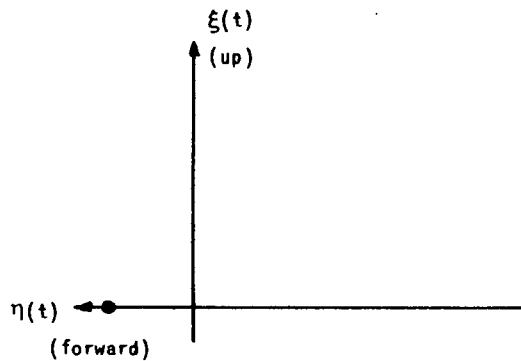
$\eta = \eta_0$ $\eta_0 \neq 0$, $\xi_0 = \dot{\xi}_0 = \dot{\eta}_0 = 0$

$\dot{\eta}_0 \neq 0$, $\xi_0 = \dot{\xi}_0 = \eta_0 = 0$
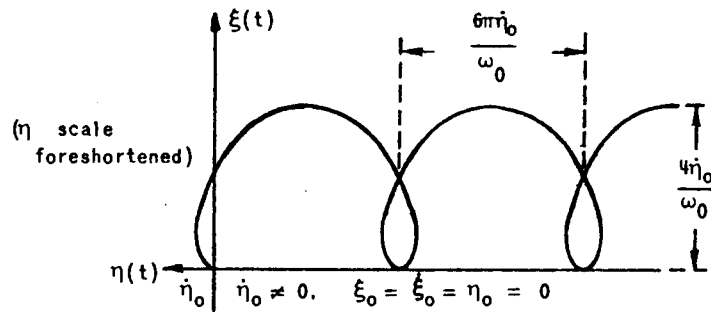
$$\Delta e = \frac{2\dot{\eta}_0}{\omega_0 r_N} \ , \quad \Delta a = \frac{2\dot{\eta}_0}{\omega_0} \ , \quad \Delta T = \frac{6\pi\dot{\eta}_0}{\omega_0 r_N} \ ,$$

to first order in e.

FIG. 4-1. MOTION RELATIVE TO A NOMINAL CIRCULAR ORBIT FOR VARIOUS RELATIVE INITIAL CONDITIONS (VIEW LOOKING IN ALONG ζ)

Either from Eq. (4-2) or Fig. 4-1 or by examination of the characteristic equation of Eqs. (1-72) and (1-73), $s^2(s^2 + \omega_0^2) = 0$, it may be seen that the free response of these equations consists of oscillations at orbit frequency plus a secular response in η which grows proportionally to t. Physically, it is obvious that if the satellite were started in a higher or lower orbit with an initial velocity equal to circular velocity at that altitude, the resulting motion would correspond to excitation of the response which corresponds to the s^2 term in the characteristic equation. It is also obvious that if the satellite were in a slightly elliptical orbit with the same period as that of the nominal orbit, the motion would contain no secular terms in t; and that this motion would correspond to the $s^2 + \omega_0^2$ term in the characteristic equation. These results may be seen analytically by inserting initial conditions which correspond to motion in a higher or lower circular orbit or initial conditions which correspond to elliptical motion with period, $2\pi/\omega_0$, into Eq. (4-2) and noting that only the terms corresponding to s^2 or to $s^2 + \omega_0^2$, respectively, appear.

These heuristic arguments may be made rigorous by considering the normal modes of Eqs. (1-72) and (1-73). The pair of normal modes corresponding to the $s^2 = 0$ roots give the initial conditions for a higher or lower circular orbit, and the pair of normal modes corresponding to the roots, $s^2 + \omega_0^2 = 0$, give initial conditions for slightly elliptical motion with period, $2\pi/\omega_0$.

The transformation to normal coordinates is

$$\underline{\alpha} = \underline{T}\, \underline{\xi} \qquad\qquad (4\text{-}3)$$

or

$$
\begin{bmatrix} \alpha_1 \\ \alpha_2 \\ \alpha_3 \\ \alpha_4 \end{bmatrix}
=
\begin{bmatrix}
2\omega_0 & 2 & -\omega_0 & 1 \\
6\omega_0^2 & 0 & 0 & 3\omega_0 \\
3\omega_0 & 1 & 0 & 2 \\
3\omega_0 & -1 & 0 & 2
\end{bmatrix}
\begin{bmatrix} \xi \\ \dot{\xi} \\ \eta \\ \dot{\eta} \end{bmatrix} .
\tag{4-4}
$$

Equation (4-4) changes the first-order form of the differential Eqs. (1-72) and (1-73) which is

$$
\dot{\underline{\xi}} = \underline{F}\,\underline{\xi} + \underline{D}\,\underline{u}
\tag{4-5}
$$

or

$$
\begin{bmatrix} \dot{\xi} \\ \ddot{\xi} \\ \dot{\eta} \\ \ddot{\eta} \end{bmatrix}
=
\begin{bmatrix}
0 & 1 & 0 & 0 \\
3\omega_0^2 & 0 & 0 & 2\omega_0 \\
0 & 0 & 0 & 1 \\
0 & -2\omega_0 & 0 & 0
\end{bmatrix}
\begin{bmatrix} \xi \\ \dot{\xi} \\ \eta \\ \dot{\eta} \end{bmatrix}
+
\begin{bmatrix}
0 & 0 \\
1 & 0 \\
0 & 0 \\
0 & 1
\end{bmatrix}
\begin{bmatrix} f_{DB\xi} \\ f_{DB\eta} \end{bmatrix} ,
\tag{4-6}
$$

into the form

$$\underline{\dot{\alpha}} = \underline{F}^D \underline{\alpha} + \underline{D}^D \underline{u} \qquad (4\text{-}7)$$

$$\begin{bmatrix} \dot{\alpha}_1 \\ \dot{\alpha}_2 \\ \dot{\alpha}_3 \\ \dot{\alpha}_4 \end{bmatrix} = \begin{bmatrix} 0 & 1 & 0 & 0 \\ 0 & 0 & 0 & 0 \\ 0 & 0 & 0 & \omega_0 \\ 0 & 0 & -\omega_0 & 0 \end{bmatrix} \begin{bmatrix} \alpha_1 \\ \alpha_2 \\ \alpha_3 \\ \alpha_4 \end{bmatrix} + \begin{bmatrix} 2 & 1 \\ 0 & 3\omega_0 \\ 1 & 2 \\ -1 & 2 \end{bmatrix} \begin{bmatrix} f_{DB\xi} \\ f_{DB\eta} \end{bmatrix} \qquad (4\text{-}8)$$

where

$$\underline{F}^D = \underline{T} \, \underline{F} \, \underline{T}^{-1} \qquad (4\text{-}9)$$

and

$$\underline{D}^D = \underline{T} \, \underline{D} \, . \qquad (4\text{-}10)$$

The free responses of Eq. (4 -8) are

$$\alpha_1(t) = \alpha_{1o} + \alpha_{2o} t \qquad (4\text{-}11)$$

$$\alpha_2(t) = \alpha_{2o}$$

which corresponds to circular motion in a higher or lower orbit, and

$$\alpha_3(t) = \alpha_{3o} \, c\omega_0 t + \alpha_{4o} \, s\omega_0 t$$

(4-12)

$$\alpha_4(t) = -\alpha_{3o} \, s\omega_0 t + \alpha_{4o} \, c\omega_0 t,$$

which corresponds to an elliptic orbit with the same period as the nominal orbit.

B. FORCED RESPONSE OF HILL'S ORBIT EQUATIONS

To analyze the effects of f_{DB} on the ball's trajectory, it is necessary to consider the response of Eqs. (1-72), (1-73), and (1-74) to two cases.

1. $\vec{f}_{DB}$ CONSTANT IN THE ξ, η, ζ REFERENCE FRAME

If

$$\vec{f}_{DB} = \begin{pmatrix} f_{DB\xi o} \\ f_{DB\eta o} \\ f_{DB\zeta o} \end{pmatrix} \triangleq \begin{pmatrix} f_{\xi o} \\ f_{\eta o} \\ f_{\zeta o} \end{pmatrix},$$

(4-13)

then for $\xi_o = \dot{\xi}_o = \eta_o = \dot{\eta}_o = 0$,

$$\xi(t) = \frac{f_{\xi o}}{\omega_0^2} (1 - c\omega_0 t) + \frac{2f_{\eta o}}{\omega_0^2} (\omega_0 t - s\omega_0 t)$$

(4-14)

$$\eta(t) = \frac{-2f_{\xi o}}{\omega_0^2} (\omega_0 t - s\omega_0 t) + \frac{f_{\eta o}}{\omega_0^2} \left[4(1 - c\omega_0 t) - \frac{3}{2} \omega_0^2 t^2 \right]$$

(4-15)

$$\zeta(t) = \frac{f_{\zeta o}}{\omega_0^2} (1 - c\omega_0 t).$$

(4-16)

SEL-64-067

If $\omega_0 t \ll 1$; $\xi(t) = 1/2\, f_{\xi o} t^2$, $\eta(t) = 1/2\, f_{\eta o} t^2$, and $\zeta(t) = 1/2 f_{\zeta o} t^2$, which is to be expected. If the constant terms and the short period terms $\Delta\omega_0 t$ and $c\omega_0 t$ are omitted, the remaining secular growth terms are

$$\xi(t) = + \frac{2f_{\eta o}}{\omega_0} t \qquad (4\text{-}17)$$

$$\eta(t) = - \frac{2f_{\xi o}}{\omega_0} t - \frac{3}{2} f_{\eta o} t^2 . \qquad (4\text{-}18)$$

The time can be eliminated between Eqs. (4-17) and (4-18) to yield the equation of the mean path

$$\left(\eta - \frac{2}{3} \frac{f_{\xi o}^2}{\omega_0^2\, f_{\eta o}} \right) = - \frac{3\omega_0^2}{8f_{\eta o}} \left(\xi + \frac{4}{3} \frac{f_{\xi o}}{\omega_0^2} \right)^2 . \qquad (4\text{-}19)$$

The degenerate case, where $f_{\xi o} = 0$, yields the path equation

$$\eta = - \frac{3\omega_0^2}{8f_{\eta o}} \xi^2 . \qquad (4\text{-}20)$$

These results are plotted in Figs. 4-2 through 4-8. Figures 4-2, 4-3, and 4-4 and Figs. 4-6, 4-7, and 4-8 each show their respective cases merely in different scale. This is done to illustrate various features of the motion that could not be brought out in a single drawing.

It is interesting to note that Eq. (4-16) has no secular terms, but that the effect of $f_{\zeta o}$ is merely to hold the orbit plane at an offset angle $f_{\zeta o}/\omega_0^2\, r_N$. If, however, the orbit is eccentric, and one considers the full nonlinear Eqs. (1-86), (1-87), and (1-88), secular terms occur which are proportional to the various powers of e. For example, the second-order equations
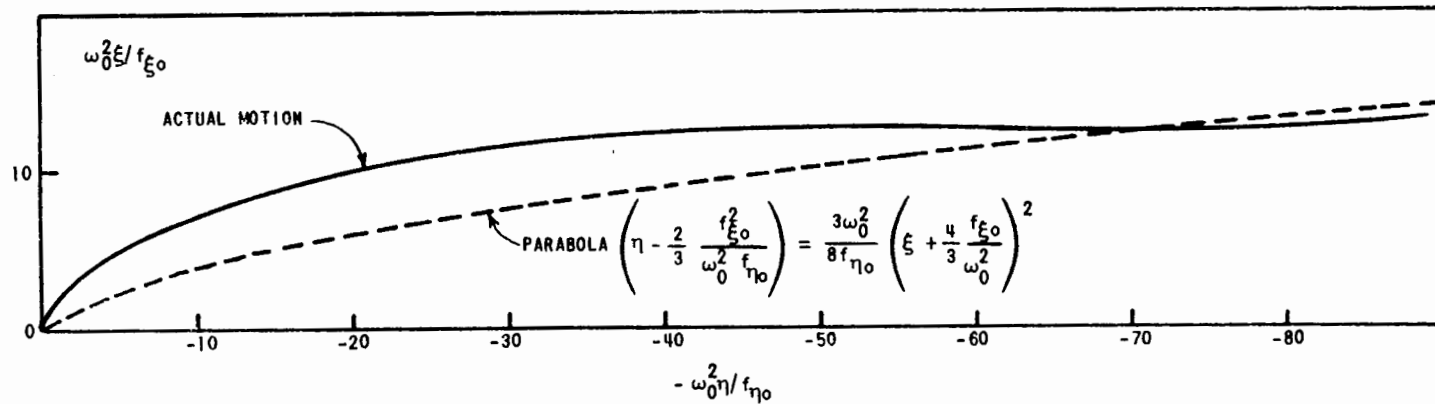
FIG. 4-2. RELATIVE PERTURBED MOTION, $\vec{f}_{DB}$ CONSTANT IN THE ξ,η FRAME. DRAWN FOR $f_{\xi o} = f_{\eta o}$ (SCALE 20 TIMES THAT OF FIG. 4-3)
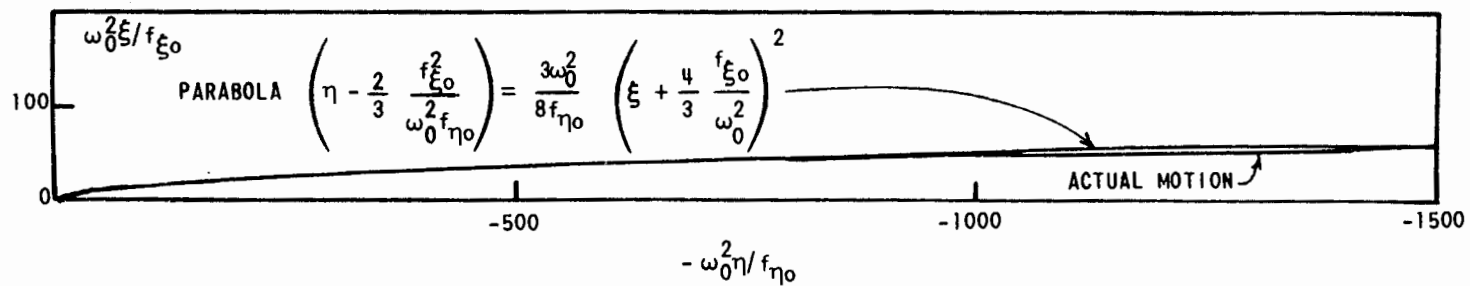
FIG. 4-3. RELATIVE PERTURBED MOTION, $\vec{f}_{DB}$ CONSTANT IN THE ξ,η FRAME. DRAWN FOR $f_{\xi o} = f_{\eta o}$ (SCALE 1/20 THAT OF FIG. 4-2)
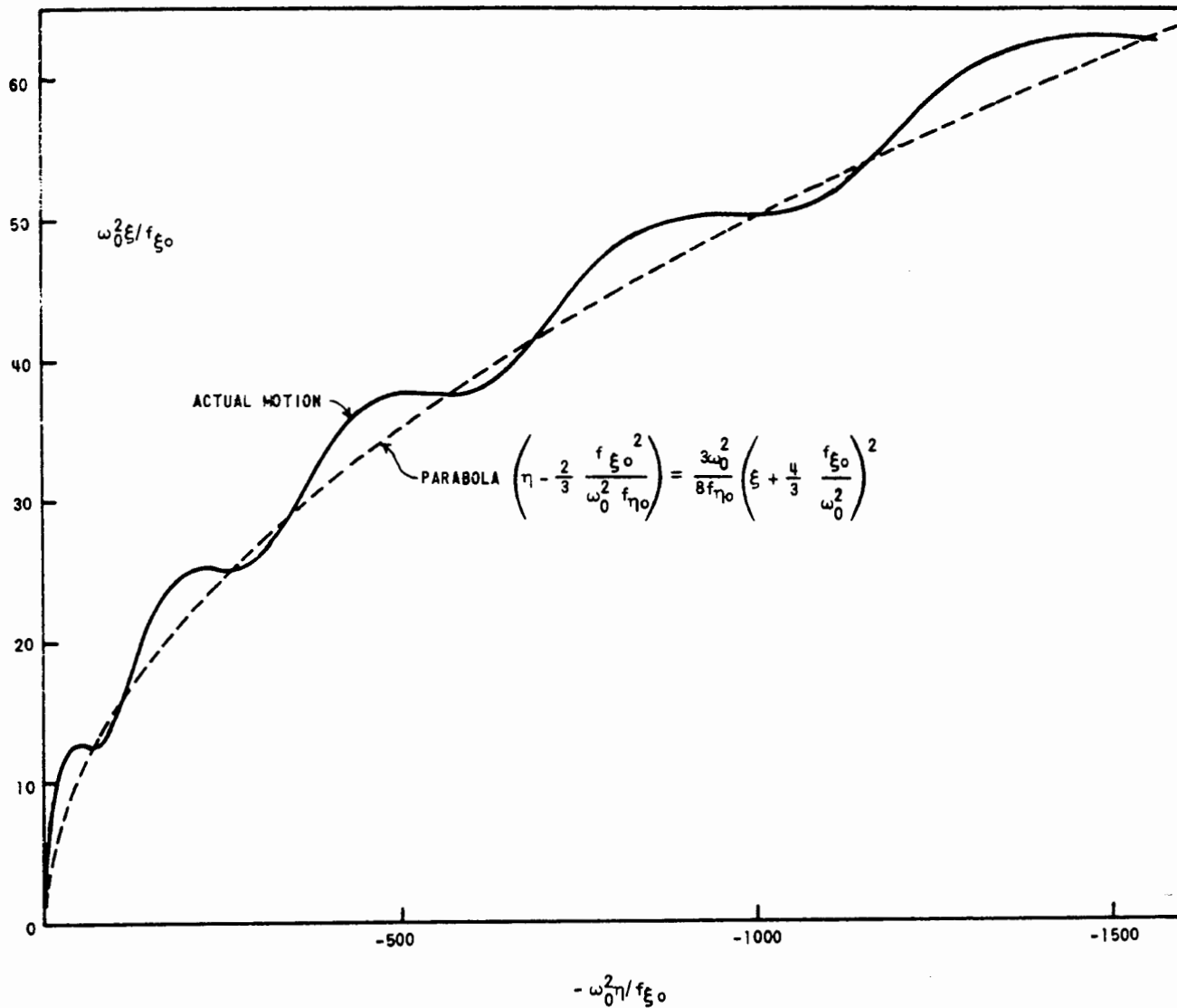
FIG. 4-4. RELATIVE PERTURBED MOTION, $\vec{f}_{DB}$ CONSTANT IN THE ξ, η FRAME. DRAWN FOR $f_{\xi o} = f_{\eta o}$ (NOTE THAT HORIZONTAL SCALE IS 1/20 OF THE VERTICAL SCALE TO EXAGGERATE SHORT PERIOD EFFECTS)
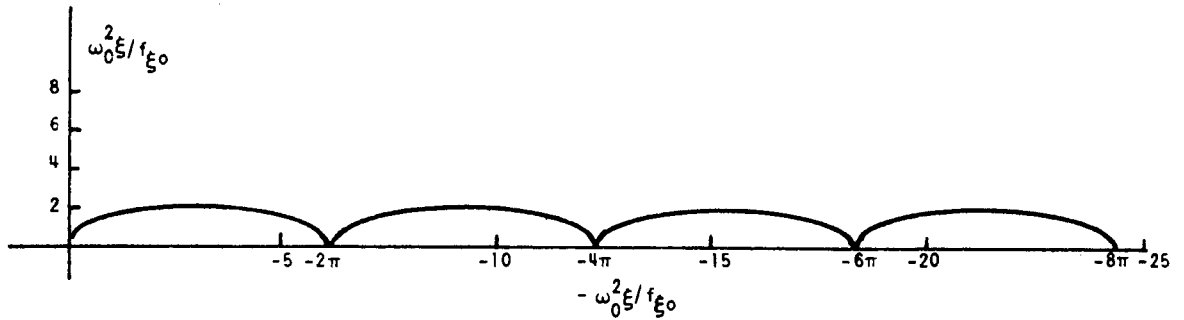
FIG. 4-5. RELATIVE PERTURBED MOTION, $\vec{f}_{DB}$ CONSTANT IN THE ξ, η FRAME — DEGENERATE CASE, $f_{\xi o} \neq 0$, $f_{\eta o} = 0$
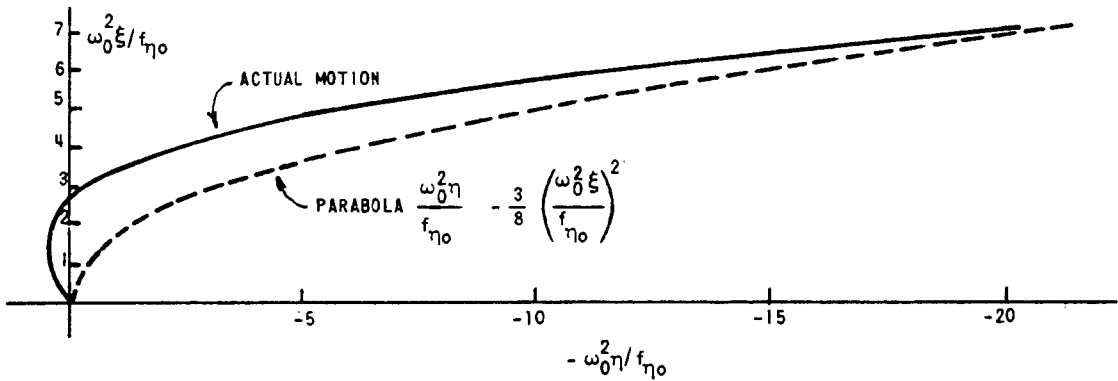
FIG. 4-6. RELATIVE PERTURBED MOTION, $\vec{f}_{DB}$ CONSTANT IN THE ξ, η FRAME — DEGENERATE CASE, $f_{\xi o} = 0$, $f_{\eta o} \neq 0$ (SCALE 10 TIMES THAT OF FIG. 4-7)
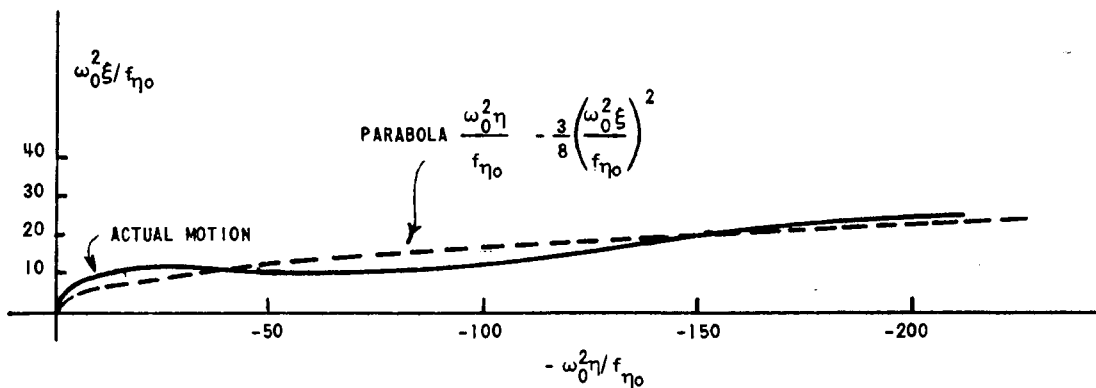
FIG. 4-7. RELATIVE PERTURBED MOTION, $\vec{f}_{DB}$ CONSTANT IN THE ξ, η FRAME — DEGENERATE CASE, $f_{\xi o} = 0$, $f_{\eta o} \neq 0$ (SCALE 1/10 THAT OF FIG. 4-6)
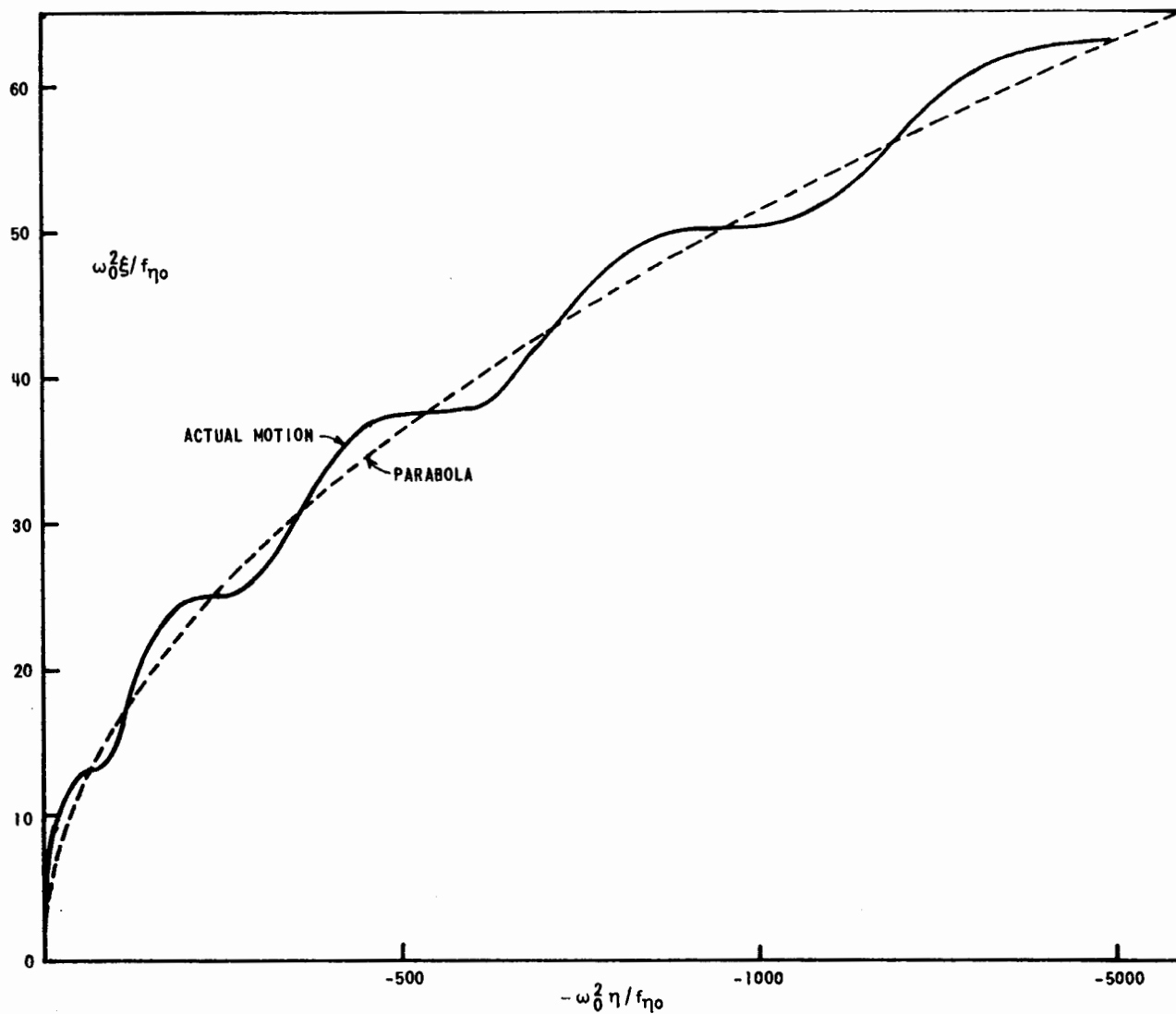
FIG. 4-8. RELATIVE PERTURBED MOTION, $\vec{f}_{DB}$ CONSTANT IN THE ξ, η FRAME —
DEGENERATE CASE, $f_{\xi o} = 0$ (NOTE THAT HORIZONTAL SCALE IS 1/20 OF THE
VERTICAL SCALE TO EXAGGERATE SHORT PERIOD EFFECTS)

FIG. 4-9. RELATIVE PERTURBED MOTION, $\vec{f}_{DB}$ CONSTANT IN INERTIAL SPACE. $\vec{f}_{DB}$ INITIALLY ALONG ξ.

PATH FOR

$f_{\xi I} = 0. \quad f_{\eta I} \neq 0$

$\dfrac{\omega_0^2 \xi}{f_{\eta I}}$

$\omega_0 t = 5\pi$

$\omega_0 t = 3\pi$

$\dfrac{\omega_0^2 \eta}{f_{\eta I}} = -10$

$\omega_0 t = \pi$

$\dfrac{\omega_0^2 \eta}{f_{\eta I}}$

$\omega_0 t = 9\pi/2$ $\omega_0 t = 5\pi/2$ $\omega_0 t = \pi/2$

$3/2$

$\omega_0 t = 3\pi/2$ $\omega_0 t = 7\pi/2$ $\omega_0 t = 11\pi/2$

$3/2$

$\omega_0 t = 2\pi$

$\omega_0 t = 4\pi$

$\omega_0 t = 6\pi$

$e = \dfrac{\xi_{max}}{r_N} \approx \dfrac{3}{2} \dfrac{f_{\eta I} t}{\omega_0 r_N}$

$\text{ARGUMENT OF PERIGEE} = \dfrac{\langle \eta \rangle_{av}}{r_N} = -\dfrac{5}{2} \dfrac{f_{\eta I}}{\omega_0^2 r_N}$
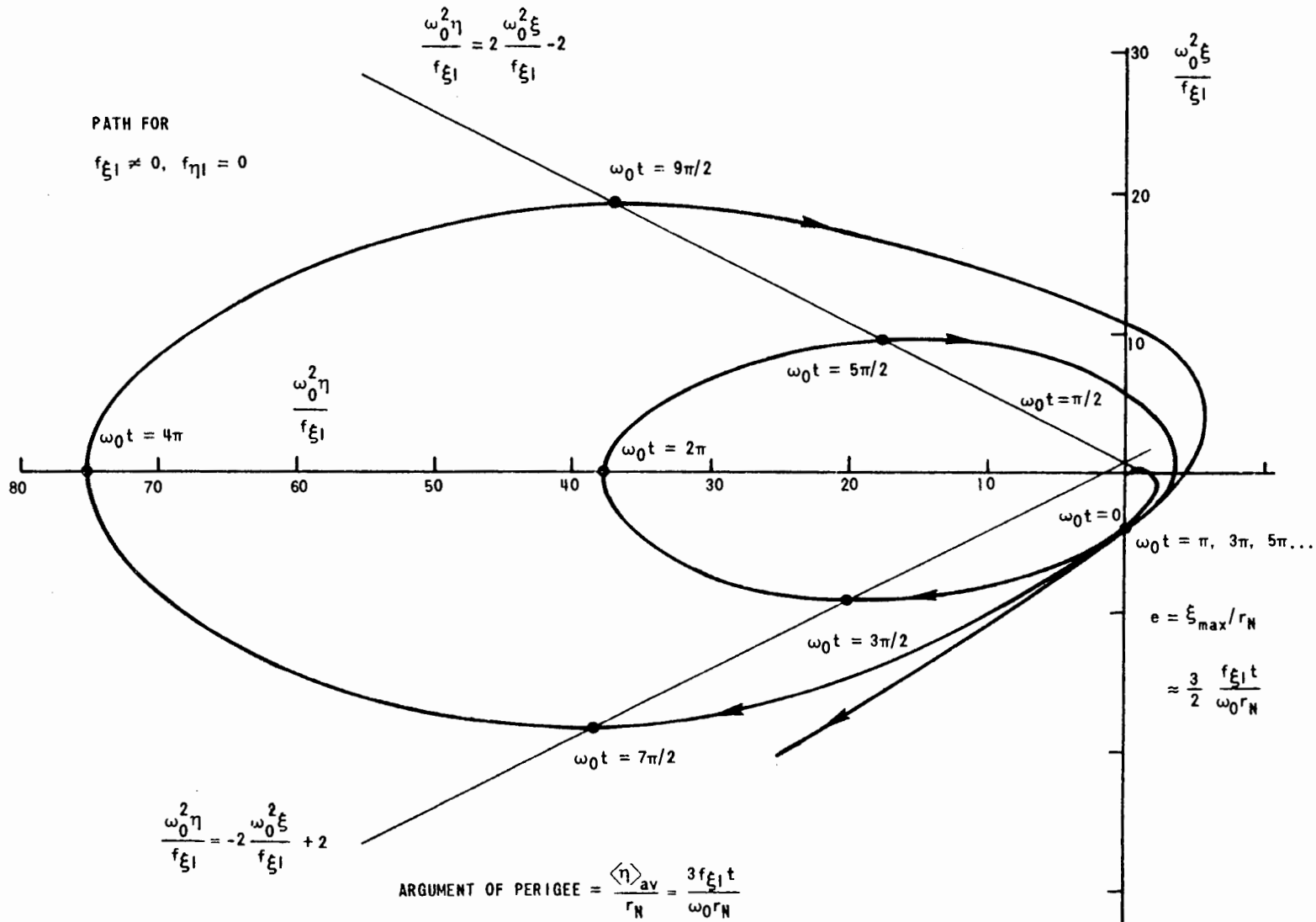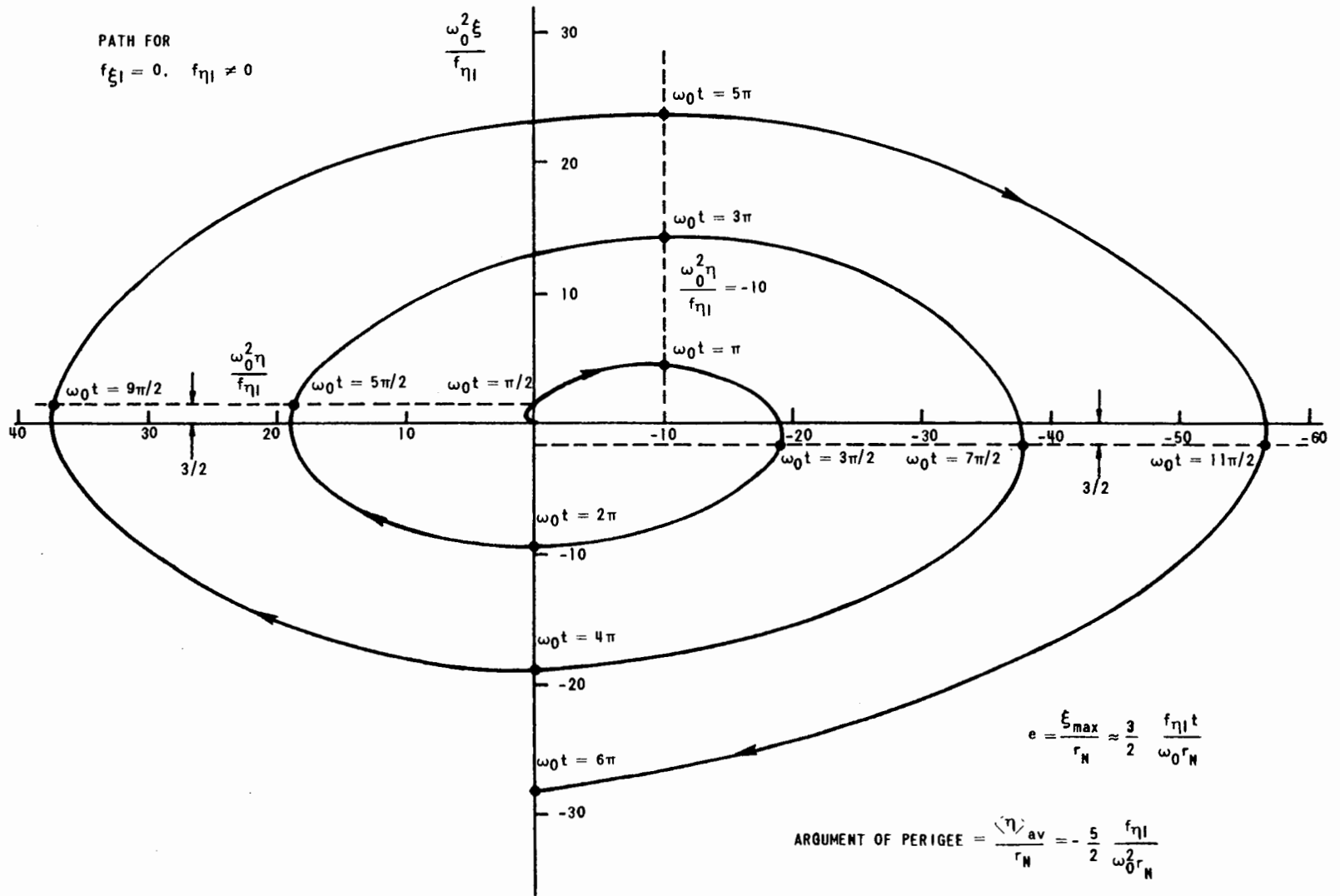
FIG. 4-10. RELATIVE PERTURBED MOTION, $\vec{f}_{DB}$ CONSTANT IN INERTIAL SPACE. $\vec{f}_{DB}$ INITIALLY ALONG η.

$$\ddot{\zeta} + \omega_0^2 \zeta = f_{\zeta o} + \frac{3\omega_0^2}{r_N} \xi\zeta \tag{4-21}$$

and

$$\xi(t) = \xi_0 \, c\omega_0 t \tag{4-22}$$

have the additional secular term (to first order in e)

$$\zeta(t) = -\frac{3e}{2} \frac{f_{\zeta o} t}{\omega_0} c\omega_0 t \ . \tag{4-23}$$

This corresponds to a slow rotation of the orbit plane at a rate,
$3e \, f_{\zeta o}/2\omega_0 r_N$. Similar results also exist for the nonlinear terms in
Eqs. (1-76) and (1-77); however, for sufficiently small t, their
effect on the satellite orbit may be neglected.

2. $\vec{f}_{DB}$ CONSTANT IN AN INERTIAL REFERENCE FRAME (ROTATING IN THE ξ, η, ζ
    FRAME)

$$\vec{f}_{DB} = \begin{pmatrix} f_{DB\xi I} \\ f_{DB\eta I} \\ f_{DB\zeta I} \end{pmatrix}_{Inertial} = \begin{pmatrix} f_{\xi I} \\ f_{\eta I} \\ f_{\zeta I} \end{pmatrix}_{Inertial} \tag{4-24}$$

$$= \begin{pmatrix} f_{\xi I} c\omega_0 t + f_{\eta I} s\omega_0 t \\ -f_{\xi I} s\omega_0 t + f_{\eta I} c\omega_0 t \\ f_{\zeta I} \end{pmatrix}_{\xi, \eta, \zeta} \tag{4-25}$$

Then for $\xi_0 = \dot{\xi}_0 = \eta_0 = \dot{\eta}_0 = 0$,

$$\xi(t) = \frac{f_{\xi I}}{\omega_0^2} \left[\frac{3}{2} \omega_0 t s\omega_0 t - 2(1 - c\omega_0 t) \right] + \frac{3}{2} \frac{f_{\eta I}}{\omega_0^2} \left[s\omega_0 t - \omega_0 t \, c\omega_0 t \right] \tag{4-26}$$

$$\eta(t) = \frac{f_{\xi I}}{\omega_0^2} \left[3\omega_0 t - 6 s\omega_0 t + 3\omega_0 t \, c\omega_0 t \right] + \frac{f_{\eta I}}{\omega_0^2} \left[3\omega_0 t s\omega_0 t - 5(1 - c\omega_0 t) \right] \tag{4-27}$$

$$\zeta(t) = \frac{f_{\zeta I}}{\omega_0^2} (1 - c\omega_0 t). \tag{4-16}$$

Again, if $\omega_0 t \ll 1$, $\xi(t) = 1/2 \, f_{\xi I} t^2$, and $\eta(t) = 1/2 \, f_{\eta I} t^2$.

The above results are shown in Figs. 4-9 and 4-10 for motion relative to the ξ,η frame; and in Fig. 4-11, the motion for several orbits is shown from the point of view of an inertial reference frame with $f_{\xi I} \neq 0$ and $f_{\eta I} = 0$.[*]

---

[*] It is rather interesting to note that in the case where $f_{\xi I} = 0$ and $f_{\eta I} \neq 0$, there is no first-order rotation of perigee (i.e., the secular term $3\omega_0 t$ is multiplied by $\Delta\omega_0 t$; whereas with $f_{\xi I} \neq 0$ and $f_{\eta I} = 0$ there is a secular term $3\omega_0 t$, which corresponds to a secular rotation of perigee at rate $3f_{\xi I}/\omega_0 r_N$. The intuitive or "physical reason" for this is that when $\vec{f}_{DB}$ begins parallel to the ξ axis, there is an initial component of force in the minus η direction for $180°$ of rotation; whereas when $\vec{f}_{DB}$ begins parallel to the η axis, the disturbing force is initially along plus η for only $90°$. In the first case, an average velocity term along the positive η axis builds up and is not cancelled by subsequent rotations, but there is not sufficient time for this to happen in the latter case. This can be seen mathematically by differentiating Eq. (4-27) to obtain the η velocity,

$$\dot{\eta}(t) = \frac{3f_{\xi I}}{\omega_0}\left[(1-c\omega_0 t) - 3\omega_0 t\Delta\omega_0 t\right] + \frac{f_{\eta I}}{\omega_0}\left[3\omega_0 t c\omega_0 t - 2\Delta\omega_0 t\right] \quad (4-28)$$

which has the constant term $3f_{\xi I}/\omega_0$.
(It is also interesting to note that an initial force acting for $180°$ along the negative η axis causes a net velocity to build up along the positive η axis. This is, of course, what would be expected from classical orbit mechanics.)
    The above situation is closely related to the motion of a point mass under the influence of a constant rotating force. (This is the model which is often used for the effect on the trajectory of a thrust vector misalignment on a spinning rocket in vacuum.) Here the equations of motion

$$\ddot{x} = fc\omega_0 t \quad \text{and} \quad \ddot{y} = f\Delta\omega_0 t \quad (4-29)$$

integrate to

$$\dot{x} = f\frac{\Delta\omega_0 t}{\omega_0} \quad \text{and} \quad \dot{y} = f\frac{1-c\omega_0 t}{\omega_0}, \quad (4-30) \text{ and } (4-31)$$

and

$$x = f\frac{1-c\omega_0 t}{\omega_0^2}, \quad y = f\frac{\omega_0 t - \Delta\omega_0 t}{\omega_0^2} \quad (4-32) \text{ and } (4-33)$$

when the initial conditions are zero.
(footnote continued on next page)
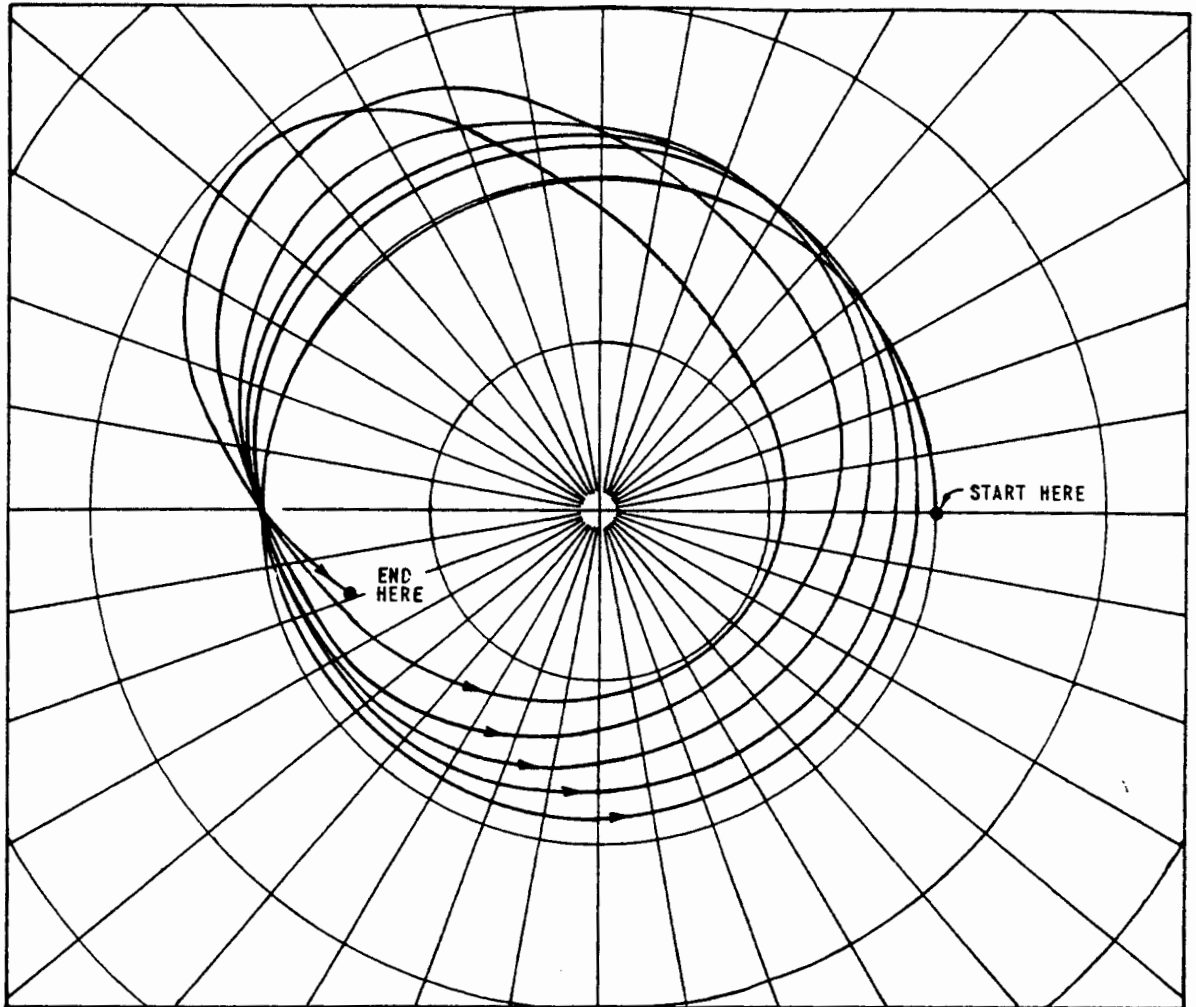
FIG. 4-11.   ORBIT PERTURBATION FOR $\vec{f}_{DB}$ CONSTANT IN INERTIAL SPACE AND
INITIALLY ALONG ξ .   DRAWN IN AN INERTIAL REFERENCE FRAME
WITH THE EFFECT GREATLY EXAGGERATED.   (NOTE INCREASING
ECCENTRICITY AND ROTATION OF THE LINE OF APSIDES.)

---

* (footnote continued from page 124)

There is a secular term in y so that the average motion pro-
ceeds in a direction 90° away from the point where the force was first
turned on.   This happens because initially the force acts in the y
direction for 180° of rotation and in the x direction for only 90°
of rotation.   A net velocity is initially built up along y which is
not cancelled by subsequent rotations, but there is not sufficient
time for this to happen along x.

C. APPLICATION TO THE DRAG-FREE SATELLITE

The forces which give rise to $\vec{f}_{DB}$ are of two basic types: those which are constant in the satellite reference frame (for a given relative position of the ball) and those which are essentially constant in an inertial reference frame. Thus the effect of the disturbances depends on the type of attitude control applied to the satellite.

1. SATELLITE ATTITUDE CONTROLLED TO A LOCALLY-LEVEL REFERENCE FRAME

When the satellite attitude control system keeps the vehicle locally level, the disturbances do not rotate in the ξ, η frame and the results of case one, page 115, apply. The dominant secular terms are

$$\xi(t) = 2f_{\eta o} t/\omega_O \tag{4-17}$$

$$\eta(t) = -2f_{\xi o} t/\omega_O - (3/2)f_{\eta o} t^2. \tag{4-18}$$

If $f_{\xi o}$ and $f_{\eta o} \approx 10^{-11} g_e \approx 10^{-10} m/sec^2{}^*$, $t = 1$ year $\approx 3 \times 10^7$ sec**, and $\omega_O \approx 10^{-3}$ rad/sec; then

$$f_{\eta o} t^2 \approx 10^5 \ m \approx 300,000 \ feet \approx 60 \ miles \tag{4-34}$$

and

$$2f_{\xi o} t/\omega_O \ or \ 2f_{\eta o} t/\omega_O = 6 \ m \approx 20 \ feet. \tag{4-35}$$

---

* See Table 4-1.
** The length of time for which the results of the linear perturbation analysis of the previous pages may be safely extrapolated depands on the effects of the nonlinear terms which have been neglected. These neglected terms will, in general, give rise to terms in the solution containing powers of $e \ \omega_O t$, and they may be neglected if $e \ \omega_O t \ll 1$. For an exactly circular initial orbit, e remains less than 10^{-6} for the case of Eq.(4-35); and a one year extrapolation appears reasonable. The results implied by the circular-orbit linear analysis are not valid for one year however if the initial conditions correspond to eccentricities of the order of 0.01. This does not imply that the results of this section are incorrect for eccentricities of this order, but merely that they do not follow from the previous considerations. If the satellite equations are linearized about a nominal elliptical orbit (linear form of Encke's method) and integrated numerically for one orbit period, the periodic part of the fundamental matrix may be factored from the part which grows with time and the effect of the perturbations for one year may be computed. When this is done, it is now Δe which remains less than 10^{-6} and the neglected terms are not significant. The results of this type of analysis are essentially the same as the circular orbit calculations.

Since a sizable component of the disturbance is almost certain to appear along η, this is clearly the worst case and can result in very large deviations from a drag-free orbit.

2. SATELLITE ATTITUDE CONTROLLED TO AN INERTIALLY-NONROTATING REFERENCE FRAME (VERY PRECISE GYROSCOPE EXPERIMENTS)

Here case two, page 122, applies and since the dominant secular terms

$$\xi(t) = \frac{3}{2} \frac{f_{\xi I}}{\omega_0} t \, \mathcal{J}\omega_0 t - \frac{3}{2} \frac{f_{\eta I}}{\omega_0} t \, c\omega_0 t \qquad (4\text{-}36)$$

$$\eta(t) = 3 \frac{f_{\xi I}}{\omega_0} t(1+c\omega_0 t) + 3 \frac{f_{\eta I}}{\omega_0} t \, \mathcal{J}\omega_0 t \qquad (4\text{-}37)$$

only increase as t and not as t^2, the deviation from a drag-free orbit can probably be limited to only a few meters per year, unless a capacitive pick-up is used as the position sensor. With a capacitive pick-up the disturbances are large enough that errors of several kilometers per year might develop.[*]

3. SATELLITE SPINNING WITH THE SPIN VECTOR NORMAL TO THE ORBIT PLANE (GEODESY, AERONOMY, AND LOW PRECISION GYROSCOPE EXPERIMENTS)

If the satellite spins with an angular velocity held normal to the orbit plane with ω_0, the effects of those forces, which are fixed in the satellite and which are not modulated at the spin rate, average to zero except along the spin axis.

Examples of forces which do not average to zero are provided by any force whose magnitude depends on the ball's position relative

---

[*] See Table 4-1.

to the satellite (since r_{SC} will not be zero and the force will be modulated at the satellite spin rate) and by the force due to the motion of a charged ball through the earth's magnetic field and the electric image attraction force (which are not fixed in the satellite). Nevertheless, with the exception of the capacitive pick-up (which can be replaced with an optical pick-up) and the non-spinning forces (which are small), the effect of the dominant disturbing acceleration (which is due to vehicle gravity) can either be attenuated by a factor of e (since Eq. (4-21) applies when the spin is normal to the orbit[*]) or by a factor equal to the percent modulation of the gravitational force at spin frequency (whichever is larger) by spinning the satellite with the spin vector normal to the orbit plane.

Under the above circumstances, the departure of the satellite from an orbit which would be caused by gravity alone could possibly be limited to only a meter/year or so, and this would truly be a drag-free satellite.

D. **CAUSES AND MAGNITUDES OF** $\vec{f}_{DB}$

The terms $\vec{f}_{SB}$ and $\vec{f}_{PB}$ act on the ball and perturb its orbit, and each source of these errors must be examined.

$\vec{f}_{SB}$ is due to:

  1) gravitational attraction of the vehicle on the proof-mass,

  2) electromagnetic forces due to stray fields in the satellite and due to stray and induced charge and magnetic moment on the proof mass,

  3) forces due to sensing the position of the proof-mass. (these can arise from optical radiation pressure or electric attraction from a capacitive pick-off), and

---

[*]It should be noted that the accuracy of this alignment need only be maintained to a factor of e.

4) gas in the satellite cavity.

$\vec{f}_{PB}$ can only arise from electromagnetic forces or possibly very energetic particle radiation since the cavity physically isolates the proof-mass from other outside disturbances.

If the control system acts to center the ball at a position where $\vec{f}_{SB} + \vec{f}_{PB} \neq 0$, the acceleration error of the satellite will be

$$\vec{f}_{SB} + \vec{f}_{PB} \triangleq \vec{f}_{DB} . \qquad (4\text{-}38)$$

For ease of comparison, all translation error forces will be expressed in terms of their corresponding accelerations of the proof-mass. The relative accelerations between the vehicle and the proof-mass are un-important except as they effect the mechanization of the control.

The sources and relative magnitudes of the various errors are summarized in Table 4-1. Typical numbers are computed for a drag-free satellite that could be used for a combined geodesy and aeronomy mission. The satellite and proof-mass are assumed to have the following typical parameters:

Nominal satellite size	$2d$ = 0.61 meters = 2 feet
Satellite mass	= 45.5 kg. = 3.12 slugs
Satellite weight	= 445 ntns = 100 lbs
Cavity radius	d_1 = 3 cm
Proof-mass radius	R_B = 2 cm
Proof-mass material	Copper
Proof-mass mass	= 0.30 kg.
Proof-mass weight	= 2.9 ntns = 0.66 lbs

The derivations of the equations in Table 4-1 and their underlying assumptions will be discussed in this section.

TABLE 4-1

ERROR SOURCES WHICH DISTURB THE ORBIT OF THE PROOF-MASS

SOURCE OF f_{SB} OR f_{PB} DISTURBANCE	RELATION	KEY MAGNITUDES	TYPICAL VALUES (acceleration in g_e's)
Vehicle Gravity	$f/g_e = 0.7 \times 10^{-10} \left(\dfrac{r_{ZB}}{d_1} \right)$	$\dfrac{r_{ZB}}{d_1} = 0.1$	10^{-11}*
Leakage Electric Field in the Cavity	$f/g_e = \dfrac{3\epsilon_o V_B E}{g_e \rho_m R_B^2}$	$V_B = 1$ volt $q_B = 2.2 \times 10^{-12}$ coul $E = 0.1$ volt/m	10^{-13}
Image Attraction of Spherical Cavity for Charged Ball with Zero Stray Field	$f/g_e = \dfrac{3\epsilon_o V_B^2}{g_e \rho_m R_B d_1^2} \left(\dfrac{r_Q}{d_1} \right)^3$	$\dfrac{r_Q}{d_1} = 0.1$	10^{-14}
Induced Magnetic Moment	$\vec{F} = (\vec{m}_{HB} \cdot \vec{\nabla})H$ $f/g_e = \dfrac{3\chi_m m_{HS}^2}{4\pi^2 \mu_o d^7 \rho_m g_e}$	$\chi_m = 10^{-5}$ $m_{HS}/\mu_o = 1 \, \text{amp-m}^2$ $d = 0.2$ m	10^{-12}
Motion through the Earth's Magnetic Field**	$f/g_e = \dfrac{3\epsilon_o V_B v_O B_e}{g_e R_B^2 \rho_m}$		10^{-13}
Electric Force from Capacitive Pick-up Sensor	$f/g_e = \dfrac{\epsilon_o A_C}{2g_e m_B} \left(\dfrac{K_C}{d_g \sigma_x} \right)^2 \left(\dfrac{\Delta d_g}{2d_g} \right)$	See discussion	10^{-8}*
Radiation Force from Optical Sensor	$f/g_e = \dfrac{W}{g_e m_B c}$	$W = 10^{-9}$ watts	10^{-18}
Gas in the Cavity	Not directly comparable but negligible	See discussion	

*These terms appear to be of the same order as the drag at very high altitudes; however, their <u>effects</u> are not of the same order since the drag always acts parallel to the velocity vector. See the section on the effects of errors. Also the large error due to a capacitive pick-off can be eliminated by using an optical pick-up. See discussion on page 141.
**This term is in fact zero inside a closed conducting cavity.

1. ERRORS DUE TO VEHICLE GRAVITY

In the vehicle there is a set of points which may be called the points of zero self-gravity or Z.S.G. points. They have the following properties:

1) The Z.S.G. points are fixed in a rigid body, and they are not the same as the center of mass or the center of gravity.

2) In a region of free space, a Z.S.G. point is a saddle point or a neutral point of the potential energy. This follows by examining the proof of Earnshaw's Theorem (see Jeans (46)).

3) The Z.S.G. point is not a unique point but may be a finite number of points, a countably infinite number or an uncountably infinite number. This is evident from the following simple examples: three point masses in a line, a dumbell with solid spheres on each end, a line mass ring, two coaxial line mass rings, a circular cylindrical shell, a hollow cylindrical body with wall of finite thickness, or a solid cylinder.

4) A Z.S.G. point is located at the center of mass of a body if $\rho_m(\vec{r}) = \rho_m(-\vec{r})$ where $\vec{r}$ is measured from the center of mass.

In the neighborhood of a Z.S.G. point, the acceleration error from the vehicle gravity is given to first order by

$$f_{BVG} = K_G \ \frac{Gm_S}{d^2} \ \left(\frac{r_{ZB}}{d} \right) \qquad (4\text{-}39)$$

where

$$r_{ZB} = |\vec{r}_C - \vec{r}_{CZ}| \;.$$

<div align="right">(4-40)</div>

d is a distance which is characteristic of the vehicle size, and K_G is a numerical factor which depends on the vehicle geometry. For example, in a hollow uniform spherical shell, $K_G = 0$; and in a solid homogeneous sphere of radius d, the factor $K_G = 1$. To obtain a rough estimate of the value of K_G might reasonably be expected to assume in a typical satellite configuration, consider a homogeneous circular cylindrical body of inner radius d_1, outer radius d_2, and height $2h_S$. The second term in the series expansion of the potential at the center is given by

$$\phi_2 = -K_{G2} \frac{Gm_S}{d_1} \left(\frac{r_{ZB}}{d_1}\right)^2 P_2 \text{ (polar angle)}$$

<div align="right">(4-41)</div>

where

$$K_{G2} = \left[\frac{\left(1 + \dfrac{h_S^2}{d_1^2}\right)^{-\frac{1}{2}} - \left(\dfrac{d_2^2}{d_1^2} + \dfrac{h_S^2}{d_1^2}\right)^{-\frac{1}{2}}}{\dfrac{d_2^2}{d_1^2} - 1}\right]$$

<div align="right">(4-42)</div>

and P_2 is the second Legendre polynomial. If, for example, $d_1 = 0.1$ feet, $d_2 = 1$ foot, and $h_S = 1$ foot, then $K_{G2} = 1/344$. If $r_{ZB} \ll d_1$, the term ϕ_2 adequately represents the potential and

$$f_{BVG} = -\frac{\partial \phi_2}{\partial r} = -2K_{G2} \frac{Gm_S}{d_1^2} \left(\frac{r_{ZB}}{d_1}\right) P_2 \text{ (polar angle)}$$

$$f_{BVGmax} = -2K_{G2} \frac{Gm_S}{d_1^2} \left(\frac{r_{ZB}}{d_1}\right) \qquad\qquad (4-43)$$

and

$$f_{BVGmax}/g_e \approx 0.7 \times 10^{-10} (r_{ZB}/d_1)$$

if $g_e m_S = 100$ lbs.

The control system can easily keep the average value of r_C to 1 mm or less, but the error in centering the control center on a Z.S.G. point could be of the order of a centimeter. In addition to this, the Z.S.G. point will shift as gas is expelled unless the location of the gas tanks is symmetrical to this point with the appropriate accuracy. Thus, under these conditions, f_{BVGmax}/g_e would probably be of the order of 10^{-11}.

There are only two possible ways to find the location of the central Z.S.G. point in the satellite. It can either be calculated from a knowledge of the mass position of each component in the satellite structure and equipment, or it might be measured with some device such as a torsion balance after the satellite is constructed. Both of these approaches present great difficulties, but they do not appear insurmountable. If, for example, the effect of a 10 gram mass located 10 cm from the central Z.S.G. point were neglected in the computation, this would cause an error of about 10^{-8} cm/sec^2 or about 10^{-11} g_e. This is equivalent to a 4.2 mm error in locating the Z.S.G. point.

SEL-64-067

2. ERRORS DUE TO ELECTRIC AND MAGNETIC FIELDS

If the ball collects a small unknown residual charge, any stray electric field will apply an unknown force to it. In addition, if the ball is located in a shielded metal cavity, the charge on the ball would be attracted to induced charges on the cavity walls. A conducting ball inside a completely enclosed metal cavity could be discharged merely by contacting the walls. The charge on the ball would be exactly zero, and the static field inside the cavity would be exactly zero. This is true even for a shield of finite conductivity. It is not possible, however, to construct a completely enclosed cavity because the position of the ball must be sensed. Furthermore, for some applications a nonconducting or even a transparent ball might be desirable; and therefore it is instructive to compute the minimum charge on the ball which could be measured and the minimum electric field in the cavity which could be detected.

a. Maximum Charge which Might Reasonably be Expected to Accumulate on the Proof-Mass

The primary mechanisms by which the proof-mass may become charged will be due to the differences in the average velocities of electrons and ions from ionized air molecules and due to the photo-electric effect from cavity illumination. At 400 km, altitude a large fraction of the air molecules are ionized, and the kinetic temperature is about $1000^{\circ}K$, but on the inside of the satellite cavity collisions with the walls should quickly discharge the ions and reduce their kinetic temperature to that of the satellite (about $300^{\circ}K$). Even if as many as half the gas molecules were ionized, the ball would probably not accumulate a negative charge much greater than one volt.

W. M. Fairbank of Stanford University has suggested to the author that if the proof-mass and the cavity walls are both coated with a photoelectric material, and if the cavity is weakly illuminated with a radiation whose wavelength is chosen to give a stopping potential of about 0.1 volt or less, that the potential on the proof-mass will

assume an equilibrium value of 0.1 volt or less. Thus it will be
assumed that, by this or some similar technique, the charge on the
proof-mass can be limited to no more than one volt, which corresponds
to a charge of

$$q_B = 4\pi\epsilon_o \times 1 \text{ volt} \times 0.02 \text{ meter} = 2.2 \times 10^{-12} \text{ coul} \approx 10^7 \text{ electrons.}$$

b. **Maximum Electric Field which Can Leak into the Cavity**

The question of what stray electric fields other than
those due to a charge on the proof-mass might be present in the cavity
can be answered in the following way. If the proof-mass were un-
charged and if the cavity walls were a completely closed conductor,
there could be no static electric field present. As a practical
matter, however, the cavity walls will need to have small holes in
them to accommodate the position sensing apparatus; and any charge
which has accumulated on the outside of the satellite will cause a
residual electric field to leak through these holes. Furthermore,
the accumulated charge on the outside of the satellite may be fairly
large, corresponding to a potential of several (or in a few cases
several hundred) volts.

If a closed conducting charged shell has an electric
field, E_n, at some point on its surface; then there will be a
field $E_n/2$ at this same point if a small hole is drilled there.
Gauss's Law implies that the charge which is then inside the closed
conductor is given by

$$q_{inside} = \frac{1}{2} \frac{A_{hole}}{A_{surface}} q_{outside} \quad \cdot \qquad (4\text{-}44)$$

The electric field on the inside will depend on how the inner charge
is distributed, but generally it will be concentrated near the hole.
If additional shields are used, each one will attenuate the charge

according to Eq. (4-44). For the purpose of a simple computation, it will be assumed that the static electric field can be limited to less than 0.1 volt/meter inside of the cavity containing the proof-mass by a series of concentric shielded cavities or, equivalently, by bringing in leads or light beams through tubes whose lengths are big compared to their diameters.

c. Force on a Charged Ball Due to Leakage Electric Field

A stray electric field of 0.1 volt/meter would cause an error acceleration on a 300 gram ball with a charge of 2.2×10^{-12} coul. which is given by

$$f/g_e = \frac{q_B E}{g_e m_B} = \frac{3\epsilon_o V_B E}{g_e \rho_m R_B^2} \approx 10^{-13} . \tag{4-45}$$

d. Force on a Charged Ball Due to Image Attraction with Zero Leakage Field

For a spherical cavity of radius d_1, the force on a point charge inside the cavity is given by

$$F = \frac{q^2}{4\pi\epsilon_o d_1^2} \left(\frac{r_Q}{d_1}\right)^3 \left[1 - \left(\frac{r_Q}{d_1}\right)^2\right]^{-1} , \frac{f}{g_e} \approx \frac{3\epsilon_o V_B^2}{g_e \rho_m R_B d_1^2} \left(\frac{r_Q}{d_1}\right)^3 \tag{4-46}$$

where r_Q is the distance of the point charge from the equilibrium point at the center. The acceleration, which corresponds to this for a 3 cm. radius cavity and a potential of one volt and a position error of 0.3 cm. is

$$f/g_e = 10^{-14} . \tag{4-47}$$

e. Magnetic Force Due to Field Gradients

The force on the ball due to stray magnetic field is

$$\vec{F} = (\vec{m}_{HB} \cdot \vec{\nabla})\vec{H} \ . \tag{4-48}$$

If the ball is constructed of nonferromagnetic materials, there will be no residual magnetic moment; and the only source of $\vec{m}_{HB}$ is a moment induced by the stray magnetic field.

Stray magnetic fields can arise from two sources, those in the satellite and those external to the satellite. The external field will be primarily due to the earth's magnetism and is of the order of 2×10^{-5} webers/meter^2. Magnetic fields in the satellite arise from current loops, ferromagnetism, and unexplained residual magnetic moments. Bandeen and Manger (47) report apparent residual values of m_{HS}/μ_o of 1 ampere meter^2 in Tiros I, and this is considerably larger than the magnetic moment expected from the electrical circuitry and is probably the largest value one might expect. The magnetic field in the satellite which corresponds to a magnetic moment of this size is of the order of the earth's field. However, its gradient is much larger than the gradient of the earth's field, and hence it can exert a much larger force on the ball. The maximum acceleration of the ball due to a residual magnetic moment, m_{HS}/μ_o, of 1 ampere-meter^2 located in the satellite a distance $d = 0.2$ meter from the ball as computed from Eq. (4-48) is

$$f_{max} = \frac{3\chi_m \ m_{HS}^2}{4\pi^2 \ \mu_o d^7 \rho_m} \approx 10^{-12} \ g_e \ . \tag{4-49}$$

f. Force Due to the Motion of a Charged Ball Through the Earth's Field

Since the charge on the ball is in motion through the earth's magnetic field, this field exerts a force on the ball given by

$$\vec{F}_{PB} = q \, \vec{v}_0 \times \vec{B}_e \; . \tag{4-50}$$

For a 300 gram ball with a stray charge of 2.2×10^{-12} coul, this corresponds to an acceleration

$$f/g_e = \frac{3\epsilon_o V_B v_0 B_e}{g_e R_B^2 \, \rho_m} \approx 10^{-13} \; . \tag{4-51}$$

The magnitude of this effect is computed for illustrative purposes only, since it is actually zero inside of a closed conducting cavity.

3. ERRORS DUE TO SENSING THE POSITION OF THE PROOF-MASS

a. Capacitive Pick-up Position Sensor

If a capacitive pick-up is used, it will exert an electric pressure on the ball given by $\epsilon_o E_n^2/2$. The electric field is proportional to the input voltage to the position circuitry, and the input voltage required depends on the precision with which the position of the ball must be resolved. Since the velocity of the ball with respect to the satellite can be inferred only from the position measurements, the minimum tolerable velocity error determines the necessary precision of the position measurements. A rough estimate of typical values for the minimum velocity error may be obtained from Table 2-2. The worst case in the table occurs at 300 miles where a velocity measurement of the order of 10^{-3} cm/sec is necessary to mechanize the control. It is assumed that the position measurement errors can be represented by white noise which is averaged by a single time constant filter with time constant $T_1 = 2\pi/\omega_1$. It is further assumed that the velocity is formed by a filter of the form

$$H(j\omega) = \frac{j\omega}{j\omega/\omega_2 + 1} \quad , \tag{4-52}$$

so that the velocity error is given in terms of the position error by

$$\sigma_{\dot{x}} = \sigma_x \left(\frac{\omega_1 \omega_2^2}{\omega_1 + \omega_2} \right)^{1/2} = \sigma_x \frac{\omega_1}{\sqrt{2}} \tag{4-53}$$

if

$$\omega_1 = \omega_2 \quad .$$

Alternately,

$$\sigma_x = \frac{\sqrt{2} \, T_1}{2\pi} \sigma_{\dot{x}} = 0.225 \, T_1 \sigma_{\dot{x}} \quad . \tag{4-54}$$

Thus to limit the velocity error to 10^{-3} cm/sec, the position must be measured to 2.25×10^{-5} cm if $T_1 = 100$ msec. If it is assumed that with a 100 volt input to the capacitive circuitry, the pick-up can resolve 10^{-4} times the nominal gap width, then it is possible to compute the force from the electric pressure. A typical capacitive pick-up would use a set of input plates to couple the input voltage to the ball and three pairs of output plates to read position in each axis. The computation of the force on the ball is rather involved but if the departure from equilibrium is small, it may be approximated by

$$f/g_e = \frac{\epsilon_o A_C}{2g_e m_B} \left(\frac{V_C}{d_g} \right)^2 \left(\frac{\Delta d_g}{2d_g} \right) \tag{4-55}$$

where d_g is the nominal gap width and A_C is the area of the plates.

SEL-64-067

If $A_C = 1 \text{ cm}^2$, $d_g = 0.2 \text{ cm}$, and $\Delta d_g / 2d_g = 0.1$; then

$$f/g_e \approx 3.76 \times 10^{-12} \, V_C^2 \quad (V_C \text{ in volts RMS}). \tag{4-56}$$

If it is assumed further that the measurement noise is additive with zero mean and is uncorrelated with position, then V_C and $\sigma_{\dot{x}}$ are related by an expression of the form

$$V_C = K_C / \sigma_{\dot{x}} \quad . \tag{4-57}$$

From Eq. (4-54) and the previous assumption of the pick-up sensitivity, it follows that $K_C = 0.1$ volt cm/sec.

Thus

$$f/g_e \approx \frac{\epsilon_o A_C}{2 g_e m_B} \left(\frac{K_C}{d_g \sigma_{\dot{x}}} \right)^2 \left(\frac{\Delta d_g}{2d_g} \right) \tag{4-58}$$

$$\approx \frac{3.76 \times 10^{-14} \text{ cm}^2/\text{sec}^2}{\sigma_{\dot{x}}^2} \quad . \tag{4-59}$$

For a given altitude the value of $\sigma_{\dot{x}}$ which can be tolerated may be inferred from Table 2-2 and is of the order of 10^{-2} cm/sec for $h_P = 100$ miles and 10^{-3} cm/sec for $h_P = 200$ or 300 miles. It follows that, for the various numerical assumptions made,

$$f_{SB}/g_e \approx 4 < 10^{-10} \text{ for } h_P = 100 \text{ miles}$$

and

$$f_{SB}/g_e \approx 4 \times 10^{-8} \text{ for } h_P = 200 \text{ or } 300 \text{ miles}. \tag{4-60}$$

For a 300 mile orbit, such a capacitive pick-up would provide about as much disturbance as the drag on the vehicle; and for missions in this altitude range or for any mission where the capacitive pick-up causes disturbances which are too large, it may be necessary to use an optical pick-up. On the other hand, for aeronomy or geodetic missions where h_p is less than 200 miles, a capacitive pick-up may be quite satisfactory.

b. Optical Position Sensor

One arrangement, which could sense the position of the ball, uses a single light source and a single photomultiplier tube. The light from the source is chopped by a vibrating reed or a linear electro-optical device and then, with the aid of fixed mirrors, is split into 6 rectangular beams, two for each axis. The chopper acts such that only one beam at a time is on, so that the output signal is time shared among the beams. To measure displacement on a given axis, the beams are aimed such that when the ball is in its centered position it intercepts about half of each beam and such that displacement along that axis covers one beam and uncovers the other. The signals from beams on opposite sides of the ball are subtracted, and this difference signal is proportional to the deviation of the ball from its centered position.

It is necessary to use a single light source and a single photomultiplier to reduce the effects of drift, and it is necessary to chop the light source in order to distinguish the beams (by time sharing), to avoid the drift problems inherent in D.C. amplifiers, and to prevent the encoding of low frequency noise on the signal.

The minimum change in position which can be detected depends on the photomultiplier noise properties. Engstrom (48) quotes minimum detectable powers of 10^{-14} watts with a bandwidth of 1.8 c/sec for photomultiplier tubes.* For a bandwidth of 10 c/sec this

---

* This noise level is reduced by about 100 times if the photomultiplier is operated at the temperature of liquid nitrogen at room pressure.

corresponds to approximately 5×10^{-14} watts. The position error, σ_x, is given by

$$\sigma_x = N d_b / 2W \qquad (4-61)$$

where d_b is the width of the beam, W is the power in the beam, and N is the noise equivalent power of the phototube. For example, if $N = 5 \times 10^{-14}$ watts, $d_b = 4$ mm, and $W = 10^{-9}$ watts

$$\sigma_x \approx 10^{-5} \text{ cm.} \qquad (4-62)$$

The disturbing force (which is due to radiative pressure) is given by

$$F = W/c$$

and

$$f/g_e = \frac{W}{g_e m_B c} \approx 10^{-18} . \qquad (4-63)$$

Thus for those applications where the capacitive pick-up would disturb the ball excessively, the use of an optical pick-up can reduce the disturbance by 9 or 10 orders of magnitude.

4. BROWNIAN MOTION OF THE PROOF-MASS

The effect of gas in the cavity will be divided into two parts, a macroscopic resistive force proportional to the velocity and a microscopic force noise with zero mean which is due to individual molecular collisions. This division of effect is to some extent arbitrary, but it has proved quite successful in the classical theory

of Brownian motion of colloidal particles. This gives the equation
of motion

$$\ddot{x}_C + \frac{p}{m_B}\dot{x}_C = f_{Dgas} . \qquad (4\text{-}64)$$

If the molecular force noise is considered to be white and
if it is assumed that equipartition of energy eventually is obtained,
the Eq. (4-64) may be integrated by the technique described in
Aseltine (49) and Kennard (50). For zero initial conditions at $t = 0$,

$$\left\langle \dot{x}_C^2 \right\rangle_{av} = \frac{kT}{m_B} (1 - e^{-2pt/m_B}) \qquad (4\text{-}65)$$

and

$$\left\langle x_C^2 \right\rangle_{av} = \frac{2kT}{p} \left[t - \frac{2m_B}{p} (1 - e^{-pt/m_B}) + \frac{m_B}{2p} (1 - e^{-2pt/m_B}) \right]. \quad (4\text{-}66)$$

p depends on the surface properties of the sphere and may be evaluated
from kinetic theory. For an order of magnitude estimate, it will be
taken as

$$p = 6\rho A_B \left(\frac{kT}{2\pi m_{av}} \right)^{\frac{1}{2}} \approx 5.6 \times 10^{-12} \frac{ntns}{m/sec} \qquad (4\text{-}67)$$

for $\rho = 6.5 \times 10^{-15}$ gm/cm^3 and $T = 300^\circ$K.

The time constant m_B/p is about 1700 years, so that

$$\left\langle \dot{x}_C^2 \right\rangle_{av} \approx \frac{2pkT}{m_B^2} t \qquad (4\text{-}68)$$

and

$$\left\langle x_C^2 \right\rangle_{av} \approx \frac{2pkT}{3m_B^2} t^3 \approx 1.4 \times 10^{-31} \ m^2/sec^3. \qquad (4\text{-}69)$$

After one year the RMS value of x_C would only be

$$\left\langle x_C^2 \right\rangle_{av}^{\frac{1}{2}} \approx 61 \ microns \qquad (4\text{-}70)$$

so that the effect of gas in the cavity is completely negligible.

CHAPTER V

THE UNSUPPORTED GYROSCOPE

A. INTRODUCTION

Perhaps the most elegant application of the drag-free satellite is as a carrier vehicle for the unsupported gyroscope. Since the proof-mass never touches the satellite walls, and since it requires no forces to support it against gravity, all of the causes of random drift of terrestrial gyroscopes which are associated with the support forces are eliminated. In this chapter the sources of random drift of the direction of the angular momentum vector of the spinning ball acting as a gyroscope will be discussed.

The very best terrestrial gyroscopes have random drift rates which are somewhat better than 10^{-3} degrees/hour. It seems possible that, by very careful refinement of present designs and techniques, improvements of a few orders of magnitude may some day be achieved. The random drifts of the present instruments are caused primarily by torques which are produced by the rotor support forces or by a lack of sphericity of the rotor; but even if these two current difficulties were overcome, there would still remain a host of reasons why perfect performance can never be achieved.

The unsupported gyroscope, which consists of a spherical spinning proof-mass in a drag-free satellite, would allow these other sources of error to be accurately studied years in advance of the time that such effects could be investigated on earth. It will be shown in this chapter that there appears to be no physical effect which will cause a spherical unsupported gyroscope to drift more than about 0.1 second of arc/year (about 3×10^{-9} degree/hour). 0.1 second of arc/year represents a theoretical upper bound on the random drift rate. With very round balls (about one part in 10^6) and with reasonable magnetic shielding, this rate can probably be made one or two orders of magnitude smaller. The limit of 0.1 second of arc/year is caused by gravity gradient torques due to the difficulty of making an exactly spherical rotor, and is based on a sphericity of about 10^{-5}. Rotors with sphericities

approaching 10^{-6} are presently available, but it may be difficult to make a simple readout which does not use an optical flat for detecting the spin axis of a rotor operating in a drag-free satellite. Such a flat would limit the sphericity to about 10^{-6}.

While the performance of terrestrial gyroscopes may be limited to only a very few orders of magnitude better than 10^{-3} degrees/hour for a number of years to come, this is by no means true for supported gyroscopes which are satellite borne. For example, the very low apparent force of gravity in a satellite reduces the required support force to the point that other effects may be the dominant sources of drift for properly designed electrostatic gyroscopes in a satellite. Thus, it seems reasonable to develop a whole new generation of gyroscopes for satellite applications and the unsupported gyroscope would allow the effects discussed in this chapter to be carefully studied.

The unsupported gyroscope offers some hope to perform a fundamental experiment in physics proposed by G. E. Pugh (13) and L. I. Schiff (4). Schiff has shown in (4) that the equations of general relativity predict that an unsupported gyroscope in a satellite in a circular orbit will have a precession of its spin axis given by

$$\dot{\phi} = \frac{g_e R_e}{r_{ES}^2} \left\{ \frac{3}{2} \left(\frac{R_e}{r_{ES}} \right) \vec{\omega}_0 - \frac{2}{5} \left(\frac{R_e}{r_{ES}} \right)^3 \left[\frac{3(\vec{\omega}_e \cdot \vec{r}_{ES})}{r_{ES}^2} \vec{r}_{ES} - \vec{\omega}_e \right] \right\}. \quad (5-1)$$

The first term in equation (5-1) is a geodetic precession caused by the curvature (due to the earth's matter) of the space around the earth, and it is always in the direction of the orbit angular velocity vector. It has a typical magnitude of about 7 seconds of arc/year which results in the greatest effect when the gyro spin vector is placed in the orbit plane.

The second term in Eq. (5-1) is called the Lense-Thirring precession and is due to the difference between the gravitational field of a rotating and a nonrotating earth. $2R_e^3 \omega_e / 5r_{ES}^3$ has a typical magnitude of about 0.1 second of arc/year. The Lense-Thirring precession consists of two parts, one anti-parallel to the orbit radius vector and one

parallel to the earth's spin vector. The part anti-parallel to $\vec{r}_{ES}$ averages to zero except along a vector which is coincident to $\vec{r}_{ES}$ at the time when it is closest to $\vec{\omega}_e$. This component has an average value of $(2R_e^3\omega_e/5r_{ES}^3)$ $(3/2)$ sin i where i is the inclination of the satellite orbit. The magnitude of the total secular Lense-Thirring effect is $(2R_e^3\omega_e/5r_{ES}^3)$ $(1 - 3/4 \sin^2 i)^{\frac{1}{2}}$ and has a maximum value when i = 0. Unfortunately it is then in the same direction as $\vec{\omega}_O$ so that it could be masked somewhat by the much larger geodetic effect. In a polar orbit with the gyro spin-axis perpendicular to both $\vec{\omega}_e$ and $\vec{\omega}_O$ the geodetic and Lense-Thirring precessions are at right angles to each other, and this is one way that they might possibly be distinguished.

Schiff explains that the geodetic precession is important because although it does not provide a check on terms in the space-time metric higher than those which may be obtained from the equivalence principle alone, it does "involve the equation of motion of matter of finite rest mass beyond the Newtonian approximation"; and that the Lense-Thirring precession is important because the detection of this effect would infer the existence of off-diagonal components of the space-time metric caused by the earth's rotation. The only other experiment which involves the equation of motion of matter of finite rest mass beyond the Newtonian approximation is the excess precession of Mercury's perihelion. Thus, general relativity rests on a weak experimental foundation.

There does not appear to be any theoretical reason why the random drift rates of the unsupported gyroscope should not be low enough, or a simple optical flat read-out system accurate enough to detect the geodetic precession. Detection of the Lense-Thirring precession, however, will be much more difficult. While it is not unreasonable to expect that unsupported gyroscopes can be constructed with random drift rates of the order of 0.01 second of arc/year, the read-out and detection of such a small angle will require the development of special equipment and may be very difficult to accomplish.

In this chapter the theoretical performance of the unsupported gyroscope will be discussed.

B. GYROSCOPE RANDOM DRIFT

The sources and magnitudes of the various torques which can cause random drift rates are summarized in Table 5-1. Typical numbers are computed for a spherical rotor with the following parameters:

Material	Silicon
Radius, R_B	2 cm
Mass, m_B	80 gms
Moment of Inertia, C	128 gm cm^2 = 1.28 $\times$ 10^{-5} kg meters^2
Spin Rate, ω_B	10^3 rad/sec $\approx$ 10^4 R.P.M.
Angular Momentum, h_B	1.28 $\times$ 10^5 dyne cm sec
	= 1.28 $\times$ 10^{-2} ntn m sec
Spericity Factors ϵ_1 and ϵ_2	10^{-5}

C. DETAILS OF THE RANDOM-DRIFT CALCULATIONS

The equations of the gyro rotor in its principal axis system are given by

$$(1 - \epsilon_1) \, \dot{\omega}_{Bx} + \epsilon_2 \, \omega_{By} \, \omega_{Bx} = M_{Bx}/C \tag{5-2}$$

$$(1 - \epsilon_2) \, \dot{\omega}_{By} - \epsilon_1 \, \omega_{Bx} \, \omega_{Bz} = M_{By}/C \tag{5-3}$$

$$\dot{\omega}_{Bz} + (\epsilon_1 - \epsilon_2) \, \omega_{Bx} \, \omega_{By} = M_{Bz}/C \tag{5-4}$$

where the principal moments of inertia are $A = C(1 - \epsilon_1)$, $B = C(1 - \epsilon_2)$, and C.

ϵ_1 and ϵ_2 are called the ellipticities and are of the order of 10^{-5}.

TABLE 5-1

UNSUPPORTED GYRO DRIFT RATES

1 sec arc/year = 3.18×10^{-8} deg/hour = 1.5×10^{-13} rad/sec

Source of Torque	Formula for $\dot{\phi}_{peak}$	Key Assumptions and Magnitudes	Typical Drift Rates (radian/sec)
Gravity Gradient	$\dfrac{3}{2} \dfrac{\omega_0^2}{\omega_B} \epsilon$	$\epsilon = 10^{-5}$; $\omega_B = 10^3$ rad/sec	5×10^{-14}
Magnetic Eddy Currents	$\dfrac{B_\perp B_\parallel \sigma}{4\rho_m}$	$B = 2\times10^{-5}$ webers/m^2 $\sigma = 10$ mhos/m	4×10^{-13}*
Barnett Effect	$\dfrac{5 \chi_m H}{\rho_m R_B^2 (e/m)g_H}$	$H = 25$ amp turns/m $g_H = 2$; $\chi_m = 10^{-5}$	10^{-15}
Einstein - de Haas	$\dfrac{5 \chi_m \dot{H}}{\rho_m R_B^2 (e/m)g_H \omega_B}$	$\dot{H}$ only due to motion through earth's field	10^{-21}
Spinning Charge	$\dfrac{15 \epsilon_o V_B B}{4 \rho_m R_B^2}$	$V_B = 1$ volt	7×10^{-16}
Tolman Effect	Neglected on the grounds that it is smaller than spinning charge		
Induced Magnetic Moment in an Ellipsoid	$\dfrac{\chi_m^2 B_o' H_o'' \epsilon}{\rho_m R_B^2 \omega_B}$		10^{-21}
Induced Magnetic Moment in Single Crystal	$\dfrac{5 B_o' H_o'' (\chi_m'' - \chi_m')}{2 \rho_m R_B^2 \omega_B}$	$\chi_m'' - \chi_m' = 10^{-6}$	10^{-12}**
Impurity Ferromagnetism	Neglected on the grounds that experimenters could not have obtained accurate values of χ_m if this were important		

TABLE 5-1 (Continued)

Source of Torque	Formula for $\dot\phi_{peak}$	Key Assumptions and Magnitudes	Typical Drift Rates (radian/sec)
Electric Moment Induced in Ellipsoid by Nonuniform Electric Field	$\dfrac{15}{4}\ \dfrac{\epsilon_o\ E_{max}^2\ \epsilon}{\rho_m\ R_B^2\ \omega_B}$	$E_{max} = 0.1$ volts/m	3×10^{-21}
Charge on the Ellipsoid plus Leakage Field	$\dfrac{15\ \epsilon_o\ V_B\ E_{max}\epsilon}{2\ \rho_m\ R_B^3\ \omega_B}$		7×10^{-18}
Charge on the Ellipsoid plus Image Field	$\dfrac{15\ \epsilon_o V_B^2\ \epsilon}{2\rho_m\ R_B^2\ d_1^2\omega_B}\left(\dfrac{r_Q}{d_1}\right)^3$	$\dfrac{r_Q}{d_1} = 0.1$	10^{-18}
Surface Electric Eddy Currents in an Ellipsoid (Power Dissipation)	$\dfrac{15\ \epsilon_o^2\ V_B^2\ \epsilon^2}{2\ t_i\ \rho_m\ R_B^3\ \sigma}$	$t_i = 10^{-10}$ m	3×10^{-21}
Surface Electric Eddy Currents (Magnetic Moment)	$\dfrac{15\ \epsilon_o\ V_B\ B\ \epsilon}{4\ \rho_m\ R_B^2}$		7×10^{-21}
Sensor Radiation Pressure	$\dfrac{15}{8\pi}\ \dfrac{W}{\rho_m\ R_B^4\ c\ \omega_B}$	$W = 10^{-9}$ watts	5×10^{-18}
Gas in Cavity	$\left\langle\phi^2\right\rangle_{av} = \dfrac{2bkT}{h_B^2}\ t$ $b = \dfrac{\pi}{9}\ R_B^4\ \rho\left(\dfrac{3kT}{m_{av}}\right)^{\frac{1}{2}}$	$T = 300°K$	$\left\langle\phi^2\right\rangle_{av}^{\frac{1}{2}} =$ 5×10^{-13} rad in one year

*This number may be reduced to 4×10^{-15} by a magnetic shield with an attenuation factor of 0.1 which is easily attained.

**In polycrystalline silicon this effect will be much smaller, and it may also be reduced by magnetic shielding.

If the terms involving ϵ_1 and ϵ_2 may be neglected, the equations of motion become with $\vec{\omega}_B = \vec{e}_\omega \, \omega_B$

$$\vec{M}_{||} = C \, \vec{e}_\omega \, \dot{\omega}_B \tag{5-5}$$

$$\vec{M}_{\perp} = \vec{\beta} \times C \, \vec{\omega}_B = \vec{\beta} \times \vec{h}_B \tag{5-6}$$

where $\vec{M}_{||}$ and $\vec{M}_{\perp}$ are the components of the disturbing torque parallel to and perpendicular to $\vec{\omega}_B$ respectively. The magnitude of the drift rate in this case is computed from equation (5-6).

The principal model which will be used for most of the torque calculations is an almost-spherical rotor of ellipsoidal shape. The shape eccentricities e_1 and e_2 are defined by

$$a^2 \triangleq c^2 (1 + e_1) \tag{5-7}$$

$$b^2 \triangleq c^2 (1 + e_2) \; ,$$

where a, b, c are the principal axis distances of the ellipsoid; and, for a rotor of constant density, the eccentricities and the ellipticities are related by

$$e_1 = 2 \, \epsilon_1$$
$$e_2 = 2 \, \epsilon_2 \tag{5-8}$$

so that

$$a = c(1 + \epsilon_1)$$
$$b = c(1 + \epsilon_2) \; . \tag{5-9}$$

It will be assumed for definiteness that

$$a > b > c \tag{5-10}$$

and

$$A < B < C \; . \tag{5-11}$$

In some of the calculations (such as gravity gradient) and in the presentation of the results (as in Table 5-1), it is convenient and appropriate to ignore the difference between ϵ_1 and ϵ_2.

In each example below the maximum value of the drift rate will be computed. In many cases, as for example with the gravity gradient torque, the actual drift will be less since part of the total effect of the torque will have zero time average.

1. GRAVITY-GRADIENT TORQUE

If it is assumed that the spinning rotor may be represented by an oblate spheroid with moments of inertia $A = B = C(1 - \epsilon)$ and C, the peak drift rate is given by Cannon (5) as

$$\dot{\phi}_{peak} = \frac{3}{2} \frac{\omega_0^2}{\omega_B} \epsilon . \qquad (5\text{-}12)$$

where ω_0 is the satellite orbit angular velocity and ω_B is the rotor spin angular velocity.

If the bulge in a homogeneous rotor is assumed to consist of a permanent bulge plus one caused by the rotation, then

$$\epsilon = \epsilon_P + \epsilon_R . \qquad (5\text{-}13)$$

It is shown in Klein and Sommerfeld (51) that

$$\epsilon_R = \frac{15}{38} \frac{\rho_m \omega_B^2 R_B^2}{E} \qquad (5\text{-}14)$$

where E is Young's modulous for the material. Thus

$$\dot{\phi}_{peak} = \frac{45}{76} \frac{\omega_0^2 \rho_m R_B^2 \omega_B}{E} + \frac{3}{2} \frac{\omega_0^2}{\omega_B} \epsilon_P . \qquad (5\text{-}15)$$

If

$$\omega_B = \left(\frac{38}{15} \frac{E \epsilon_P}{R_B^2 \rho_m} \right)^{\frac{1}{2}} \approx 1.7 \times 10^3 \frac{rad}{sec} \text{ for silicon,} \qquad (5\text{-}16)$$

then $\dot{\phi}_{peak}$ has its minimum value of

$$\dot{\phi}_{peak\ min} = 3\ \omega_0^2 \left(\frac{15}{38}\ \frac{R_B^2\ \rho_m\ \epsilon_P}{E} \right)^{\frac{1}{2}} . \qquad (5\text{-}17)$$

The expression for the precession given in Eq. (5-12) is only the peak value. The time average of all the components of the precession are zero except along an axis which is in the plane formed by $\vec{\omega}_O$ and $\vec{\omega}_B$ and which is perpendicular to $\vec{\omega}_B$. Along this axis

$$\left\langle \dot{\phi} \right\rangle_{av} = \frac{3}{4}\ \frac{\omega_0^2}{\omega_B}\ \epsilon\ \sin\ 2\underline{/\vec{\omega}_B, \vec{\omega}_O} . \qquad (5\text{-}18)$$

Equation (5-18) neglects kinematic rectification drift which would prevent the net drift rate from being exactly zero when Eq. (5-18) is zero. But apart from kinematic rectification drift, the average drift rate is very small when the gyro spin vector is either nearly parallel to or nearly perpendicular to the orbit plane. This result is not as useful as one might guess, however, since in any meaningful experiment the direction of the spin axis must be compared with a pre-chosen "fixed" star, since the orbit plane is partially determined by the launch constraints, and since the orbit plane slowly rotates due to various perturbations such as the earth's oblateness. By careful design of the experiment, it may be possible to take advantage of this result to improve the gyro performance by about one order of magnitude.

One other condition which mitigates the problem of gravity gradient drift is that it is not strictly random. While in experiments of this nature it would be better not to have to calibrate out some known effect, such a calibration could be done here so that the gravity gradient drift could be included in any extremely precise experiments.

2. MAGNETIC EDDY-CURRENT TORQUE

The solution of the boundary value problem which calculates the eddy currents in a rotating sphere is a classical problem, but most

discussions in the literature are somewhat incomplete as applied to the unsupported gyroscope. (See references (26), (27), (28), and (52).) Smythe (26) has shown that if a rotating magnetic field of the form

$$B_\perp(t) = B_\perp \, e^{j\omega_B t} \tag{5-19}$$

is assumed, then this field will induce a magnetic moment

$$m_H = 2\pi \, B_\perp \, D \tag{5-20}$$

in the sphere where

$$\frac{D}{R_B^3} = \frac{3 \, v \, I_{-\frac{1}{2}}(v) - 3 \, I_{\frac{1}{2}}(v) - v^2 \, I_{\frac{1}{2}}(v)}{\chi_m \left[v \, I_{-\frac{1}{2}}(v) - I_{\frac{1}{2}}(v) \right] + v^2 \, I_{\frac{1}{2}}(v)} \tag{5-21}$$

$$v \triangleq (j \, \mu_o \, \sigma \, \omega_B)^{\frac{1}{2}} \, R_B \tag{5-22}$$

and

$$I_{\frac{1}{2}}(v) = \left(\frac{2}{\pi \, v} \right)^{\frac{1}{2}} \sinh v \tag{5-23}$$

$$I_{-\frac{1}{2}}(v) = \left(\frac{2}{\pi \, v} \right)^{\frac{1}{2}} \cosh v \tag{5-24}$$

are spherical Bessel's functions with imaginary arguments. For non-ferrous materials $\chi_m \approx 10^{-5}$ and the term in Eq. (5-21) involving χ_m is negligible when v is large. When v is small

$$v \, I_{-\frac{1}{2}}(v) - I_{\frac{1}{2}}(v) \xrightarrow[v \to 0]{} \frac{1}{3} \left(\frac{2}{\pi \, v} \right)^{\frac{1}{2}} \left[v^3 + \frac{v^5}{10} \right] \tag{5-25}$$

and

$$v^2 \, I_{\frac{1}{2}}(v) \xrightarrow[v \to 0]{} \left(\frac{2}{\pi \, v} \right)^{\frac{1}{2}} \left[v^3 + \frac{v^5}{6} \right] \tag{5-26}$$

so that when v is small the χ_m term is also negligible. Thus

$$\frac{D}{R_B^3} = -1 - \frac{3}{v^2} + \frac{3}{v} \coth v \qquad (5\text{-}27)$$

$$\coth v = \frac{\cosh \left[\frac{1}{2}(1+j)\, x\right]}{\sinh \left[\frac{1}{2}(1+j)\, x\right]} \qquad (5\text{-}28)$$

$$= \frac{\cosh x + \cos x}{\sinh x + j \sin x} \qquad (5\text{-}29)$$

where

$$x \triangleq \left(2\, \mu_o\, \sigma\, \omega_B\right)^{\frac{1}{2}} R_B \;. \qquad (5\text{-}30)$$

Thus

$$\frac{D}{R_B^3} = -\left[1 - \frac{3}{x}\, \frac{\sinh x - \sin x}{\cosh x - \cos x}\right] - j\left[\frac{3}{x}\, \frac{\sinh x + \sin x}{\cosh x - \cos x} - \frac{6}{x^2}\right] \qquad (5\text{-}31)$$

$$\triangleq -R - j\, I \qquad (5\text{-}32)$$

so that

$$R \triangleq \left[1 - \frac{3}{x}\, \frac{\sinh x - \sin x}{\cosh x - \cos x}\right] \qquad (5\text{-}33)$$

and

$$I \triangleq \left[\frac{3}{x}\, \frac{\sinh x + \sin x}{\cosh x - \cos x} - \frac{6}{x^2}\right] \;. \qquad (5\text{-}34)$$

Equation (5-31) was first published without proof by Houston (27).
Equations (5-33) and (5-34) are plotted in Fig. 5-1.

One of the most remarkable properties of Eq. (5-31) is the
accuracy with which its asymptotic expansions approximate its behavior
over most of its range.

$$R \xrightarrow[x \to 0]{} \frac{x^4}{630} \qquad (5\text{-}35)$$

$$R \xrightarrow[x \to \infty]{} 1 - \frac{3}{x} \qquad (5\text{-}36)$$
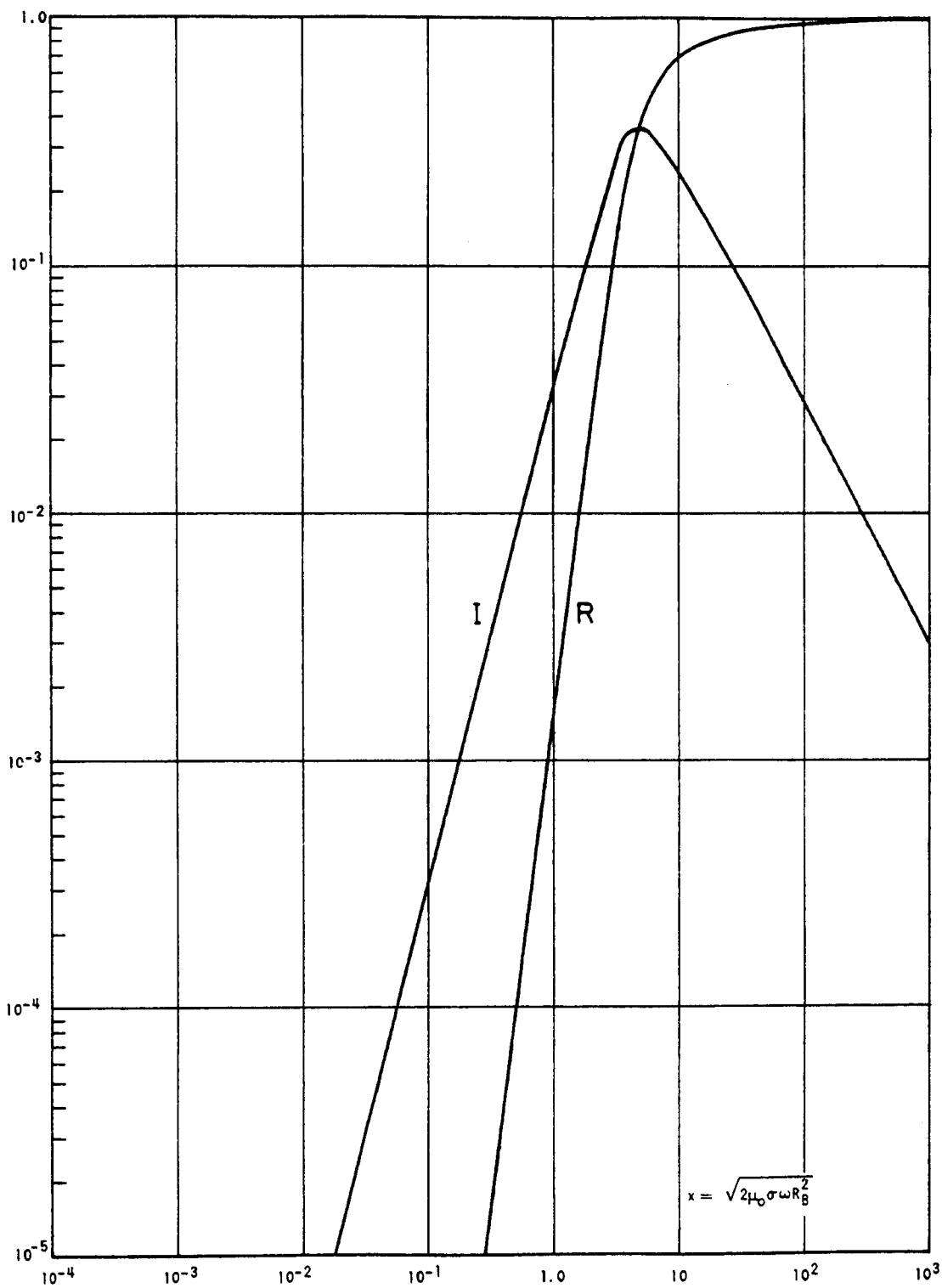
FIG. 5-1. REAL AND IMAGINARY COMPONENTS OF EDDY-CURRENT TORQUE ON A
ROTATING SOLID SPHERE

$$x = \sqrt{2\mu_o \sigma \omega R_B^2}$$

$$I \xrightarrow[x \to 0]{} \frac{x^2}{30} \qquad\qquad (5\text{-}37)$$

$$I \xrightarrow[x \to \infty]{} \frac{3}{x} \left(1 - \frac{2}{x} \right) \qquad\qquad (5\text{-}38)$$

These curves are plotted in Fig. 5-2 and this figure shows that the appropriate asymptotic expression is a very accurate approximation for R or I except over the relatively narrow range, $2 \leq x \leq 5$.

Thus the magnetic moment induced in the sphere is given by

$$m_H = - 2 \pi B_\perp R_B^3 [R + j I] \qquad\qquad (5\text{-}39)$$

and the eddy current torque on the sphere is given by

$$\vec{M} = \vec{m}_H \times \frac{\vec{B}}{\mu_o} . \qquad\qquad (5\text{-}40)$$

Figure 5-3 shows the various components of these torques and the resulting precession rates. There are three basic effects:

1) A damping torque given by $- 2 \pi B_\perp^2 R_B^3 I/\mu_o$,
2) A precession torque given by $- 2 \pi B_\perp B_{\|} R_B^3 R/\mu_o$, and
3) A precession torque given by $- 2 \pi B_\perp B_{\|} R_B^3 I/\mu_o$.

Effects (1) and (2) were reported by Houston and Alers (28), but they make no mention of (3) which is the dominant cause of the precession of a silicon rotor.

It is instructive to compute the spin decay time constant and the precession rate for both copper and silicon rotors. For a copper sphere of radius $R_B = 2$ cm, $x = [(2 \omega_B \mu_o \sigma)^{\frac{1}{2}} R_B] = 7.7$, and the time constant is given by

$$\text{Spin Decay Time Constant} = \frac{4 \rho_m}{B_\perp^2 \sigma} \left(\frac{x^4}{90(x-2)} \right) \qquad\qquad (5\text{-}41)$$

where $B_\perp$ is taken as 2×10^{-5} webers/m^2 (approximately the earth's field). If $B_{\|}$ is assumed to be approximately equal to $B_\perp$, then $\dot{\phi}$ due to I is given by
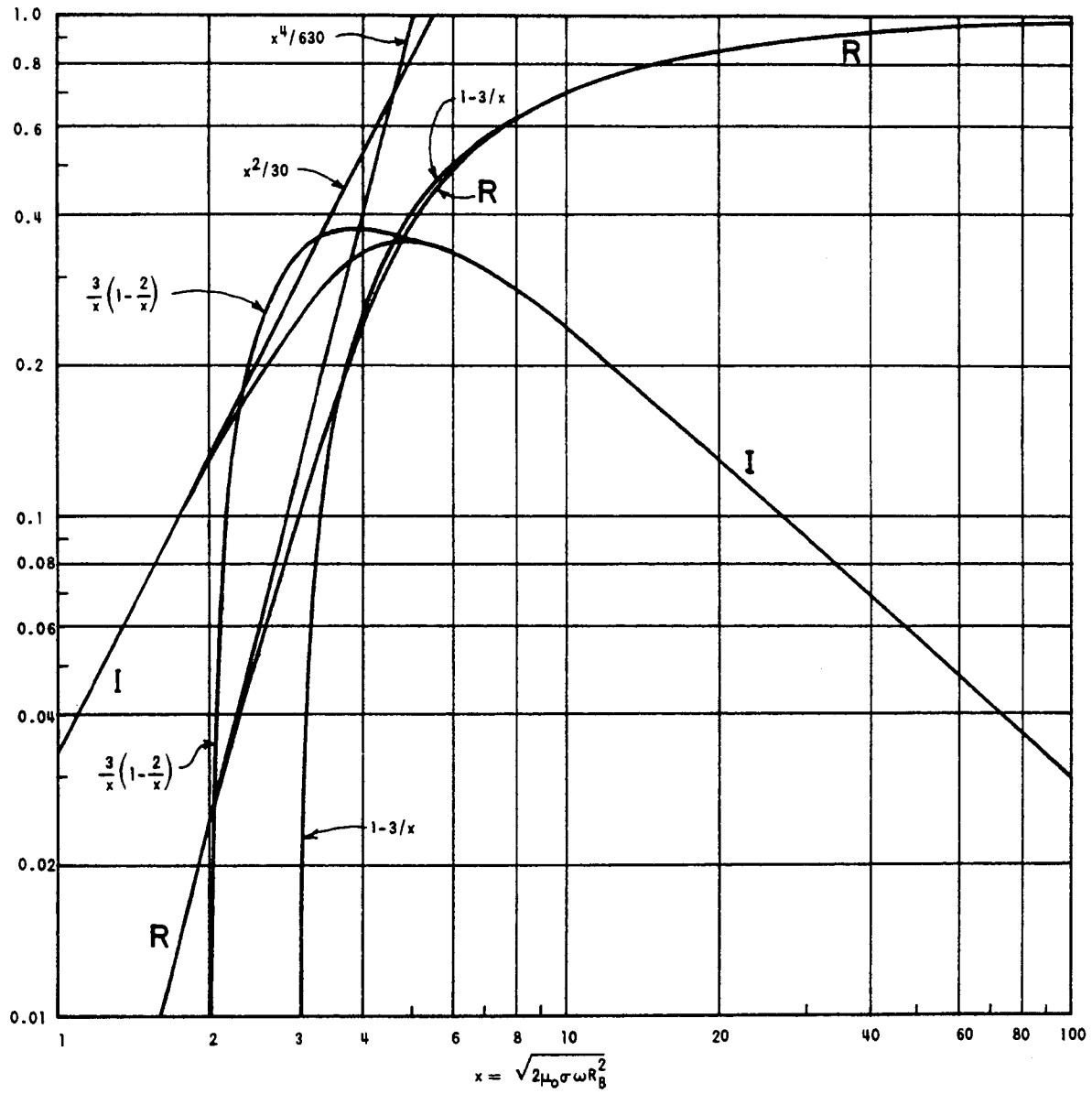
FIG. 5-2. ASYMPTOTIC EXPANSIONS OF R AND I

$$\vec{m}_H = -2\pi B_\perp R_B^3\ (\vec{R} + \vec{1})$$

$$\vec{M} = \vec{m}_H \times \vec{H}$$

$$\vec{M}_\parallel = -2\pi B_\perp R_B^3\ \frac{\vec{1} \times \vec{B}_\perp}{\mu_o} = \vec{e}_\omega C \dot{\omega}_B$$

$$\vec{M}_\perp = \frac{\vec{m}_H \times \vec{B}_\parallel}{\mu_o} = \dot{\vec{\phi}} \times \vec{h}_B$$

FIG. 5-3.   DAMPING AND PRECESSION OF A SPHERICAL ROTOR BY MAGNETIC EDDY
CURRENT TORQUES (SPIN AXIS PERPENDICULAR TO PAPER)

$$\dot{\phi} = \frac{B_\parallel\ B_\perp\ \sigma}{4\ \rho_m} \left(\frac{90(x - 2)}{x^4} \right) \tag{5-42}$$

$$= 0.75 \times 10^{-7}\ \text{rad/sec}$$

and $\dot{\phi}$ due to R by

$$\dot{\phi} = \frac{B_\parallel\ B_\perp\ \sigma}{4\ \rho_m} \left(\frac{30(x - 3)}{x^3} \right) \tag{5-43}$$

$$= 2 \times 10^{-7}\ \text{rad/sec.}$$

SEL-64-067

To obtain performance in the neighborhood of only 10^{-13} rad/sec would require a magnetic shield with an attenuation of 10^{-3}. This is somewhat difficult to obtain with present-day techniques.

On the other hand, the shielding requirements for a silicon rotor are not nearly so stringent. For silicon, $x = 2.8 \times 10^{-3}$ and the time constant is given by

$$\text{Spin Decay Time Constant} = \frac{4 \, \rho_m}{B_\perp^2 \, \sigma} \tag{5-44}$$

$$= 0.74 \times 10^5 \text{ years.}$$

Again for the case where $B_\parallel$ and $B_\perp$ are taken as approximately equal, $\dot{\phi}$ due to I is

$$\dot{\phi} = \frac{B_\parallel \, B_\perp \, \sigma}{4 \, \rho_m} \tag{5-45}$$

$$= 4.3 \times 10^{-13} \text{ rad/sec}$$

and $\dot{\phi}$ due to R is

$$\dot{\phi} = \frac{B_\parallel \, B_\perp \, \sigma}{4 \, \rho_m} \frac{x^2}{21} \tag{5-46}$$

$$= 2 \times 10^{-20} \text{ rad/sec.}$$

Thus it is clear that for silicon, I makes the dominant contribution to the precession, and that the shielding requirements to reduce the drift below 10^{-15} rad/sec are moderate.

Finally, Tabakin (52) has calculated the torque on a spinning ferromagnetic sphere caused by an alternating field. In every case he shows that the high frequency torques are less than the corresponding value at D.C.

3. THE BARNETT AND EINSTEIN-de HAAS EFFECTS

Because of the definitions of angular momentum and magnetic moment, there is a unique relation between the mechanical angular momentum and the magnetic moment of a classical charged system. This relation is

still true for atomic systems but it must be modified by an empirical constant, the gyromagnetic ratio, g_H. For a classical system $g_H = 1$, for electron spin $g_H = 2$, and for a typical atom g_H is slightly less than 2.

$$\vec{m}_H = \frac{g_H \, \mu_o \, (e/m)}{2} \vec{h} \tag{5-47}$$

If a constant magnetic field, $\vec{H}$, is applied to the charged system, the equation of motion

$$\frac{d\vec{h}}{dt} = \vec{m}_H \times \vec{H} = - \frac{g_H \, \mu_o \, (e/m)}{2} \vec{H} \times \vec{h} \tag{5-48}$$

implies precession about the field at the Larmour frequency

$$\vec{\omega}_\ell = - \frac{g_H \, \mu_o \, (e/m)}{2} \vec{H} \; . \tag{5-49}$$

Conversely rotation of a charged system induces a magnetic moment,

$$\vec{m}_H = - \frac{2V \, \chi_m \, \vec{\omega}_\ell}{g_H \, (e/m)} \; . \tag{5-50}$$

This effect has been observed experimentally (53) and is known as the Barnett effect.

In a spinning gyro rotor this magnetic moment can interact with the earth's field and cause an unwanted precession

$$\dot{\phi} = \frac{5 \, \chi_m \, H_e}{\rho_m \, R_B^2 \, (e/m) \, g_H} \tag{5-51}$$

$$= 1.15 \times 10^{-15} \text{ rad/sec.}$$

In addition, an applied field induces a magnetic moment in a material body which in turn changes the net atomic angular momentum. A time varying external field applies a torque to ponderable matter. This effect has also been observed (53) and is known as the Einstein–deHaas effect.

The torque is given by

$$\vec{M} = \frac{d\vec{h}}{dt} = \frac{2}{\mu_o \, g_H \, (e/m)} \, \dot{\vec{m}}_H \tag{5-52}$$

$$= \frac{2V \, \chi_m \, \dot{\vec{H}}_e}{g_H \, (e/m)} \, . \tag{5-53}$$

If the only time varying field is considered to be the earth's magnetic field, then

$$\dot{\phi}_{peak} = \dot{\phi}_{peak \; Barnett} \left(\frac{4 \; \omega_o}{\omega_B} \right) \tag{5-54}$$

so that the Einstein–deHaas effect is generally quite small in comparison with the Barnett effect.

4. ELECTROMAGNETIC TORQUES DUE TO ELLIPTIC GEOMETRY

The simplest model which takes into account the geometrical imperfections of any practical "sphere" and which is still analytically tractable is the ellipsoid. There are a number of electromagnetic torques that arise from the ellipsoidal shape.

a. Induced Magnetic Moment

Stratton (54) computes the torques on an ellipsoid from a constant external field in terms of the magnetization integrals

$$A_1 \triangleq \int_0^\infty \frac{ds}{(s + a^2) \, R_s}$$

$$A_2 \triangleq \int_0^\infty \frac{ds}{(s + b^2) \, R_s} \tag{5-55}$$

$$A_3 \triangleq \int_0^\infty \frac{ds}{(s + c^2) \, R_s}$$

$$R_s \triangleq [(s + a^2)(s + b^2)(s + c^2)]^{\frac{1}{2}} .$$

Equations (5-55) are elliptic integrals; but when the eccentricities are small, they may be evaluated in powers of e_1 and e_2; and all but the first power may be neglected. When this is done

$$A_1 = \frac{2}{3c^3} [1 - 3/10 (e_1 + e_2)] \qquad (5\text{-}56)$$

$$A_2 = \frac{2}{3c^3} [1 - 3/10 (e_1 + 3e_2)] \qquad (5\text{-}57)$$

$$A_3 = \frac{2}{3c^3} [1 - 3/10 (e_1 + e_2)] \qquad (5\text{-}58)$$

and

$$A_3 - A_2 = \frac{2e_2}{5c^3} \qquad (5\text{-}59)$$

$$A_1 - A_3 = \frac{-2e_1}{5c^3} \qquad (5\text{-}60)$$

$$A_2 - A_1 = \frac{2(e_1 - e_2)}{5c^3} . \qquad (5\text{-}61)$$

The torque induced in an ellipsoid with susceptibility χ_m by a constant external field $\vec{H}_o$ can be computed from Eqs. (5-59), (5-60), and (5-61).

$$\underline{M} = \chi_m^2 V \frac{abc}{5c^3} \begin{bmatrix} B_{oy} H_{oz} e_2 \\ -B_{oz} H_{ox} e_1 \\ B_{ox} H_{oy} (e_1 - e_2) \end{bmatrix} \qquad (5\text{-}62)$$

Using prime, double prime, and e to represent those components of Eqs. (5-62) which give the largest component of $\underline{M}$, the peak precession caused by this torque is given by

$$\dot{\phi}_{peak} = \frac{\chi_m^2 B_o' H_o'' e}{2 \rho_m R_B^2 \omega_B} \approx 10^{-21} \text{ rad/sec.} \qquad (5\text{-}63)$$

This source of drift is completely negligible.

b. Torques From an Electric Field or From Excess Charge

The drift rate produced by induced electric moments and by charge on an ellipsoid may be bounded by the following procedure.

The torque on an uncharged ellipsoid in a nonuniform external electric field is given by

$$\vec{M} = -\frac{\epsilon_o}{2} \int\limits_{surface} E^2 \, \vec{r} \times d\vec{S}_B \qquad (5\text{-}64)$$

since the electric field is normal to the surface.

For example, the y component of M is

$$M_y = \frac{\epsilon_o}{2} \int\limits_{surface} E^2 \, \frac{x_B \, z_B \left(\frac{1}{a^2} - \frac{1}{c^2}\right) d\,S_B}{\sqrt{\dfrac{x_B^2}{a^4} + \dfrac{y_B^2}{b^4} + \dfrac{z_B^2}{c^4}}} \qquad (5\text{-}65)$$

$$= - e_1 \frac{\epsilon_o}{2c^2 (1 + e_1)} \int\limits_{surface} \frac{E^2 \, x_B \, z_B \, dS_B}{\sqrt{\dfrac{x_B^2}{a^4} + \dfrac{y_B^2}{b^4} + \dfrac{z_B^2}{c^4}}} \quad . \qquad (5\text{-}66)$$

Since the ellipsoid is almost spherical, the radical in the denominator may be replaced by $1/c$. When this is done, only errors of the order of e_1 and e_2 are introduced.

Hence

$$M_y \approx \frac{e_1 \, \epsilon_o}{2c} \int\limits_{surface} E^2 \, x_B \, z_B \, dS_B \quad . \qquad (5\text{-}67)$$

Since the maximum value of $x_B z_B$ differs from $c^2/2$ only by terms of order e_1 and e_2,

$$M_y \; < \; \pi \, \epsilon_o \, E_{av}^2 \, c^3 \, e_1 \quad . \qquad (5\text{-}68)$$

$\overset{\bullet}{\phi}_{peak}$ due to M_y is given by

$$\overset{\bullet}{\phi}_{peak} < 15/4 \ \frac{\epsilon_o \ E_{av}^2 \ \epsilon_1}{\rho_m \ R_B^2 \ \omega_B} \tag{5-69}$$

with similar relations for the other axes.

The bounds on the torque from excess charge and the other electric phenomena listed in Table 5-1 may be computed in a similar manner. In addition, the torques from the position sensor radiation pressure and gas in the cavity were bounded in the same manner.

5. MAGNETIC TORQUES DUE TO CRYSTALLINE ANISTTROPY

If the rotor is constructed of a single crystal, χ_m will be a tensor except in a few special cases. The results in Stratton are easily extended to included this case.

If $\underline{H}_o$ is a 3 × 1 column matrix of components of the constant external field and if $\underline{H}^-$ is the matrix of the internal field, then the magnetic energy, U, is given by Stratton (55).

$$U = 1/2 \int_V \underline{H}^{-T} \ (\underline{\mu}_2 - \underline{\mu}_1) \ \underline{H}_o \ dV \tag{5-70}$$

where

$$\underline{\mu}_2 \overset{\triangle}{=} \mu_o \begin{bmatrix} 1 & 0 & 0 \\ 0 & 1 & 0 \\ 0 & 0 & 1 \end{bmatrix} \tag{5-71}$$

and

$$\underline{\mu}_1 \overset{\triangle}{=} \mu_o \begin{bmatrix} 1 + \chi_{mx} & 0 & 0 \\ 0 & 1 + \chi_{my} & 0 \\ 0 & 0 & 1 + \chi_{mz} \end{bmatrix} \tag{5-72}$$

$$U = 1/2 \ V \ \underline{H}^{-T} \ (\underline{\mu}_2 - \underline{\mu}_1) \ \underline{H}_o \ . \tag{5-73}$$

But from the boundary value problem of the sphere $\underline{H}^-$ and $\underline{H}_o$ are related by a constant matrix

$$\underline{H}^- = \underline{\underline{S}} \; \underline{H}_o \qquad\qquad (5\text{-}74)$$

where

$$\underline{\underline{S}} \triangleq \begin{bmatrix} \dfrac{1}{1 + 1/3 \; \chi_{mx}} & 0 & 0 \\[3mm] 0 & \dfrac{1}{1 + 1/3 \; \chi_{my}} & 0 \\[3mm] 0 & 0 & \dfrac{1}{1 + 1/3 \; \chi_{mz}} \end{bmatrix} . \qquad (5\text{-}75)$$

Thus,

$$U = 1/2 \; V \; \underline{H}_o^T \; \underline{\underline{S}} \; (\underline{\underline{\mu}}_2 - \underline{\underline{\mu}}_1) \; \underline{H}_o \qquad\qquad (5\text{-}76)$$

and for a small variation in the field $\delta \underline{H}_o$

$$\delta U = V \; \underline{H}_o^T \; \underline{\underline{S}} \; (\underline{\underline{\mu}}_2 - \underline{\underline{\mu}}_1) \; \underline{H}_o \; . \qquad\qquad (5\text{-}77)$$

If $\delta \underline{H}_o$ is caused by a small rotation $\delta \underline{\Phi}$

$$\delta \underline{H}_o = \underline{H}_o \times \delta \underline{\Phi} \qquad\qquad (5\text{-}78)$$

and

$$\delta U = - \; V \; \underline{H}_o \times (\underline{\underline{\mu}}_2 - \underline{\underline{\mu}}_1) \; \underline{\underline{S}} \; \underline{H}_o \cdot \delta \underline{\Phi} \; . \qquad (5\text{-}79)$$

By comparison, the work done by the rotation is

$$\delta U = - \; \underline{M} \cdot \delta \underline{\Phi} \qquad\qquad (5\text{-}80)$$

so that the torque induced by the field is

$$\underline{M} = \underline{H}_o \times (\underline{\underline{\mu}}_2 - \underline{\underline{\mu}}_1) \; \underline{\underline{S}} \; \underline{H}_o \; . \qquad\qquad (5\text{-}81)$$

For example, the y component of this torque

$$M_y = V\, B_{oz}\, H_{oy} \left(\frac{\chi_{mx}}{1 + 1/3\ \chi_{mx}} - \frac{\chi_{mz}}{1 + 1/3\ \chi_{mz}} \right) \tag{5-82}$$

$$\approx V\, B_{oz}\, H_{ox}\ (\chi_{mx} - \chi_{mz}) \tag{5-83}$$

leads to a precession of

$$\dot{\phi} = \frac{5\ B_{oz}\ H_{ox}\ (\chi_{mx} - \chi_{mz})}{2\ \rho_m\ R_B^2\ \omega_B} \quad . \tag{5-84}$$

6. SURFACE ELECTRIC EDDY CURRENTS

The surface electric eddy currents are due to the fact that the charge distribution of a charged ellipsoid in an electric field must vary as the orientation of the ellipsoid varies. The results quoted in Table 5-1 are estimates based on the approximation that a fraction ϵ_1 or ϵ_2 of the total charge circulates around the ellipsoid at a frequency $\omega_B/2$.

7. GAS TORQUES

The gas in the cavity tends to slow down the rotation and to precess the spin axis. The resistance is approximately proportional to ω_B and may be computed from kinetic theory. For the purposes of an order of magnitude estimate b will be taken as

$$b = \frac{\pi}{9}\ R_B^4\ \rho \left(\frac{3kT}{m_{av}} \right)^{\frac{1}{2}} \approx 1.8 \times 10^{-16} \text{ joule-sec} . \tag{5-85}$$

The spin-down time-constant due to T can be computed from the equation

$$C\,\dot{\omega}_B + b\ \omega_B = M_{\parallel} \quad , \tag{5-86}$$

and the result is

$$\text{Spin-Down Time-Constant} = C/b \approx 2200 \text{ years.} \tag{5-87}$$

SEL-64-067

The random walk of the spin axis may be evaluated by the same procedure as that outlined in Chapter IV. The RMS drift angle of the spin axis is given by

$$\left\langle \phi^2 \right\rangle_{av} = \frac{2bkT}{h_B^2} t \ .$$ (5-88)

Equation (5-88) predicts a drift of

$$\left\langle \phi^2 \right\rangle_{av}^{\frac{1}{2}} \approx 5.4 \times 10^{-13} \text{radians}$$ (5-89)

in one year, which is entirely negligible.

D. GYROSCOPE READOUT

One of the most difficult questions, and one which will not be discussed in this thesis, is the spin or angular momentum vector readout technique. Stanford University, Minneapolis-Honeywell, and the University of Illinois are all working on feasible readout schemes. It is felt by the author that any description of the details of the various systems should be given by these groups. It does appear, however, that readout to this order of accuracy is quite possible and that it can be done without causing excessive drift rates.

One complication which arises when one tries to read the direction of the angular momentum vector of an almost iso-inertial gyro rotor is that the preferred axis of rotation (i.e., the axis of maximum moment of inertia) is difficult to identify in advance. This means that readout schemes which depend on body-fixed patterns are not quite as useful as they are on rotors where one axis of inertia is much larger than the other two. This is true because the angular velocity vector may move a considerable distance in the rotor body-fixed axis if the spin is not started parallel to the preferred axis. For an almost spherical rotor with principal moment of inertia $A = C(1 - \epsilon_1)$, $B = C(1 - \epsilon_2)$, and C (where ϵ_1 and ϵ_2 are of the order of 10^{-5}); it can be shown that the

angle, ψ, between the angular momentum vector and the angular velocity vector is given by

$$\psi = \left[\epsilon_1^2 \left(\frac{\sin 2\alpha}{2} \right)^2 + \epsilon_2^2 \left(\frac{\sin 2\beta}{2} \right)^2 - 2\epsilon_1\epsilon_2 \cos^2\alpha \cos^2\beta \right]^{\frac{1}{2}}$$

(5-90)

$$= \epsilon_1 \frac{\sin 2\gamma}{2} \qquad \text{if } \epsilon_1 = \epsilon_2 \ .$$

α, β, and γ are the respective angles from the rotor x_B, y_B, and z_B principle axes to the angular velocity vector. ψ has a maximum value of the order of ϵ_1 or ϵ_2, and when viewed from an inertial reference frame, the angular velocity vector rotates about the angular momentum vector at a rate which is practically equal to the angular velocity. If ϵ_1 and ϵ_2 are of the order of 10^{-5}, it would appear that any readout which does not have a response time faster than $2\pi/\omega_B$ will tend to read the average direction of ω_B which, of course, is the direction of the angular momentum. Thus, it seems at the present time that sufficiently accurate readout schemes can be developed. Further details on this subject will have to await papers by the above groups.

CONCLUSION

It has been shown that there appears to be no fundamental physical or engineering reason why a drag-free satellite cannot be built at this time. Such a vehicle would yield useful immediate results in geodesy and aeronomy and would lay the foundations for the construction of very good gyroscopes and possibly open the way to do the Pugh-Schiff Relativity Experiment. In addition, the actual mechanization of the translation control would not be overly complex. For simple vehicles no attitude control is necessary since three medium-quality rate gyros will give sufficient attitude information to implement the control. The jet thrust levels and attainable fuel lifetimes are quite reasonable and should cause no difficulty.

A spinning drag-free satellite with its spin vector normal to the orbit plane and with an optical position sensor would depart from a purely-gravitational orbit by only a meter per year. Distances this small cannot be detected by any present or foreseeable tracking apparatus, and such performance would be drag free in every practical sense.

LIST OF REFERENCES

1. Kaula, W. M., "Celestial Geodesy," NASA Technical Note D-1155, Mar 1962.

2. Jacchia, L. G., "Variations in the Earth's Upper Atmosphere as Revealed by Satellite Drag," Smithsonian Astrophysical Observatory Report, 31 Dec 1962.

3. Sharp, G. W., Hanson, W. B., and McKibbin, D. D., "Atmospheric Density Measurements with a Satellite Borne Microfilm Gauge," J. Geophys. Res., 67, 1962, pp. 375-382.

4. Schiff, L. I., "Motion of a Gyroscope According to Einstein's Theory of Gravitation," Proc. Natl. Acad. Sci. U. S., 20, Oct, Nov, Dec 1959, pp. 1288-1302, 1405-1421, and 1517-1532.

5. Cannon, R. H., Jr., "Requirements and Design for a Special Gyro for Measuring General Relativity Effects from an Astronomical Satellite," Kreiselprobleme, edited by H. Ziegler, Springer-Verlag, Berlin, 1963, pp. 146-160.

6. Dicke, R. H., "The Nature of Gravitation," Science in Space, Part 2, edited by L. V. Beoknev and H. Odishaw, McGraw-Hill, New York, 1961, pp. 91-118.

7. Dicke, R. H., Hoffmann, W. F., and Krotkov, R., "Tracking and Orbit Requirements for Experiment to Detect Variations in Gravitational Constant," Space Research II - Proceedings of the Second International Space Science Symposium, Interscience Publishers, New York, 1961, pp. 287-291.

8. Rider, L., "Impulsive Orbit Sustaining Techniques for Low Altitude Satellites," Aerospace Corporation Technical Report, T.N. 594-1105-2, 5 Dec 1960.

9. Bruce, R. W., "Satellite Orbit Sustaining Techniques," ARS Journal, Sep 1961, pp. 1237-1241.

10. Roberson, R. E., "An Intermittent Orbit Sustaining Technique," Astronautica Acta, 8, Fasc. 1, 1962, pp. 42-48.

11. Gerathewohl, S. J., Zero-G Devices and Weightlessness Simulators, National Academy of Sciences - National Research Council, Publication 781, 1961.

12. Ericke, K. A., "The Satelloid," Astronautica Acta, 2, Fasc. 2, 1956.

13. Pugh, G. E., WSEG Research Memorandum No. 11, Weapons Systems Evaluation Group, The Pentagon, Washington 25, D. C., 12 Nov 1959.

14. MacDonald, G. J. F., and Cohlan, B. F., "Sustaining Orbiting Geophysical Observatory" (unpublished proposal), Institute of Geophysics and Planetary Physics, University of California at Los Angeles, Dec 1962.

LIST OF REFERENCES (CONT)

15. Proceedings of the Conference on Experimental Tests of the Theories of Relativity (unpublished), Stanford University, Jul 1961.

16. Wheelon, A. D., "An Introduction to Mid-Course and Terminal Guidance," Space Technology Laboratory Report, G.M.-T.M.-0165-00252, 10 Jun 1958.

17. Geyling, F. T., "Satellite Perturbations from Extra-Terrestrial Gravitation and Radiation Pressure," J. Franklin Inst., May 1960, pp. 375-407.

18. Eggleston, J. M., and Beck, H. D., "A Study of the Positions and Velocities of a Space Station and a Ferry Vehicle During Rendevous and Return," NASA Technical Report, No. R-87, 1961.

19. Tempelman, W. H., "Circular Orbit Partial Derivatives," AIAA Journal, 1, 5, May 1963, pp. 1187-1189.

20. Nelson, R. L., "The Motions of Rolling Symmetrical Missiles Referred to a Body-Axis System," NACA Report, TN 3737, Nov 1956.

21. Kanno, J. S., "The Effect of Nonlinear Aerodynamic Coefficients on Free-Spinning Ballistic Behavior and Its Application to the Evaluation of Flight Measurements," Lockheed Missiles and Space Co. Technical Report, LMSD-703013, Jun 1960.

22. Leon, H. I., "Spin Dynamics of Rockets and Space Vehicles in Vacuum," Space Technology Laboratory Report, TR-59-0000-00787, 16 Sep 1959.

23. Freed, L. E., "Attitude Control System for a Spinning Body," ARS Journal, 32, 3, Mar 1962, pp. 396-400.

24. Gaylord, R. S., and Keller, W. N., "Attitude Control System Using Logically Controlled Pulses," Progress in Astronautics and Rocketry, Vol. 8, Guidance and Control, edited by R. E. Roberson and J. S. Farrior, American Rocket Society, New York, 1962, pp. 629-648.

25. Dahl, Aldrich, and Herman, "Limit Cycles in Reaction Jet Attitude Control Systems Subject to External Torques," ibid., pp. 599-628.

26. Smythe, W. R., Static and Dynamic Electricity, McGraw-Hill, New York, 1950, p. 398.

27. Houston, W. V., and Muench, N., "Electromagnetic Forces on a Superconductor," Phys. Rev., 79, 6, 15 Sep 1950, pp. 967-970.

28. Alers, P. B., McWhirter, J. W., and Squire, C. F., "Eddy Currents and Supercurrents in Rotating Metal Spheres at Liquid Helium Temperatures," Phys. Rev., 84, 1, 1 Oct 1951, pp. 104-107.

29. Smart, W. M., Celestial Mechanics, Longmans, London, 1953, pp. 291 f.

30. Lagrange, J. L., "Theorie de la Libration de la Lune," Oeuvres, Tomb V, p. 1.

LIST OF REFERENCES (CONT)

31. Roberson, R. E., "Gravitational Torque on a Satellite Vehicle," J. Franklin Inst., 265, 1, Jan 1958.

32. DeBra, D. B., "The Large Attitude Motions and Stability, Due to Gravity, of a Satellite with Passive Damping in an Orbit of Arbitrary Eccentricity about an Oblate Body," Stanford University Technical Report, SUDAER No. 126, May 1962.

33. Groves, G. V., "Determination of Upper-Atmosphere Air Density and Scale Height from Satellite Observations," Proc. Roy. Soc. (London) 252A(1268):16-34, 25 Aug 1959.

34. Jacchia, L. G., "The Effect of a Variable Scale Height on Determinations of Atmospheric Density from Satellite Accelerations," Smithsonian Inst. Astrophys. Obs., Res. in Space Sci., Spec. Rept. No. 46:1-4, 11 Jul 1960.

35. Smelt, R., "Upper Atmosphere Properties Derived from Discoverer Satellites," Technical Report SUDAER No. 111, Department of Aeronautics and Astronautics, Stanford University, 1961.

36. Kane, T. R., Marsh, E. L., and Wilson, W. G., Letter to the Jour. Astro. Sci., 9, 4, Winter 1962, pp. 108-109.

37. Curtis, E. C., "Coordinate Transformation Problems Made Easy with Signal Flow," Lockheed Missiles and Space Co. Technical Report, 25 Mar 1963.

38. Graham, D., and McRuer, D., Analysis of Nonlinear Control Systems, Wiley, New York, 1961, pp. 370-393.

39. Rott, N., and Pottsepp, L., "Simplified Calculation of the Jet Damping Effects," AIAA Journal, 2, 4, Apr 1964, pp. 764-766.

40. Koelle, H. H., Handbook of Astronautical Engineering, McGraw-Hill, New York, 1961, pp. 2-63, 3-74, 3-75.

41. Beard, D. B. and Johnson, F. S., "Charge and Magnetic Field Interaction with Satellites," J. Geophys. Res., 65, 1, Jan 1960.

42. Sissenwine, N., "Announcing the U. S. Standard Atmosphere - 1962," Astronautics, 7, 8, Aug 1962, pp. 52-53.

43. Flügge-Lotz, I., Discontinuous Automatic Control, Princeton University Press, 1953.

44. Flügge-Lotz, I., "Discontinuous Automatic Control," App. Mech. Rev., 14, 8, Aug 1961.

45. Kalman, R. E., and Bertram, J. E., "Control System Analysis and Design Via the Second Method of Lyapunov Part I - Continuous Time Systems," Trans. ASME, Jour. Basic Eng., Jun 1960, pp. 371-393. (Aizerman's original paper is referenced and discussed in this work. The actual reference is in Russian and is inaccessible to most readers.)

LIST OF REFERENCES (CONT)

46.   Jeans, J., _The Mathematical Theory of Electricity and Magnetism_, Cambridge Press, 1960, pp. 167-168.

47.   Bandeen, W. R., and Manger, W. P., "Angular Motion of the Spin Axis of Tyros I Meterological Satellite due to Magnetic and Gravitational Torques," _J. Geophys. Rev._, 65, 1960, pp. 2992-5.

48.   Engstrom, R. W., _J. Opt. Soc. Am._, 37, 1947, p. 420.

49.   Aseltine, J. A., _Transform Method in Linear System Analysis_, McGraw-Hill, New York, 1958, pp. 240-241.

50.   Kennard, E. H., _Kinetic Theory of Gases_, McGraw-Hill, New York, 1938, pp. 280-283.

51.   Klein, F., and Sommerfeld, A., _Theorie des Kreisels_, Heft III, Die Störenden Einflüsse. Astronomische und Geophysikalische Anwendungen, Leipzig, Druck und Verlag, von G. B. Teubner, 1903, pp. 692-696.

52.   Tabakin, F., "Torque on a Spinning Metallic Sphere Induced by a Time Dependent Magnetic Field," Space Technology Laboratories, Inc. Technical Report, BSD-61-25, Sep 1961.

53.   Harnwell, G. P., _Principles of Electricity and Electromagnetism_, McGraw-Hill, New York, 1949, pp. 377-381.

54.   Stratton, J. A., _Electromagnetic Theory_, McGraw-Hill, New York, 1941, pp. 201-217.

55.   Stratton, pp. 112-113.